

SYNTHESIS OF NEW MULTIFUNCTIONAL  
POLYFLUORENE  
&  
DONOR ACCEPTOR TYPE POLYFLUORENE DERIVATIVES

A THESIS SUBMITTED TO  
THE GRADUATE SCHOOL OF NATURAL AND APPLIED SCIENCES  
OF  
MIDDLE EAST TECHNICAL UNIVERSITY

BY

BUKET BEZGİN ÇARBAŞ

IN PARTIAL FULFILLMENT OF THE REQUIREMENTS  
FOR  
THE DEGREE OF DOCTOR OF PHILOSOPHY  
IN  
CHEMISTRY

MAY 2013



Approval of the thesis:

**SYNTHESIS OF NEW MULTIFUNCTIONAL  
POLYFLUORENE  
&  
DONOR ACCEPTOR TYPE POLYFLUORENE DERIVATIVES**

submitted by **BUKET BEZGİN ÇARBAŞ** in partial fulfillment of the requirements for the degree  
of **Doctor of Philosophy in Chemistry Department, Middle East Technical University** by,

Prof. Dr. Canan Özgen  
Dean, Graduate School of **Natural and Applied Sciences**

\_\_\_\_\_

Prof. Dr. İlker Özkan  
Head of Department, **Chemistry**

\_\_\_\_\_

Prof. Dr. Ahmet M. Önal  
Supervisor, **Chemistry Dept., METU**

\_\_\_\_\_

**Examining Committee Members**

Prof. Dr. Teoman Tinçer  
Chemistry Dept., METU

\_\_\_\_\_

Prof. Dr. Ahmet M. Önal  
Chemistry Dept., METU

\_\_\_\_\_

Assoc. Prof. Dr. Ali Cirpan  
Chemistry Dept., METU

\_\_\_\_\_

Assoc. Prof. Dr. Atilla Cihaner  
Chem. Eng. And App. Chem. Dept., ATILIM UNIVERSITY

\_\_\_\_\_

Assoc. Prof. Dr. H. Emrah Ünalın  
Metallurgical and Materials Engineering Dept., METU

\_\_\_\_\_

**Date:** 10.05.2013

**I hereby declare that all information in this document has been obtained and presented in accordance with academic rules and ethical conduct. I also declare that, as required by these rules and conduct, I have fully cited and referenced all materials and rules that are not original to this work.**

Name, Last Name: Buket Bezgin Çarbaş

Signature :



## ABSTRACT

### SYNTHESIS OF NEW MULTIFUNCTIONAL POLYFLUORENE & DONOR ACCEPTOR TYPE POLYFLUORENE DERIVATIVES

Bezgin Çarbaş, Buket  
Ph. D., Department of Chemistry  
Supervisor: Prof. Dr. Ahmet M. Önal

May 2013, 144 pages

This dissertation focuses on the synthesis of polyfluorene and its derivatives via chemical or electrochemical polymerization for various applications (i.e. ambipolar property in organic electronics, fluorometric sensors PLEDs, and electrochromism). Fluorene based homo- and co-polymers have been integrated to these kinds of applications because of their facile synthesis and unique optical and electronic properties. The research can be divided into three parts.

In the first part, a new anodically coloring polymer, poly (fluorene-carboxylic acid) **P(FCA)**, was synthesized via electrochemical polymerization in the presence of the Lewis acid, borontrifluoride diethyletherate, yielding a clear to brownish-orange electrochromism. Furthermore, a dual type electrochromic device based on **P(FCA)** was constructed exhibiting a good open circuit memory.

In the second part, the thienylene fluorenes were under investigation and their analogues to produce electrochromic polymers with moderate band gaps and to determine the role of the donor groups in the D-A-D polyfluorene derivatives. The methylene bridge of the fluorene was also functionalized by different substituents based on -ketone (fluorenone), -quinoxaline and -xanthene pendant units to see the effect of the functional groups on the main chain backbone. For this purpose, eight D-A-D typed monomers- functionalized from C9 position of the fluorene structure and their corresponding polymers, (**P(TFT)** (poly(2,7-di-thiophen-2-yl-fluorene-9-one)), **P(EFE)** (poly(2,7-bis-(2,3-dihydro-thieno[3,4-b][1,4]dioxin-5-yl)-fluorene-9-one)), **P(PFP)** (poly (2,7-bis-(3,3-dihexyl-3,4 dihydro-2H-thieno[3,4-b][1,4]dioxepin-6-yl)-fluorene-9-one)) as fluorene-one; **P(TQT)** (poly(2,7-di(thiophen-2-yl)-5'H-spiro[fluorene-9,4'-pyrrolo[1,2-a]quinoxaline])), **P(EQE)** (poly(2,7-bis(2,3-dihydrothieno[3,4-b][1,4]dioxin-5-yl)-5'H-spiro[fluorene-9,4'-pyrrolo[1,2-a]quinoxaline])), **P(PQP)** (poly(2,7-bis(3,3-dihexyl-3,4-dihydro-2H-thieno[3,4-b][1,4]dioxepin-6-yl)-5'H-spiro[fluorene-9,4'-pyrrolo[1,2-a]quinoxaline]) ) as fluorene-quinoxaline and **P(TXT)** (poly(3',6'-bis(octyloxy)-2,7-di(thiophen-2-yl)spiro[fluorene-9,9'-xanthene])), **P(EXE)** (poly (2,7 bis(2,3-dihydrothieno[3,4-b][1,4]dioxin-5-yl)-3',6'-bis(octyloxy)spiro[fluorene-9,9'-xanthene])) as fluorene-xanthene derivatives were synthesized. The obtained polymers exhibited attractive optical and electronic properties and utilized for some applications. For instance; D-A-D type fluorenone derivatives exhibited ambipolar property with orange light emission and one with fluorene-quinoxaline derivatives showed high sensitivity towards the Fe<sup>2+</sup> ions with red light emission. The last derivative, fluorene-xanthene spiro structure, indicated strong thermal stability with blue light emission together with high quantum efficiency.

In the last part, a novel blue emitting and electrochromic conjugated polymer based on 9,9'-dioctylfluorene and spiro (fluorene-9,9'-xanthene) was prepared. Optical, photophysical and electrochemical characterizations have been conducted for the synthesized polymer; **P(F8-SFX)**. Switching of the corresponding polymer between yellow and purple states was demonstrated, and blue emission with Commission Internationale de L'Eclairage (CIE) coordinate at (0.19, 0.15) was obtained from the fabricated polymer light emitting diode.

**Keywords:** Polyfluorene and its derivatives, Electrochromism, D-A-D approach, PLED, Ambipolar polymers, Ion sensitivity, Electrochromic Device.

## ÖZ

### ÇOK FONKSİYONLU YENİ POLİFLOREN SENTEZİ & DONÖR AKSEPTÖR TİPİ POLİFLOREN TÜREVLERİ

Bezgin Çarbaş, Buket  
Doktora, Kimya Bölümü  
Tez Yöneticisi: Prof. Dr. Ahmet M. Önal

May 2013, 144 pages

Bu tez, değişik kullanım alanları olan (organik cihazlarda kullanılan ambipolar özellikli polimerler, florometrik tesbit, PLED'ler ve elektrokromizm gibi) kimyasal veya elektrokimyasal yöntemlerle elde edilen polifloren ve türevlerinin üzerinde odaklanmıştır. Floren bazlı homo- ve ko-polimerler eşsiz optiksel ve elektronik özelliklerinden dolayı bu tür uygulama alanlarına entegre edilebilmektedirler. Bu bilimsel çalışma 3 bölümden oluşmaktadır.

İlk bölümde, floren karboksilik asit monomerinin borontriflorür dietileter varlığında elektrokimyasal polimerizasyonu ile anodikli renkli polimer poly(floren karboksilik asit), **P(FCA)**, elde edilmiştir. Şeffaf olan **P(FCA)** filmi elektrokimyasal yükseltgenme esnasında kahverengimsi-turuncu renge dönüşerek elektrokromik özellik göstermiştir. Ayrıca, **P(FCA)** bazlı çift yönlü elektrokromik cihaz oluşturulmuş ve açık devre hafızasının oldukça iyi olduğu bulunmuştur.

İkinci bölümde ise, düşük band aralıklı elektrokromik polimerler elde etmek ve D-A-D polifloren türevlerindeki elektron verici grupların görevini belirleyebilmek için tienil florenleri ve türevlerine odaklanılmıştır. Floren yapısındaki metilen köprüsü, farklı işlevsel grupların ana zincir üzerindeki etkisini incelemek amacı ile, keto (florenon), -kinoksalin ve -ksanten gibi farklı gruplar ile işlevselleştirilmiştir. Bu nedenle florenin C9 pozisyonundan fonksiyonlanmış D-A-D tipi 8 değişik monomer ve onların karşılığı olan polimerleri (**P(TFT)** (poly(2,7-di-thiophen-2-yl-fluorene-9-one)), **P(EFE)** (poly(2,7-bis-(2,3-dihydro-thieno[3,4-b][1,4]dioxin-5-yl)-fluorene-9-one)), **P(PFP)** (poly (2,7-bis-(3,3-dihexyl-3,4 dihydro-2H-thieno[3,4-b][1,4]dioxepin-6-yl)-fluorene-9-one)) florenon; **P(TQT)** (poly(2,7-di(thiophen-2-yl)-5'H-spiro[fluorene-9,4'-pyrrolo[1,2-a]quinoxaline])), **P(EQE)** (poly(2,7-bis(2,3-dihydrothieno[3,4-b][1,4]dioxin-5-yl)-5'H-spiro[fluorene-9,4'-pyrrolo[1,2-a]quinoxaline])), **P(PQP)** (poly(2,7-bis(3,3-dihexyl-3,4-dihydro-2H-thieno[3,4-b][1,4]dioxepin-6-yl)-5'H-spiro[fluorene-9,4'-pyrrolo[1,2-a]quinoxaline])), floren-kinoksalin **P(TXT)** (poly(3',6'-bis(octyloxy)-2,7-di(thiophen-2-yl)spiro[fluorene-9,9'-xanthene])), **P(EXE)** (poly (2,7 bis(2,3-dihydrothieno[3,4-b][1,4]dioxin-5-yl)-3',6'-bis(octyloxy)spiro[fluorene-9,9'-xanthene])) floren-ksanten türevleri olarak sentezlenmiştir. Elde edilen polimerler ilgi çekici optiksel ve elektronik özellikler göstermiştir. Örneğin, D-A-D florenon türevleri turuncu ışık yayımı ile birlikte ambipolar özelliği göstermiştir ve fluorene- kinoksalin türevleri ise kırmızı ışık yayımı ile Fe<sup>2+</sup> katyonuna karşı aşırı duyarlılık göstermiştir. Son türev floren-ksanten spiro yapısı ise yüksek kuantum verimi ile mavi ışık yayabilen güçlü termal kararlılık göstermiştir.

Son bölümde ise, yeni bir mavi ışık yayabilen ve elektrokromik konjuge 9.9'-dioktilfluorene ve (spiro fluorene-9.9'-ksanten) bazlı yeni bir konjuge polimer hazırlanmış, ve elde edilen polimerin optiksel, fotofiziksel ve elektrokimyasal özellikleri incelenmiştir. Polimerin sarı ve eflatun renkleri arasında anahtarlandığı ve polimerden elde edilen PLED cihazının Commission Internationale de L'Eclairage (CIE) (0.19, 0.15) koordinatlarında mavi ışık yayabildiği ayrıca bulunmuştur.

**Anahtar Sözcükler:** Polifloren ve türevleri, Elektrokromizm, D-A-D Yaklaşımı, PLED, Ambipolar polimerler, İyon duyarlılığı, Elektrokromik cihaz.

To My Lovely Daughter and My Family ....  
*For your endless support and love*

## ACKNOWLEDGMENTS

I would like to acknowledge thanks to all the people who helped me during my all studies and the preparation of this thesis:

I wish to express my deepest appreciation to my advisor, Prof. Dr. Ahmet M. Önal, for his support and tremendous encouragement during my research. He was not only my supervisor, but also was one of my friends and especially my second father in the university. I thank him very much for everything. It was an honor to work with him. Words can not express my gratitude.

I owe great thanks to Assoc. Prof. Dr. Atilla Cihaner for his help, technical support and answering my questions anytime in the laboratory, besides their kind friendship not only for his support throughout my studies but also treated me like a brother.

I also want to thanks to Prof. Dr. Metin Zora and Prof. Dr. Leyla Aras for their lab support during my organic synthesis.

I wish to thank Assoc. Prof. Dr. Arif Kıvrak for his endless help, never-ending support during my studies and trust even though he is thousands of kilometers away.

Special thanks go to my dear friends, Asist. Prof. Dr. Seha Tirkeş, Demet Asil, Nurdan Atılğan, Samed Atak, Barış Karabay, Arzu Güneş, Esra Oğuztürk, Ece Gizem Kubat, Halil İpek, Özden Çelikkilek, Jetmire Mersini, Esra Eroğlu, Salih Ertan , Emine Gül Cansu for useful conversations and cooperation. I also would like to thank all my labmates in our research group for their kind friendship.

I also wish to thank all my colleagues in Chemistry Department of METU. I would also like to thank the staff at METU Chemistry Department for their efforts and helps.

I would like to express my sincere thanks to Dr. Arzu Büyükyavaş Yavuz, Dr. Yasin Kanbur, Tuğba Efe, Yasemin Çetin, Cansel Kadioğlu, Mahir Kaya, Serhat Odabaş, for their endless support, patience and motivation throughout this work.

I would like to thank to TÜBİTAK for supplying financial support during my PhD. I would like to extend my deepest thanks to Gaziosmanpaşa University and OYP programme for supporting me to complete my PhD. in the Chemistry Department of METU.

I thank to my parents Gülser and Mustafa Yaşar Bezgin for believing in me and giving me endless support. My parents without whom, I would not be the person that I am today. My love for them is eternal. I also want to thanks to my second family; Hayriye and Süreyya Çarbaş for their support and love. Many thanks to my sisters Dilek Toklu, Nükhet Erdem and Ayşegül Çarbaş for their priceless advices in every step of my life. I also want to express my special thanks to my brother in law, Dr. Mehmet Davut Toklu. Without his support and encouragement, I wouldn't be able to make this career. Thanks for everything....

Finally, I give my special thanks to my spouse, Serdar, for his endless love and support no matter how unbearable I get. He is the source of my inspiration and my ultimate.

## TABLE OF CONTENTS

|  |       |
|--|-------|
| ABSTRACT .....   | v     |
| ÖZ .....   | vi    |
| ACKNOWLEDGMENTS .....  | viii  |
| TABLE OF CONTENTS .....  | ix    |
| LIST OF FIGURES .....  | xii   |
| LIST OF TABLES .....   | xvi   |
| LIST OF SCHEMES .....  | xvii  |
| ABBREVIATIONS .....  | xviii |
| CHAPTERS .....   | 1     |
| 1. INTRODUCTION .....  | 1     |
| 1.1. A Brief Introduction to Conducting Polymers .....   | 1     |
| 1.2. Conductivity Mechanism of Conjugated Polymers .....                                       | 2     |
| 1.2.1. Structure and Conjugation .....   | 2     |
| 1.2.2. Band Gap .....  | 3     |
| 1.2.3. Doping Process .....  | 3     |
| 1.2.4. Hopping Process .....   | 5     |
| 1.3. Synthesis of CPs .....  | 5     |
| 1.3.1. Chemical Polymerization .....   | 5     |
| 1.3.2. Electrochemical Polymerization .....  | 6     |
| 1.3.2.1. Electroanalytical Methods for Electropolymerization and Characterization of CPs. .... | 7     |
| 1.3.2.1.1. Cyclic Voltammetry (CV) .....   | 8     |
| 1.3.2.1.2. Differential Pulse Voltammetry (DPV) .....  | 8     |
| 1.3.2.1.3. Controlled Potential Coulometry .....   | 9     |
| 1.4. Intrinsic Properties of CPs .....   | 9     |
| 1.4.1. Band Gap .....  | 9     |
| 1.4.1.1. Donor Acceptor Approach .....   | 9     |
| 1.4.1.2. Measurement Methods of Band Gap .....   | 9     |
| 1.4.1.2.1. Electroanalytical Methods .....   | 10    |
| 1.4.1.2.2. Spectroelectrochemical Methods .....  | 11    |
| 1.4.2. Electrochromism .....   | 12    |
| 1.4.2.1. Optical contrast .....  | 13    |
| 1.4.2.2. Switching Time .....  | 14    |
| 1.4.2.3. Coloration Efficiency ( $\eta$ ) .....  | 14    |
| 1.4.3. Fluorescence .....  | 14    |
| 1.4.3.1. Quantum Yield ( $\Phi_f$ ) .....  | 15    |
| 1.4.4. Electroluminescence .....   | 16    |
| 1.5. Polyfluorenes .....   | 17    |
| 1.5.1. Chemical Structure .....  | 17    |
| 1.5.2. Synthesis of Polyfluorenes .....  | 17    |
| 1.5.2.1. Synthesis of PFs via chemical approaches .....  | 17    |
| 1.5.2.2. Synthesis of PFs via electrochemical oxidation .....                                  | 18    |
| 1.5.2.2.1. Fluorene Homopolymers .....   | 18    |
| 1.5.2.2.2. Alternating Donor Acceptor Type Polyfluorene Derivatives .....                      | 19    |
| 1.5.2.3. Functionalization of Polyfluorene Derivatives at C9 position .....                    | 20    |
| 1.5.2.3. Fluorene Copolymers .....   | 22    |
| 1.5.3. Some Selected Applications of PF Derivatives .....                                      | 22    |

|            |  |    |
|------------|--|----|
| 1.5.3.1.   | Electrochromic Devices .....   | 22 |
| 1.5.3.2.   | Fluorometric Detection .....   | 23 |
| 1.5.3.3.   | PLEDs .....  | 24 |
| 1.6.       | Aim of This Study .....  | 25 |
| 2.         | EXPERIMENTAL .....   | 29 |
| 2.1.       | Materials.....   | 29 |
| 2.2.       | General methods.....   | 29 |
| 2.3.       | Electrochemistry.....  | 29 |
| 2.4.       | Spectroelectrochemistry (SPEL) .....   | 30 |
| 2.5.       | PLED Device Characterization .....   | 31 |
| 2.6.1.     | Synthesis of D-A-D type fluorene monomers .....  | 31 |
| 2.6.1.1.   | Preparation of Donor Moieties .....  | 32 |
| 2.6.1.1.1. | Tributyl (thiophen-2-yl) stannane (i).....   | 33 |
| 2.6.1.1.2. | Tributyl (2, 3-dihydrothieno [3, 4- <i>b</i> ][1, 4] dioxin-7-yl)stannane (ii) ..                                | 33 |
| 2.6.1.1.3. | Tributyl-(3, 3-dihexyl-3, 4-dihydro-2H-thieno[3,4- <i>b</i> ][1,4]dioxepin-6-yl)-stannane (iii) .....            | 33 |
| 2.6.1.2.   | Synthesis of Donor-Acceptor-Donor-Acceptor Moieties.....   | 35 |
| 2.6.1.2.1. | Synthesis of D-A-D monomer based on fluorenone moiety .....  | 35 |
| 2.6.1.2.3. | Synthesis of D-A-D monomer based on xanthene moiety.....   | 38 |
| 2.6.1.3.   | Electropolymerization of D-A-D type fluorene derivatives and their characterization .....                        | 39 |
| 2.6.1.4.   | Chemical Polymerization of D-A-D type fluorene derivatives.....  | 40 |
| 2.6.2.     | Electropolymerization of FCA .....   | 40 |
| 2.6.3.     | Chemical coupling polymerization of spirofluorene-co-9,9'-dioctylfluorene ...                                    | 41 |
| 3.         | RESULTS AND DISCUSSION .....   | 43 |
| 3.1.       | Electrochemical polymerization of 9-fluorene-carboxylic acid and its electrochromic device application .....     | 43 |
| 3.1.1.     | Electrochemical behavior of FCA and its electrochemical polymerization.....                                      | 43 |
| 3.1.2.     | Polymer Characterization .....   | 44 |
| 3.1.3.     | Thermal Characterization .....   | 44 |
| 3.1.4.     | Spectroelectrochemical properties of P(FCA). .....   | 45 |
| 3.1.5.     | Electrochromic switching of P(FCA) film in solution.....   | 46 |
| 3.1.6.     | P(FCA) / PEDOT Electrochromic Device Application .....   | 47 |
| 3.2.       | D-A-D type Polyfluorene derivatives .....  | 49 |
| 3.2.1.     | Fluorenone functionalized D-A-D type Polyfluorene derivatives .....  | 49 |
| 3.2.1.1.   | Electrochemical behavior of TFT, EFE and PFP .....   | 49 |
| 3.2.1.2.   | Electrochemical polymerization of TFT, EFE and PFP .....   | 50 |
| 3.2.1.3.   | Electrochemical behaviour of P(TFT), P(EFE) and P(PFP) .....   | 51 |
| 3.2.1.4.   | Band gap analysis of P(TFT), P(EFE) and P(PFP) via electrochemical methods. P(TFT), P(EFE) and P(PFP) .....      | 51 |
| 3.2.1.5.   | Band gap analysis of P(TFT), P(EFE) and P(PFP) via spectroelectrochemical methods P(TFT), P(EFE) and P(PFP)..... | 51 |
| 3.2.1.6.   | Energy band diagram of polymers .....  | 56 |
| 3.2.1.7.   | Spectroelectrochemical and Switching Behaviors of Polymers P(TFT), P(EFE) and P(PFP) .....                       | 58 |
| 3.2.1.8.   | Fluorescence Properties of Polymers P(TFT), P(EFE) and P(PFP) .....  | 60 |
| 3.2.2.     | Fluorene-quinoxaline functionalized D-A-D type Polyfluorene derivatives .....                                    | 61 |
| 3.2.2.1.   | Electrochemical behavior of FQ, TQT, EQE and PQP .....   | 61 |
| 3.2.2.2.   | Electrochemical polymerization of TQT, EQE and PQP .....   | 62 |
| 3.2.2.3.   | Electrochemical behaviour of P(TQT), P(EQE) and P(PQP).....  | 63 |
| 3.2.2.4.   | Polymer characterization of P(TQT), P(EQE) and P(PQP) .....  | 64 |
| 3.2.2.5.   | Spectroelectrochemical behaviour of P(TQT), P(EQE) and P(PQP) .....  | 64 |

|          |   |     |
|----------|---|-----|
| 3.2.2.6. | Fluorescence Study .....  | 69  |
| 3.2.3.   | Fluoren-xanthene functionalized D-A-D type Polyfluorene derivatives ..... | 71  |
| 3.2.3.1. | Electrochemical behavior of FX, TXT and EXE .....                         | 71  |
| 3.2.3.2. | Electrochemical polymerization of TXT and EXE .....                       | 72  |
| 3.2.3.3. | Electrochemical behaviour of P(TXT) and P(EXE).....                       | 73  |
| 3.2.3.4. | Spectroelectrochemistry of P(TXT) and P(EXE).....                         | 75  |
| 3.2.3.5. | Fluorescence study for P(TXT) and P(EXE) .....                            | 79  |
| 3.2.3.6. | Thermal Characterization of P(TXT) and P(EXE).....                        | 80  |
| 3.2.3.7. | Characterization of P(TXT) and P(EXE) .....                               | 81  |
| 3.3.     | Polyfluorene copolymer synthesis.....                                     | 82  |
| 3.3.1.   | Synthesis and Properties of P(F8-SFX) .....                               | 82  |
| 3.3.2.   | Electrochemical characterization of P(F8-SFX) .....                       | 84  |
| 3.3.3.   | Optical Characterization of P(F8-SFX) .....                               | 85  |
| 3.3.4.   | Electrochromic Properties of P(F8-SFX) .....                              | 86  |
| 3.3.4.1. | Electrochromic properties of P(F8-SFX) and its switching property .....   | 86  |
| 3.3.4.2. | Optical Properties of the P(F8-SFX)/PEDOT electrochromic device .....     | 87  |
| 3.3.5.   | PLED Characterization .....   | 89  |
| 4.       | CONCLUSIONS.....  | 93  |
|          | REFERENCES.....   | 101 |
|          | APPENDICIES .....   | 105 |
| A.       | FTIR SPECTRA OF MONOMERS AND POLYMER .....                                | 105 |
| B.       | NMR SPECTRA OF MONOMERS .....   | 117 |
| C.       | NMR SPECTRA OF POLYMERS .....   | 137 |
| D.       | ELEMENTAL COMPOSITION REPORT OF MONOMERS.....                             | 139 |
| E.       | MASS ANALYSIS REPORT OF POLYMER .....                                     | 142 |
|          | CURRICULUM VITAE .....  | 143 |

## LIST OF FIGURES

### FIGURES

|   |    |
|---|----|
| Figure 1.1. Some common aromatic conjugated polymers. ....  | 1  |
| Figure 1.2. A schematic illustration of the structure and atomic orbitals involved in the electronic structure (left) and the energy diagram (right) of a) polyethylene, b) transpolyacetylene. ....  | 2  |
| Figure 1.3. Valence (VB) and Conduction (CB) bands in conductor, semiconductor, and insulator. ....   | 3  |
| Figure 1.4. A schematic description of the formation of (a) polyene, (b) polaron, and (c) bipolaron (d) soliton pair on a trans-polyacetylene chain by doping. ....   | 4  |
| Figure 1.5. Illustration of hopping mechanism .....   | 5  |
| Figure 1.6. Electrochemical polymerization mechanism of EDOT.....   | 6  |
| Figure 1.7. (a) Illustration of an electrochemical cell used for electrochemical polymerization (b) a typical cyclic voltammogram.....  | 8  |
| Figure 1.8. Orbital interaction between donor and acceptor units lowers the band gap of conjugated polymers. ....   | 9  |
| Figure 1.9. Evaluation of the band gap value by using CV technique .....  | 10 |
| Figure 1.10. Evaluation of the band gap value by using DPV technique .....  | 11 |
| Figure 1.11. Evaluation of band gap by using SPEL method .....  | 11 |
| Figure 1.12. Types of the electrochromic of CPs (1) Multielectrochromic typed, (2a) Cathodically colored, (2b) Anodically colored, (3) two distinct colored polymer.....  | 12 |
| Figure 1.13. The relationship between polymer color and absorption spectrum of the material.....  | 13 |
| Figure 1.14. Chronoabsorptometry and chronocoulometry experiments for the polymer of 4-((2,5-dithiophen-2-yl)thiophen-3-yl)pyrrolo[1,2-a]quinoxaline at 530 nm in 0.1 M TBAPF <sub>6</sub> /DCM. ....   | 14 |
| Figure 1.15. The schematic illustration of the fluorescence property in a molecule .....  | 15 |
| Figure 1.16. Illustration of electroluminescence (EL) in a conjugated polymer material. ....  | 16 |
| Figure 1.17. Chemical structure of fluorene.....  | 17 |
| Figure 1.18. Oxidative synthesis of poly[(9,9'-dihexyl)-2,7-fluorene]. ....   | 17 |
| Figure 1.19. Synthesis of 9,9'-dialkylated polyfluorene via Yamamoto coupling. ....   | 18 |
| Figure 1.20. Synthesis of 9,9'-dialkylated polyfluorene via Suzuki cross coupling. ....   | 18 |
| Figure 1.21. Previously reported fluorene derivatives polymerized via electrochemical polymerization .....  | 19 |
| Figure 1.22. Previously reported hybrid fluorene derivatives polymerized via electrochemical polymerization .....   | 20 |
| Figure 1.23. The mechanism for the generation of keto-defect sites .....  | 21 |
| Figure 1.24. Chemical structure and 3-D image of spirofluorene .....  | 21 |
| Figure 1.25. Examples of fluorene copolymers used in various applications .....   | 22 |
| Figure 1.26. A typical illustration of electrochromic device construction. ....   | 23 |
| Figure 1.27. (a) The Stern–Volmer plots of polyfluorene derivative in the presence of various metal ions (each 5–40 mM). Metal ion solutions were prepared from Fe(NO <sub>3</sub> ) <sub>3</sub> ·9H <sub>2</sub> O, Cu(NO <sub>3</sub> ) <sub>2</sub> ·3H <sub>2</sub> O, Ni(NO <sub>3</sub> ) <sub>2</sub> ·6H <sub>2</sub> O, Zn(NO <sub>3</sub> ) <sub>2</sub> ·6H <sub>2</sub> O, AgNO <sub>3</sub> , Hg(NO <sub>3</sub> ) <sub>2</sub> , Pb(NO <sub>3</sub> ) <sub>2</sub> , Cd(NO <sub>3</sub> ) <sub>2</sub> ·4H <sub>2</sub> O in THF, (b) K <sub>sv</sub> values, (c) the fluorescence emission spectra of polyfluorene derivative with successive addition of 5–40 mM Fe <sup>3+</sup> aqueous solution. .... | 24 |
| Figure 1.28. Representation of a PLED. ....   | 25 |
| Figure 3. 1. Cyclic voltammograms of (a) FCA and (b) P(FCA) at scan rates from 25 mV/s to 250 mV/s in 25 mV increments in 0.1 M TBABF <sub>4</sub> in nitromethane containing 4% BFEE. ....   | 43 |
| Figure 3. 2. Thermogram of P(FCA).....  | 45 |



|  |    |
|--|----|
| Figure 3.3. In-situ absorption spectra of P(FCA) (50 mC/cm <sup>2</sup> on ITO) recorded in 0.1 M TBABF <sub>4</sub> /nitromethane containing 4% BFEE at various applied potentials.....   | 45 |
| Figure 3. 4. Optical response of P(FCA) at 490 nm as a function of time in 0.1 M TBABF <sub>4</sub> /nitromethane containing 4% BFEE under an applied square voltage signal between 0.0 V (the neutral state) and 1.2 V (the oxidized state). ....   | 46 |
| Figure 3. 5. Optical characterization of P(FCA) / PEDOT electrochromic device by applying potentials between – 1.0 V and + 2.0 V.....  | 47 |
| Figure 3. 6. Optical response of P(FCA) /PEDOT electrochromic device at 600 nm as a function of time under an applied square voltage signal between – 1.0 V (transparent) and + 2.0 V (dark blue color) with a switch time of 10 s. ....   | 48 |
| Figure 3. 7. Open circuit memory of P(FCA)/PEDOT device after applying – 1.0 V and + 2.0 V for 5 s, respectively.....  | 48 |
| Figure 3. 8. First oxidation potential comparison of FO, TFT ,EFE and PFP in 0.1 M TBAPF <sub>6</sub> /DCM at 100 mV/s onto a Pt disc (area = 0.02 cm <sup>2</sup> ) vs. Ag/AgCl. ....   | 49 |
| Figure 3. 9. Electropolymerization of 10 mM (a) TFT (b) EFE in 0.1 M TBAPF <sub>6</sub> / DCM (c) PFP in 0.1 M TBAPF <sub>6</sub> / DCM / ACN (1/9-v/v) at 100 mV/s by potential scanning to give P(TFT), P(EFE), and P(PFP), respectively. ....   | 50 |
| Figure 3. 10. Scan rate dependence study for (a) P(TFT), (b) P(EFE) and (c) P(PFP) in 0.1 M TBAPF <sub>6</sub> /ACN at applied scan rates between 20 mV/s and 200 mV/s in 20 mV increments. Insets: relationship of anodic (i <sub>anodic</sub> ) and cathodic (i <sub>cathodic</sub> ) current peaks as a function of scan rate for (a) p-doped (b) n-doped films in 0.1 M TBAPF <sub>6</sub> /CAN.....   | 52 |
| Figure 3. 11. Cyclic voltammograms of p- and n-doped (a) P(TFT), (b) P(EFE) and (c) P(PFP) films in TBAPF <sub>6</sub> /ACN at scan rate 100 mV/s. Insets: differential pulse voltammetry of p- and n-doped films in TBAPF <sub>6</sub> /ACN with a step time of 0.1 s and a step size of 10 mV.....   | 53 |
| Figure 3. 12. Electronic absorption spectra of (a) P(TFT) ( between 0 V and 1.4 V ), (b) P(EFE) (between 0 V and 1.10 V ) and (c) P(PFP) (between 0 V and 1.10 V ) films on ITO in 0.1 M TBAPF <sub>6</sub> /ACN at various applied potentials. Inset: Electronic absorption spectra of (i) P(TFT) ( between 0 V and -1.5 V ) (ii) P(EFE) ( between 0 V and -1.6 V ) and (iii) P(PFP) ( between 0 V and -1.8 V ) films on ITO in 0.1 M TBAPF <sub>6</sub> /ACN (50 cycles) on ITO in 0.1 M TBAPF <sub>6</sub> /ACN at various applied potentials. .... | 55 |
| Figure 3. 13. SPEL and electrochemical data for various fluorene derivatives.....  | 57 |
| Figure 3. 14. Chronoabsorptometry experiments for P(PFP) on ITO in 0.1 M TBAPF <sub>6</sub> / ACN while the polymer was switched between -0.2 V and 1.2 V with a switching time of 10 s during 5 minutes at 441 nm, 684 nm and 1050 nm.....  | 59 |
| Figure 3. 15. Emission (excited at 420 nm) and absorption spectra of P(EFE) in THF.....  | 60 |
| Figure 3. 16. Emission (excited at 355 nm) and absorption spectra of P(PFP) in THF. Inset (a) spray coating of P(PFP) in THF (b) photograph of P(PFP) under UV light .....   | 60 |
| Figure 3. 17. Cyclic voltammograms of FQ, TQT, EQE and PQP on a Pt disk electrode at 100 mV/s in 0.1 M TBAClO <sub>4</sub> /ACN vs. Ag / AgCl. (Insets: Cyclic voltammogram of FQ, after peak clipping at 1.10 V.) .....   | 61 |
| Figure 3. 18. Repeated potential scan electropolymerization of 2 mM (a) TQT in 0.1 M TBAClO <sub>4</sub> /ACN:BFEE;1:1, (b) EQE in 0.1 M TBAClO <sub>4</sub> /ACN (c) PQP in 0.1 M TBAPF <sub>6</sub> /ACN on a Pt disk electrode at 100 mV/s. ....  | 62 |
| Figure 3. 19. Scan rate dependence of (a) P(TQT), (b) P(EQE), (c) P(PQP) film (25 cycle) on a Pt disk electrode at different scan rates between 20 mV/s and 100 mV/s (20 mV s <sup>-1</sup> increments) in 0.1 M TBAClO <sub>4</sub> /ACN. (Insets: Relationship of anodic (I <sub>anodic</sub> ) and cathodic (I <sub>cathodic</sub> ) current peaks as a function of scan rate). ....  | 63 |
| Figure 3. 20. Electronic absorption spectra of (a) P(TQT), (b) P(EQE), (c) P(PQP) on ITO (25 cycles) in 0.1 M TBAClO <sub>4</sub> /ACN solution during anodic oxidation of the polymer film. ....  | 65 |
| Figure 3. 21. Schematic illustration of energy band diagrams for P(TQT), P(EQE) and P(PQP)..   | 66 |

|   |    |
|---|----|
| Figure 3. 22. Chronoabsorptimetry experiments for (a) P(TQT) and (b) P(EQE), with a switching between 0 V and 1.0 V in 10 and 5 s. ....   | 67 |
| Figure 3. 23. Optical stability experiments of P(PQP) at (a) 569 nm, (b) 874 nm and (c) 1017 nm in a switching between 0 V and 1.0 V in 10 s.....   | 68 |
| Figure 3. 24. The Stern–Volmer plots of (a) PQP, (b) P(PQP), in the presence of various metal ions (each 0.02–0.1 mM). Metal ions prepared from $\text{Fe}(\text{NO}_3)_3 \cdot 9\text{H}_2\text{O}$ , $\text{Cu}(\text{NO}_3)_2 \cdot 3\text{H}_2\text{O}$ , $\text{Ni}(\text{NO}_3)_2 \cdot 6\text{H}_2\text{O}$ , $\text{Zn}(\text{NO}_3)_2 \cdot 6\text{H}_2\text{O}$ , Pb, $\text{AgNO}_3$ in THF. Inset: (a) Fluorescence emission spectra of (a) PQP (b) P(PQP) (1 mg in 20 ml THF) with successive addition of 0.02–0.1 mM $\text{Fe}^{2+}$ ion. (b) $K_{sv}$ values of (a) PQP (b) P(PQP) in the presence of $\text{Cu}^{2+}$ , $\text{Ag}^+$ , $\text{Ni}^{2+}$ , $\text{Fe}^{2+}$ , $\text{Zn}^{2+}$ , $\text{Fe}^{3+}$ (each 0.02–0.1 mM). .... | 70 |
| Figure 3. 25. Emission colors of (1) PQP, (2) PQP in the presence of $\text{Fe}^{2+}$ ion, (3) P(PQP) , (4) P(PQP) in the presence of $\text{Fe}^{2+}$ ion in THF under handheld UV lamp. ....  | 71 |
| Figure 3. 26. First oxidation potential comparison of FX, TXT and EXE in 0.1M $\text{TBAPF}_6/\text{ACN}$ at 100 mV/s onto a Pt disc (area = 0.02 $\text{cm}^2$ ). ....   | 72 |
| Figure 3. 27. (a) Cyclic voltammogram of 10 mM (a) TXT 0.1M $\text{TBAPF}_6$ in DCM: ACN = 1:10 and (b) EXE 0.1M $\text{TBAPF}_6$ in ACN on a Pt disc electrode at scan rate of 100 $\text{mVs}^{-1}$ (25 cycle). ....  | 73 |
| Figure 3. 28. Cyclic voltammograms of (a) P(TXT) and (b) P(EXE) film in $\text{TBAPF}_6/\text{ACN}$ at a scan rate of 100 mV/s. ....  | 74 |
| Figure 3. 29. Stability test for a P(EXE) (25 $\text{mC cm}^{-2}$ ) film in 0.1 M $\text{TBAPF}_6/\text{ACN}$ by a square wave potential method between -0.30 V and 0.90 V and cyclic voltammograms of A: 1 <sup>st</sup> ; B: 500 <sup>th</sup> ; C: 1,000 <sup>th</sup> cycles at a scan rate of 200 $\text{mVs}^{-1}$ : (a) $i_{pa}$ (anodic peak current), (b) $Q_a$ (Anodic charge stored) (c) $i_{pc}$ (cathodic peak current). ....  | 75 |
| Figure 3. 30. Electronic absorption spectra of (a) P(TXT) and (b) P(EXE) on ITO in 0.1 M $\text{TBAPF}_6/\text{ACN}$ at various applied potentials. (Inset: The color of oxidized and neutral forms of polymers ).....  | 76 |
| Figure 3. 31. Chronoabsorptimetry experiments for (a) P(TXT) and (b) P(EXE) film on ITO in 0.1 M $\text{TBAPF}_6/\text{ACN}$ while the polymer was switched with a switching time of 10 s. ....   | 78 |
| Figure 3. 32. Emission and absorbance spectrum of P(TXT) (a) in chloroform solution (b) in solid state (inset ; Emission spectrum of P(EXE) in different solutions). ....   | 80 |
| Figure 3. 33. Thermogram of (a) P(TXT) and (b) P(EXE). ....   | 81 |
| Figure 3. 34. Thermal gravimetric analysis of P(F8-SFX).....  | 83 |
| Figure 3. 35.. DSC analysis of P(F8-SFX).....   | 83 |
| Figure 3. 36. DPV of P(F8-SFX) measured in the solid state on a glassy carbon disk electrode in the medium of an electrolyte of 0.1 M ( $\text{TBAPF}_6$ ) in ACN at a scan rate of 100 $\text{mV s}^{-1}$ . ....   | 84 |
| Figure 3. 37. PL-spectra of polymer film in 1,2 DCB (15 mg/ml) after annealing (170°C) in ambient atmosphere and normal indoor light. ....  | 85 |
| Figure 3. 38. UV-vis absorption and PL spectra of P(F8-SFX) in $\text{CHCl}_3$ . ....   | 86 |
| Figure 3. 39. Optical characterization of P(F8-SFX) by applying different potentials between oxidized and neutral states with an inset of photographs. ....   | 87 |
| Figure 3. 40. Optical characterization of P(F8-SFX)/PEDOT electrochromic device by applying different potentials between oxidized and neutral states (Inset (a) the colors of oxidized and neutral states and (b) illustration of electrochromic device construction). ....   | 88 |
| Figure 3. 41. (a) Chronoabsorptimetry (b) chronocoloumetry and (c) current density experiments for P(F8-SFX) electrochromic device at $\lambda_{\text{max}}$ (562 nm) under an applied square voltage signal between -0.5 V and 2.0 V. (d) Electrochemical stability of P(F8-SFX)/PEDOT electrochromic device. ....   | 89 |
| Figure 3. 42. Behaviour of the single layer device.....   | 90 |
| Figure 3. 43. (a) Schematic illustration of ITO/PEDOT/F8-TFB/P(F8-SFX) /Ca(20 nm)/Al(100 nm) PLED device and its energy band diagram (b) Device performance and normalized ECL spectrum of the device ITO/PEDOT:PSS/CAV-2/ P(F8-SFX) /Ca-Al. (c)  |    |

|   |    |
|---|----|
| Electroluminescence spectrum of single layer device (black) and the device with thin CAV-2 layer. (d) Comparison of ECL spectrum P(F8-SFX) and CAV-2- P(F8-SFX).....  | 91 |
| Figure 4.1. The chemical structure of FCA and electrochromic performance of its polymer P(FCA) in the neutral and oxidized states. ....   | 96 |
| Figure 4.2. Emission (i) colors and (ii) spectrum of (a) P(PFP), (b) P(PQP) and (c) P(TXT) in the presence of in THF under handheld UV lamp. ....   | 95 |
| Figure 4.3. Electrochromic colors of the D-A-D type fluorene derivatives. ....  | 96 |
| Figure 4.4. An illustration of quinoxaline functionality over the metal cations when it acts a pendant unit over the polymer chain. Fluorescence intensity decreases upon successive addition of $\text{Fe}^{n+}$ ion due to energy transfer between $\text{Fe}^{n+}$ ions and Fluorene quinoxaline fluorophore ..... | 97 |

## LIST OF TABLES

### TABLES

|  |    |
|--|----|
| Table 3.1 Voltammetric and SPEL data for P(FCA) in 0.1 M TBABF <sub>4</sub> /nitromethane containing 4% BFEE. ....   | 47 |
| Table 3. 2 Optical and switching time data of electrochemically synthesized P(TFT), P(EFE), and P(PFP).....  | 58 |
| Table 3. 3. Optical and switching time data of electrochemically synthesized P(TQT), P(EQE), and P(PQP). ....  | 69 |
| Table 3. 4. Voltammetric and spectroelectrochemical data for PFX, P(TXT), and P(EXE), in 0.1M TBAPF <sub>6</sub> / ACN. S (soluble), PS (partially soluble). *The values were predicted with respect to reference 107 and ** $\Phi_f$ of P(TXT) (chemically prepared) were found from anthracene as standard in cyclohexane..... | 77 |
| Table 3. 5. Optical and switching time data of electrochemically synthesized P(TXT) and P(EXE). ....   | 79 |
| Table 3. 6. Comparison of the characteristics properties P(F8-SFX) with its analogues. ....  | 84 |
| Table 3. 7. Summary of optical properties of P(F8-SFX) .....   | 85 |
| Table 3. 8. Electronic and electrochromic properties of the P(F8-SFX) and its electrochromic device ( <sup>a</sup> CIE L x a x b system: luminance (L), hue (a) and saturation (b). <sup>b</sup> Redox states for PEDOT layer.) .....  | 88 |
| Table 4. 1. A summary of electrochemical and optical data for DAD type fluorene derivatives.. ....   | 98 |

## LIST OF SCHEMES

### SCHEMES

|  |    |
|--|----|
| Scheme 1.1. Chemical structure of P(FCA).....  | 26 |
| Scheme 1.2. Chemical Structures of D-A-D type polyfluorene derivatives, P(TFT), P(TQT), P(TXT), P(EFE), P(EQE), P(EXE), P(PFP) and P(PQP).....   | 27 |
| Scheme 1.3. The chemical structure of P(F8-SFX).....   | 27 |
| Scheme 2.1. Structure of D-A-D type monomers, TFT, EFE, PFP; TQT, EQE, PQP; TXT, EXE.....  | 32 |
| Scheme 2.2. Chemical structure of Tributyl (thiophen-2-yl) stannane (1), Tributyl (2, 3-dihydrothieno [3, 4- <i>b</i> ][1, 4] dioxin-7-yl)stannane (2), Tributyl-(3, 3-dihexyl-3, 4-dihydro-2H-thieno[3,4- <i>b</i> ][1,4]dioxepin-6-yl)-stannane (3). ....  | 32 |
| Scheme 2.3. Synthesis of 3,3-Dihexyl-3,4-dihydro-2H-thieno[3,4- <i>b</i> ][1,4]dioxepine (3). ....   | 34 |
| Scheme 2.4. Synthesis of 2,7-dibromo-9-fluorenone (4). ....  | 35 |
| Scheme 2.5. Synthesis route of 2,7-Di-thiophen-2-yl-fluoren-9-one (TFT) , 2,7-Bis-(2,3-dihydrothieno[3,4- <i>b</i> ][1,4]dioxin-5-yl)-fluoren-9-one (EFE), 2,7-Bis-(3,3-dihexyl-3,4-dihydro-2H-thieno[3,4- <i>b</i> ][1,4]dioxepin-6-yl)-fluoren-9-one (PFP). ....   | 36 |
| Scheme 2.6. Synthesis route of 2, 7-di(thiophen-2-yl)-5' <i>H</i> -spiro[fluorene-9,4'-pyrrolo[1,2- <i>a</i> ]quinoxaline] (TQT), 2,7-bis(2,3-dihydrothieno[3,4- <i>b</i> ][1,4]dioxin-5-yl)-5' <i>H</i> -spiro[fluorene-9,4'-pyrrolo[1,2- <i>a</i> ]quinoxaline] (EQE), 2,7-bis(3,3-dihexyl-3,4-dihydro-2H-thieno[3,4- <i>b</i> ][1,4]dioxepin-6-yl)-5' <i>H</i> -spiro[fluorene-9,4' pyrrolo[1,2- <i>a</i> ]quinoxaline] (PQP). .... | 37 |
| Scheme 2.7. Synthesis route of spiro[fluorene-9,9'-(2',7'-di- <i>n</i> -octyloxy)xanthene] (5) ; 2,7-Dibromospiro[fluorene-9,9'-(2',7'-di- <i>n</i> -octyloxy)xanthene] (6). ....  | 38 |
| Scheme 2.8. Synthesis route of 3',6'-bis(octyloxy)-2,7-di(thiophen-2-yl)spiro[fluorene-9,9'-xanthene] (TXT), 2,7-bis(2,3-dihydrothieno[3,4- <i>b</i> ][1,4]dioxin-5-yl) 3',6'-bis(octyloxy)spiro[fluorene-9,9'-xanthene] (EXE). ....   | 39 |
| Scheme 2.9. Reaction scheme of polymer synthesis, electrochemically. ....  | 40 |
| Scheme 2.10. Reaction scheme of P(FCA), electrochemically. ....  | 40 |
| Scheme 2.11. Synthesis of P(F8-SFX) by Suzuki–Miyaura coupling. ....   | 41 |
| Scheme 4. 1. Chemical structures of a series of new fluorene derivatives bearing different pendant units with different donor units.....   | 92 |

## ABBREVIATIONS

|         |                                     |
|---------|-------------------------------------|
| ACN     | Acetonitrile                        |
| A.U.    | Absorbance Unit                     |
| CB      | Conduction Band                     |
| CE      | Counter Electrode                   |
| CP      | Conducting Polymer                  |
| CV      | Cyclic Voltammetry                  |
| D-A-D   | Donor Acceptor Donor                |
| DCM     | Dichloromethane                     |
| DMF     | Dimethylformamide                   |
| DMSO    | Dimethylsulfoxide                   |
| DPV     | Differential Pulse Voltammetry      |
| DSC     | Differential Scanning Calorimetry   |
| EDOT    | Ethylenedioxythiophene              |
| FTIR    | Fourier Transform Infrared          |
| HOMO    | Highest Occupied Molecular Orbital  |
| ITO     | Indium Tin Oxide                    |
| LED     | Light Emitting Diode                |
| LUMO    | Lowest Unoccupied Molecular Orbital |
| NMR     | Nuclear Magnetic Resonance          |
| PEDOT   | Poly(3,4-ethylenedioxythiophene)    |
| PF      | Polyfluorene                        |
| Pro-DOT | Propylenedioxythiophene             |
| PTSA    | Para Toluene Sulphonic Acid         |
| RE      | Reference Electrode                 |
| SCE     | Saturated Calomel Electrode         |
| SPEL    | Spectroelectrochemical              |
| TGA     | Thermogravimetric Analysis          |
| THF     | Tetrahydrofuran                     |
| VB      | Valance Band                        |
| WE      | Working Electrode                   |

## CHAPTER 1

### INTRODUCTION

#### 1.1. A Brief Introduction to Conducting Polymers

The development of the synthetic polymers started in the 20<sup>th</sup> century and today, people have found many applications in nearly every industry and area of life such as; adhesives, lubricants as well as structural components for products ranging from children's toys to aircrafts. It was originally believed that all of the polymers were insulators and therefore polymeric materials were especially used in electronic industry with for insulation purposes. But, this general belief has been changed by three scientists, Alan MacDiarmid, Hideki Shirakawa and Alan Heeger in 1977. They have showed that polyacetylene could be made to conduct electricity upon exposure to iodine vapor [1, 2]. This event endowed a new door for polymer science.

In his Nobel Lecture [3], Heeger stated, "Conducting polymers offer the promise of achieving a new generation of polymers: Materials which exhibit the electrical and optical properties of metals or semiconductors, retain the attractive mechanical properties and processing advantages of polymers." These were the key words for organic conducting- and semiconducting-polymers, and have allowed them to find some applications such as electrochromic devices [4, 5], optical displays [6], smart windows [7, 8], mirrors [9, 10] and camouflage materials [11, 12] in which traditional metal or inorganic semiconductors cannot be used.

Recently, conducting polymers are used for the fabrication of various organic electronic devices such as light emitting diodes [13-16], photovoltaic cells [17-21], sensors [22-26], batteries [27-30], actuators (artificial muscles) [31,32] and similar devices which are applicable on numerous kinds of portable and stationary electronics.

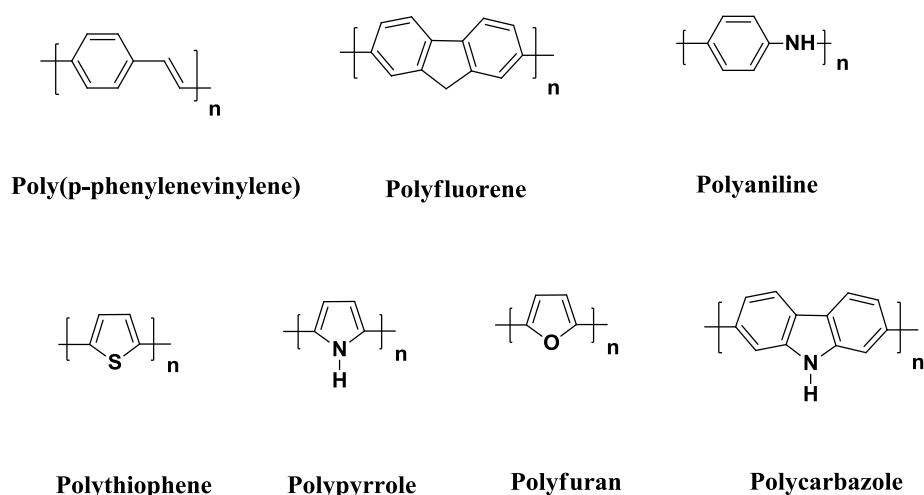


**Figure 1. 1.** Structures of some common aromatic conjugated polymers.

Polyacetylene, the first synthesized conjugated conducting polymer, has certain limitations such as improcessability and instability towards air oxidation in the doped state. Therefore, the research in

conducting polymers focuses on some popular aromatic polymers such as poly(*p*-phenylenevinylene), polyfluorene, polyaniline, polythiophene, polypyrrole, polyfuran, polycarbazole (**Figure 1.1**) and their derivatives. These aromatic polymeric materials are more stable than the non-aromatic polyacetylene. To date, a large number of conjugated polymers have been designed and characterized by many research groups. Furthermore, several of these conductive polymer types have been commercialized and are sold by a variety of polymer manufacturers.

In order to use the synthesized materials in the desired technological applications, some properties of the conducting polymers (i.e., stability, solubility, electronic and optical behaviors, etc.) should be controlled by the modification of the starting monomers [33].

## 1.2. Conductivity Mechanism of Conjugated Polymers

### 1.2.1. Structure and Conjugation

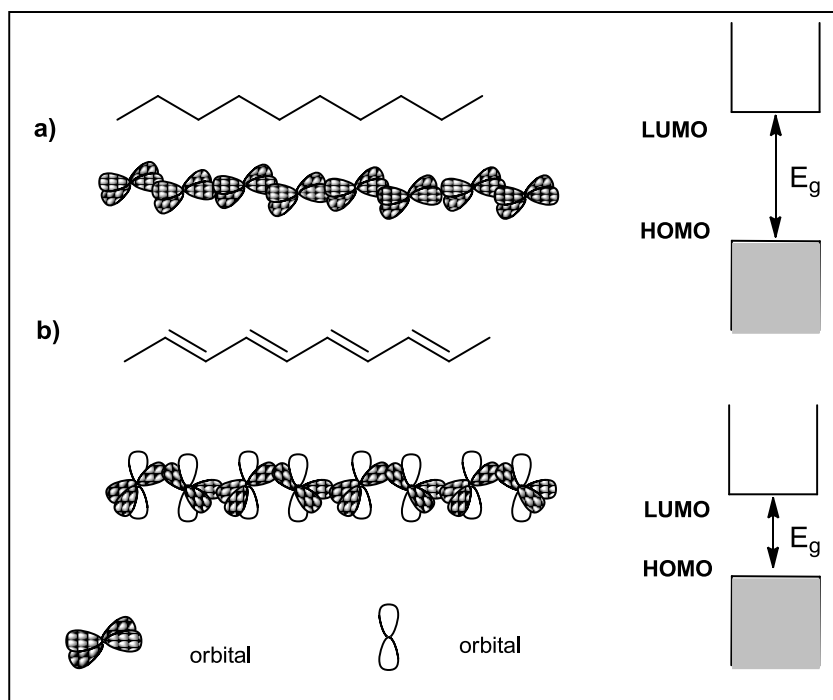


**Figure 1. 2.** A schematic illustration of the structure and atomic orbitals involved in the electronic structure (left) and the energy diagram (right) of a) polyethylene, b) trans polyacetylene.

The conjugated structure with alternating single and double bonds coupled with atoms providing p-orbitals for a continuous orbital overlap (e.g. N, S) is necessary for polymers to become intrinsically conducting. The highest occupied molecular orbital (HOMO) constitute the valence band (VB) and the lowest unoccupied molecular orbital (LUMO), the conduction band (CB). To make a polymer electronically conductive it is necessary to contain not only charge carriers but also an orbital system that allows the charge carriers to move through a continuous overlapping of  $\pi$ -orbitals along the polymer backbone [34]. The width of the forbidden band, or band gap ( $E_g$ ), between the VB and CB determines the electrical properties of the material. Therefore, similar to semiconductor materials, they can conduct electricity [35]. As shown in **Figure 1.2**, for



polyethylene each carbon atom forms four  $\sigma$  bonds with other atoms (2 carbon and 2 hydrogen atoms), whereas in the case of polyacetylene three  $\sigma$  bonds and one  $\pi$  bond are formed, resulting in alternating single and double bonds. The difference between HOMO and LUMO defines the band gap  $E_g$  of the neutral polymer chain [36].

### 1.2.2. Band Gap

The band gap generally refers to the energy difference between the top of VB and the bottom of CB. This is equivalent to the energy required to free an outer shell electron from its orbit about the nucleus to become a mobile charge carrier, able to move freely within the material. So the band gap is a major factor determining the electrical conductivity of a polymer. Substances with large band gaps are generally insulators, those with smaller band gaps are semiconductors, while conductors either have a very small band gap or none, due to the overlapping of VB and CB [37] (**Figure 1.3**).

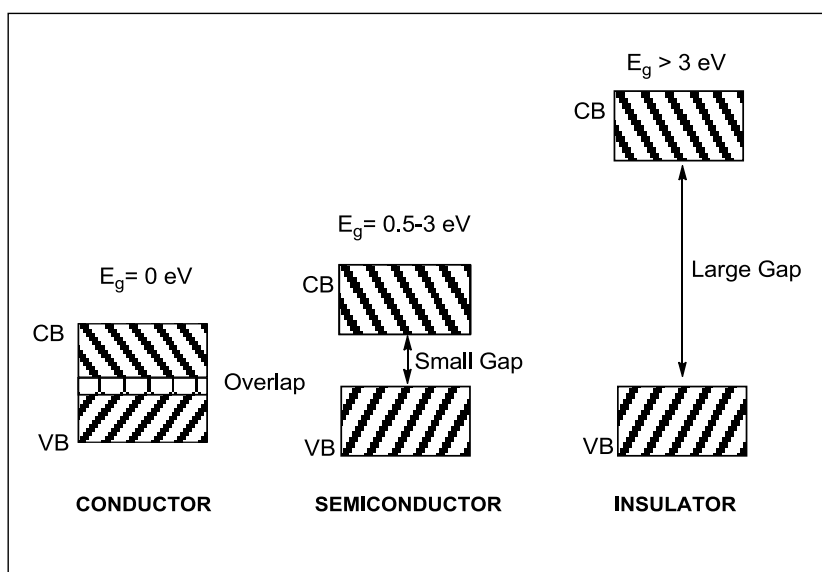


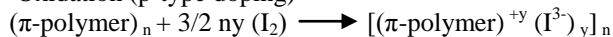
**Figure 1. 3.** Band structures in solids.

### 1.2.3. Doping Process

In general, conjugated polymers are insulators in their neutral state and become conducting upon oxidation or reduction. To increase the conductivity of the conjugated polymers, doping of these materials is necessary. Since the conjugated polymers don't possess intrinsic charge carriers, they can be provided by partial oxidation (p-doping) of the polymer chain with electron acceptors or by partial reduction (n-doping) with electron donors. CPs can be doped in two different ways; chemical and electrochemical doping.

Chemical doping involves charge-transfer redox chemistry:

(a) Oxidation (p-type doping)



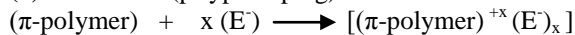
(b) Reduction (n-type doping)



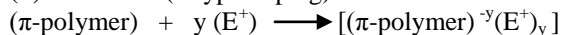
Although the chemical doping seems to be an efficient and easy process, the control of the process may cause incomplete doping in the system due to inhomogeneous intermediate structure. For that reason, electrochemical doping is mostly used to solve this problem [38].

Electrochemical doping is illustrated by the following examples:

(a) Oxidation (p-type doping)



(b) Reduction (n-type doping)



(E = electrolyte; E<sup>+</sup> cation, E<sup>-</sup> anion) (x and y; doping degree)

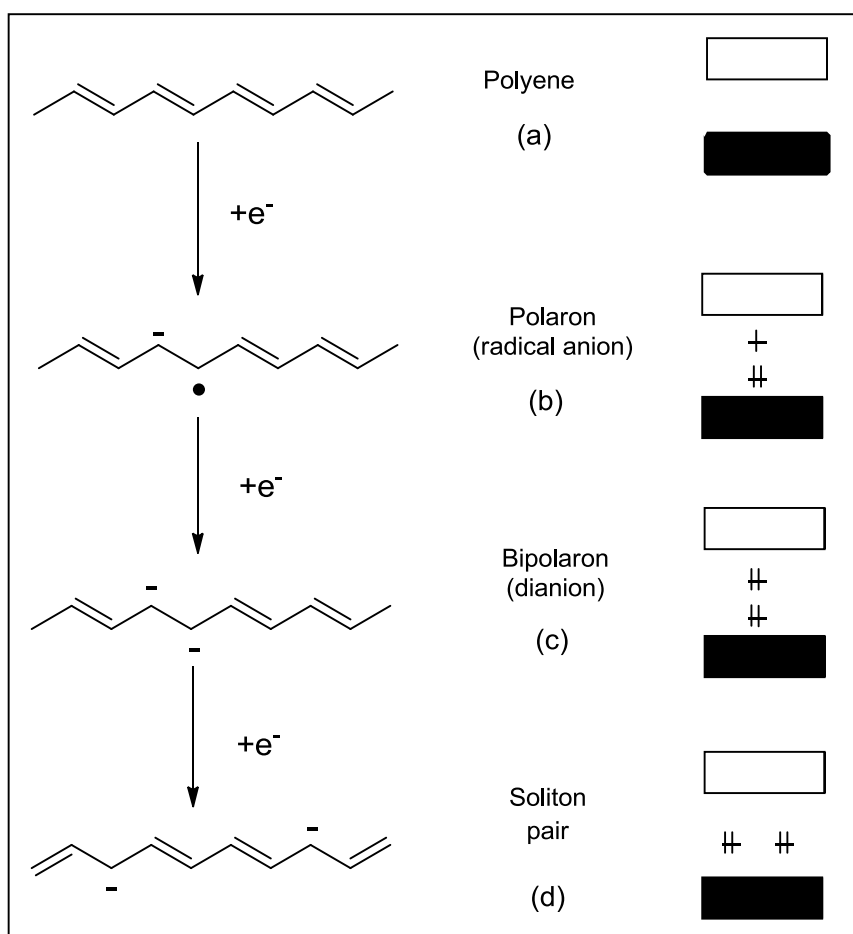


**Figure 1. 4.** A schematic description of the formation of (a) polyene, (b) polaron, and (c) bipolaron and (d) soliton pair on a trans-polyacetylene chain by doping.

The redox process is very simple for this doping type by adjusting appropriate potential in an electrochemical cell. The charge on the polymer chain is then neutralized by the counter ion from the electrolyte solution. During a doping process, charged defects, termed as polaron, bipolaron and solitons are formed (**Figure 1.4**).

As shown in **Figure 1.4a**, the polymer is in its neutral state before doping or oxidation/reduction process and called shortly as polyene. When an electron is added to the lower part of CB or removed from the top of the VB of a conjugated polymer, the CB becomes partially filled and a radical anion or cation, commonly called as a polaron. A polaron carries both spin (1/2) and charge (**Figure 1.4b**). Addition or removal of a second electron from the polymer chain which is already possessing a negative (positive) polaron forms a bipolaron through dimerization of two polarons (**Figure 1.4c**).

In conjugated polymers, like trans-polyacetylene with a degenerate ground state, the bipolarons can further lower their energy by dissociating into two spinless solitons (**Figure 1.4d**). However, solitons do not form in conjugated polymers with nondegenerate ground states, such as in polypyrrole, polythiophene, polyaniline and other popular conjugated polymers.

#### 1.2.4. Hopping Process

The overall mobility of charge carriers in conducting polymers depends on two components; intra-chain and inter-chain mobilities. In intra-chain mobility, the charge transfer occurs along the polymer chain. On the other hand, in inter-chain movement the charge jumps from one chain or crystalline to another by hopping or tunneling mechanism (**Figure 1.5**) [39].

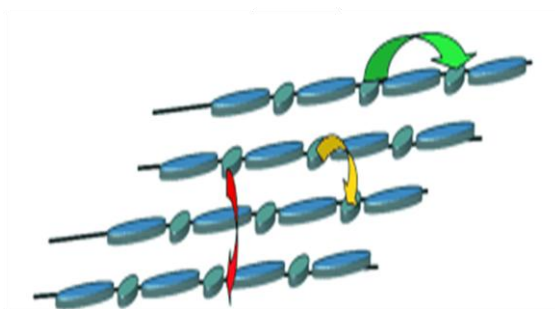
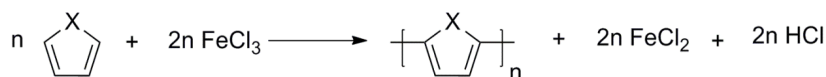


**Figure 1. 5.** Illustration of hopping mechanism

### 1.3. Synthesis of CPs

There are many ways to synthesize CPs, which includes chemical, electrochemical, photochemical, biocatalyzed, and solid-state synthesis, etc. The most popular and widely used techniques are chemical and electrochemical polymerization [40].

#### 1.3.1. Chemical Polymerization



where X= S, O, Se, N

(Equation 1. 1)

Chemical polymerization is the least expensive and most widely used method for the preparation of CPs. Chemical polymerizations are fulfilled by exposing the monomer to a two-electron stoichiometric amount of oxidizing agent, resulting in the formation of the polymer in its doped

and conducting state. In this type of polymerization strong chemical oxidants, such as ammonium peroxydisulfate ((NH<sub>4</sub>)<sub>2</sub>S<sub>2</sub>O<sub>8</sub>, APS), ferric ions, permanganate or bichromate anions, or hydrogen peroxide are utilized. In **Equation 1.1** oxidative polymerization with FeCl<sub>3</sub> of a five membered heterocyclic compound is shown [41].

Although chemical polymerization conditions can be easily scaled-up and yield large quantities of polymer, the process has some disadvantages that often result in poor quality polymers, such as limited degree of polymerization and overoxidation of the system [42-44].

### 1.3.2. Electrochemical Polymerization

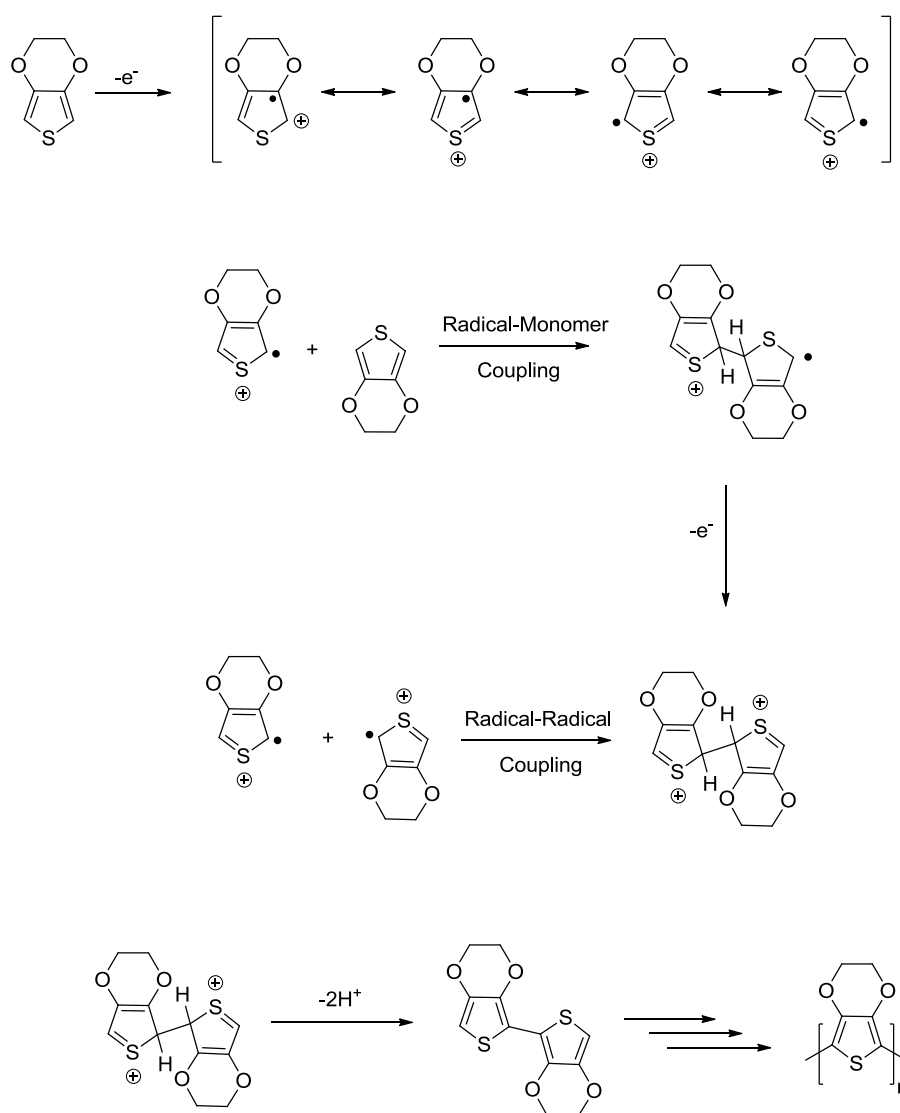


**Figure 1. 6.** Electrochemical polymerization mechanism of EDOT.

Electrochemical polymerization is also an easy and fast method which allowing the synthesis of the desired polymer on an electrode's surface in a proper electrolyte medium. Furthermore, rapid

characterization of conjugated polymers is also possible utilizing electroanalytical methods such as potentiostatic, or galvanostatic techniques. In electrochemical polymerization, a suitable potential (usually the oxidation potential of monomer) is applied to the working electrode which results in the formation of reactive radical cations due to the oxidation of monomer in the electrolytic medium. In **Figure 1.6** the mechanism for the electrochemical polymerization of 3,4-ethylenedioxythiophene (EDOT) is depicted. As seen from the figure, EDOT is converted to its radical cation by the removal of an electron under an applied electric field. This intermediate is stabilized by the ethylenedioxy group and either attack to a neutral monomer or may couple with another intermediate. Both of the routes yield an intermediate that produces the loss of two protons and then gives a dimer unit. Repeated coupling terminates in synthesis of the polymer [45].

#### 1.3.2.1. Electroanalytical Methods for Electropolymerization and Characterization of CPs

A large variety of electroanalytical methods can be applied to investigate the properties of CPs. The information obtained, for example, from oxidation/reduction potentials, electrochemical band gap, electrochemical stability, presents a deeper understanding of important physical properties of CPs. Among these methods, cyclic voltammetry (CV), Differential Pulse Voltammetry (DPV) and controlled potential coulometry have become increasingly favorite to study redox behaviour of a monomer or a polymer, because of their simplicity and versatility. Furthermore, CV reveals information regarding the stability of the product during multiple redox cycles.

Applied potential, solvent medium, supporting electrolyte, temperature and type of electrode are the most important factors affecting electrochemical polymerization.

##### Solvent choice

Solvents used for the electrochemical studies must have a high dielectric constant ( $\epsilon$ ) to be sure about the ionic conductivity of electrolytic medium and a good electrochemical resistance against decomposition at the potentials to oxidize the monomer. Furthermore, it is also essential that the solvent has a wide enough potential region for the study of the redox process of interest [46].

Acetonitrile (ACN) ( $\epsilon=37$ ) is one of the most frequently used solvent due to its inert electrochemical properties. It has +3.0 V anodic and -3.0 V cathodic limits vs. saturated calomel electrode (SCE).

The second choice of electrochemists is dichloromethane (DCM) ( $\epsilon=9$ ) for organic oxidation studies. It is stable up to + 3.0 V like ACN

Dimethylformamide (DMF) and dimethylsulfoxide (DMSO), which are aprotic solvents, have very good dissolving properties for ionic species. Although these solvents are good choice for reduction process (limit up to  $\sim -3.0$  V vs. SCE), the solvents decomposes in the potential regions above +1.0 V.

Water ( $\epsilon=80$ ) is the cheapest solvent and can form highly conductive solutions. It could get reduced or oxidized to  $H_2$  and  $O_2$  very easily. Furthermore, it can react so well with radicals. For that reason, it is not suitable for radical ion studies. In addition, some organic molecules are less soluble in water.

Other solvents such as propylene carbonate, ethanol, nitromethane and tetrahydrofuran (THF) are also among the most widely used organic solvents [47-49].

##### Supporting Electrolyte

All ionic salts or ionizable compounds in a solvent are called as supporting electrolyte. They must remain electroinactive in the potential region of interest. Solubility is a very important parameter for the selection of supporting electrolytes in the aprotic solvent medium. While  $LiClO_4$  is quite soluble in a few aprotic solvents,  $NaClO_4$  is less soluble. Tetraalkylammonium salts, on the other hand, possess high solubility in aprotic media and they are widely employed for this purpose.

Perchlorate ( $\text{ClO}_4^-$ ) ions are usually oxidized at about +1.6 V vs. SCE, tetrafluoroborate ( $\text{BF}_4^-$ ) and hexafluoro phosphate ( $\text{PF}_6^-$ ) are at least up to +3.0 V vs. SCE [50].

#### Working, Counter and Reference Electrodes

Voltammetric measurements are carried out using an electrochemical cell containing three electrodes immersed in a solution containing the analyte and the supporting electrolyte. One of three electrodes is working electrode (WE) at which the redox process of interest is taking place. It is generally made of platinum, gold, silver, glassy carbon, nickel, or palladium. For spectroelectrochemical measurements ITO coated glass electrode is also used.

The second electrode is reference electrode (RE). The requirement for the RE is that the potential should not change when the external potential is applied in the WE and RE system of the cell. Examples of commonly used reference electrodes are the normal hydrogen electrode, Ag/AgCl electrode and calomel electrode. The RE keeps the potential between itself and the WE constant. Potential measurements from different laboratories are often difficult to compare during usage of different reference electrodes. For that reason, a standard reference couple of known potential is used to check from time to time or corrected to a common scale. Ferrocene, which is most commonly used couple is reversibly oxidized to the ferrocenium ion at +0.48 V vs. Ag/Ag<sup>+</sup> in ACN. [51].

The third electrode is CE, which conducts electricity from the signal source through the solution to the other electrodes. It is wise to keep the surface area of the CE relatively larger than WE because the inaccuracies may occur due to the additional resistance imposed by CE. It should be made of electrochemically inert material such as platinum or graphite.

#### 1.3.2.1.1. Cyclic Voltammetry (CV)

**Figure 1.7** below shows a schematic of a CV cell and typical cyclic voltammogram. It has three different electrodes; WE, CE and RE. A cyclic voltammogram is obtained by measuring the current between WE and CE by applying constant potential. Therefore, the WE sets up its potential with respect to RE which has deposited on the electrode [52].

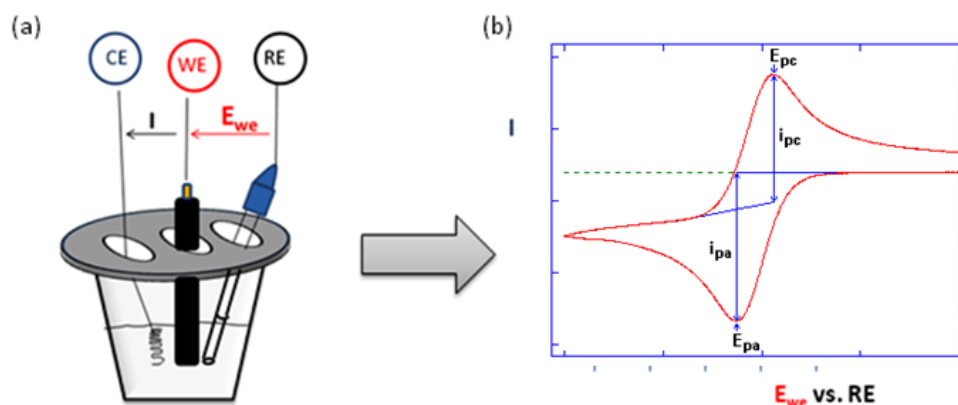


**Figure 1. 7.** (a) Illustration of an electrochemical cell used for electrochemical polymerization and (b) a typical cyclic voltammogram ( $E_{pc}$ = oxidation potential,  $E_{pa}$ = reduction potential,  $i_{pc}$ = oxidation current  $i_{pa}$ =reduction current).

#### 1.3.2.1.2. Differential Pulse Voltammetry (DPV)

DPV is another common electroanalytical technique, which is designed to minimize background charging currents. Measurements are taken at the end of each potential change during the

experiment. Current is given twice in each pulse period; before the pulse and at the end of the pulse. The difference between these two currents is plotted vs. the cell's staircase potential [54]. DPV is very important and an alternative way to CV during the characterization of electroactive polymer.

#### 1.3.2.1.3. Controlled Potential Coulometry

Controlled potential coulometry is one of the electrochemical methods, in which electroactive species are fully oxidized or reduced. Meanwhile the instrument measures and integrates the current. The total charge (Coulombs) passing through the system during the experiment allows the calculation of the number of electrons transferred in the electrochemical reaction [53].

### 1.4. Intrinsic Properties of CPs

#### 1.4.1. Band Gap

For many organic electronics such as LEDs (Light Emitting Diode), solar cells or electrochromic devices, the value of the band gap is very important, because it plays a role in the color of the emitted or absorbed light. According to the band model, the magnitude of the band gap is critical in determining the properties of the material. The presence of an energy gap of between 1 eV and 3 eV allows for the absorption and emission of photons in the visible wavelength range. Narrow band gap polymers are promising candidates for solar cells as well as n-type conductors and multicolor electrochromic polymers.

##### 1.4.1.1. Donor Acceptor Approach

One of the popular way to decrease the band gap of CPs is using donor-acceptor (D-A) approach. The concept of D-A approach means that a polymer with a delocalized  $\pi$ -electron system that involves alternating electron-rich (D) and electron-deficient (A) repeat units. The combination of high-lying HOMO levels and low-lying LUMO levels results in an overall narrow band gap for the polymer, as depicted in **Figure 1.8**. The magnitude of the polymer band gap can be controlled and narrowed on the basis of the choice of D and A units [54].

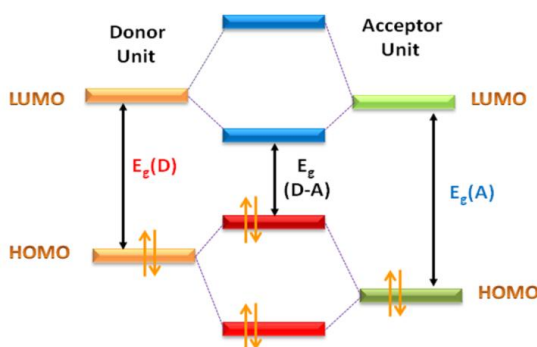


**Figure 1. 8.** Orbital interaction between D and A units lowers the band gap of CPs

##### 1.4.1.2. Measurement Methods of Band Gap

The band gap of CPs can be obtained using several techniques, such as electroanalytical methods (CV, DPV) and spectroelectrochemical methods.

#### 1.4.1.2.1. Electroanalytical Methods

Voltammetric measurements can be used to determine the oxidation (p-doping) and reduction peak (n-doping) potentials of the polymer. After the analysis of data obtained by CV and DPV measurements, the electronic band gap is obtained. Since an electron is taken from VB during the oxidation of polymer and an electron enters into CB during the reduction, oxidation potential ( $V_{ox}$ ) and reduction potential ( $V_{red}$ ) give information about the HOMO and LUMO energies, respectively. The energy gap (in electron volts) is simply the difference between the two potentials (onsets) multiplied the charge on the electron  $e=-1$  eV/V.

$$E \text{ (eV)} = e (V_{red} - V_{ox}) \quad \text{(Equation 1.6.)}$$

Although it seems that CV is a reliable method, recent studies show that oxidation or reduction peak onsets of the polymer sometimes changes depending on the scan rate [56]. DPV provides advantage over CV to determine same basic values for polymer films. First of all, the measurement with DPV is faster than CV over the same potential range. Second, it is very easy to determine the values of onset potentials for a polymer since for a reversible system; the peak potential is the same on the forward and reverse scans [56]. As shown in **Figure 1.9** and **1.10** the band gap values obtained from DPV and CV measurements are identical for the same polymer. The difference between the onset of oxidation and reduction potentials of the polymer is used to calculate the band gap.

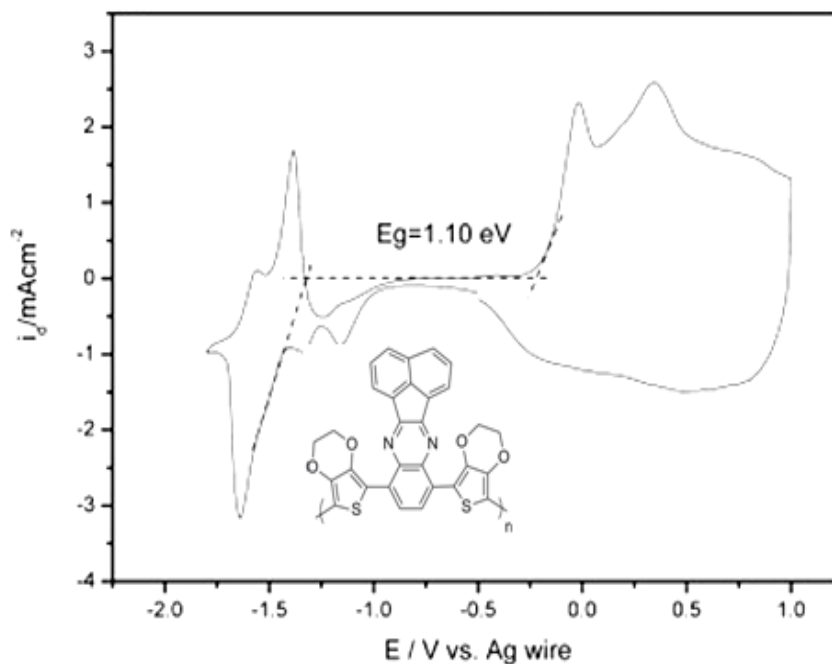


**Figure 1. 9.** Evaluation of the band gap value by using CV technique [55]



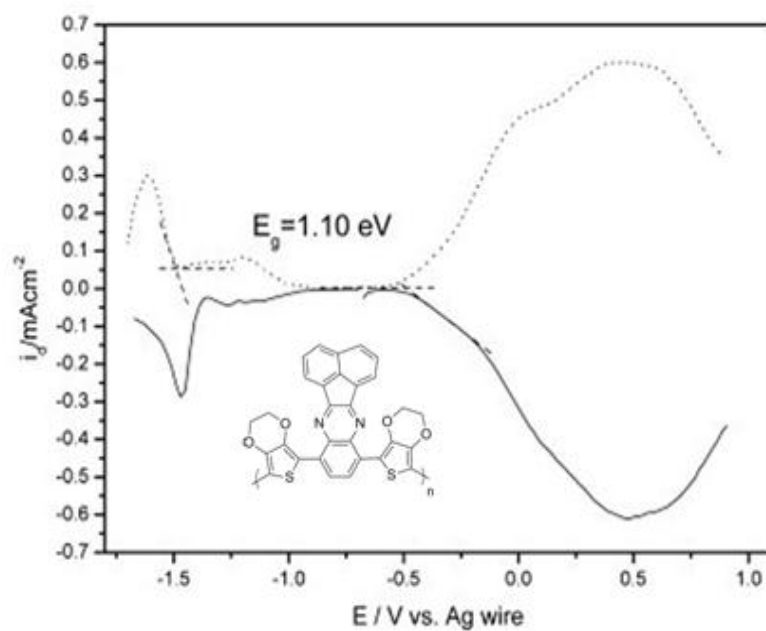


**Figure 1. 10.** Evaluation of the band gap value by using DPV technique [55].

Although the band gap of the polymer is the same, the calculations for HOMO and LUMO differ depending on the type of the techniques used. For both techniques, the onsets of the oxidation and reduction potential values are taken.

#### 1.4.1.2.2. Spectroelectrochemical Methods

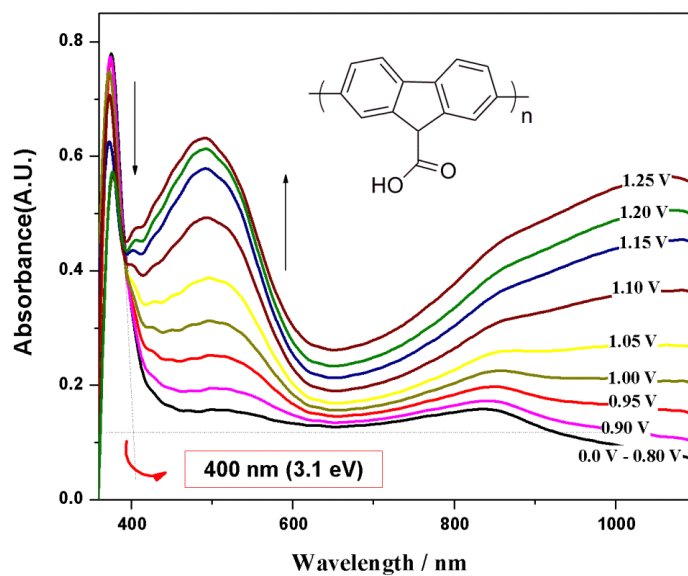


**Figure 1. 11.** Evaluation of the band gap value by using SPEL method [57].

Spectroelectrochemical (SPEL) measurements are conducted not only to evaluate the band gap values of the polymers but also to investigate their electrochromic behaviors. It is possible to determine the band gap by extrapolating the onset of  $\pi$  to  $\pi^*$  absorbance to the background. From the commencement on the low energy end of the  $\pi$ - $\pi^*$  transition band in the neutral state, the band gap value of 3.1 eV was found for poly(9-fluorene-2,7-dicarboxylic acid) **P(FCA)**, as shown in **Figure 1.11** [57]. In order to get reliable results, the polymer should be in its neutral form with no more shoulders except for  $\pi$ - $\pi^*$  transition.

#### 1.4.2. Electrochromism

Electrochromism is the reversible color change of a substance induced by external voltage. It is not necessary that the color change must be in the visible region. It can also transmit/reflect the light in the near-IR region.

Three classes of electrochromic materials (metal oxide films, molecular dyes and conducting polymers) are known. Among them CPs present additional advantages, such as, low processing cost, enhanced mechanical properties, no dependence with angle of vision, good UV stability high coloration efficiency, fast switching ability and fine-tuning of the band gap through the modification of polymer's chemical structure [58]. CPs can be divided into three groups depending on the color change. The first class is multicolored electrochromic polymers, which is represented by multicolored electrochromes including a bleached state or not. This kind of CPs and copolymers have multiple redox states. The second one is exhibiting at least one colored and one bleached state (anodically and cathodically coloring polymers). The third class polymers show two distinct colored states [59]. The examples of some electrochromic polymers are depicted in **Figure 1.12**.

In its neutral state, the color of CPs depends on the energy gap between HOMO and LUMO level. New charge carriers (polaron and bipolaron) upon oxidation determine the color of oxidized state. Color changes are also related with the movement of counter ions into and out of the matrix. New charged species enter this matrix and migrates through the film.

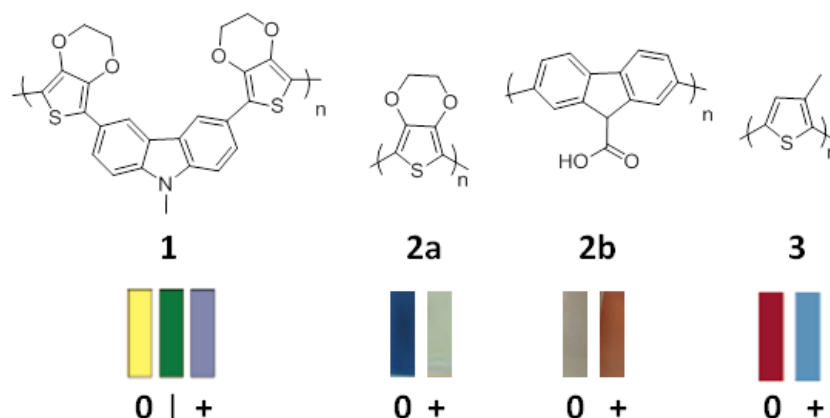


**Figure 1. 12.** Types of the electrochromic of CPs; (1) multielectrochromic typed [61], (2a) cathodically colored [60], (2b) anodically colored [58] and (3) two distinct colored polymer [62]. (0 = neutral state, 1 = intermediate state, + = oxidized state)

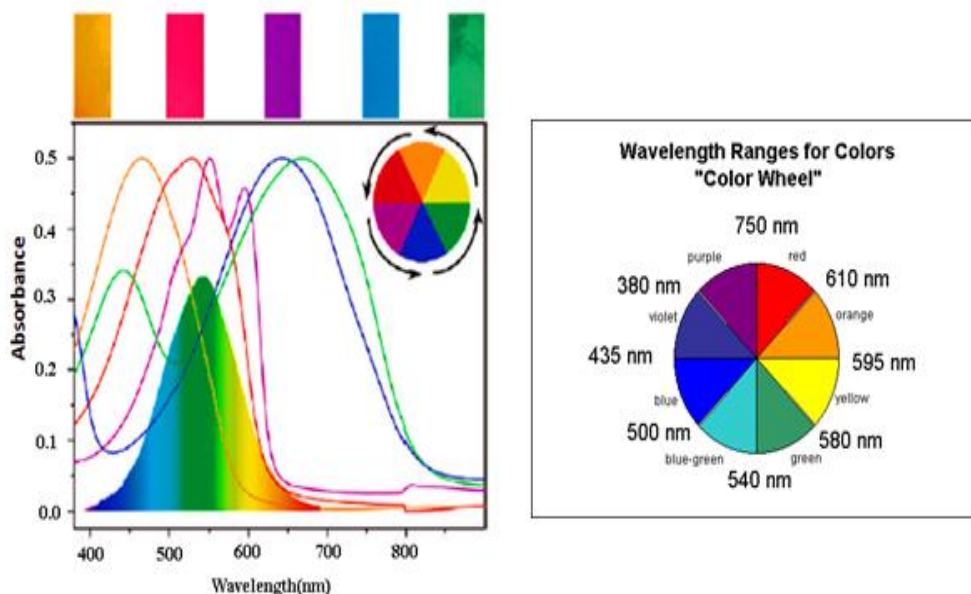


**Figure 1. 13.** The close relationship between the color of the polymer and its UV-vis absorption spectrum [63].

The interpretation and estimation of the polymer color are very important. For that reason, UV-vis spectrometry is used for the characterization of the polymer. There is a relationship between observed color and absorption spectrum of the material. The orange, red, purple, blue, and green colored conjugated polymers are shown in **Figure 1.13**. Each has a special maximum wavelength as shown in the graph depending on the wavelength range of complementary colors in the color wheel [62].

Colorimetry method is a method used to quantify and describe physically the human color perception. In this method, it is necessary to provide approximately a standard uniform color scale which could be used by everyone. Thus, the color of the materials can be compared with each other, safely. In colorimetry, there are three components; hue (dominant wavelength or chromatic color), saturation (chroma, intensity, or purity), and brightness (lightness or luminance). In 1976, The CIE (Commission Internationale de l'Eclairage) developed the CIELAB and CIELUV colour spaces ( $L^*a^*b^*$ ). It is mostly used by electrochemists to define the color or light transmission changes for electrochromic polymers when an external voltage is applied. The  $L^*$  character indicates lightness of the polymer color (0 = black, 100 = diffuse white).  $a^*$  and  $b^*$  letters give information about the red-green balance and yellow-blue balance, respectively.

Some parameters, such as optical contrast, coloration efficiency, switching time and stability are also important while describing the characteristics of an electrochromic polymer [63].

#### 1.4.2.1. Optical contrast

It is generally defined as a percent transmittance change ( $\Delta T$  %) at a given wavelength. Electrochromic contrast can be monitored and recorded upon application of square-wave potential steps (neutral to oxidation) to the electroactive film placed in front of the beam of a spectrophotometer [59]. The results obtained chronoabsorptometry and chronocoulometry experiments at the given wavelength for a polymer are obtained from **Figure 1.14**.

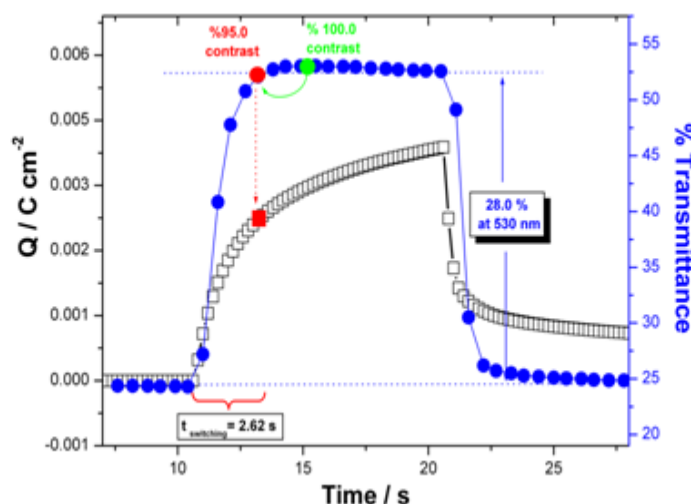


**Figure 1.14.** Chronoabsorptometry and chronocoulometry experiments for the polymer of 4-((2,5-dithiophen-2-yl)thiophen-3-yl)pyrrolo[1,2-a]quinoxaline at 530 nm in 0.1 M TBAPF<sub>6</sub>/DCM [64].

While the polymer film is switched between its neutral and oxidized states via electroanalytical methods, the chronoabsorptometry results are also monitored in-situ. Therefore, optical contrast can be found using **Equation 1.7**.

$$\Delta\%T = (\%T_{\text{bleached}} - \%T_{\text{colored}}) \quad (\text{Equation 1.7})$$

#### 1.4.2.2. Switching Time

Switching rate is also an important parameter and can be defined as the time needed for an electrochrome to switch from one redox state to the other. This parameter mostly depends on the ability of the electrolyte to conduct ions and the ease of diffusion of the counterbalancing ionic species across polymer chain, the thickness and morphology of the obtained polymer film. Since human eye can perceive 95 % of the full contrast; switching time is calculated by taking this fact into consideration.

#### 1.4.2.3. Coloration Efficiency ( $\eta$ )

Coloration efficiency value ( $\eta$ ) can be defined as total optical density change ( $\Delta OD$ ) for a polymer per density of injected or ejected charge ( $Q_d$ ) during its redox process. It is necessary to make chronoabsorptometry and chronocoulometry experiments at the same time to find these parameters as shown in **Figure 1.14**. The amount of charge ( $Q_d$ ) is also necessary to produce the optical change between colored ( $T_{\text{colored}}$ ) and bleached states ( $T_{\text{bleached}}$ ). The equations below are used to calculate  $\eta$  [60].

$$\eta = \Delta OD / Q_d = \log (T_{\text{bleached}} / T_{\text{colored}}) / Q_d \quad (\text{Equation 1.8})$$

#### 1.4.3. Fluorescence

Fluorophore is a molecule that is capable of fluorescence. Most of CPs with this important property can be used in many applications such as PLEDs, sensors and solar cells. The fluorescent property of a molecule is summarized in **Figure 1.15**.

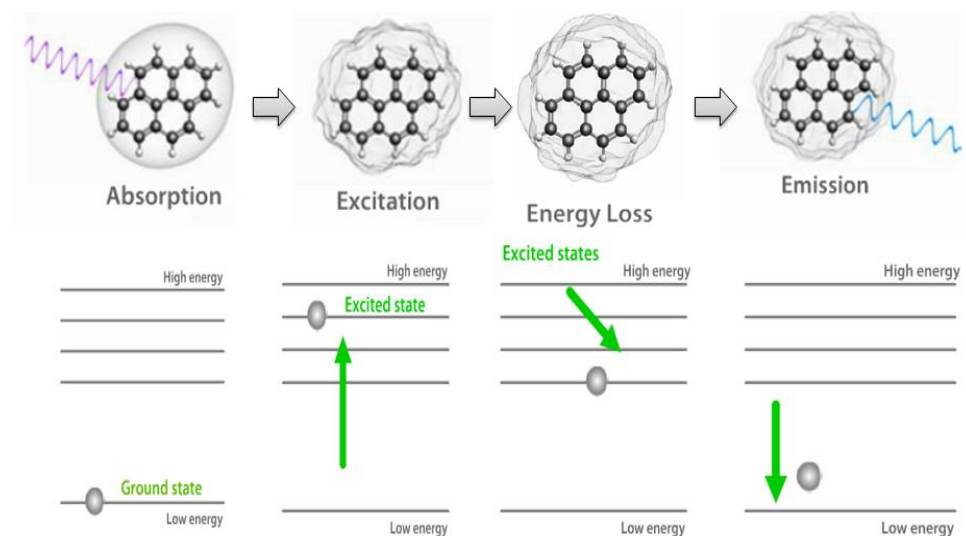


**Figure 1. 15.** The schematic illustration of the fluorescence property in a molecule.

In the ground state, fluorophore is in its relatively low energy and a stable configuration and is not fluorescent. When a light from external source hits the fluorophore, the molecule can absorb the light energy. When the energy is sufficient, the molecule reaches a higher energy state as called excited state. This process is known as excitation. There are a lot of excited states, which fluorophore can obtain depending on the wavelength of the energy of external light source. Since the fluorophore is unstable in high energy configuration, it eventually adopts the lower energy excited state, which is semistable. The length of time the fluorophore in excited states is called as excited life time which is in the range of  $10^{-15}$  to  $10^{-9}$  seconds. Next, the fluorophore rearranges from semistable excited state to the ground state relieving the excess energy in the form of emitted light.

#### 1.4.3.1. Quantum Yield ( $\Phi_F$ )

The efficiency of the fluorescence process can be calculated by the quantum yield. The quantum yield sometimes differ from one author to another for even identical experiments, which makes some people unwilling to consider fluorescence spectroscopy as a reliable quantitative tool. Quantum yield is defined as the ratio of the number of emitted photons to the number of absorbed photons per time unit. Calculation of  $\Phi_F$  is usually done by using relative materials with fluorophore property. Following equation is used for that purpose.

$$\phi_{F,x} = \left( \frac{A_s}{A_x} \right) \times \left( \frac{F_x}{F_s} \right) \times \left( \frac{n_x^2}{n_s^2} \right) \times \phi_{F,s} \quad \text{(Equation 1.9.)}$$

,where  $\Phi_F$  is the fluorescence quantum yield, A is the absorbance at the excitation wavelength, F is the area under the corrected emission curve, and  $n$  is the refractive index of the solvents used. The letters s and x refer to the standard and unknown, respectively. There are some rules during measurements and choosing the reference chemicals.

#### Choice of Standard

It is advantageous,

- to choose a standard with absorption and emission bands close to those of the unknown
- to excite both compounds at the same wavelength [65].

#### Absorbance measurement

During fluorescence measurements, absorbance intensity must be between 0.05 and 0.04. If absorbance is above 0.05, the emission intensity can no longer be assumed proportional to the concentration of the analyte. On the other side, if the absorbance is too low, impurities from the medium may become important with respect to the amount of analyte [66].

#### 1.4.4. Electroluminescence

Electroluminescence is an optical phenomenon defined as the generation of light by the application of an electric field. Electroluminescence results in the formation of light, which the excited electrons release as photons due to the radiative recombination of electrons and holes in a material (usually a semiconductor). Many semiconducting materials, including CPs are used in luminescent applications (light emitting diodes) due to the variety of their colors and broad energy range characterizing the radiation emitted by electroluminescent devices today.

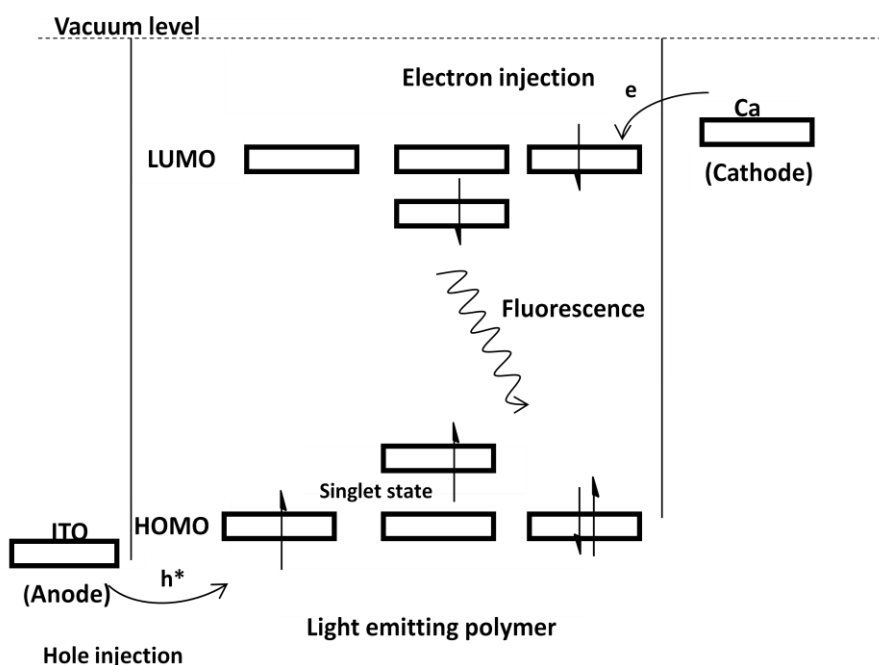


**Figure 1. 16.** Illustration of electroluminescence (EL) in a conjugated polymer material.

In electroluminescence as seen in **Figure 1.16**, the injection of the holes is formed at the ITO anode. The electrons are removed from HOMO level and give positive charged carriers. Radical anions are also formed at the calcium cathode where electrons are injected. The new charged species migrate from the polymer chain by hopping process when applied to the electric field. As a result of the combination of two opposite charges the excitons (singlet and triplet excited states) are formed. The color of the emission is dependent on the size of HOMO-LUMO energy gap (visible light (380-780 nm)) [67].

## 1.5. Polyfluorenes

### 1.5.1. Chemical Structure

Polyfluorenes are one of the rigid-rod polymers. The monomer, fluorene is composed of rigid planar biphenyl units, bridged by a carbon atom in position 9, which provides a high degree of conjugation (**Figure 1.17**). Fluorene received its name due to strong violet fluorescence which arises from highly conjugated planar p-electron system. The methylene bridge (C9 position) in fluorene structure offers an opportunity to modify the processability or functionality of the polymer by substituents. For instance, replacement of labile H atom at C-9 position of fluorenes with alkyl groups improves the solubility of polyfluorenes [68].

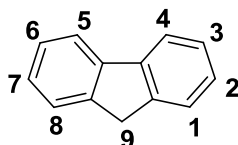


**Figure 1. 17.** Chemical structure of fluorene

Furthermore, the 2 and 7 positions in fluorene structure, which are the most reactive sites towards electrophilic attack, provides construction of a fully conjugated rigid-rod polymer chain by substitution reactions. Many electron donor or acceptor groups are introduced along this backbone to form an alternative copolymer to tune the band-gap or electronic properties and to enhance stabilities [69-72].

### 1.5.2. Synthesis of Polyfluorenes

#### 1.5.2.1. Synthesis of PFs via chemical approaches

The earliest report about the synthesis of soluble polyfluorenes was in 1989 by Yoshino et al. They synthesized poly(9,9-dihexylfluorene) oxidatively using  $\text{FeCl}_3$ . However, product was a low molar mass polymer ( $M_n$  of 5000 g/mol) with imperfect regioselectivity, which is due to some defects in the desired 2,7-linkage of polyfluorene [73]. The synthesis is outlined in **Figure 1.18**.

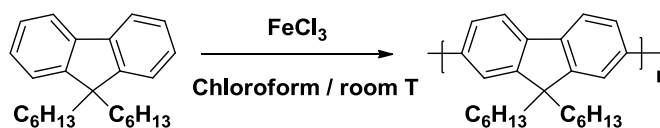


**Figure 1. 18.** Oxidative synthesis of poly[(9,9'-dihexyl)-2,7-fluorene].

After this attempt, to synthesize higher molecular weighted polymers, the transition metal catalyzed aryl-aryl couplings were used, as shown in **Figure 1.19**.  $\text{Ni}(\text{COD})_2$  (Bis(1,5-cyclooctadiene)nickel(0)) is used most of the time for this kind of polymer synthesis. Higher molecular weight polymer (200000 g/mol) was obtained by the Yamamoto coupling [74]. The disadvantage of this coupling method is that polymers with a degree of polymerization greater than 50 are difficult to obtain due to low solubility in the highly polar aprotic reaction medium [75].

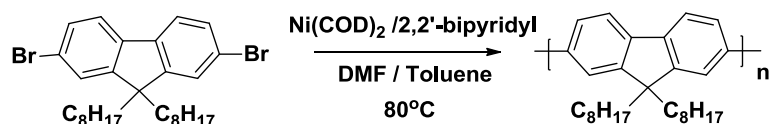


**Figure 1. 19.** Synthesis of 9,9'-dialkylated polyfluorene via Yamamoto coupling.

A high grade method is based on the palladium-catalyzed reaction of mixed phenylboronic acids and arylbromides to give biphenyls. By using this method (**Figure 1.20**), polymers with molecular weights ranging from 10000 to 500000 g/mol and are generated with high yields.[76].

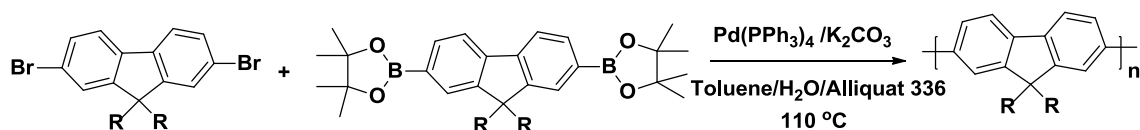


**Figure 1. 20.** Synthesis of 9,9'-dialkylated polyfluorene via Suzuki cross coupling.

### 1.5.2.2. Synthesis of PFs via electrochemical oxidation

#### 1.5.2.2.1. Fluorene Homopolymers

Many homo-polyfluorene derivatives with good redox activity and stability were successfully achieved via electrochemical polymerization when their proper medium was found for electropolymerization, such as alkyl chains **7** [77], amino **8**, **9** [78-79], halogen **10,11** [80, 81] carboxyl **4**, **5**, **6** [57, 83-84] and carbonyl groups **2** [85-86], as depicted in **Figure 1.21**. It has been found that the incorporation of suitable functional groups at C9 position of fluorene monomer tunes the optoelectronic properties of corresponding CPs. All this kind of polymers shows electrochromic behaviors with high coloration efficiency values.

For electropolymerization of fluorene derivatives, the choice of the polymerization medium is very important. While some researchers [88-89] reported the impossibility of obtaining polyfluorenone (**PFO**) by oxidative coupling in ACN and synthesized **PFO** via different methods, the electropolymerization was succeeded in DCM using TBABF<sub>4</sub> as supporting electrolyte[86, 87]. After this information, it is also found that the low-potential electropolymerization of polyfluorene derivatives in boron trifluoride diethyl etherate (BFEE) led to facile electrodeposition of high quality polymeric films on the electrode surface [81].



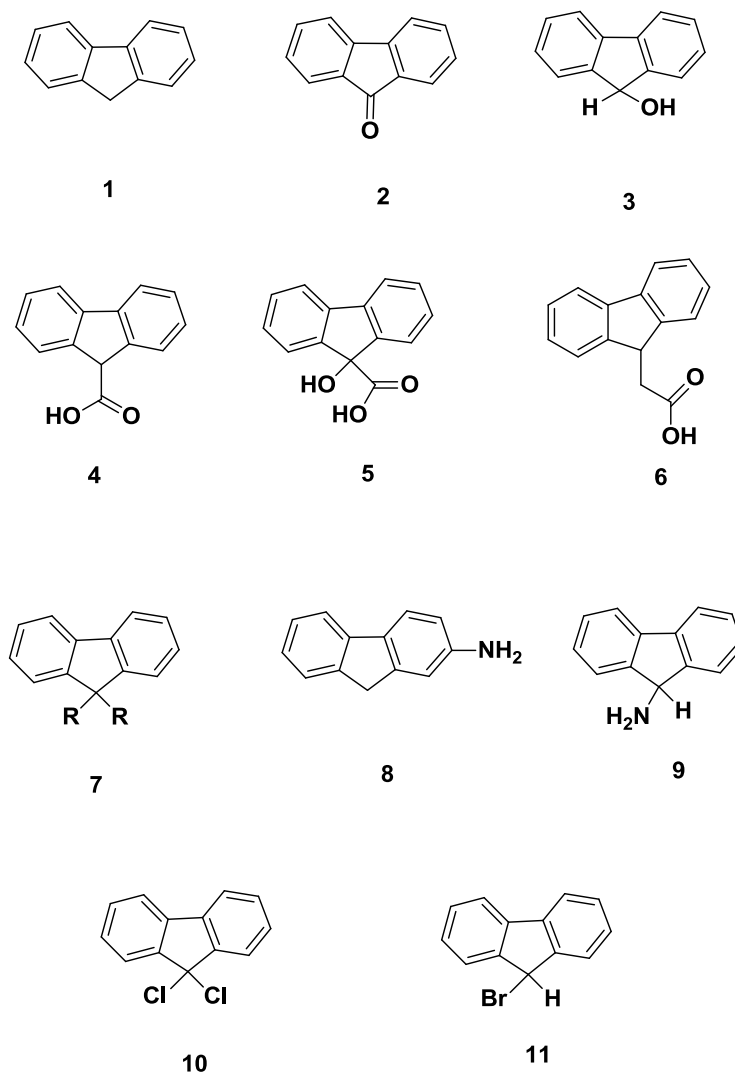


**Figure 1. 21.** Previously reported fluorene derivatives polymerized via electrochemical polymerization [77-86].

#### 1.5.2.2.2. Alternating Donor Acceptor Type Polyfluorene Derivatives

Since an alternating sequence of D–A units along the polymer chain reduces the band gap, interest in the preparation of such copolymers increased and more recently various D–A type copolymers based on fluorene were reported [70-72, 90-94]. Thiophene, furan, EDOT and pyrrole are the examples of most popular donor groups used for this kind of applications (**Figure 1.22.**).

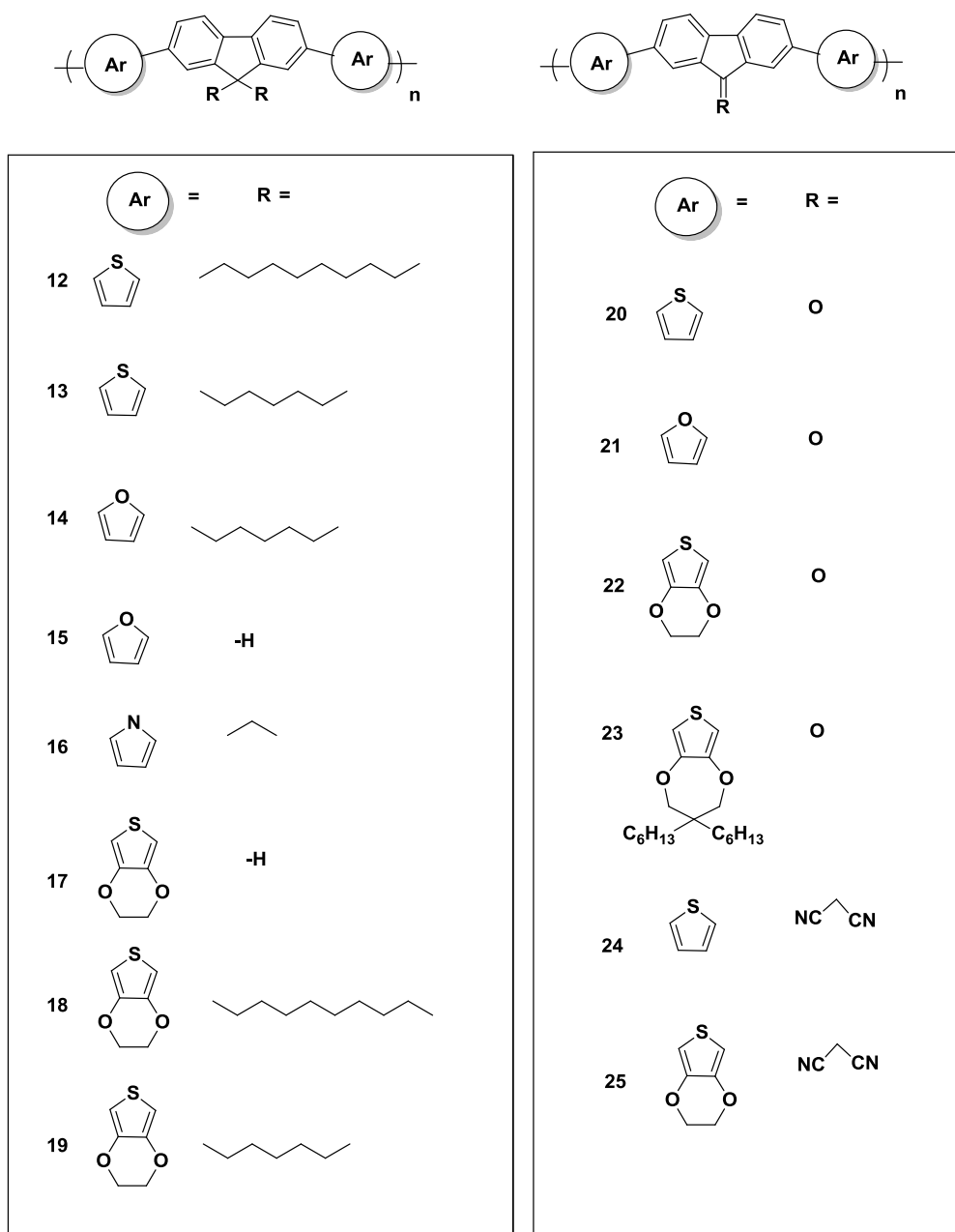


**Figure 1. 22.** Previously reported hybrid fluorene derivatives polymerized-via electrochemical polymerization **12** [70]; **13**, **19** [89]; **14**, **15**, **21** [90]; **16**, **18** [69]; **17** [71]; **20**, **24**, **25** [91]; **22** [92]; **23** [93].

### 1.5.2.3. Functionalization of Polyfluorene Derivatives at C9 position

Polyfluorenes, which are mostly used in LEDs, have suffered from an unwanted green emission band (535 nm) along with the desired blue emission. The origin of the green emission was believed to be due to the intermolecular excimer formation between polyfluorene chains. Fluorenone is believed to be formed after fabrication of the devices. The certain mechanism of the fluorenone formation is not known but it is supposed that monoalkylated fluorene units are formed as impurity in poly(dialkylfluorenes), which are the sites sensitive to oxidation, as depicted in **Figure 1.23**. [94].

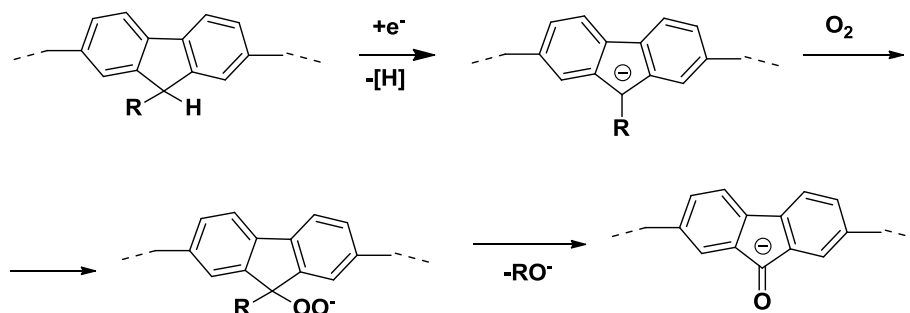


**Figure 1. 23.** The mechanism for the generation of keto-defect sites in PFs [94].

Polyfluorene at the methylene bridge can be functionalized without distorting the conjugation between monomer units. This is widely used to control the undesirable green emission and to modify charge injection and mobility in the emissive layer. Furthermore, by using bulky pendant groups the thermal properties of the polymers can be improved [95-98]. To circumvent all these obstacles, a tremendous amount of research has been presented both to reduce the formation of excimer or keto defects and to enhance the color stability of PFs. These approaches are;

- The introduction of low band gap chromophores at the end and or middle of the polymer chain [99].
- End-capping with cross linkable moieties or hole trapping groups [100, 101].
- Kinking the backbone structure [102].
- Encapsulating the polymer backbone within bulky/dendrimer bulky side chains [103-105].
- Incorporating siloxane bridges or polyhedral oligomeric silsesquioxane units [96,106].
- The introduction of spiro structures [104].

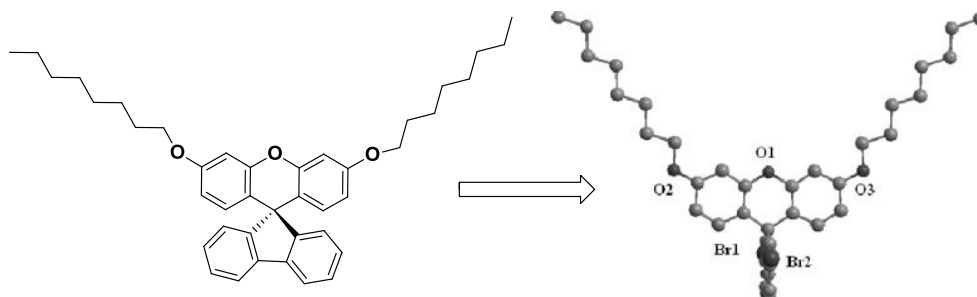


**Figure 1. 24.** Chemical structure and 3-D image of spirofluorene [108].

One of the most promising ways to overcome these problems is to introduce spiro structures at the bridge position of fluorene (i.e. C-9 position), which provides the control of the polymer solubility, interchain interactions in the film state, while also offering the ability to tune the optical properties of the PF derivatives [107]. One of the examples for spirofluorene structure is seen in **Figure 1.24**.

While most of the functionalized polyfluorenes have been used for their characteristic blue light emission in the application of LEDs, the facile functionalization of C9 position of fluorene unit

provides the opportunity to improve solubility in common solvents, and processability for some applications, such as fluorometric detection and biosensors, etc.

### 1.5.2.3. Fluorene Copolymers

Copolymerization of fluorene derivatives with different aromatic units presents color tuning through modification of the band gap. Copolymers consisting of 9,9-substituted fluorenes are mostly used for solar cell, LED and biosensor applications. (**Figure 1. 25**) [107-110].

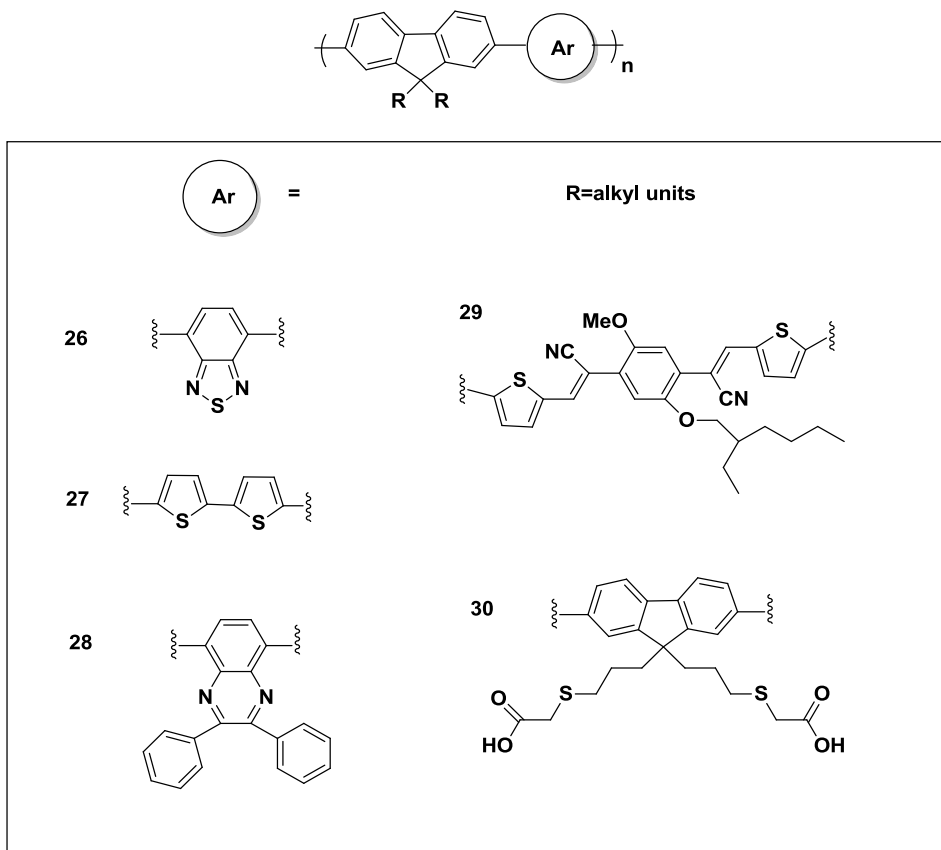


**Figure 1. 25.** Examples of fluorene copolymers used in various applications [107-110].

## 1.5.3. Some Selected Applications of PF Derivatives

### 1.5.3.1. Electrochromic Devices

Electrochromic devices are mostly used in displays and military interests for absorbers, depending on the consumer interests. They also took place in commercial applications such as electrochromic mirrors in cars and eventually in dial-tint windows for residential and business uses. Most of the CPs including PFs and their derivatives, present faster switching times and can be modified to provide different colors based on research in band gap modification [111]. **Figure 1.26** shows an illustration of a typical electrochromic device to test its performance. For this device, electroactive, transparent electrodes (ITO) are used. Two different complementary CPs are coated onto each electrode and then the device was constructed using the electrochromic electrodes stacked face-to-face separated by a gel electrolyte.

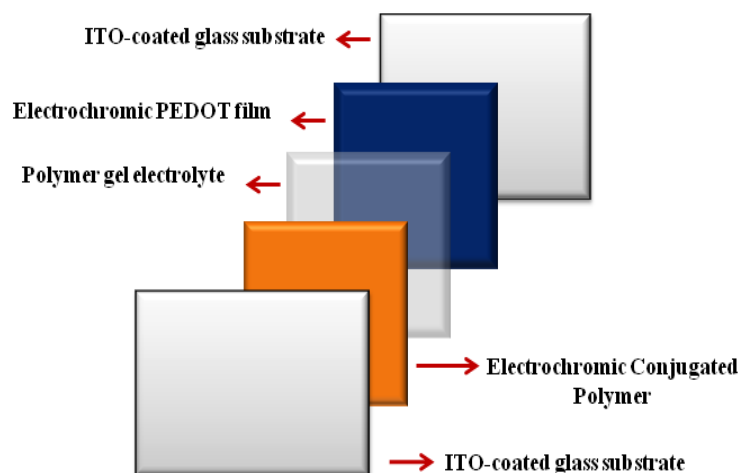


**Figure 1. 26.** A typical electrochromic device construction of a conjugated polymer.

### 1.5.3.2. Fluorometric Detection

CPs is important due to the sensitivity towards heavy metal ions, organic vapors, and explosives through fluorescence quenching via Stern-Volmer behavior. The classical sensing methods such as atomic absorption spectrometry, anodic stripping voltammetry and X-ray fluorescence spectrometry are expensive methods for this kind of application [112]. For that reason, fluorescence quenching of CPs in the presence of an analyte is an inexpensive method for the sensing of chemicals.

Fluorescence quenching comprises the fluorophore and the quencher. While, a fluorophore chemical emits fluorescence, when excited, a quencher reduces the fluorescence of a fluorophore. The quantitative analysis of fluorescence quenching achieved utilizing with the Stern-Volmer equation.

$$I_0/I = 1 + K_{SV} [Q] \quad \text{(Equation 1.10)}$$

,where

- $I_0$  = the measured fluorescence intensity without quencher present
- $I$  = the measured fluorescence intensity with quencher present
- $K_{SV}$  = the Stern-Volmer constant
- $[Q]$  = the quencher concentration

The Stern-Volmer constant,  $K_{SV}$ , can be obtained from the slope of  $I_0 / I$  vs.  $[Q]$  plot. A higher value for the slope corresponds to higher sensitivity towards the target [113].

The usage of fluorene-based CPs as a fluorescent sensor is becoming the highly attractive because of high fluorescent quantum yields and the suitable ligands which have ability to coordinate with the desired ions. These properties make the fluorene derivatives suitable in detection of biologically and environmentally important metal ions and at high detection limit [114-120]. As seen in **Figure 1.27**, an example of polyfluorene derivative, substituted with thioglycolic acid groups from C9 position, is a promising candidate as a metal ion sensor with a remarkably high fluorescent quenching efficiency and an ability to detect  $Fe^{3+}$  ions selectively in organic solvents [110].

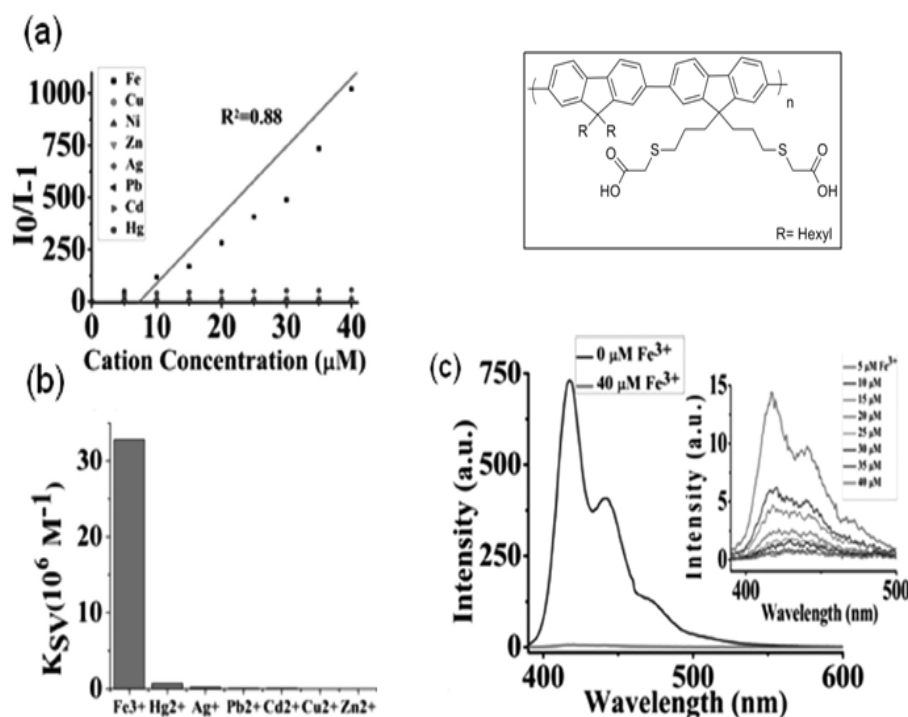


**Figure 1. 27.** (a) The Stern–Volmer plots of polyfluorene derivative in the presence of various metal ions (each 5–40 mM). Metal ion solutions were prepared from  $\text{Fe}(\text{NO}_3)_3 \cdot 9\text{H}_2\text{O}$ ,  $\text{Cu}(\text{NO}_3)_2 \cdot 3\text{H}_2\text{O}$ ,  $\text{Ni}(\text{NO}_3)_2 \cdot 6\text{H}_2\text{O}$ ,  $\text{Zn}(\text{NO}_3)_2 \cdot 6\text{H}_2\text{O}$ ,  $\text{AgNO}_3$ ,  $\text{Hg}(\text{NO}_3)_2$ ,  $\text{Pb}(\text{NO}_3)_2$ ,  $\text{Cd}(\text{NO}_3)_2 \cdot 4\text{H}_2\text{O}$  in THF, (b)  $K_{sv}$  values, (c) the fluorescence emission spectra of polyfluorene derivative with successive addition of 5–40 mM  $\text{Fe}^{3+}$  aqueous solution [110].

### 1.5.3.3. PLEDs (Polymer Light Emitting Diodes)

PLEDs convert electrical power into visible light. This is mostly related to the fluorescence of polymers where UV light is converted into visible light. The construction of PLEDs is illustrated in **Figure 1.28**. A PLED device is a sandwiched system containing mainly three parts, an anode, a cathode and a conducting material. A transparent electrode with a high work function (ITO) is mostly selected as the anode. The conjugated polymer is chosen as a conducting material, a layer of PLED material. For cathodic material, a low work function material is preferred. When the current is applied, electrons and holes are injected at each electrode and then they combine to produce light. Depending on the device performance, it can be optimized with different layers between the electrodes. After discovery of the PLEDs many researchers make new CPs emitting different colors from violet to red. Among them, PFs possess a high band gap range. It means that PFs are the only family of CPs, which can emit the entire visible light with high efficiency. Furthermore, the device constructed using PFs requires low operating voltage during PLEDs performance [121].

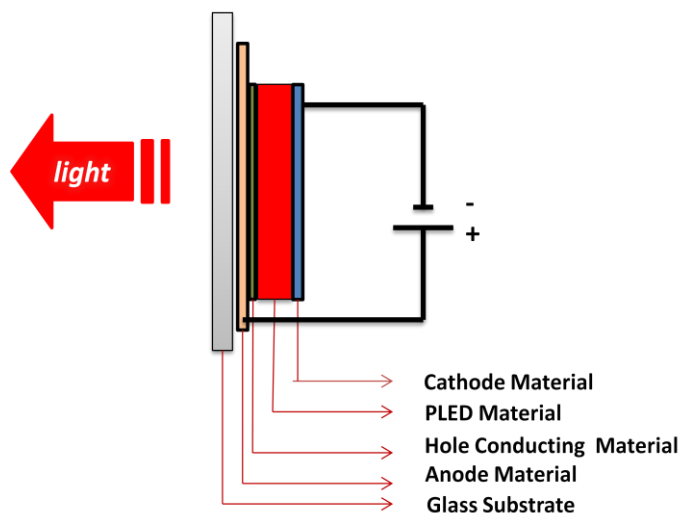


**Figure 1. 28.** The schematic structure of a PLED device.

Since, PFs have high band gap, it is possible to obtain different colors by tuning the band gap by incorporating comonomers into fluorene main chain backbone. For example, the green light can be obtained by coupling a thiophene monomer with fluorene monomer. Stability of the colors is mainly important. The characteristic blue color emission of PFs is still under investigation as mentioned before.

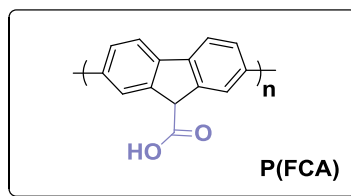
#### 1.6. Aim of This Study

This work, presents the synthesis and characterization of CPs based on fluorene derivatives with an intention to use them for various applications. The goal of this research is to develop new synthetic routes and methods towards fluorene based polymers, as well as to assess and compare the optical and electrical properties of the resulting material. As mentioned before, the thesis contains three different parts.

##### First Part:

It is well known that PFs possessing specific properties are interesting due to their applications in organic electronics. Polyfluorenes were mainly synthesized either by chemical approaches via Suzuki, Yamamoto and Stille reactions [122, 123] or by electrochemical oxidations [88, 124–127]. In electrochemical polymerization various solvents were applied for different fluorene derivatives. Recently, Xu and his/her coworkers reported that quality of polyfluorene films can be improved using boron trifluoride diethyl etherate (BFEE) as solvent and supporting electrolyte due to its catalytic effect since it is not easy to electropolymerize most of the fluorene derivatives in commonly used solvent electrolyte media [83,84]. 9-fluorene-carboxylic acid (**FCA**), which is functionalized from C9 position of the fluorene, is one of the kinds of polyfluorene derivatives, which can not be electropolymerized in common solvent electrolyte couples.

Keeping this in mind, our aim was to obtain a well-defined and processable polyfluorene derivative, **P(FCA)** by electrochemical oxidation of **FCA** (**Scheme 1.1**). The spectroscopic and electrochromic behaviors of the polymer film were also investigated. Furthermore, **P(FCA)** film was used to construct a dual type electrochromic device.



**Scheme 1. 1.** Chemical structure of **P(FCA)**.

### Second Part:

It is known that low band gap polymers can be prepared utilizing D–A units along the polymer chain. Furthermore, the co-polymerization of  $\pi$ -rich unit, such as thiophenes with electron deficient fluorene derivatives has been found to facilitate the p-doping process, lower the band gap and improve the stability of the resulting copolymers [69]. It means that the anodic electropolymerization in common solvent-electrolyte medium becomes easier. In the light of this information, various new D-A type fluorene derivatives functionalized from C9 position were prepared.

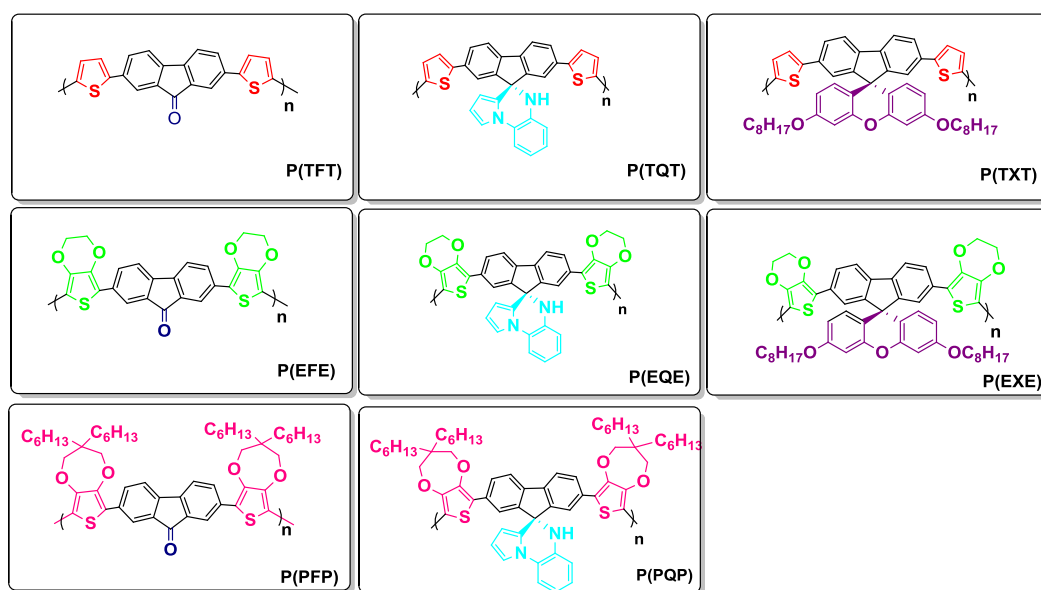
For this purpose **Th** (thiophene), **EDOT** (3,4-ethylenedioxythiophene) and **ProDOT** (dialkyl substituted 3,4-propylenedioxythiophene) were chosen as donor groups. It is expected that the presence of dialkyl substituted **ProDOT** units would not only enhance the solubility but also change the optoelectronic properties by changing the band gap. Furthermore, the polymer is expected to be regioregular, which is also an important factor in determining the optical properties of conjugated polymers, and most PFs suffer from the problem of low regioregularity due to branching through positions other than 2 and 7 positions of PF. In order to elucidate the effect of donor group, the results obtained for polymers were compared.

Three different acceptor units were also selected. Fluorenone, which is an attractive precursor material to produce low band-gap polymers with a low LUMO energy level, provides sites for facile and stable n-doping copolymers of fluorenone with different donor groups. For this purpose, three new D-A-D type fluorenone derivatives (**TFT** (2,7-di-thiophen-2-yl-fluoren-9-one), **EFE** (2,7-bis-(2,3-dihydro-thieno[3,4-b][1,4]dioxin-5-yl)-fluoren-9-one), **PFP** (2,7-bis-(3,3-dihexyl-3,4 dihydro-2H-thieno[3,4-b][1,4]dioxepin-6-yl)-fluoren-9-one) were synthesized. Their corresponding polymers (**P(TFT)** (poly(2,7-di-thiophen-2-yl-fluoren-9-one)), **P(EFE)** (poly(2,7-bis-(2,3-dihydro-thieno[3,4-b][1,4]dioxin-5-yl)-fluoren-9-one)), **P(PFP)** (poly (2,7-bis-(3,3-dihexyl-3,4 dihydro-2H-thieno[3,4-b][1,4]dioxepin-6-yl)-fluoren-9-one)) were prepared via electrochemical polymerization. Repeating units of the polymers are depicted in **Scheme 1.2**.

A series of new fluorene derivatives bearing pendant quinoxaline moieties with different donor groups were also synthesized. It is known that both polyfluorene derivatives [110] and quinoxaline functional units [64] are selective towards  $\text{Fe}^{+n}$  ions. A hybrid material prepared by combining quinoxaline, a high electronegativity fluorescence material, with fluorene and its polymer would be an interesting new material not only for sensor applications but also for light emitting devices., Three different fluorene-quinoxaline derivatives with different units (**TQT** (2,7-di(thiophen-2-yl)-5'*H*-spiro[fluorene-9,4'-pyrrolo[1,2-a]quinoxaline]), **EQE** (2,7-bis(2,3-dihydrothieno[3,4-b][1,4]dioxin-5-yl)-5'*H*-spiro[fluorene-9,4'-pyrrolo[1,2-a]quinoxaline]), **PQP** (2,7-bis(3,3-dihexyl-3,4-dihydro-2*H*-thieno[3,4-b][1,4]dioxepin-6-yl)-5'*H*-spiro[fluorene-9,4'-pyrrolo[1,2 a]quinoxaline]) were synthesized. Their corresponding polymers (**P(TQT)** (poly(2,7-di(thiophen-2-yl)-5'*H*-spiro[fluorene-9,4'-pyrrolo[1,2-a]quinoxaline])), **P(EQE)** (poly(2,7-bis(2,3-dihydrothieno[3,4-b][1,4]dioxin-5-yl)-5'*H*-spiro[fluorene-9,4'-pyrrolo[1,2-a]quinoxaline])), **P(PQP)** (poly(2,7-bis(3,3-dihexyl-3,4-dihydro-2*H*-thieno[3,4-b][1,4]dioxepin-6-yl)-5'*H*-spiro[fluorene-9,4'-pyrrolo[1,2-a]quinoxaline])) were prepared utilizing electrochemical polymerization techniques. Repeating units of the polymers are depicted in **Scheme 1.2**.

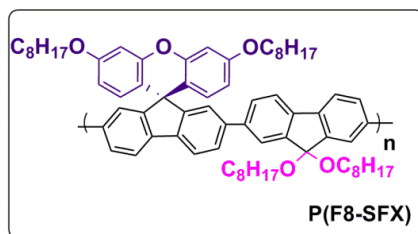


The spirobifluorene derivatives, which constitute a perpendicular arrangement of their two biphenylene planes, possess a great potential for applications in optical and optoelectronic devices since they have high glass transition temperature and superior morphological stability [107]. Currently, spiro compounds with hetero-atoms in the spiro-skeleton have been synthesized for use as building blocks of  $\pi$ -conjugated oligomers and polymers to improve their charge injecting and transporting properties [128-131]. Another way to improve charge injection and optical properties is to associate the donor groups such as **Th** and **EDOT** (Scheme 1.2.). Two new D-A-D type fluorene-xanthene derivative monomers (**TXT** (3',6'-bis(octyloxy)-2,7-di(thiophen-2-yl)spiro[fluorene-9,9'-xanthene]), **EXE** (2,7-bis(2,3-dihydrothieno[3,4-b][1,4]dioxin-5-yl)-3',6'-bis(octyloxy)spiro[fluorene-9,9'-xanthene]) and their corresponding polymers; **P(TXT)** (poly(3',6'-bis(octyloxy)-2,7-di(thiophen-2-yl)spiro[fluorene-9,9'-xanthene])), **P(EXE)** (poly(2,7-bis(2,3-dihydrothieno[3,4-b][1,4]dioxin-5-yl)-3',6'-bis(octyloxy)spiro[fluorene-9,9'-xanthene])) were also synthesized to investigate the effect of spiro groups on the thermal and photophysical properties of polyfluorenes.



**Scheme 1. 2.** Chemical Structures of D-A-D type polyfluorene derivatives, **P(TFT)**, **P(TQT)**, **P(TXT)**, **P(EFE)**, **P(EQE)**, **P(EXE)**, **P(PFP)** and **P(PQP)**.

### Third Part:



**Scheme 1. 3.** The chemical structure of **P(F8-SFX)**.

Since polyfluorenes are blue light emitters with high quantum yields, they are potential candidates for PLED applications. However, the solubility problems and low thermal stability together with the formation of keto defects limit their applications. Furthermore, the examples of organic polymers and oligomers having both electrochromism and photo- or electroluminescence are scarce in the literature. In the light of this knowledge, we attempted to synthesize a novel **P(F8-SFX)** polymer by Suzuki-Miyaura coupling method as a multipurpose material (**Scheme 1.3**) having both electrochromic and electroluminescent properties. The electrochemical, electrochromic and electroluminescence properties of **P(F8-SFX)** was investigated.

## CHAPTER 2

### EXPERIMENTAL

#### 2.1. Materials

All chemicals were purchased from Sigma Aldrich Chemical and used as received except for lithium aluminum hydride (Acros Chemicals). For electrochemical experiments, tetrabutylammonium hexafluorophosphate (TBAPF<sub>6</sub>), tetrabutylammonium tetrafluoroborate (TBABF<sub>4</sub>) and tetrabutylammonium perchlorate (TBAClO<sub>4</sub>) dissolved in freshly distilled acetonitrile (ACN) and dichloromethane (DCM) (over CaH<sub>2</sub> under N<sub>2</sub> or Ar atm) solvents were used as electrolyte solutions. Tetrahydrofuran (THF) was refluxed with sodium/benzophenone and distilled under Ar(g) atmosphere. The molecular sieves (4 Å) and alumina were activated at 250 °C and 450 °C, respectively, for several hours.

#### 2.2. General methods

<sup>1</sup>H NMR and <sup>13</sup>C NMR spectra of the monomers and chemically obtained polymer were recorded on a Bruker-Instrument-NMR Spectrometer (DPX-400) with CDCl<sub>3</sub> and d-acetone as the solvents and chemical shifts (δ) were given relative to tetramethylsilane as the internal standard. Chemical shifts are reported in ppm and CDCl<sub>3</sub> 7.27 ppm and d-acetone 2.05 ppm as the reference signals for <sup>1</sup>H NMR (see Appendix B and C). FTIR spectra were recorded on Nicolet 510 FT-IR spectrophotometer with an attenuated total reflectance (ATR) (see Appendix A). UV measurements were carried out with a Hewlett-Packard 8453A diode array UV-vis and SPECORD S 600 spectrometers using a well-considered designed three electrode cell to allow potential application as monitoring the absorption spectra. The molecular weight of the polymer was determined by gel permeation chromatography (GPC, Polymer Laboratories PL-GPC 220) using THF as a solvent (see Appendix E). A Waters, Synapt HRMS instrument was used for the high resolution mass spectrometry analysis of the monomers (see Appendix D). Differential scanning calorimetry (DSC) and thermal gravimetric analysis (TGA) were performed using a Perkin Elmer Diamond and Perkin Elmer Pyris 1 TGA under nitrogen atmosphere with 10 °C/min heating rate, respectively. Colorimetry measurements were done via Minolta CS-100 spectrophotometer. A Varian Cary Eclipse Fluorescence Spectrophotometer was used for fluorescence measurements.

#### 2.3. Electrochemistry

CV and electrolysis experiments were carried out a Gamry PCI4/300 potentiostat-galvanostat for *in-situ* spectroelectrochemical studies and electroanalytical measurement. This method consists of cycling the potential of an electrode, which is immersed in an unstirred solution, and measuring the resulting current at the WE. Therefore, the obtained voltammogram is a display of current (vertical axis) vs. potential (horizontal axis). The reducing or oxidizing strength of the WE is precisely controlled by the applied potential. A glassy carbon disc (0.07 cm<sup>2</sup>) or a Pt disc electrode (0.02 cm<sup>2</sup>) was used as a WE, and a Pt wire was used as a CE. Potentials were reported vs. Ag/AgCl and calibrated vs. internal ferrocene standard.

Prior to electrochemical measurements electrolytic medium was purged with Ar(g) to remove oxygen. After electropolymerization, the electrode is removed from the monomer solution and carefully rinsed with monomer-free electrolyte solution. The rinsed electrode was then placed into another three-electrode cell filled with a monomer-free electrolyte solution to study the redox behavior of the polymer film.

## 2.4. Spectroelectrochemistry (SPEL)

SPEL measurements provide information about the material's band gap and intraband states created upon doping as well as give electrochromic properties of CPs at various applied potentials. Measurements were carried out with a HP 8453A diode array UV-vis spectrometer using a specially designed three-electrode cell to allow potential application while monitoring the absorption spectra.

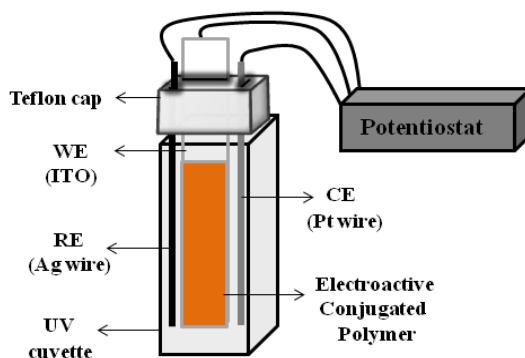


**Figure 2. 1.** Spectroelectrochemical characterization setup of a polymer with three electrodes system.

The UV cuvette used for this experiment has the dimensions of 1.0 x 1.0 x 4.5 cm and a cutoff value of 190 nm in ACN. A teflon cap is pierced from 3 parts of it due to place the three electrodes into UV cuvette, as seen in **Figure 2.1**. The WE is an ITO fitting the SPEL cuvette (0.7 cm wide). Ag-wire pseudo reference is used as a RE and a Pt wire is used as a CE. For potential control, all three electrodes were connected to a Gamry PCI4/300 potentiostat/ galvanostat.

In a typical SPEL experiment, monomer free solution and blank ITO (no polymer on it) with other electrodes is placed into UV cuvette and then the background is taken beginning at 300 nm via UV-vis spectrophotometer. After that, the polymer on ITO is replaced with blank ITO in the cuvette. The characterization of the polymer is started with switching between oxidation and reduction potentials while monitoring the change in the absorbance of the polymer.

The characterization of the electrochromic device is also carried out with this method. During the measurement of the blank for the device, two uncoated ITO are taken and sandwiched with a transparent gel electrolyte, as shown in **Figure 2.2a**. The composition of the gel electrolyte may differ depending on the choices. A widely used receipt consist of TBABF<sub>4</sub>, ACN, poly(methyl methacrylate) and polycarbonate in the ratio of 3:70:7:20 by weight due to the transparency and easiness of the preparation and coating over the ITO electrodes. After that each electrodes were coated with predetermined electrochromic polymers. The device was constructed using them stacked face-to face separated by the gel electrolyte as depicted in **Figure 2.2b**. After drying step, the potential range of the device was determined from the measurements of each polymer via electroanalytical methods. The electrodes were plugged into the potentiostat and then the measurements were taken by monitoring absorbance in the UV-vis spectrometer during switching with electroanalytical methods.

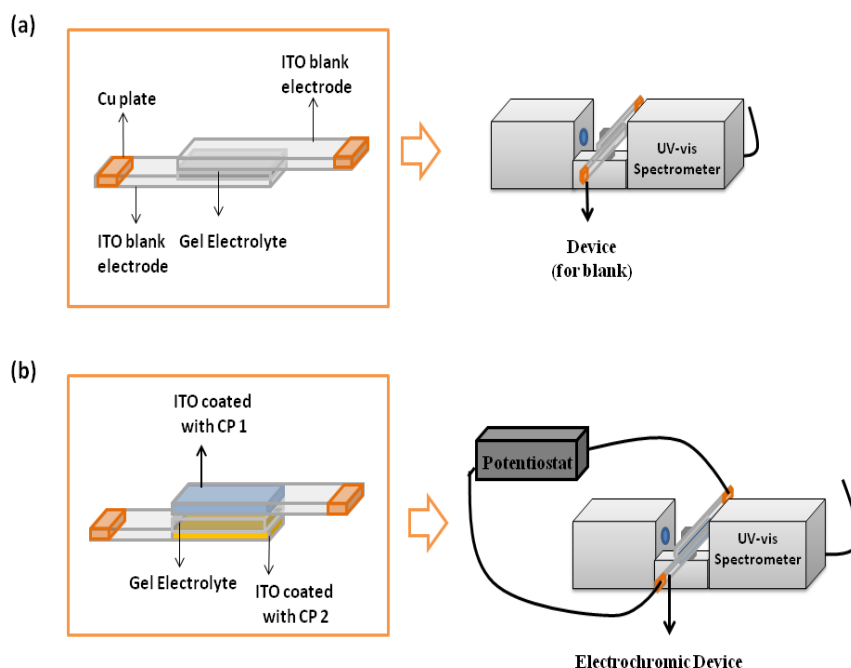


**Figure 2. 2.** Schematic design of an electrochromic device with two electrode system. **(a)** Measurement of the blank and **(b)** characterization of electrochromic device.

## 2.5. PLED Device Characterization

Current density (Keithley 2400 source measurement unit) and brightness (Keithley 2000 multimeter) versus applied voltage (Keithley 2400 sourcemeter) characteristics for the LEDs were measured in air using a calibrated reference Si photodetector located in the forward direction, typically at a distance of 42 mm from the substrate. Electroluminescence (EL) spectra were recorded with a multimode optical fiber (diameter = 600  $\mu\text{m}$ ) attached to an intensity calibrated Ocean Optics USB2000 spectrometer.

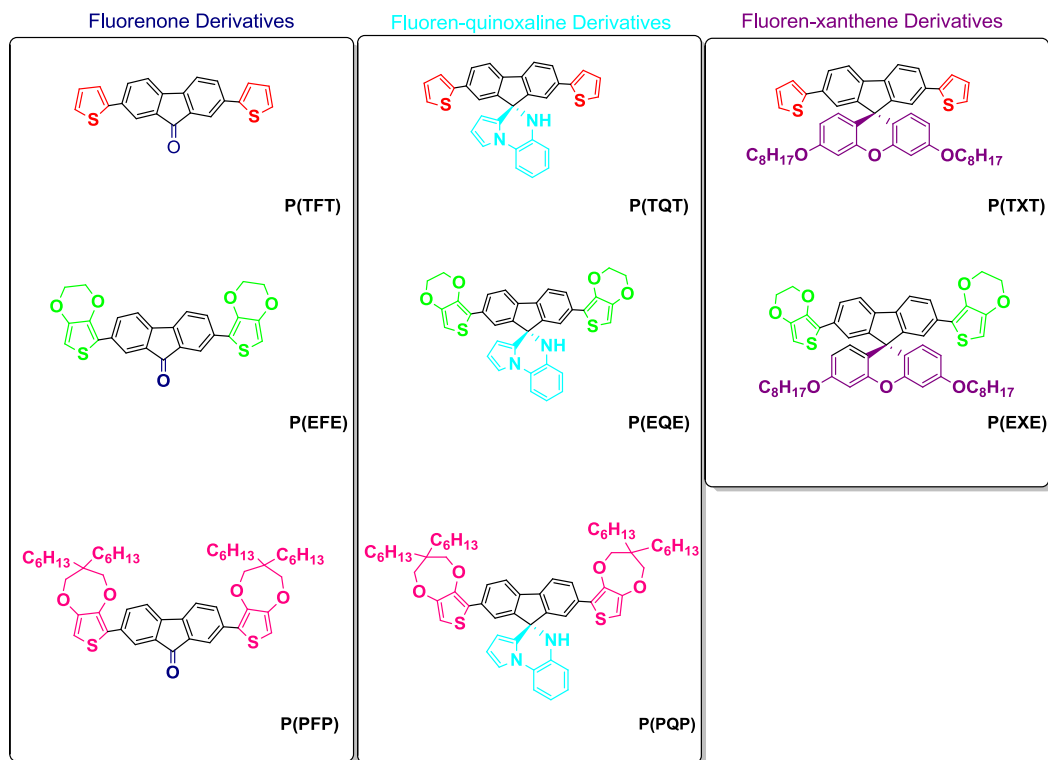
## 2.6. Synthesis of Chemicals

To synthesize the desired multifunctional fluorene derivatives, the synthesis part was divided into 3 parts.

- Synthesis of D-A-D type fluorene monomers and their electropolymerization; fluorenone, fluoren-quinoxaline and fluoren-xanthene.
- Electropolymerization of 9-fluorene-carboxylic acid.
- Chemical coupling polymerization of spirofluorene-co-9,9'-dioctylfluorene.

### 2.6.1. Synthesis of D-A-D type fluorene monomers

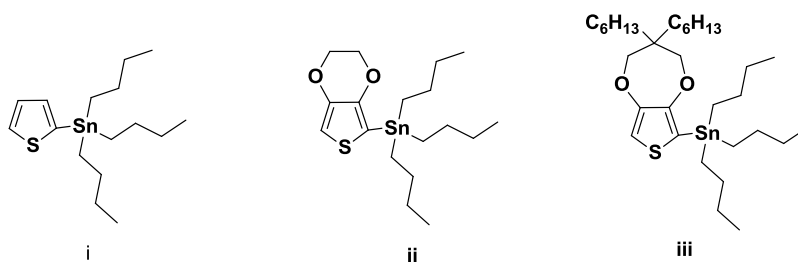
Eight D-A-D type monomers were synthesized before electropolymerization step (**Scheme 2.1**).



**Scheme 2. 1.** Structures of D-A-D type monomers, **TFT**, **EFE**, **PFP**; **TQT**, **EQE**, **PQP**; **TXT** and **EXE**.

#### 2.6.1.1. Preparation of Donor Moieties

In order to prepare the Stille reagent, tributyltin substituted thiophene; ProDOT and EDOT were prepared in high yield by lithiation with *n*-butyl lithium and subsequent quenching with tributyltin chloride (**Scheme 2.2**).



**Scheme 2. 2.** Chemical structure of tributyl (thiophen-2-yl) stannane (**i**), tributyl (2, 3-dihydrothieno [3, 4-*b*][1, 4] dioxin-7-yl)stannane (**ii**), tributyl-(3, 3-dihexyl-3, 4-dihydro-2H-thieno[3,4-*b*][1,4]dioxepin-6-yl)-stannane (**iii**).

#### 2.6.1.1.1. Tributyl (thiophen-2-yl) stannane (i)

A solution of thiophene (31.2 mmol, 2.5 mL) in 30 mL of anhydrous THF under argon was cooled to -78 °C in a dry ice/o-xylene cooling bath. To the stirred precooled solution, 26.9 mL of 2.5 M n-butyllithium were added dropwise and the mixture was stirred at this temperature under argon for 2 h. Then tributylstannyl chloride (34.3 mmol, 9.3 mL) was added, and the mixture was stirred at -78 °C for 1.5 h. The solvent was evaporated under vacuum after stirring the mixture at room temperature for 12 h. The residue was poured into saturated aqueous NaHCO<sub>3</sub> and extracted with dichloromethane. The organic phase was separated and washed with saturated aqueous brine and then dried over an anhydrous sodium sulfate. The solvent was removed at a reduced pressure. The title compound was obtained as oil which was used without any further purification for the next step.

**i:** Yellow viscous liquid. Yield: 83%.

<sup>1</sup>H NMR (400 MHz, CDCl<sub>3</sub>, δ, ppm) : 7.69 (s, 1H, ArH), 7.25 (m, 1H, ArH), 7.17 (m, 1H, ArH), 1.63 (t, 6H, *J* = 7.2 Hz), 1.32 (m, 6H), 1.15 (m, 6H), 0.89 (t, 9H, *J* = 6.82 Hz); <sup>13</sup>C NMR (100 MHz, CDCl<sub>3</sub>, δ, ppm): 136.2, 134.2, 130.7, 127.7, 28.7, 27.2, 16.6, 13.8.

#### 2.6.1.1.2. Tributyl (2, 3-dihydrothieno [3, 4-*b*][1, 4] dioxin-7-yl)stannane (ii)

A 2.5 mL (23.5 mmol) sample of 2,3-dihydrothieno[3,4-*b*][1,4]dioxine in 50 mL of anhydrous THF was treated dropwise with 16.1 mL of 2.5 M n-butyllithium at -78 °C under argon in a dry ice/o-xylene cooling bath. After the solution was stirred for 1.5 h at -78 °C, 6.98 mL (25.8 mmol) of tributylstannyl chloride was added to this solution. The solution was stirred at -78 °C under argon for 4 h. Then the solution was warmed to room temperature. The solvent was removed by rotary evaporation after the solution was stirred overnight. After the removal of the solvent at a reduced pressure, the residue was poured into saturated aqueous NH<sub>4</sub>Cl and extracted with dichloromethane. The organic phase was separated and washed with saturated aqueous brine and then dried over an anhydrous magnesium sulfate. The solvent was removed at a reduced pressure to afford tributyl(2,3-dihydrothieno[3,4-*b*][1,4]dioxin-7-yl)stannane as a yellow liquid. The compound was used for the next reactions as obtained, with no further purifications.

**ii:** Light yellow viscous liquid. Yield: 43%

<sup>1</sup>H NMR (400 MHz, CDCl<sub>3</sub>, δ, ppm) : 6.50 (s, 1H, ArH), 4.18 (s, 4H), 1.60 (t, 6H, *J* = 7.2 Hz), 1.35 (m, 6H), 1.10 (m, 6H), 0.90 (t, 9H, *J* = 6.82 Hz); <sup>13</sup>C NMR (100 MHz, CDCl<sub>3</sub>, δ, ppm): 148.4, 142.2, 115.8, 105.3, 64.7, 28.9, 27.5, 26.9, 16.6, 13.6.

#### 2.6.1.1.3. Tributyl-(3, 3-dihexyl-3, 4-dihydro-2H-thieno[3,4-*b*][1,4]dioxepin-6-yl)-stannane (iii)

3,3-Dihexyl-3,4-dihydro-2H-thieno[3,4-*b*][1,4]dioxepine (**iii**) was prepared in 3 steps as seen in **Scheme 2.3** [132].

1<sup>st</sup> step:

500 mL two-necked flask equipped with reflux condenser was filled with dry ethanol (160 mL). Sodium metal (0.2 mol, 3.25 eq.) was added and stirred to resolve all of the sodium. After slow addition of diethyl malonate (0.062 mol, 1 eq.), the reaction mixture was heated to reflux. When it starts to reflux, 1-bromoalkyl (0.23 mol, 3.65 eq.) in 30 mL ethanol was added slowly and refluxed 4 days. After removing the ethanol, cold water was added and extracted with cold ether. Organic layer was dried with anhydrous MgSO<sub>4</sub> and the solvent was removed under reduced

**iii (a):** Colorless liquid. Yield: 75 %

<sup>1</sup>H NMR (400 MHz, CDCl<sub>3</sub>, δ, ppm): 4.18 (q, 4H, *J* = 7.2 Hz), 1.90 (m, 2H, *J* = 7.2 Hz), 1.43-1.00 (m, 26H), 0.90 (t, 6H, *J* = 7.3 Hz); <sup>13</sup>C NMR (100 MHz, CDCl<sub>3</sub>, δ, ppm): 171.68, 60.4, 31.3, 30.6, 29.4, 25.3, 22.38, 13.89.

2<sup>st</sup> step :

LiAlH<sub>4</sub> (72 mmol, 1.79 eq.) was placed in a 250 mL two-necked flask equipped with reflux condenser under N<sub>2</sub> atmosphere. After that a 100 mL dry THF solvent was added to the reaction flask. Diethyl-2,2-dialkylmalonate (40 mmol, 1 eq.) was added with a syringe. The reaction was stopped after one day. 0.1 M H<sub>2</sub>SO<sub>4</sub> solution was added with a syringe very slowly, drop by drop. A salty solution was observed. Then solution was extracted with diethyl ether.

**iii (b):** Yellow liquid, Yield %56

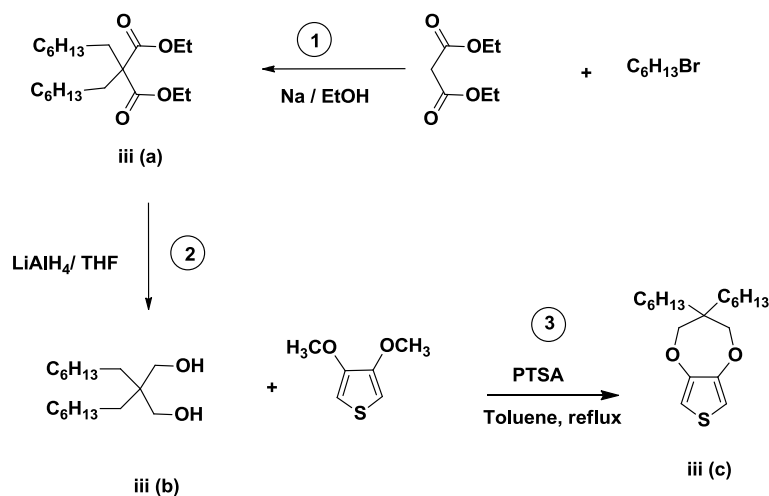
<sup>1</sup>H NMR (400 MHz, CDCl<sub>3</sub>, δ, ppm): 3.60 (s, 4H), 2.12 (s, br, 2H), 1.41-1.00 (m, 20H), 0.88 (t, 6H, *J*= 7.3 Hz); <sup>13</sup>C NMR (100 MHz, CDCl<sub>3</sub>, δ, ppm): 67.3, 36.5, 31.8, 31.6, 29.9, 25.2, 22.7, 14.1.

3<sup>rd</sup> step:

To an argon degassed solution of 3,4-dimethoxythiophene (5.42 mmol, 1 eq.), 2,2-dihexylpropane-1,3-diol (10.84 mmol, 2 eq.) and p-toluenesulfonic acid (PTSA) (0.542 mmol, 0.1 eq.) were mixed in dry toluene (20 mL) and the mixture was heated under reflux during 24 h. After cooling to rt, the solvent was removed under reduced pressure. The crude mixture was chromatographed on silica gel by eluting with DCM: hexane (1:3, v/v) to give ProDOT-C<sub>6</sub>.

**iii (c):** Yellow liquid. Yield: 62 %

<sup>1</sup>H NMR (400 MHz, CDCl<sub>3</sub>, δ, ppm): 6.41 (s, 2H, ArH), 3.83 (s, 4H); 1.31-1.28 (m, 20H); 0.91 (t, 6H, *J*= 6.82 Hz); <sup>13</sup>C NMR (100 MHz, CDCl<sub>3</sub>, δ, ppm): 149.74; 104.63; 43.75; 31.89; 31.73; 30.14; 22.78; 22.64; 14.05;



**Scheme 2. 3.** Synthesis of 3,3-Dihexyl-3,4-dihydro-2H-thieno[3,4-b][1,4]dioxepine (3).

A solution of 3,3-dihexyl-3,4-dihydro-2H-thieno[3,4-b][1,4]dioxepine (6.2 mmol, 2.13 mL) in anhydrous THF (30 mL) under argon was cooled to -78 °C in a dry ice/acetone cooling bath. A 3.33 mL of 1.6 M *n*-BuLi was added dropwise, via syringe, to this precooled solution. After 1.5 h stirring at -78 °C, (12.9 mmol, 3.5 mL) tributylstannyl chloride was added slowly and the solution was stirred for further 4 h at -78 °C under argon. After 4 h, the solution was warmed to room temperature and stirred overnight. The solvent was removed at a reduced pressure. The residue was poured into saturated aqueous sodium hydrogen carbonate and extracted with dichloromethane. The solvent was removed at a reduced pressure.



**iii:** Colorless oil. Yield: 85 %

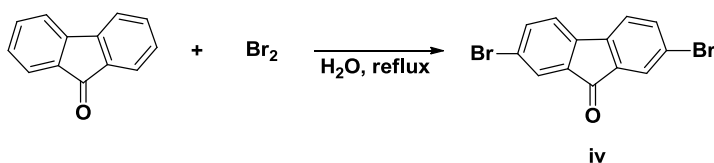
$^1\text{H}$  NMR (400 MHz,  $\text{CDCl}_3$ ,  $\delta$ , ppm): 6.66 (s, 1H), 3.84 (s, 4H), 1.28 (br, 38H), 0.89 (t, 15H,  $J=6.82$  Hz);  $^{13}\text{C}$  NMR (100 MHz,  $\text{CDCl}_3$ ,  $\delta$ , ppm): 155.6, 150.4, 114.7, 110, 76.71, 43.6, 32.08, 31.75, 30.2, 29.01, 27.9, 22.8, 22.66, 17.53, 14.05, 13.72, 10.61.

### 2.6.1.2. Synthesis of Donor-Acceptor-Donor-Acceptor Moieties.

#### 2.6.1.2.1. Synthesis of D-A-D monomer based on fluorenone moiety

To get the fluorenone products, reactant, fluorenone was firstly brominated in aqueous medium (**Scheme 2.4**).  $\text{Br}_2$  (0.16 mol, 3.99 mL) and water (85 mL) mixture was added to fluorenone (0.056 mol, 10 g) and mixed perfectly. After reflux at 95-100°C for 3 h the reaction was neutralized. After two stages bromine was added  $\text{Br}_2$  (0.12 mol, 4 mL) and  $\text{Br}_2$  (0.078 mol, 2.98 mL) and the same procedure was repeated in the first part and the reaction time was 4 h instead of 3 h. The reaction mixture was cooled to room temperature and filtered. The crude product was purified by column chromatography over silica gel (2:1; chloroform: hexane). The product was taken as 98% yield (yellow solid).

**iv:**  $^1\text{H}$  NMR (400 MHz,  $\text{CDCl}_3$ ,  $\delta$ , ppm): 7.73 (s, 2H, Ar-H), 7.60 (s, 2H, Ar-H), 7.35 (s, 2H, Ar-H);  $^{13}\text{C}$  NMR (100 MHz,  $\text{CDCl}_3$ ,  $\delta$ , ppm): 191, 142.4, 137.6, 155.4, 128.0, 123.5, 122.0.



**Scheme 2. 4.** Synthesis of 2,7-dibromo-9-fluorenone (**iv**).

A general procedure was applied to synthesis of D-A-D monomer based on fluorenone moiety as seen in **Scheme 2.5**. A mixture of **iv**,  $\text{Pd}(\text{PPh}_3)_2\text{Cl}_2$  (0.02 equiv.) and **i**, **ii** or **iii** (2.5 equiv.) in dry toluene was refluxed under an argon atmosphere until the starting materials were consumed. The reaction mixture was evaporated and the crude product was purified by column chromatography over silica gel.

**TFT:** Red solid. Yield: 48%, Hexane/ $\text{CHCl}_3$  (1:1)

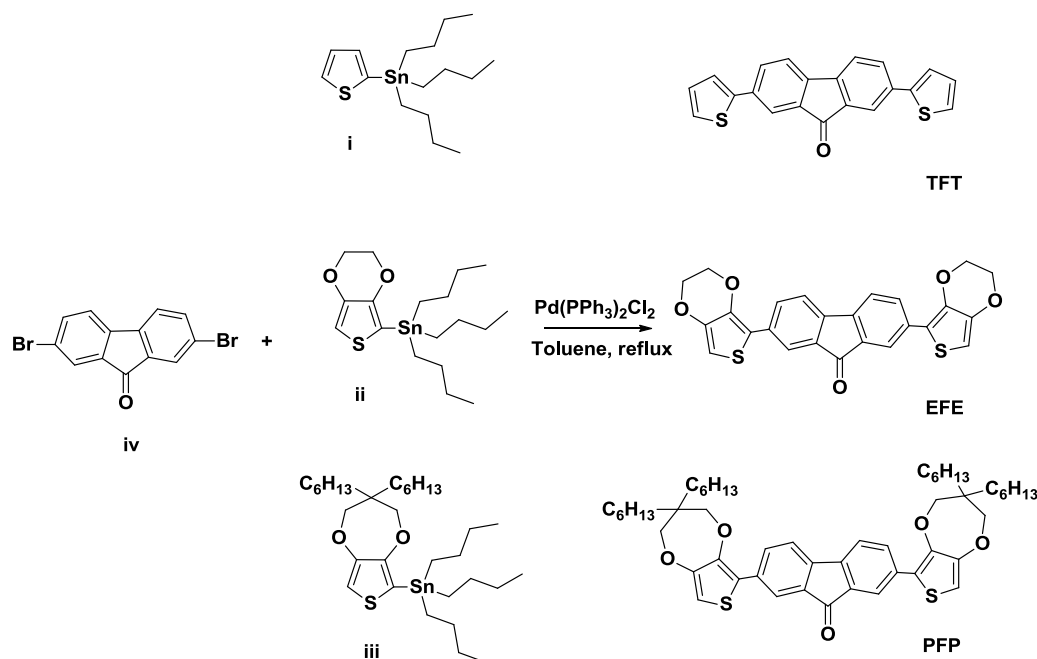
$^1\text{H}$  NMR (400 MHz,  $\text{CDCl}_3$ )  $\delta$  (ppm): 7.94 (s, 2H), 7.75 (d,  $J = 6.5$  Hz, 2H), 7.54 (d,  $J = 7.5$  Hz, 2H), 7.41 (d,  $J = 4.0$  Hz, 2H), 7.34 (d,  $J = 5.5$  Hz, 2H), 7.12 (t,  $J = 9.5$  Hz, 2H).  $^{13}\text{C}$  NMR (100 MHz,  $\text{CDCl}_3$ )  $\delta$  (ppm): 127.6, 128.0, 128.1, 128.6, 131.2, 131.7, 132.3, 139.9, 140.3, 144.1, 193.8.

**EFE:** Red solid. Yield: 60%, Hexane/EtOAc (4:1)

$^1\text{H}$  NMR (400 MHz,  $\text{CDCl}_3$ )  $\delta$  (ppm): 7.98 (s, 2H), 7.73 (d,  $J = 9.6$  Hz, 2H), 7.4 (d,  $J = 8$  Hz, 2H), 6.29 (s, 2H), 4.3 (dt,  $J = 8$  Hz, 4H), 4.2 (dt,  $J = 8$  Hz, 4H).  $^{13}\text{C}$  NMR (100 MHz,  $\text{CDCl}_3$ )  $\delta$  (ppm): 64.45, 64.87, 98.323, 116.52, 120.42, 121.86, 131.57, 134.14, 134.89, 138.95, 142.04, 142.31, 187.0.

**PFP:** Red viscous oil, Yield: 25%, Hexane.

$^1\text{H}$  NMR (400 MHz,  $\text{CDCl}_3$ )  $\delta$  (ppm): 7.98 (s, 2H), 7.80 (d,  $J = 9.6$  Hz, 2H), 7.45 (d,  $J = 8$  Hz, 2H), 6.5 (s, 2H), 3.65 (s, 4H), 3.75 (s, 4H), 1.34–0.95 (m, 52H).  $^{13}\text{C}$  NMR (100 MHz,  $\text{CDCl}_3$ )  $\delta$  (ppm): 193.7, 155.7, 150.5, 146.7, 142.3, 138.2, 135.2, 134.5, 132.4, 114.7, 100.5, 62.5, 43.6, 32.1, 31.8, 30.3, 29.1, 27.9, 22.9, 22.7, 14.1.



**Scheme 2. 5.** Synthesis route of **TFT**, **EFE** and **PFP**.

#### 2.6.1.2.2. Synthesis of D-A-D monomer based on quinoxaline moiety

All monomers (**FQ**, **TQT**, **EQE** and **PQP**) were prepared by the reaction of 1-(2-aminophenyl)pyrrole with corresponding 9H-fluoren-9-one derivatives according to a modified literature procedure [133], the details of which will be published somewhere else in due course (**Scheme 2.6**).

**FQ:** Brown solid. Yield: 79%.

$^1\text{H}$  NMR (400 MHz,  $\text{CDCl}_3$ ):  $\delta$  7.69 (dd,  $J = 1.2, 7.2$  Hz, 2H), 7.49 (dd,  $J = 1.6, 7.6$  Hz, 1H), 7.39 (m, 4H), 7.31 (dd,  $J = 1.2, 3.2$  Hz, 1H), 7.22 (t,  $J = 7.2$  Hz, 2H), 6.99 (m, 2H), 6.69 (dd,  $J = 1.6, 7.6$  Hz, 1H), 6.22 (t,  $J = 3.2$  Hz, 1H), 5.51 (dd,  $J = 1.6, 3.6$  Hz, 1H), 4.18 (br s, 1H, NH);  $^{13}\text{C}$  NMR (100 MHz,  $\text{CDCl}_3$ ):  $\delta$  (ppm) 149.1, 138.9, 135.8, 130.1, 129.2, 128.5, 126.0, 125.0, 124.95, 120.2, 119.8, 116.3, 115.1, 114.7, 110.6, 104.4, 65.3.

**TQT:** Red solid. Yield: 61%.

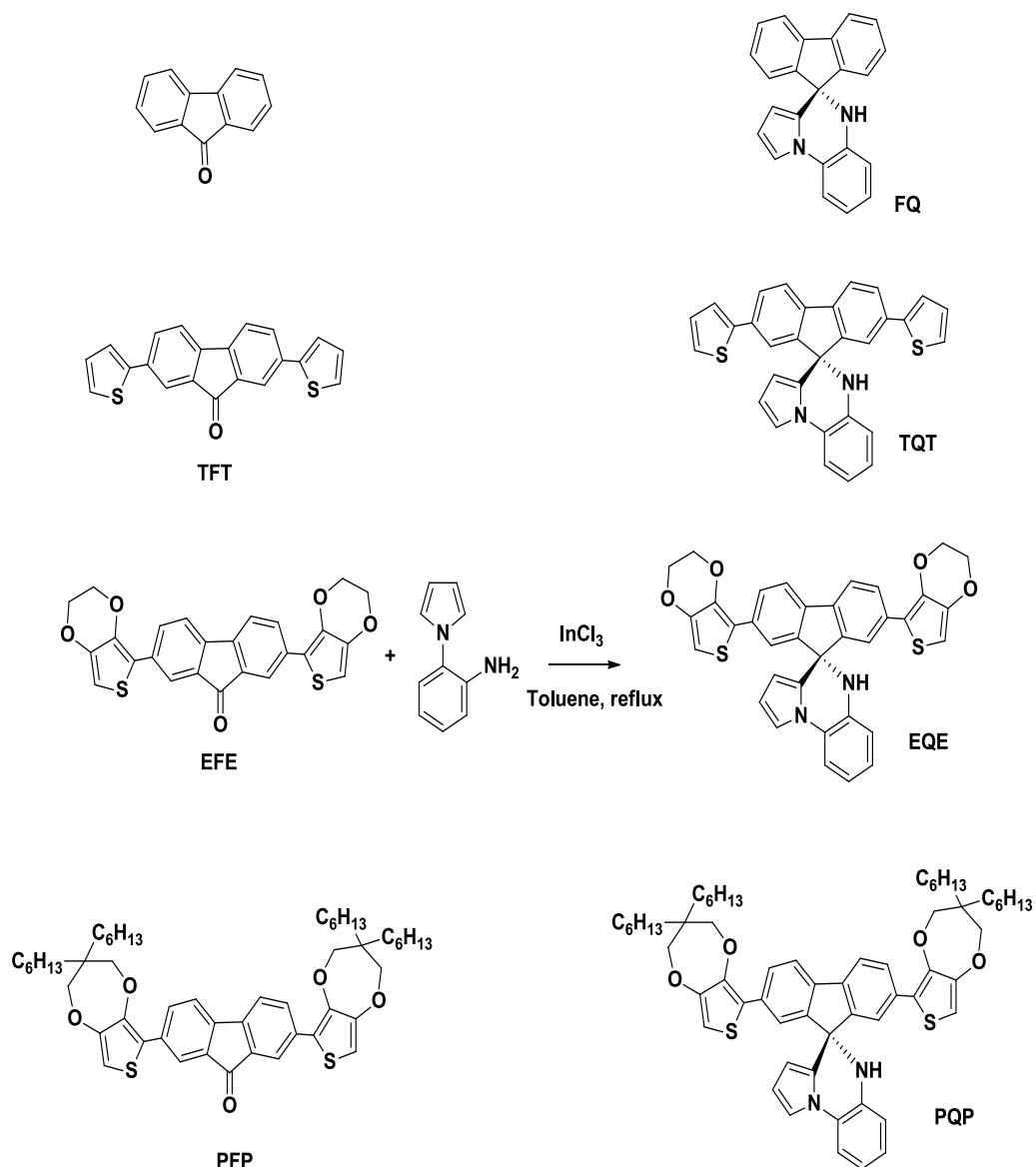
$^1\text{H}$  NMR (400 MHz,  $\text{CDCl}_3$ ):  $\delta$  7.85 (m, 6H), 7.53 (m, 1H), 7.34 (m, 1H), 7.23 (dd,  $J = 5.2, 1.2$  Hz, 2H), 7.19 (dd,  $J = 3.6, 1.2$  Hz, 2H), 7.03 (m, 4H), 6.73 (m, 1H), 6.24 (m, 1H), 5.60 (dd,  $J = 7.6, 1.6$  Hz, 1H), 4.23 (brs, 1H, NH).  $^{13}\text{C}$  NMR (100 MHz,  $\text{CDCl}_3$ ):  $\delta$  150.1, 144.4, 137.9, 135.7, 134.7, 129.9, 128.3, 127.2, 126.3, 125.2, 125.1, 123.5, 122.3, 120.7, 120.3, 116.6, 115.4, 114.9, 110.7, 104.8, 65.3.

**EQE:** Red solid. Yield: 54%

$^1\text{H}$  NMR (400 MHz,  $\text{CDCl}_3$ ):  $\delta$  7.81 (d,  $J = 1.6$  Hz, 2H), 7.66 (dd,  $J = 1.6, 8.0$  Hz, 2H), 7.60 (d,  $J = 8.0$  Hz, 2H), 7.49 (dd,  $J = 1.6$  Hz, 1H), 7.30 (m, 1H), 7.00 (m, 2H), 6.75 (dd,  $J = 1.2, 7.6$  Hz, 1H), 6.25 (s, 2H), 6.21 (t,  $J = 3.2$  Hz, 1H), 5.56 (m, 1H), 4.16 (s, 8H);  $^{13}\text{C}$  NMR (100 MHz,  $\text{CDCl}_3$ ):  $\delta$  (ppm) 149.5, 142.4, 138.5, 136.9, 136.1, 133.2, 130.4, 126.7, 126.5, 124.8, 122.4, 120.2, 119.7, 117.6, 116.7, 115.1, 114.6, 110.6, 104.6, 97.8, 64.7, 64.5, 60.4.

**PQP:** Red viscous oil, Yield: 30%, Hexane. HRMS Calculated for  $\text{C}_{61}\text{H}_{77}\text{N}_2\text{O}_4\text{S}_2$ : 965.4808. Found 965.5325.

$^1\text{H}$  NMR (400 MHz,  $\text{CDCl}_3$ ):  $\delta$  7.74 (d,  $J = 1.2$  Hz, 2H), 7.66 (m, 4H), 7.49 (d,  $J = 8.0$  Hz, 1H), 7.30 (m, 1H), 7.02 (td,  $J = 1.2, 7.6$  Hz, 1H), 6.93 (td,  $J = 1.2, 8.0$  Hz, 1H), 6.77 (dd,  $J = 1.2, 7.6$  Hz, 1H), 6.35 (s, 2H), 6.21 (m, 1H), 5.54 (m, 1H), 4.30 (br s, 1H. NH), 3.85 (m, 4H), 3.75 (m, 4H), 1.33 (m, 40H), 0.94 (m, 12 H);  $^{13}\text{C}$  NMR (100 MHz,  $\text{CDCl}_3$ ): 150.4, 149.5, 146.2, 137.3, 136.0, 133.6, 130.1, 127.7, 126.3, 124.9, 123.1, 122.0, 120.2, 119.8, 116.5, 115.1, 114.6, 110.8, 104.8, 102.8, 77.9, 77.8, 65.3, 43.9, 32.3, 32.0, 30.4, 23.0, 22.9, 14.3.



**Scheme 2. 6.** Synthesis route of **TQT**, **EQE** and **PQP**.

### 2.6.1.2.3. Synthesis of D-A-D monomer based on xanthene moiety

Before coupling reaction, acceptor moiety was synthesized in two steps (**Scheme 2.7**).

1<sup>st</sup> step:

A mixture of 9-fluorenone 2,7-dibromo-9-fluorenone (**4**, 6.00 g, 17.71 mmol), resorcinol (6.82 g, 62.00 mmol), and ZnCl<sub>2</sub> (555 mg, 4.07 mmol) was stirred and heated at 140 °C for 2 h. The melt was then heated with concentrated HCl (aqueous, 20 mL) under reflux for another 1 h. The reaction mixture was poured into water (300 mL). The precipitate was washed with water, dried, and purified by column chromatography.

2<sup>nd</sup> step:

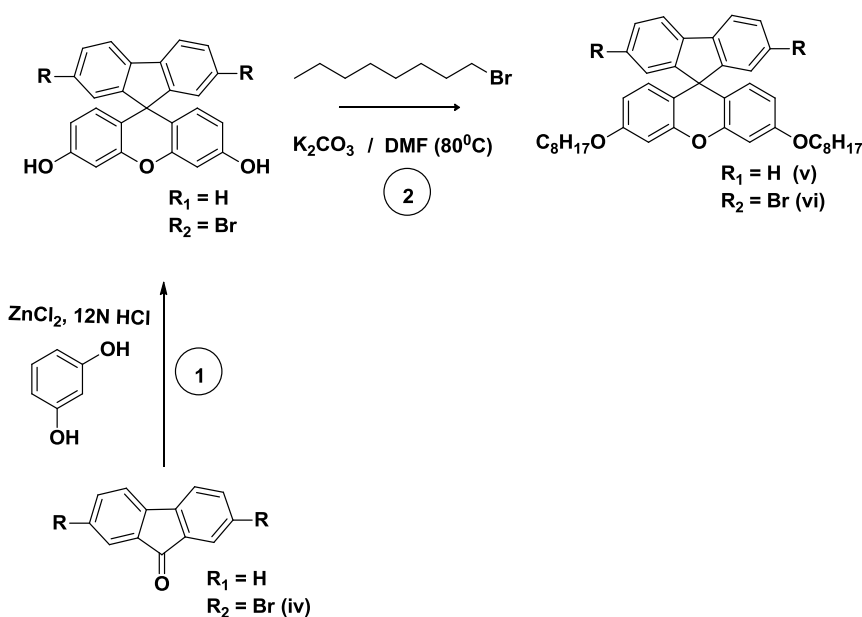
A mixture of 2,7-Dibromospiro[fluorene-9,9'-(2',7'-dihydroxyxanthene)] (7.80 g, 14.99 mmol), 1-bromooctane (10.42 g, 53.98 mmol), K<sub>2</sub>CO<sub>3</sub> (5.38 g, 38.98 mmol), and DMF (132 mL) was stirred and heated at 80 °C for 12 h under N<sub>2</sub>. The resulting mixture was poured into water (200 mL) and extracted with EtOAc (3x 100 mL). The combined extracts were dried (MgSO<sub>4</sub>), and the solvent was evaporated in vacuum. The crude product was purified by column chromatography.

**v**: Yellow viscous oil, Yield: 67.0% , Hexane/EtOAc (4:1)

<sup>1</sup>H NMR (400 MHz, acetone-d<sub>6</sub>): δ 0.87 (t, 6H) , 1.27-1.43 (m, 20H), 1.71-1.80 (m, 4H), 3.92 (t, *J* = 6.5 Hz, 4H), 6.23 (d, *J* = 8.7 Hz, 2H), 6.38 (dd, *J* = , 2.7 Hz, 2H), 6.71 (d, *J* = Hz, 2H), 7.08 (d, *J* = 7.8 Hz, 2H), 7.21 (dd, *J* = , 7.6 Hz, 2H), 7.41 (dd, *J* = 7.6 Hz, 2H), 7.88 (d, *J* = 7.8 Hz, 2H); <sup>13</sup>C NMR (100 MHz, acetone-d<sub>6</sub>): δ (ppm) 159.3, 157.1, 151.9, 137.4, 131.1, 129.0, 128.6, 122.3, 121.3, 114.7, 111.3, 101.8, 68.2, 53.5, 31.8, 29.3, 29.21, 29.2, 26.0, 22.6, 14.1.

**vi**: Yellow viscous oil, Yield: 61.8% , Hexane

<sup>1</sup>H NMR (400 MHz, acetone-d<sub>6</sub>): δ 0.87 (t, 6H) , 1.27-1.43 (m, 20H), 1.71-1.80 (m, 4H), 3.92 (t, *J* = 6.5 Hz, 4H), 6.23 (d, *J* = 8.7 Hz, 2H), 6.38 (dd, *J* = 8.7 , 2.5 Hz, 2H), 6.71 (d, *J* = 2.4 Hz, 2H), 7.21 (d, *J* = 1.5 Hz, 2H), 7.45 (dd, *J* = 8.1, 1.7 Hz, 2H), 7.58 (d, *J* = 8.1 Hz, 2H); <sup>13</sup>C NMR (100 MHz, acetone-d<sub>6</sub>): δ (ppm) 159.3, 157.1, 151.9, 137.4, 131.1, 129.0, 128.6, 122.3, 121.3, 114.7, 111.3, 101.8, 68.2, 53.5, 31.8, 29.3, 29.21, 29.15, 26.0, 22.6, 14.1.



**Scheme 2. 7.** Synthesis route of spiro[fluorene-9,9'-(2',7'-di-*n*-octyloxyxanthene) (**5**) ; 2,7-Dibromospiro[fluorene-9,9'-(2',7'-di-*n*-octyloxyxanthene) (**6**).

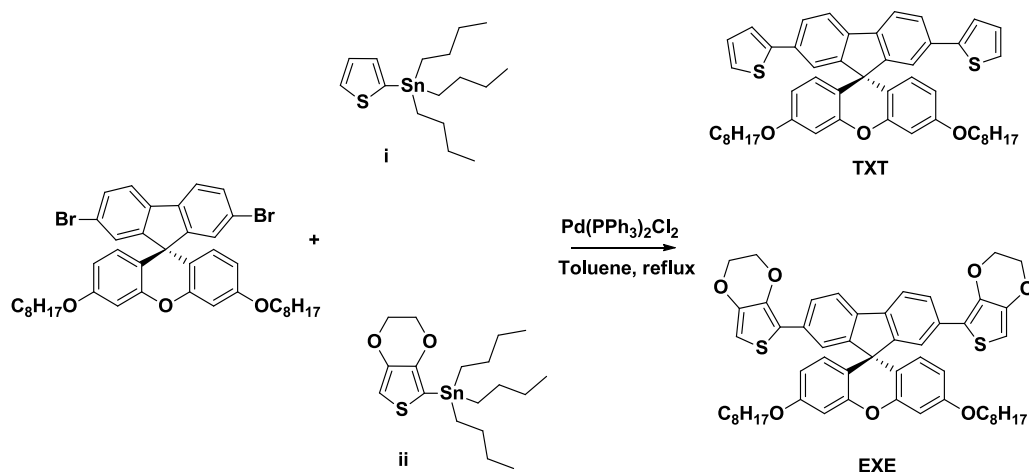
We performed a general procedure to synthesize **TXT** and **EXE** monomers via a Stille coupling between 2, 7-Dibromospiro [fluorene-9, 9'-(2', 7'-di-*n*-octyloxyxanthene)] [107] and two amounts of **i** or **ii**. 3',6'-bis(octyloxy)-2,7-di(thiophen-2-yl)spiro[fluorene-9,9'-xanthene] (**TXT**) (**Scheme 2.8**).

**TXT**: Yellow viscous solid (yield 35%). HRMS calculated for C<sub>49</sub>H<sub>52</sub>O<sub>3</sub>S<sub>2</sub>: 752.3358. Found 752.3292.

<sup>1</sup>H NMR (400 MHz, CDCl<sub>3</sub>): δ (ppm) 7.76 (d, *J* = 8.0 Hz, 2H), 7.62 (dd, *J* = 1.6, 8.0 Hz, 2H), 7.35 (m, 2H), 7.21 (m, 4H), 7.00 (m, 2H), 6.75 (d, *J* = 8.0 Hz, 2H), 6.38 (m, 4H), 3.94 (t, *J* = 8.0 Hz, 4H), 1.71–1.80 (m, 4H) 1.27–1.43 (m, 20H), 0.87 (t, *J* = 8.0 Hz, 6H). <sup>13</sup>C NMR (100 MHz, CDCl<sub>3</sub>): δ (ppm) 159.0, 156.5, 152.0, 151.1, 147.7, 130.71, 130.6, 128.6, 127.9, 125.9, 125.8, 125.4, 124.7, 123.2, 122.9, 116.2 111.1, 68.2, 60.9, 29.3, 29.2, 29.0, 26.0, 22.6, 14.1 FTIR (ATR) 3060–3035 cm<sup>-1</sup>(Aromatic C-H) and 1160–1265(C-O).

**EXE**: Green solid (yield 25%). HRMS Calculated for C<sub>51</sub>H<sub>52</sub>O<sub>7</sub>S<sub>2</sub>: 868.3573. Found 868.3467.

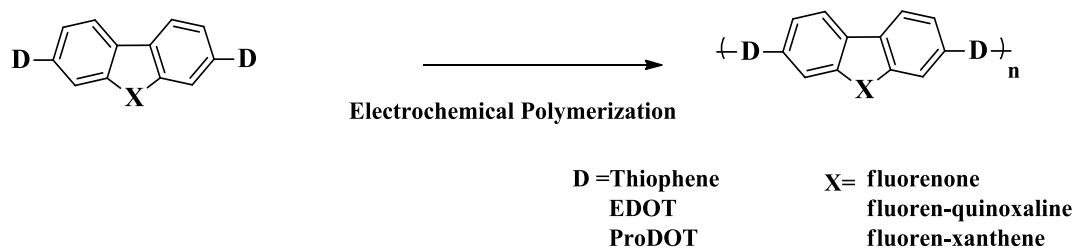
<sup>1</sup>H NMR (400 MHz, CDCl<sub>3</sub>): δ (ppm) 7.74 (m, 4H), 7.40 (s, 2H), 6.75 (s, 2H), 6.38 (m, 4H), 6.23 (s, 2H), 4.20 (m, 8H), 3.94 (t, *J* = 8.0 Hz, 4H), 1.71–1.80(m, 4H) 1.27–1.43 (m, 20H), 0.87 (t, *J* = 8.0 Hz, 6H). <sup>13</sup>C NMR: δ (ppm) (100 MHz, CDCl<sub>3</sub>): δ 159.1, 156.2, 152.3, 142.3, 138.2, 137.9, 133.3, 128.9, 125.9, 123.1, 120.0, 117.9, 116.9, 111.1, 101.9, 97.7, 68.3, 65.1, 64.8, 64.5, 31.9, 29.9, 29.5, 29.2, 26.2, 22.8, 14.3. FTIR (ATR) 3060–3035 cm<sup>-1</sup>(Aromatic C-H), and 1160–1265(C-O).



**Scheme 2.8.** Synthesis route of **TXT** and **EXE**.

### 2.6.1.3. Electropolymerization of D-A-D type fluorene derivatives and their characterization

Polymer films were obtained via repetitive cycling in their proper medium and their electrochemical and optical behaviors were investigated in monomer free electrolyte solutions (**Scheme 2.9**). For spectroelectrochemical studies, platinum and silver (calibrated externally using 5 mM solution of ferrocene/ferrocenium couple) wires were used as counter and reference electrodes, respectively. An indium-tin oxide (ITO, Delta Tech. 8–12 Ω, 0.7 cm × 5 cm) coated by the polymer film was used as the WE. The polymer films were switched between neutral and doped states several times in order to equilibrate its redox behavior in monomer-free electrolytic solution, prior to SPEL investigations.



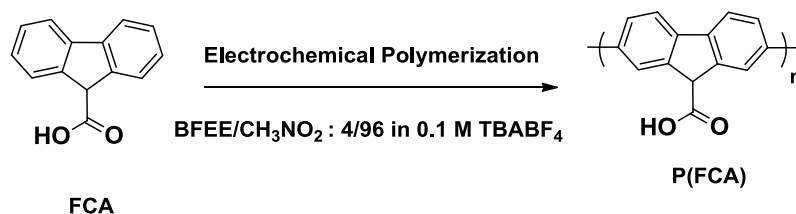
**Scheme 2.9.** Reaction scheme for the electrochemical polymerization of monomers.

#### 2.6.1.4. Chemical Polymerization of D-A-D type fluorene derivatives

The soluble polymers in common organic solvents were synthesized according to a general procedure. A solution of anhydrous  $\text{FeCl}_3$  (444 mg, 2.74 mmol, 5 equiv) in nitromethane was added dropwise over a period of 45 min. to the stirred monomer solution at room temperature. A suspension of anhydrous  $\text{FeCl}_3$  in  $\text{CHCl}_3$  of equal volume was added to the monomer solution for 1 h at 0 °C under  $\text{Ar(g)}$  atmosphere used to remove the generated  $\text{HCl}$  as well as keep the iron catalyst in its active  $\text{Fe}^{3+}$  oxidation state. The final concentration for the monomer and  $\text{FeCl}_3$  was 0.05 M and 0.2 M, respectively. When the addition was complete, the mixture was stirred for 24 h at room temperature and the reaction mixture was poured into methanol, and a precipitate formed. This was filtered and washed with methanol and ether, respectively. The solid was then dried under vacuum at 50 °C.

#### 2.6.2. Electropolymerization of FCA

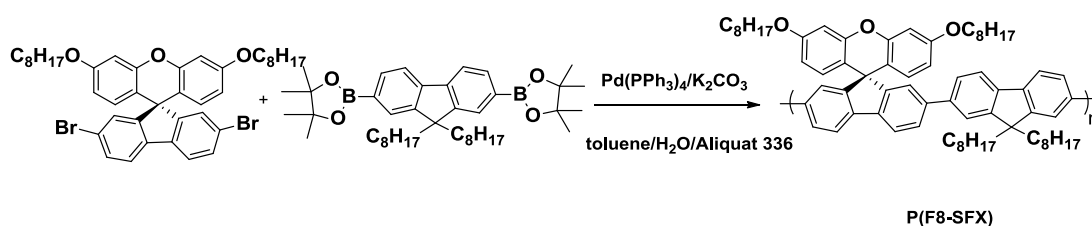
All electrochemical investigations and polymer synthesis were performed in a one-compartment cell utilizing Gamry PCI4/300 potentiostat. The working and counter electrodes for electrochemical measurements were platinum wires and a Ag-wire was used as a pseudo-reference electrode. The pseudo-reference electrode was calibrated externally using a 5 mM solution of ferrocene ( $E_p(\text{Fc} / \text{Fc}^+) = 0.41 \text{ V}$  vs Ag-wire and 0.45 V vs  $\text{Ag}/\text{AgCl}$ ). Measurements were made in a mixture of nitromethane containing 4% BFEE (v/v) and 0.1 M  $\text{TBABF}_4$  at room temperature (**Scheme 2.10**). Electrochemical polymerization of **FCA** was achieved via constant potential electrolysis at 1.15 V vs Ag-wire from a 25 mM monomer solution in nitromethane/BFEE solvent mixture. At the end of the electrolysis the coated film on the electrode surface was peeled off and washed with nitromethane and then ethanol. The polymer was dried under vacuum at 55 °C for 24 h.



**Scheme 2.10.** Reaction scheme for the electrochemical polymerization of **FCA**.

### 2.6.3. Chemical coupling polymerization of spirofluorene-co-9,9'-dioctylfluorene

100.0 mg (0.12 mmol) of 2,7-dibromospiro[fluorene- 9, 9'-2''7''-di-n-octyloxyxanthene)], 88.0 mg (0.12 mmol) of 9,9-dioctylfluorene-2,7-diboronic acid bis(1,3-propanediol) ester, 5.0 mg (4.3  $\mu$ mol) of  $\text{Pd}(\text{PPh}_3)_4$ , and 1.1 mL of 2 M  $\text{K}_2\text{CO}_3$  were combined in 2.2 mL of toluene and the mixture was degassed via freeze-pump-thaw (3 cycles), backfilling with  $\text{N}_2$ . The reaction was heated to reflux under nitrogen atmosphere for 3 days, the end groups were capped by heating the mixture under reflux for 12 h with benzeneboronic acid (28.0 mg, 0.24 mmol) and then for 12 h with bromobenzene (37.0 mg, 0.24 mmol). The reaction mixture was cooled to room temperature and then precipitated with methanol. The precipitate was collected via centrifugation and the excess solvent was decanted off. The polymer was dried under vacuum and polymer was reprecipitated three times by dissolving in 50 mL of THF, concentrating to ca. 10 mL, precipitating with methanol, centrifuging, decanting and then drying under vacuum. The polymer was dried under vacuum to give 105.0 mg of purified material (**Scheme 2.11.**).



**Scheme 2. 11.** Synthesis of **P(F8-SFX)** by Suzuki–Miyaura coupling.

**P(F8-SFX):** Ashed colored solid. Yield 91.08 %.

$^1\text{H}$  NMR (400 MHz,  $\text{CDCl}_3$ ):  $\delta$  7.66-7.80 (m, 8H), 7.40- 7.56 (m, 8H), 7.24-7.36 (m, 8H), 6.64-6.71(m, 2H), 6.23-6.34(m, 4H), 3.92(t,  $J$  = 8.0 Hz, 4H), 1.71-1.94(m, 6H) 1.27-1.43 (m, 40 H), 0.87 (b, 6H).





## CHAPTER 3

### RESULTS AND DISCUSSION

#### 3.1. Electrochemical polymerization of 9-fluorencarboxylic acid and its electrochromic device application

##### 3.1.1. Electrochemical behavior of FCA and its electrochemical polymerization

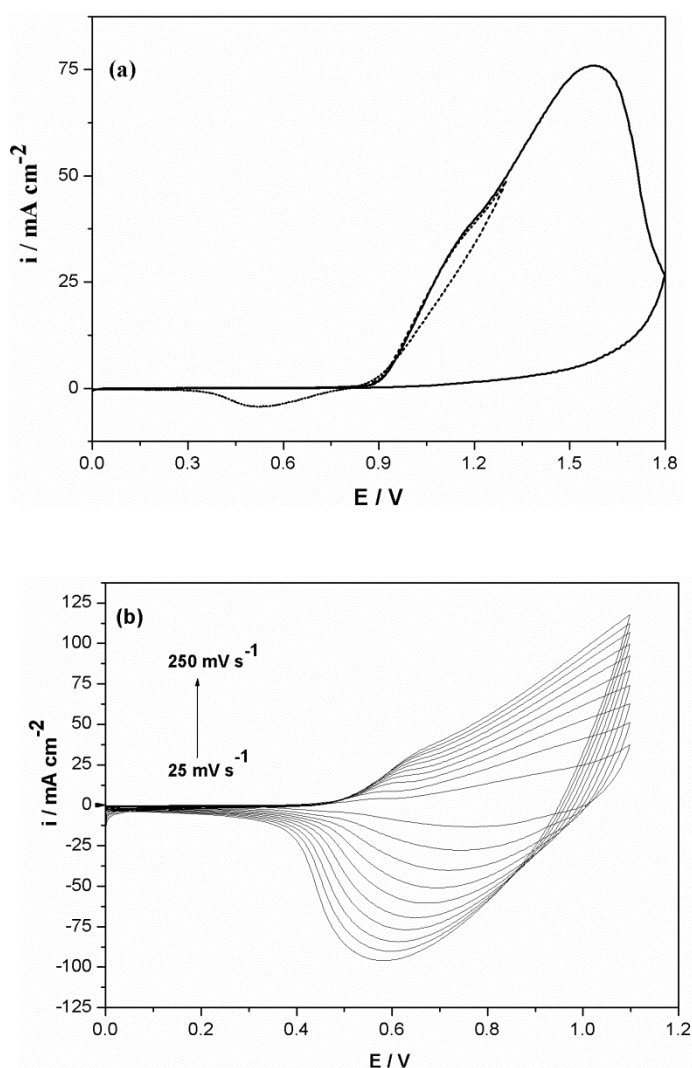


**Figure 3. 1.** Cyclic voltammograms of (a) FCA and (b) P(FCA) at scan rates from 25  $\text{mV/s}$  to 250  $\text{mV/s}$  in 25  $\text{mV}$  increments in 0.1 M TBABF<sub>4</sub> in nitromethane containing 4% BFEE.

Electrochemical behavior of **FCA** was investigated in nitromethane/BFEE solvent mixture (96/4-v/v) using 0.1 M TBABF<sub>4</sub> as supporting electrolyte. During the anodic scan two oxidation peaks at 1.20 and 1.55 V vs. Ag-wire were observed. A reduction peak was also noted during the reverse scan which intensified after scan reversal at 1.30 V. (**Figure 3.1(a)**). This reduction peak is accompanied with an oxidation peak during repetitive cycling between 0.0 and 1.30 V. This reversible peak gained intensity upon successive anodic scans, indicating deposition of conducting polymer on the WE. These observations imply that the first oxidation peak at 1.20 V can be ascribed to the oxidation of **FCA** and the second one could be due to the overoxidation of oligomeric species formed in the vicinity of the WE.

After repeated scans, the polymer coated WE was removed from the monomer solution and rinsed with nitromethane and ethanol to remove the oligomeric species and the electrolyte. The electrochemical behavior of the polymer film was investigated in monomer-free electrolyte solution. The polymer film was found to exhibit one a half wave of quasi reversible redox couple representing the doping and de-doping of the polymer film at 0.80 V vs. Ag-wire. It is found that both anodic and cathodic peak currents increase linearly with increasing scan rate, indicating that the redox process is non-diffusional and the polymer film is well-adhered to the WE (**Figure 3.1(b)**).

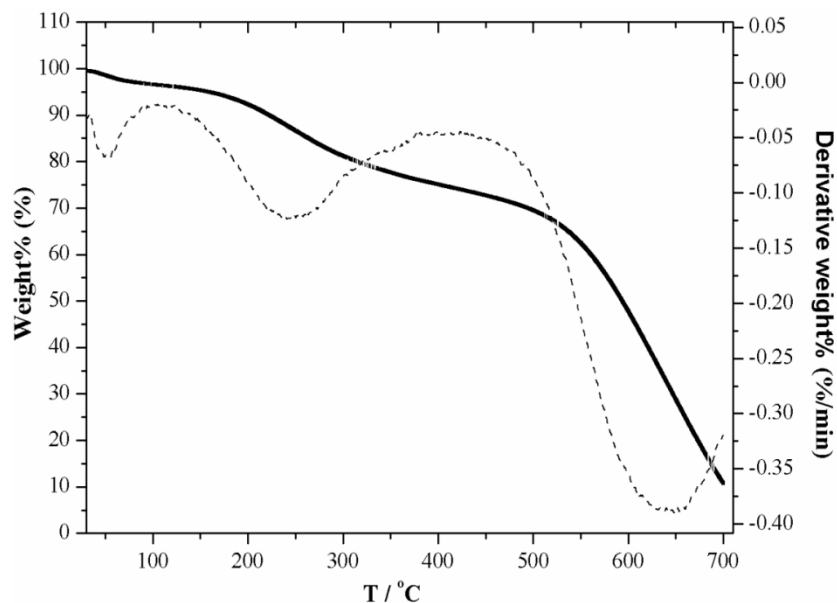
### 3.1.2. Polymer Characterization

The preparative formation of **P(FCA)** was achieved in the same solvent/electrolyte medium using 1.0 cm<sup>2</sup> Pt-plate working electrode. Constant potential electrolysis was used for this purpose and the optimum potential (1.15 V) was chosen on the basis of chronoamperometric investigations carried out under the same conditions used for CV studies. During electrolysis, a brownish-orange film is rapidly formed on the WE surface. The product was washed with nitromethane and ethanol and then dried under vacuum at 55 °C.

Most of the bands observed in the FT-IR spectrum of monomer are also present in that of the polymer. The peak at around 1700 cm<sup>-1</sup> in the polymer spectrum indicates the presence of C=O group. 1,2-disubstituted and 1,2,4-trisubstituted benzene absorption peaks are characteristic peaks, which arise from the in-plane and out-of-plane CH bending modes observed in the range of 730 and 850 cm<sup>-1</sup>. The 730 cm<sup>-1</sup> peak in the spectrum of the monomer belongs to the 1,2-disubstituted benzene ring. This peak loses its intensity and a peak appears at about 830 cm<sup>-1</sup>, attributed to 1,2,4-trisubstituted benzene ring. This indicates that **FCA** undergoes polymerization via 2,7-positions [85]. Also, the peak at 1083 cm<sup>-1</sup> corresponds to the vibration bands of the dopant ion, BF<sub>4</sub><sup>-</sup>.

### 3.1.3. Thermal Characterization

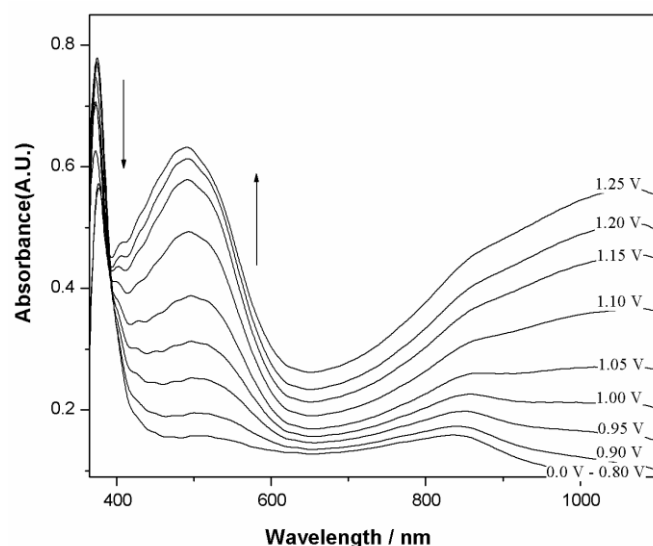
Thermal stability of **P(FCA)** was investigated utilizing TGA in the range of 30 °C and 750 °C. As seen from **Figure 3.2**, there are three-stage thermal degradation processes. The initial weight loss between 30 °C and 100 °C could be attributed to the loss of the moisture. The second weight loss occurs between 150 °C and 350 °C, which could be assigned to the loss of dopant anions, which was confirmed by the appearance of dopant related peak (1100 cm<sup>-1</sup>) in the FT-IR spectrum recorded for the evolved gases during TGA experiment. The last weight loss between 500 °C and 750 °C is because of the thermal degradation of the main polymer chain. These results indicate that **P(FCA)** has high thermal stability.



**Figure 3. 2.** Thermogram of **P(FCA)**.

#### 3.1.4. Spectroelectrochemical properties of **P(FCA)**.

**P(FCA)** films can be used as an active element in smart windows and electrochromic display devices on the basis of obtained electro-optical properties. For this aim, the polymer film ( $50 \text{ mC/cm}^2$ ) was deposited on ITO and its transition between the neutral (dedoped) and oxidized (doped) states was studied in monomer-free electrolyte solution.

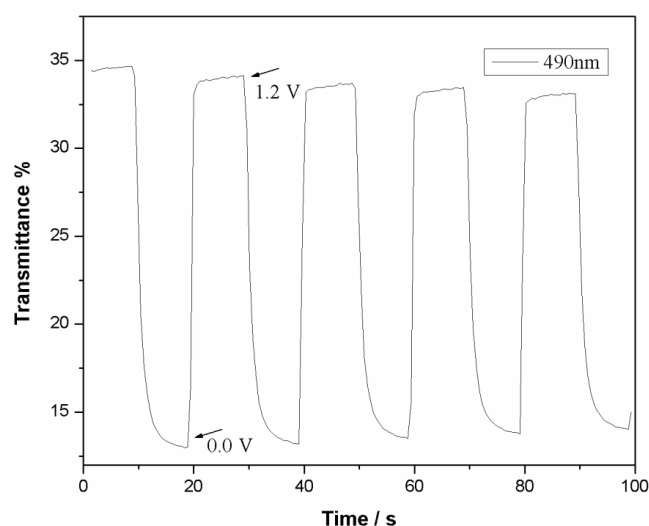


**Figure 3.3.** In-situ absorption spectra of **P(FCA)** ( $50 \text{ mC/cm}^2$  on ITO) recorded in  $0.1 \text{ M TBABF}_4$ /nitromethane containing 4% BFEE at various applied potentials.

**Figure 3.3** shows the in-situ absorption spectra of the polymer recorded at various applied potentials in terms of the reversible redox couple of **P(FCA)** between 0.0 V and 1.25 V in 0.1 M TBABF<sub>4</sub>/nitromethane containing 4% BFEE. **P(FCA)** forms smooth films on ITO that can be switched from a transparent neutral state to a brownish-orange oxidized state. In the neutral state, polymer film exhibits an absorption band at 374 nm due to the  $\pi$ - $\pi^*$  transition. From the commencement on the low energy end of the  $\pi$ - $\pi^*$  transition band in the neutral state, the band gap value of 3.1 eV was found. The evolution of the spectra upon electrochemical doping shows a simultaneous increase of the absorbance at 490 and 850 nm (2.53 eV and 1.46 eV), together with an isosbestic point at 391 nm indicating one step reaction due to polaron formation. Upon further doping (beyond 1.1 V) a broad band centered at 1066 nm starts to intensify indicating bipolaron formation [77].

### 3.1.5. Electrochromic switching of P(FCA) film in solution



Switching times and optical contrast in polymer film on ITO were determined with a change in transmittance at 490 nm in the visible region between redox states. Therefore, square wave potential step method was coupled with optical spectroscopy to investigate the switching ability of **P(FCA)** between its neutral and doped states (**Figure 3.4**).



**Figure 3. 4.** Optical response of **P(FCA)** at 490 nm as a function of time in 0.1 M TBABF<sub>4</sub>/nitromethane containing 4% BFEE under an applied square voltage signal between 0.0 V (the neutral state) and 1.2 V (the oxidized state).

The polymer film coated on ITO was reversibly switched between 0.0 V and 1.2 V vs. Ag-wire for each 10 s. The maximum transmittance difference between the oxidized and neutral states was found to increase with increasing polymerization charge. Values are commonly reported at 95% of a full switch, beyond which the naked eye cannot sense the difference. From this knowledge, both  $\Delta OD$  and  $\eta$  of the **P(FCA)** film coated on ITO were found to increase with increasing polymerization charge (**Table 3.1**). The time required to attain 95% of the total transmittance difference was found to be 4.9 s from the neutral to oxidized states and 1.2 s from the oxidized to neutral states. It shows that **P(FCA)** (50 mC/cm<sup>2</sup>) can be rapidly switched to the neutral state.

**Table 3.1** Voltammetric and SPEL data for **P(FCA)** in 0.1 M TBABF<sub>4</sub>/nitromethane containing 4% BFEE.

| Polymerization Charge (mC/cm <sup>2</sup> ) | T <sub>bleached</sub> | T <sub>colored</sub> | Δ%T  | ΔOD  | η (cm <sup>2</sup> /C) | neutral state   | oxidized state  |
|---|-----------------------|----------------------|------|------|------------------------|---|---|
| 12  | 51.7                  | 61.1                 | 9.4  | 0.07 | 143                    |  |  |
| 24  | 23.2                  | 34.2                 | 11   | 0.17 | 161                    |   |   |
| 36  | 25.0                  | 44.8                 | 19.8 | 0.25 | 178                    |   |   |
| 50  | 13.1                  | 34.1                 | 21   | 0.42 | 226                    |   |   |
| 75  | 8.5                   | 31.4                 | 22.9 | 0.57 | 232                    |   |   |

### 3.1.6. P(FCA) / PEDOT Electrochromic Device Application

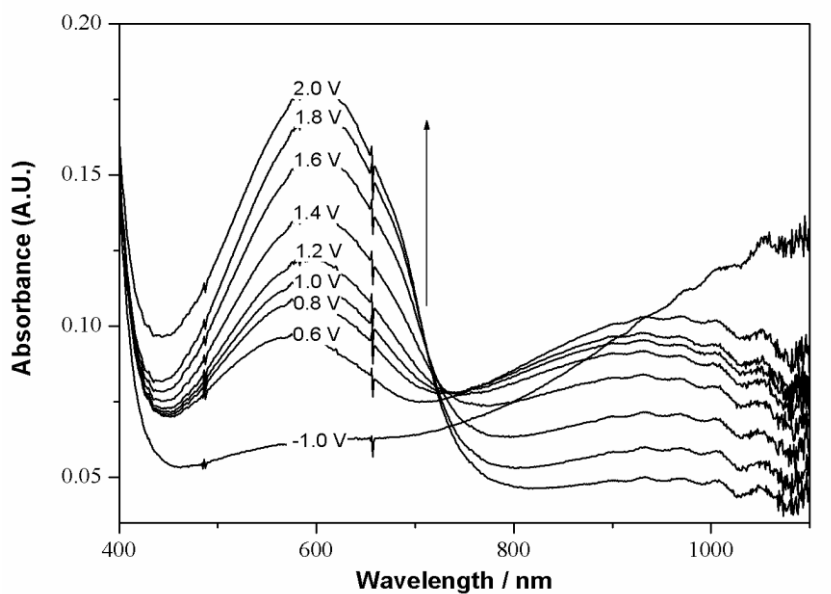


**Figure 3. 5.** Optical characterization of P(FCA) / PEDOT electrochromic device by applying potentials between  $-1.0$  V and  $+2.0$  V.

A dual type electrochromic device consisting of **P(FCA)** and PEDOT was constructed and its SPEL behavior was investigated by recording the optical absorbance spectra at different applied potentials. Electrochromic device showed a more reversible response in a potential range of  $-1.0$  V (neutral) and  $2.0$  V (oxidized) in **Figure 3.5**. At  $-1.0$  V, the polymer was transparent and

PEDOT was also transparent in its oxidized state; therefore, the device at  $-1.0$  V was transparent. As the applied potential was increased, an absorption band at  $600$  nm was observed due to the neutral state of PEDOT layer. The color of the device at  $2.0$  V became dark blue.

Kinetic studies were done in order to determine the response time needed to perform switching between the colored states and optical contrast of device. Under a square potential input of  $-1.0$  V and  $2.0$  V with a residence time of  $10$  s at each potential, the optical response at  $600$  nm for the device was monitored in **Figure 3.6**. The switching time was calculated as  $2.5$  s at  $90\%$  of the maximum transmittance for neutral state and  $2.0$  s for oxidized state and the optical contrast was calculated as  $30\%$ .

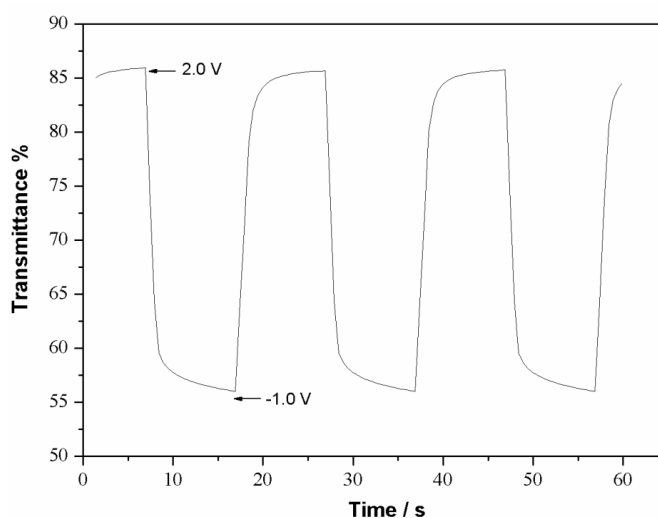


**Figure 3. 6.** Optical response of **P(FCA) /PEDOT** electrochromic device at  $600$  nm as a function of time under an applied square voltage signal between  $-1.0$  V (transparent) and  $+2.0$  V (dark blue color) with a switch time of  $10$  s.

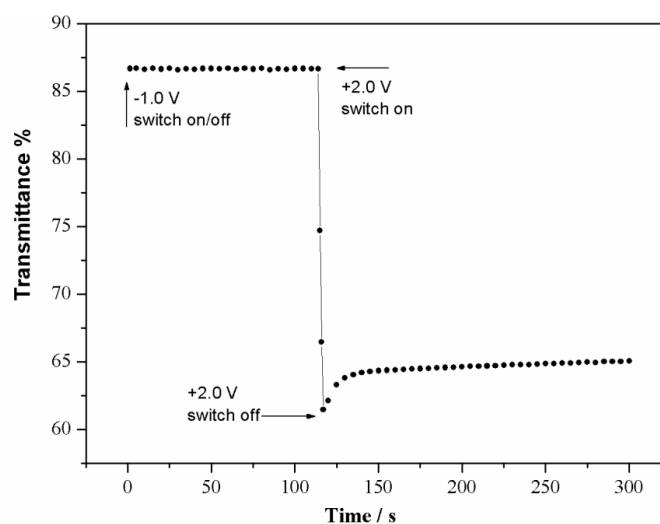


**Figure 3. 7.** Open circuit memory of **P(FCA)/PEDOT** device after applying  $-1.0$  V and  $+2.0$  V for  $5$  s, respectively.

The optical memory is an important parameter to characterize an electrochromic device. The optical memory was measured when the device retains its color under open circuit conditions. Device shows quite a good optical memory in the neutral state with almost no transmittance. It also device has a good optical memory in the oxidized state with a slow decrease in transmittance up to a certain value. For example, transmittance changes at 600 nm when polarized by an applied pulse for 5 s and then kept under open circuit conditions; device keeps its blue color without significant loss, retaining 80% of its optical activity for 24 h. This means that for practical purposes the device wouldn't need a refreshing current for maintaining its color for both neutral (transparent) and oxidized (dark blue) states (see **Figure 3.7**).

### 3.2. D-A-D type Polyfluorene derivatives

#### 3.2.1. Fluorenone functionalized D-A-D type Polyfluorene derivatives

The first group of D-A-D type fluorene derivatives consists of fluorenone as the acceptor unit and three different (thiophene, EDOT and ProDOT) donor units.

##### 3.2.1.1. Electrochemical behavior of TFT, EFE and PFP

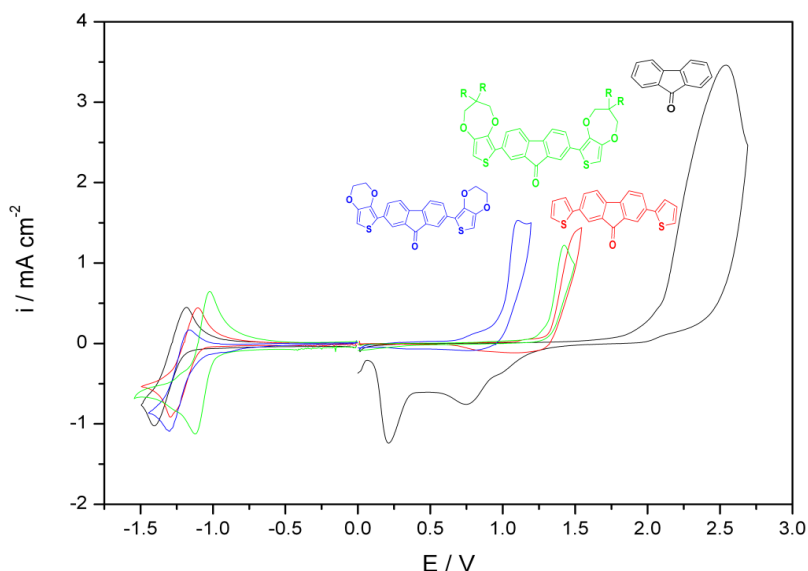


**Figure 3. 8.** First oxidation potential comparison of **FO**, **TFT**, **EFE** and **PFP** in 0.1 M TBAPF<sub>6</sub>/DCM at 100 mV/s onto a Pt disc (area = 0.02 cm<sup>2</sup>) vs. Ag/AgCl.

Prior to electrochemical polymerization, electrochemical behavior of the monomers were investigated not only to find the suitable polymerization potential but also to understand the effect of different donor units on the electrochemical behavior of the monomers. The cyclic voltammograms of **FO**, **TFT**, **EFE** and **PFP** were recorded in 0.1 M TBAPF<sub>6</sub> dissolved in DCM for this purposes and the results are depicted in **Figure 3.8**. An inspection of **Figure 3.8** reveals that, the oxidation potentials for **TFT**, **EFE** and **PFP** are much lower than that of **FO**, indicating clearly the effect of donor units on the ease of oxidation of monomers. Among the four monomers investigated, **EFE** has the lowest first oxidation potential indicating that EDOT is a stronger donor unit than ProDOT. On the other hand, reversible reduction peaks due to formation of stable radical anions are very close for the monomers investigated, which shows that the acceptor group, **FO**, is determining the ease of reduction process, as expected.

### 3.2.1.2. Electrochemical polymerization of TFT, EFE and PFP

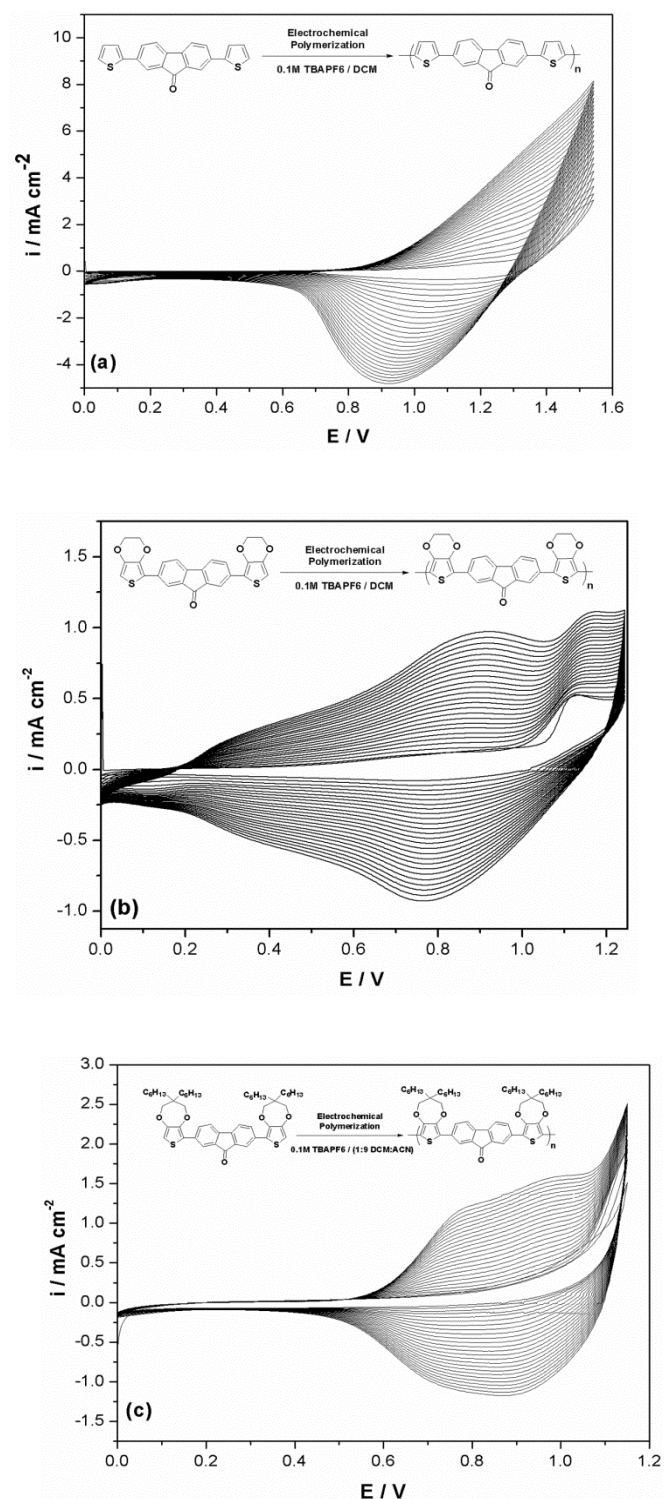


**Figure 3. 9.** Electropolymerization of 10 mM (a) **TFT** (b) **EFE** in 0.1 M TBAPF<sub>6</sub> / DCM (c) **PFP** in 0.1 M TBAPF<sub>6</sub> / DCM / ACN (1/9-v/v) at 100 mV/s by potential scanning to give **P(TFT)**, **P(EFE)**, and **P(PFP)**, respectively.



The electrochemical polymerization of **TFT** and **EFE** were achieved in electrolyte solution consisting of 0.1 M TBAPF<sub>6</sub> dissolved in DCM via repetitive cycling. In the case of **PFP**, 0.1 M TBAPF<sub>6</sub> dissolved in DCM /ACN mixture (1:9 by volume) was used as the electrolytic medium. Polymer films, **P(TFT)**, **P(EFE)** and **P(PFP)**, were deposited on the WE surface via potential cycling from 0.0 V to 1.50 V (for **TFT**); 0.0 V to 1.25 V (for **EFE**); 0.0 V to 1.15 V (for **PFP**). New intensifying redox couples were also observed during successive scans. The increase in the current intensities of this new redox couples clearly indicated the formation of the polymer films, **P(TFT)**, **P(EFE)** and **P(PFP)**, on the electrode surface (**Figure 3.9**).

### 3.2.1.3. Electrochemical behaviour of **P(TFT)**, **P(EFE)** and **P(PFP)**

After electrodeposition, the polymer film coated electrode was washed with ACN to remove any unreacted monomer and oligomeric species. The redox behavior of polymer films were investigated by recording the cyclic voltammograms in monomer free electrolytic solution and the results are given in **Figure 3.10**. In order to represent the ability of n- and p- type doping of the polymer films, they were scanned both anodically and cathodically in the monomer free solution of 0.1 M TBAPF<sub>6</sub>/ACN.

When **P(TFT)**, **P(EFE)**, and **P(PFP)** were scanned anodically in monomer-free electrolyte solution, they exhibited well-defined quasi-reversible redox couples due to p-doping ( $E_{pa} = 1.2$  V for **P(TFT)**;  $E_{pa} = 0.75$  V for **P(EFE)** and  $E_{pa} = 0.65$  V for **P(PFP)**). A linear increase in the peak currents as a function of the scan rates confirmed well-adhered electroactive polymer films on the electrode surface as well as non-diffusional redox process (**Figure 3.10 insets (a)**).

The redox behaviors of **P(TFT)**, **P(EFE)**, and **P(PFP)** were also examined during n-doping in **Figure 3.10**. The polymer films showed well-defined reversible n-doping process. ( $E_{pc} = -1.35$  V for **P(TFT)**;  $E_{pc} = -1.40$  V for **P(EFE)** and  $E_{pc} = -1.48$  V for **P(PFP)**). During n-doping process, it was observed that intensities of the anodic and cathodic peak currents were increasing linearly as a function of scan rate, proving that redox process was non-diffusion-controlled (**Figure 3.10 insets (b)**).

These results indicate that the donor units of the polymer films during p doping process are dominant depending on the donor strength of Th, EDOT, and ProDOT. However, in the case of n-doping process, the values did not change too much. N-type doping process was also confirmed and supported by SPEL studies as well as CV measurements.

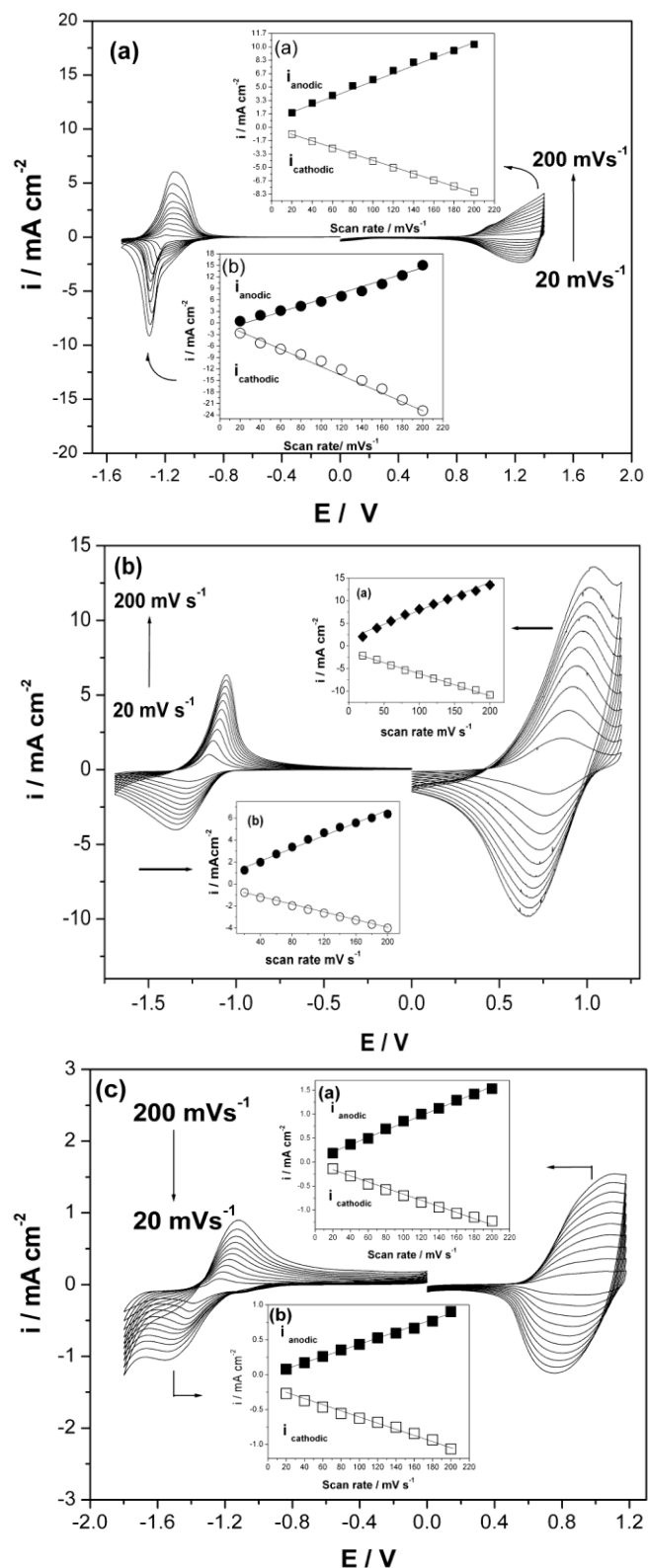


**Figure 3. 10.** Scan rate dependence study for (a) P(TFT), (b) P(EFE) and (c) P(PFP) in 0.1 M TBAPF<sub>6</sub>/ACN at applied scan rates between 20 mV/s and 200 mV/s in 20 mV increments. Insets: relationship of anodic ( $i_{\text{anodic}}$ ) and cathodic ( $i_{\text{cathodic}}$ ) current peaks as a function of scan rate for (a) p-doped (b) n-doped films in 0.1 M TBAPF<sub>6</sub>/CAN.

### 3.2.1.4. Band gap analysis of P(TFT), P(EFE) and P(PFP) via electrochemical methods

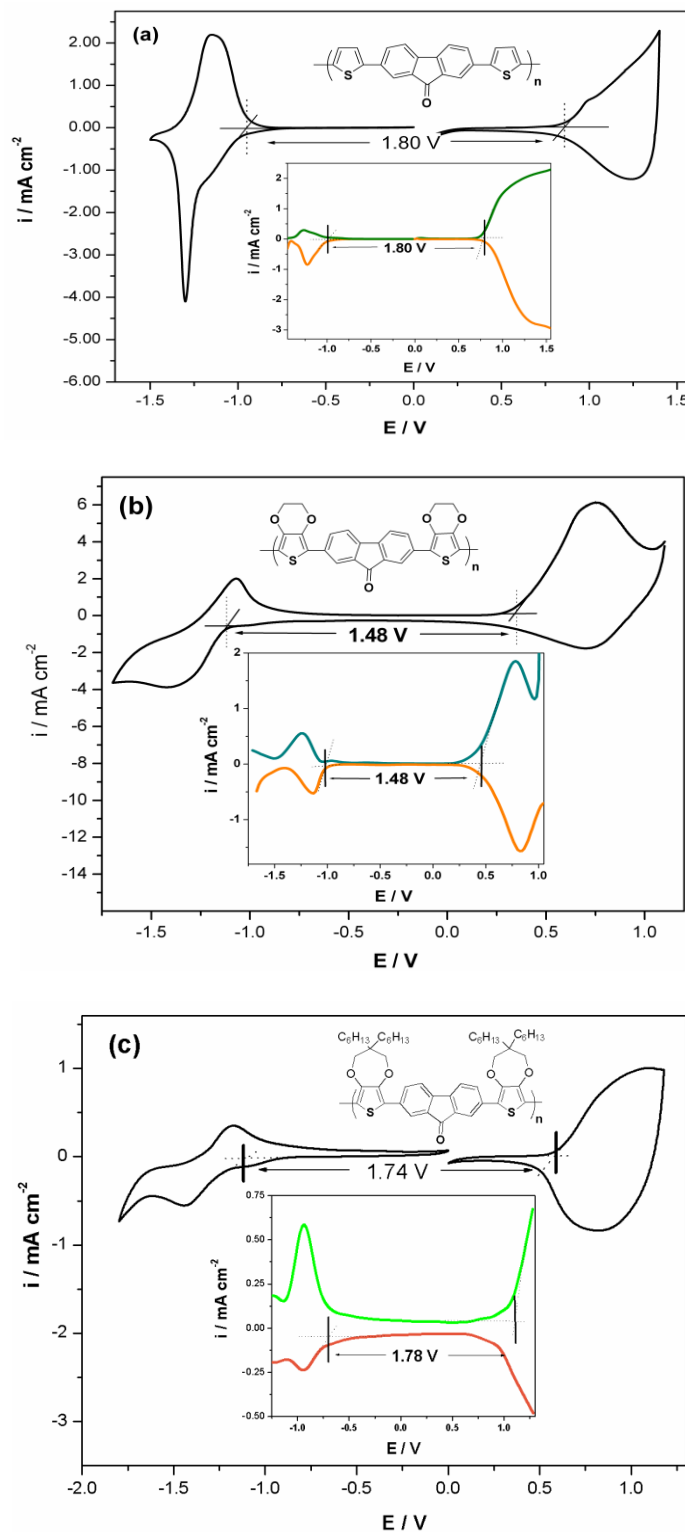


**Figure 3. 11.** Cyclic voltammograms of p- and n-doped (a) P(TFT), (b) P(EFE) and (c) P(PFP) films in TBAPF<sub>6</sub>/ACN at scan rate 100 mV/s. Insets: differential pulse voltammetry of p- and n-doped films in TBAPF<sub>6</sub>/ACN with a step time of 0.1 s and a step size of 10 mV.

The linear correlation between the scan rate and anodic peak current supports the idea that the rate of the redox processes is surface bound. It means that the onset of oxidation value changes with increasing scan rate. For that reason, the onset of oxidation was also determined by DPV. The cyclic voltammogram of the films at a scan rate of  $100 \text{ mV s}^{-1}$  were investigated and compared with the data of DPV. Electrochemical measurements, both DPV and CV, revealed very close values for all polymers (**Figure 3.11** and its insets). These values are lower than that of **PFO** [85] due to band gap lowering effect of donor-acceptor arrangement.

#### 3.2.1.5. Band gap analysis of **P(TFT)**, **P(EFE)** and **P(PFP)** via spectroelectrochemical methods

In order to elucidate the electrochromic features and to get information about charge carriers polymer films were deposited on ITO working electrode via potential cycling and the transitions between the neutral (dedoped), oxidized (p-doped) and reduced (n-doped) states were studied in monomer-free electrolyte solution and the results were depicted in **Figure 3.12**.

The changes in the electronic absorption spectrum were recorded during potential scanning from 0.0 V to 1.4 V with a voltage scan rate of  $100 \text{ mV/s}$  and the results are depicted in **Figure 3.12 a**. An inspection of figure reveals that **P(TFT)** film, in its neutral state, exhibits two absorption bands at 412 nm and a shoulder at 520 nm, which correspond to internal charge transfer between donor and acceptor groups [59]. The  $E_g$  of the **P(TFT)** was found as 2.00 eV by the commencement on the low energy end of the  $\pi-\pi^*$  transitions at 520 nm. Upon increasing the potential, the color of the **P(TFT)** film turns from yellow to green, which is accompanied with the corresponding changes in the absorption bands. The promising n-doping property of the **P(TFT)** film, observed with CV, was also confirmed by in-situ monitoring the UV-vis spectra during reduction process (see inset of **Figure 3.12 (a)**).

For **P(EFE)**, the electronic absorption spectrum of the neutral form of the polymer film consists of a broad band at about 466 nm due to  $\pi-\pi^*$  transition followed by a shoulder at 555 nm as shown in **Figure 3.12 b**. The evolution of the spectra upon electrochemical doping shows a simultaneous decrease of the absorbance at 466 nm, which is accompanied by the formation of a new ill-defined absorption band at 800 nm in the potential range  $-0.20 \text{ V}$  to  $0.40 \text{ V}$  indicating the formation of charge carriers. Upon further doping, this band undergoes a blue shift to 620 nm and a new broad band beyond 1006 nm starts to intensify due to further formation of charge carriers. The polymer film also exhibits a color change from brown (neutral) to blue (oxidized). All spectra recorded during potential cycling between  $-0.2 \text{ V}$  and  $1.2 \text{ V}$  passes through a clear isosbestic points at 520 nm, indicating that polymer film was being interconverted between its neutral and oxidized states. The  $E_g$  was found to be 1.68 eV from the commencement on the low energy end of 555 nm band. The n-doping behavior of the **P(EFE)** film was also confirmed by recording the changes in the electronic absorption spectrum during reduction. When the polymer film was reduced its color changes from brown to yellow. These color changes are accompanied with the corresponding changes in the absorption bands. The band at 570 nm began to decrease and the band at 454 nm started to intensify. A new intensifying absorption band centered at 728 nm was also noted with a concomitant appearance of an isosbestic point at 533 nm which indicates the presence of only two phases during the n-doping process (see inset of **Figure 3.12 (b)**).

It is interesting to note that the changes in the electronic absorption spectrum of **P(TFT)** and **P(EFE)** recorded during n-doping are not symmetrical as the one recorded during p-doping. Although this observation seems to be unexpected, there are also examples in which spectral changes for p- and n-doping are not symmetrical [134] and [135]. One of the reasons for such contradictory observations might be the change in the band gap [136].

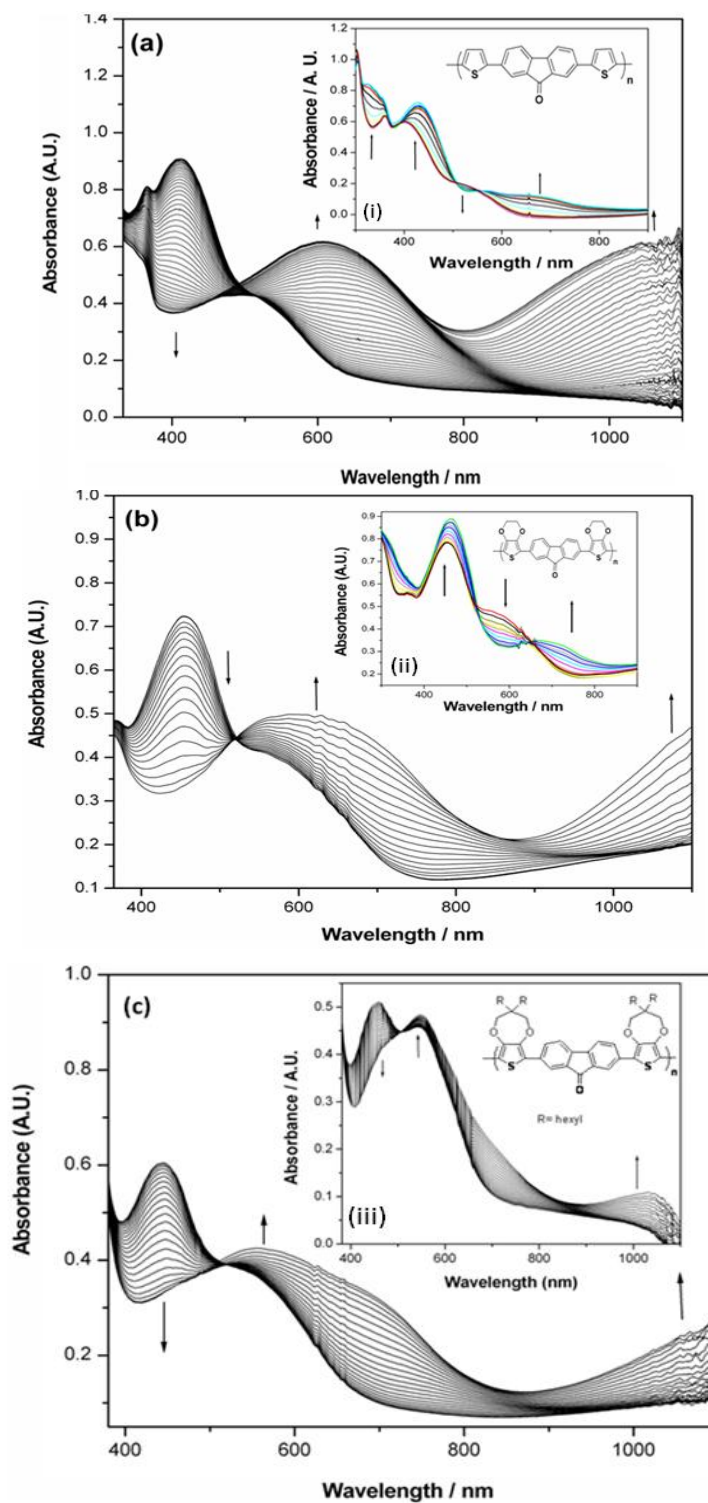
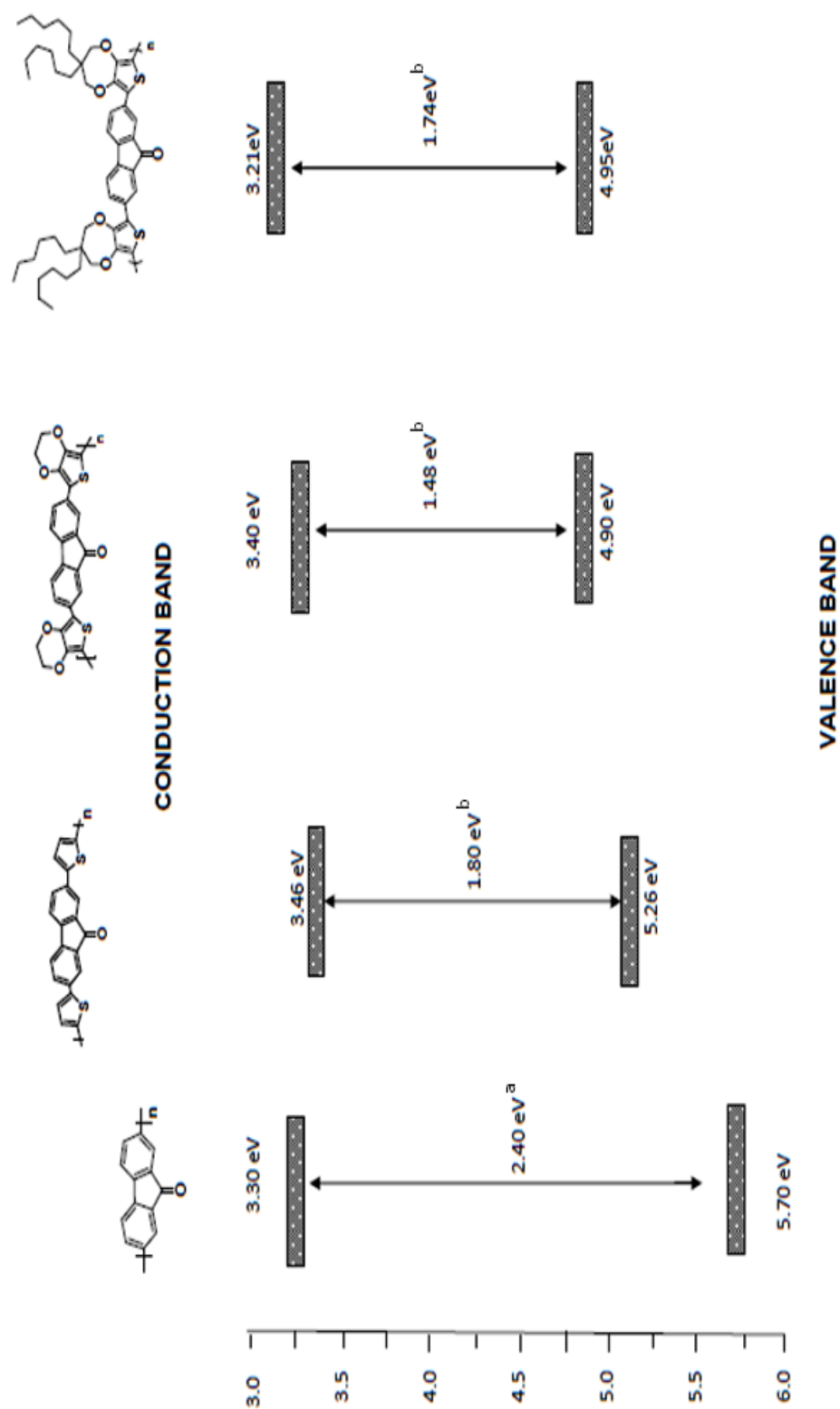


**Figure 3. 12.** Electronic absorption spectra of (a) P(TFT) ( between 0 V and 1.4 V ), (b) P(EFE) (between 0 V and 1.10 V ) and (c) P(PFP) ( between 0 V and 1.10 V ) films on ITO in 0.1 M TBAPF<sub>6</sub>/ACN at various applied potentials. Inset: Electronic absorption spectra of (i) P(TFT) ( between 0 V and -1.5 V ) (ii) P(EFE) ( between 0 V and -1.6 V ) and (iii) P(PFP) ( between 0 V and -1.8 V ) films on ITO in 0.1 M TBAPF<sub>6</sub>/ACN (50 cycles) on ITO in 0.1 M TBAPF<sub>6</sub>/ACN at various applied potentials.

In the case of **P(PFP)**, the electronic absorption spectrum of neutral form of **P(PFP)** film exhibits an absorption band at 445 nm due to  $\pi$ - $\pi^*$  transition and a shoulder at 540 nm as shown in **Figure 3.12 c**. Upon oxidation, the valance-conduction band at 445 nm diminishes and a new band starts to intensify at about 740 nm in the potential range 0.0 to 0.40 V due to formation of charge carriers. Upon further doping, this band undergoes a blue shift to 620 nm and a new broad band beyond 1040 nm starts to intensify due to further formation of charge carriers. All spectra recorded during potential cycling between 0.0 and 1.2 V passes through a clear isosbestic points at 516 nm, indicating that polymer film was being interconverted between its neutral and oxidized states. The changes in the electronic absorption spectra of **P(PFP)** film is also accompanied by a color change from orange to dark blue indicating that **P(PFP)** film exhibits electrochromic behavior. The n-doping behavior of the **P(PFP)** film was also confirmed by recording the changes in the electronic absorption spectra during cathodic scan from 0.0 to -1.8 V vs Ag/AgCl. Upon reduction the intensity of 445 nm band starts losing its intensity which is accompanied by the formation of an ill defined band at about 760 nm during the potential cycling from 0.0 to -0.95 V with a concomitant appearance of an isosbestic point at 505 nm. Appearance of a new absorption band at 1040 nm beyond -0.95 V was also noted (see inset of **Figure 3.12 c**). Although there are several examples reporting unsymmetrical changes during p and n doping [137, 138], in the case of **P(PFP)**, the changes recorded during n doping is very similar to the one recorded during p doping.

### 3.2.1.6. Energy band diagram of polymers

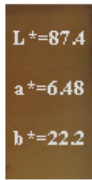
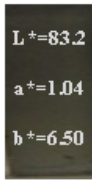
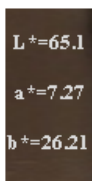
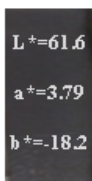
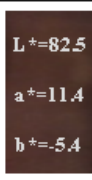
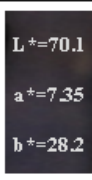
The band gaps ( $E_g$ ) of **P(TFT)**, **P(EFE)**, and **P(PFP)** were calculated from the onset of the low energy end of the  $\pi$ - $\pi^*$  transitions to be 2.00 eV, 1.68 eV, and 1.79 eV, respectively, which were in well agreement with the band gaps calculated from cyclic voltammogram and DPV data. It can be easily concluded that the smallest band gap can be obtained when EDOT units were attached. It may be because of the effective intramolecular charge transfer between the D and the A units. Oxidation potentials are reported vs.  $\text{Fc}/\text{Fc}^+$  to calculate of HOMO and LUMO levels of polymers. The energy level of  $\text{Fc}/\text{Fc}^+$  was taken as 4.4 eV below vacuum [137]. The oxidation onset potential of  $\text{Fc}/\text{Fc}^+$  was measured as 0.36 V vs. Ag/AgCl. HOMO and LUMO energy levels were obtained from the onset potential of the oxidation and reduction potentials of polymers, respectively (**Figure 3.13**).



**Figure 3.13.** SPEL and electrochemical data for various fluorene derivatives. <sup>a</sup> The band gap was obtained from SPEL data <sup>b</sup> Calculated from CV measurements.

### 3.2.1.7. Spectroelectrochemical and Switching Behaviors of Polymers P(TFT), P(EFE) and P(PFP)

**Table 3. 2** Optical and switching time data of electrochemically synthesized **P(TFT)**, **P(EFE)**, and **P(PFP)**.

| Polymer       | $\lambda_{\max}$<br>(nm) | $\eta$<br>(cm <sup>2</sup> / C) | Switching<br>time<br>(s) | Color   |   |
|---------------|--------------------------|---------------------------------|--------------------------|---|---|
|               |                          |                                 |                          | Neutral   | Oxidized  |
| <b>P(TFT)</b> | 394                      | 6.71                            | 2.9                      | <br>L <sup>+</sup> =87.4<br>a <sup>+</sup> =6.48<br>b <sup>+</sup> =22.2   | <br>L <sup>+</sup> =83.2<br>a <sup>+</sup> =1.04<br>b <sup>+</sup> =6.50   |
|               | 697                      | 46.80                           | 8.6                      |   |   |
|               | 1050                     | 9.32                            | 1.6                      |   |   |
| <b>P(EFE)</b> | 462                      | 250.0                           | 4.8                      | <br>L <sup>+</sup> =65.1<br>a <sup>+</sup> =7.27<br>b <sup>+</sup> =26.21 | <br>L <sup>+</sup> =61.6<br>a <sup>+</sup> =3.79<br>b <sup>+</sup> =18.2  |
|               | 697                      | 242.6                           | 1.9                      |   |   |
|               | 1050                     | 217.7                           | 2.3                      |   |   |
| <b>P(PFP)</b> | 441                      | 144.0                           | 3.1                      | <br>L <sup>+</sup> =82.5<br>a <sup>+</sup> =11.4<br>b <sup>+</sup> =5.4  | <br>L <sup>+</sup> =70.1<br>a <sup>+</sup> =7.35<br>b <sup>+</sup> =28.2 |
|               | 684                      | 422.0                           | 1.9                      |   |   |
|               | 1050                     | 93.0                            | 3.2                      |   |   |

Due to its importance in electrochromic applications, switching times and optical contrast of polymeric films on ITO were also investigated under square wave input of determined potential ranges in 10 s intervals by monitoring the transmittance and the kinetic responses of the film at given wavelengths in **Table 3.2**. As seen in **Figure 3.14**, **P(PFP)** film shows a reversible response within the range of applied potential pulses with a response time of 1.9 s at 95% of the maximum transmittance and the optical contrast ( $\Delta\%T$ ) was 22.7%, 28.8% and 25.4% at 441, 684 and 1050 nm, respectively. It is noteworthy that these values did not change within the applied potential regime, indicating the optical stability of **P(PFP)** film. Besides response time and optical contrast,  $\eta$  a measure of power efficiency, is also important for electrochromic materials. **P(PFP)** has  $\eta$  of 144 and 92.8 cm<sup>2</sup>/C at 441 and 1050 nm, respectively. On the other hand, at 684 nm, its  $\eta$  was found to be 422 cm<sup>2</sup>/C (95% of the full switch), which is much higher than that of most inorganic and polymeric electrochromics [138].  $\eta$  values for all PF derivatives with different donor groups are tabulated in **Table 3.2** for comparison reasons. Among the three derivatives **P(PFP)** exhibits highest value (422 cm<sup>2</sup>/C) indicating that **P(PFP)** is a promising candidate for electrochromic device applications.



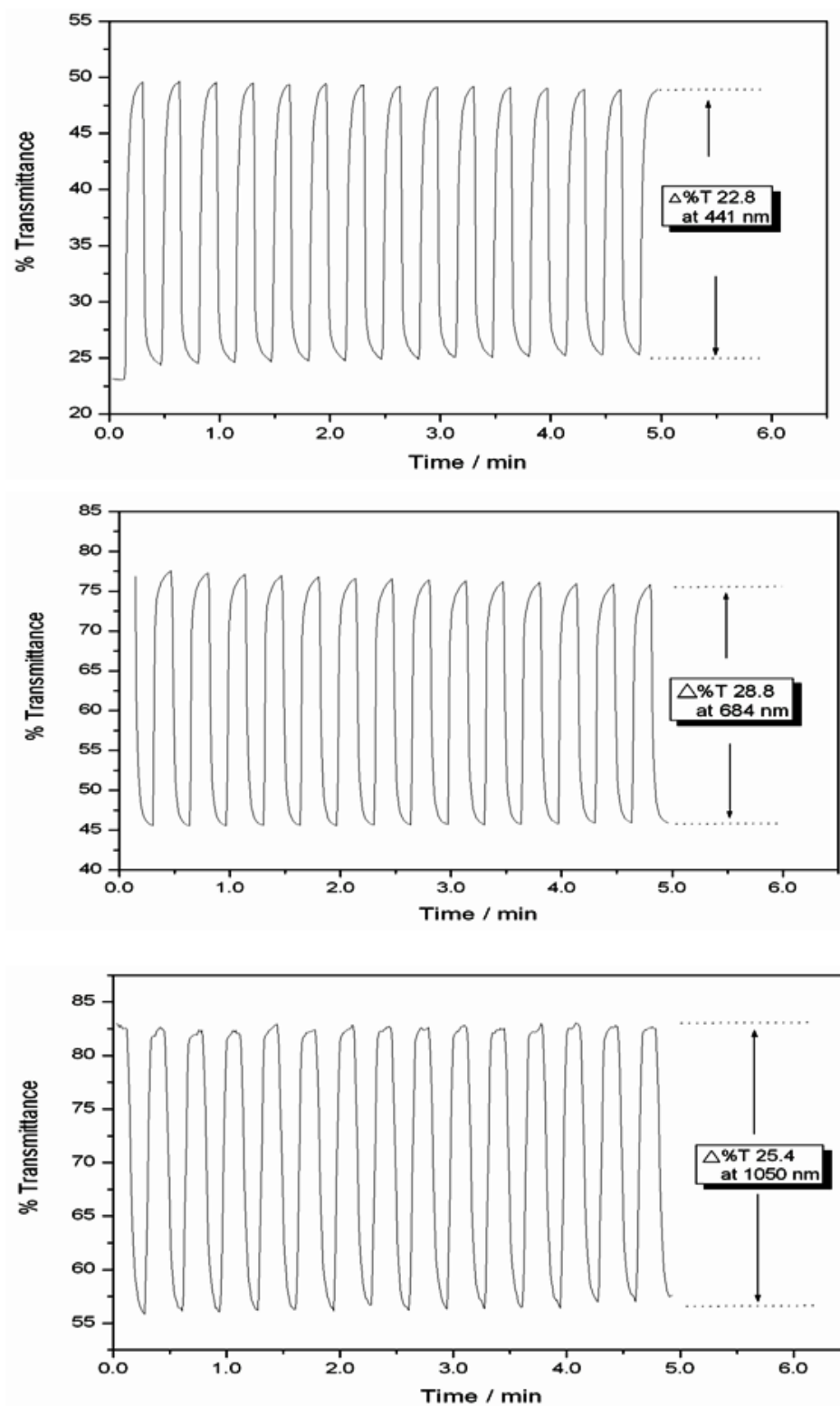


**Figure 3. 14.** Chronoaabsorptometry experiments for P(PFP) on ITO in 0.1 M TBAPF<sub>6</sub> / ACN while the polymer was switched between -0.2 V and 1.2 V with a switching time of 10 s during 5 minutes at 441 nm, 684 nm and 1050 nm.

### 3.2.1.8. Fluorescence Properties of Polymers P(TFT), P(EFE) and P(PFP)

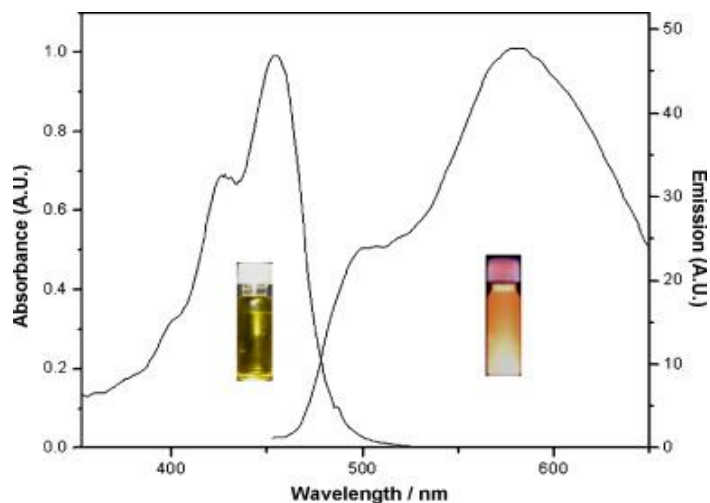


**Figure 3. 15.** Emission (excited at 420 nm) and absorption spectra of **P(EFE)** in THF.

Since the electrochemically synthesized **P(EFE)** film was found to be partially soluble in THF, its fluorescence property was also investigated and its absorption/emission spectrum recorded in this solvent is depicted in **Figure 3.15**. As it seen from **Figure 3.15**, excitation at 420 nm resulted in the formation of a weak and relatively intense emission bands at about 500 nm and at 580 nm. The higher wavelength emission band corresponds to orange color indicating that this partially soluble polymer is an orange light emitter.

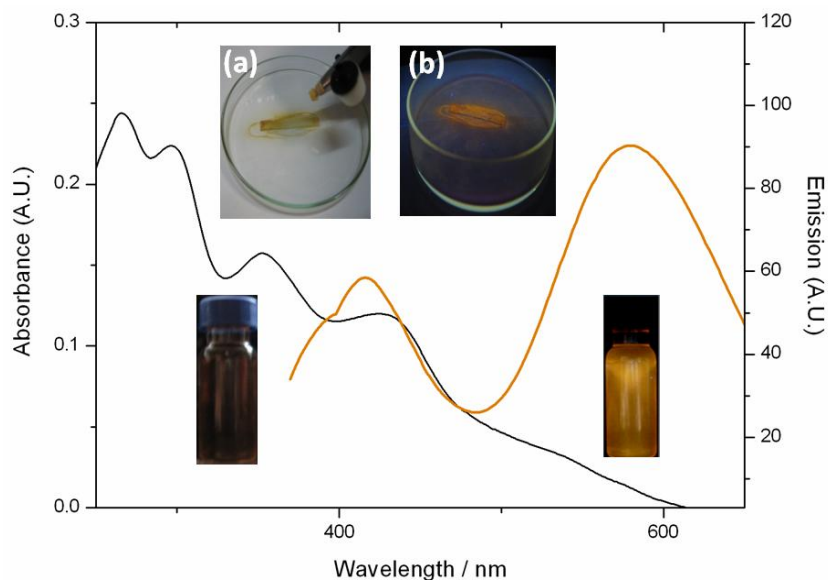


**Figure 3. 16.** Emission (excited at 355 nm) and absorption spectra of **P(PFP)** in THF. Inset (a) spray coating of **P(PFP)** in THF (b) photograph of **P(PFP)** under UV light.

Electrochemically obtained polymer **P(PFP)** on the other hand, was quite soluble in common organic solvents: DCM, THF,  $\text{CHCl}_3$ , and DMF. Its fluorescence property was also investigated. The absorption/emission spectrum **P(PFP)** dissolved in THF is shown in **Figure 3.16**. As it seen from the figure, excitation at 355 nm resulted in the formation of a weak and relatively intense emission bands at about 420 and 577 nm, respectively. The higher wavelength emission band corresponds to orange color, indicating that this soluble polymer is an orange light emitter. This orange emission is clearly seen in the inset of **Figure 3.16**.

### 3.2.2. Fluoren-quinoxaline functionalized D-A-D type Polyfluorene derivatives

Electrochemical polymerization of **TQT**, **EQE** and **PQP** were achieved via potential cycling and electrochemical, electro-optical and electrochromic properties of their corresponding polymers were investigated using CV and in-situ SPEL techniques. Furthermore, the fluorescence properties of **PQP** and its polymer were investigated in THF. The effect of various metal cations on the fluorescence intensity was also determined.

#### 3.2.2.1. Electrochemical behavior of FQ, TQT, EQE and PQP

The electrochemical behavior of fluorene based monomers bearing quinoxaline moieties, **FQ**, **TQT**, **EQE** and **PQP**, were investigated by CV in an electrolyte solution consisting of 0.1 M  $\text{TBAClO}_4$  dissolved in ACN. During the first anodic scan **FQ** exhibits a quasi reversible (about 1.0 V vs. Ag/AgCl) and an irreversible oxidation peak (at about 1.80 V vs. Ag/AgCl) as shown in **Figure 3.17**. The latter could be ascribed to the loss of an electron from the fluorene based electroactive centers. On the other hand, the quasi reversible peak corresponds to the loss of electrons from the quinoxaline moiety of the monomer (see inset of **Fig. 3.17**). When donor side groups are attached to 2 and 7 positions of fluorene moiety, the irreversible peak shifts to lower potentials as expected, with almost no appreciable change in the position of quasi- reversible peak.

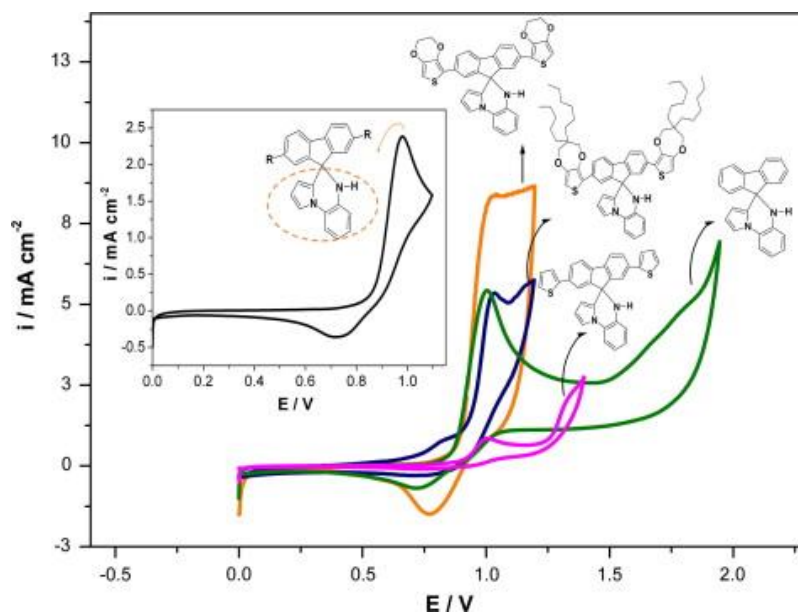


**Figure 3. 17.** Cyclic voltammograms of **FQ**, **TQT**, **EQE** and **PQP** on a Pt disk electrode at 100 mV/s in 0.1 M  $\text{TBAClO}_4/\text{ACN}$  vs. Ag / AgCl. (Insets: Cyclic voltammogram of **FQ**, after peak clipping at 1.10 V.)

### 3.2.2.2. Electrochemical polymerization of TQT, EQE and PQP

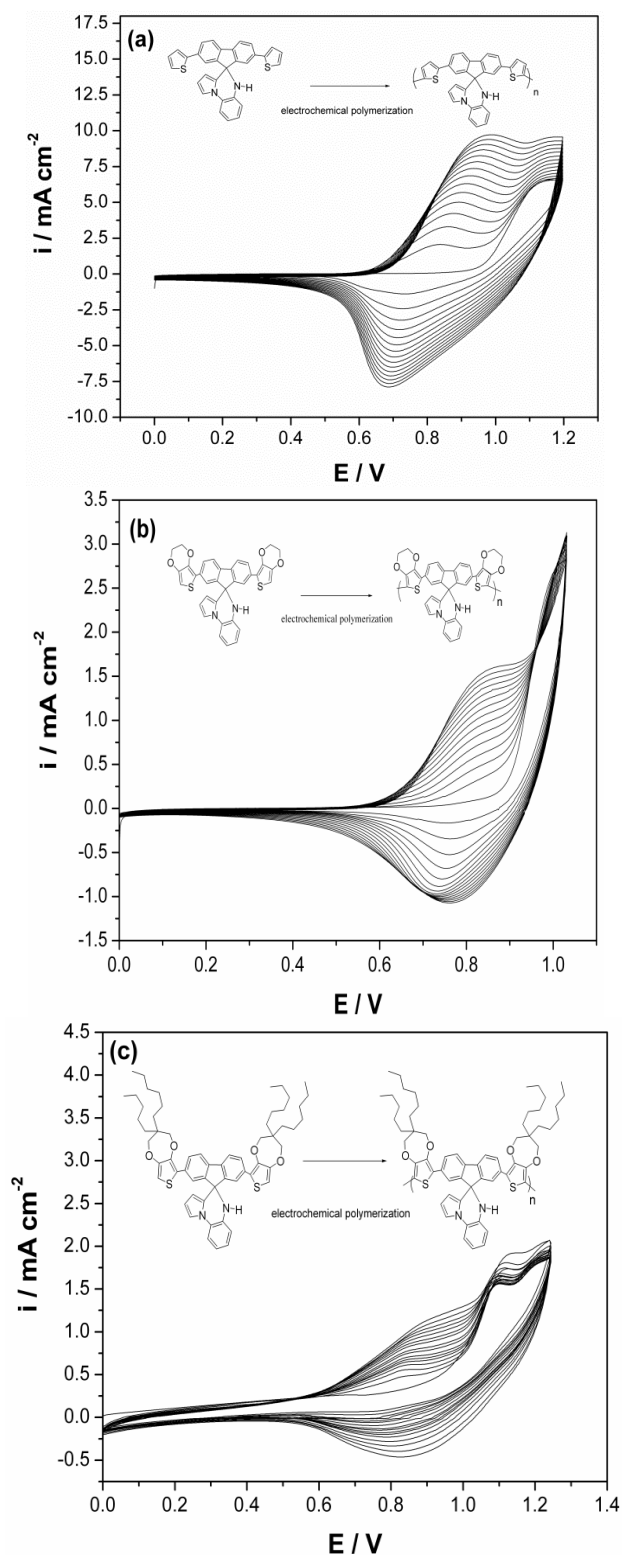


**Figure 3. 18.** Repeated potential scan electropolymerization of 2 mM (a) TQT in 0.1 M TBAClO<sub>4</sub>/ACN:BFEE;1:1, (b) EQE in 0.1 M TBAClO<sub>4</sub>/ACN (c) PQP in 0.1 M TBAPF<sub>6</sub>/ACN on a Pt disk electrode at 100 mV/s.

The electrochemical polymerization of **EQE** and **PQP** were achieved in an electrolyte solution consisting of 0.1 M TBAClO<sub>4</sub> and TBAPF<sub>6</sub>, respectively, dissolved in ACN via repetitive cycling. On the other hand, for the electrochemical polymerization of **TQT**, a 1:1 (v:v) mixture of ACN/BFEE was used in the presence of 0.1 M TBAClO<sub>4</sub> as supporting electrolyte to improve the film quality. As shown in **Figure 3.18**, during second anodic scan, new reversible redox couples appeared around 0.8 V, and after each successive scan, the peak currents were intensified, indicating the formation of an electroactive polymer film on the working electrode with increasing polymer film thickness. After electrodeposition, the polymer film coated electrodes were washed with ACN to remove any unreacted monomer and oligomeric species.

### 3.2.2.3. Electrochemical behaviour of P(TQT), P(EQE) and P(PQP)

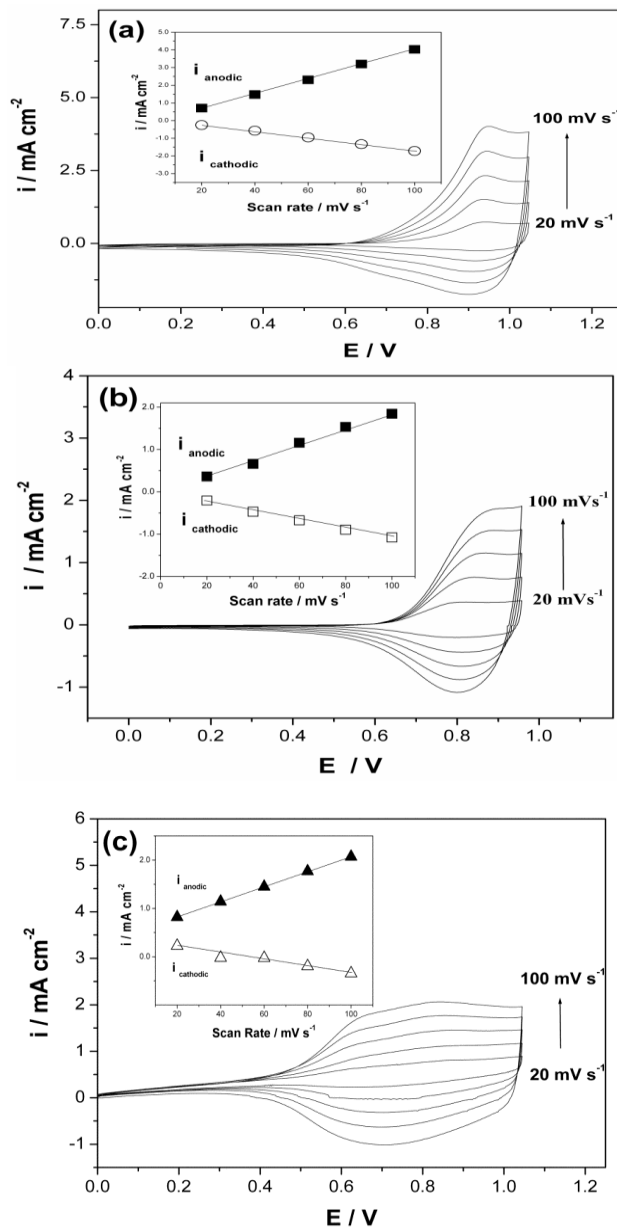


**Figure 3. 19.** Scan rate dependence of (a) P(TQT), (b) P(EQE), (c) P(PQP) film (25 cycle) on a Pt disk electrode at different scan rates between 20 mV/s and 100 mV/s (20  $\text{mV s}^{-1}$  increments) in 0.1 M TBAClO<sub>4</sub>/ACN. (Insets: Relationship of anodic ( $I_{\text{anodic}}$ ) and cathodic ( $I_{\text{cathodic}}$ ) current peaks as a function of scan rate).

To compare the electrochemical behavior of **P(TQT)**, **P(EQE)** and **P(PQP)** polymer films, the obtained polymers via repetitive cycles were scanned anodically in a monomer-free electrolytic solution containing 0.1 M TBAClO<sub>4</sub>/ACN and the results are given in **Figure 3.19**.

As seen from **Figure 3.19**, three polymer films exhibit well defined redox couples due to p-doping at 0.95, 0.90 and 0.80 V for **P(TQT)**, **P(EQE)** and **P(PQP)**, respectively. Although the reversible peaks obtained for **P(TQT)** and **P(EQE)** are similar in appearance, cyclic voltammogram of **P(PQP)** is rectangular shaped, showing capacitive behavior, in the range of 0.4 to 1.0 V. This might be due to the presence of long alkyl chains on Pro-DOT side groups which may effect the incorporation of dopant ion into the polymer matrix during doping process. Scan rate dependence experiments showed that both anodic and cathodic peak currents increase linearly with increasing scan rate, indicating a well-adhered polymer film on the WE surface and a non-diffusional redox process, which was shown in the inset of **Figure 3.19**.

#### 3.2.2.4. Polymer characterization of **P(TQT)**, **P(EQE)** and **P(PQP)**

The polymer films formed after 15 consecutive cycles in the potential range of 0.0 to 1.10 V for **EQE**, 0.0 to 1.25 V for **PQP** and 0.0 to 1.20 V **TQT** were washed with ACN and then dried. The FTIR spectra of polymer films, **P(TQT)**, **P(EQE)** and **P(PQP)**, and their corresponding monomers together with **FQ**, were recorded. The FTIR spectrum of the acceptor part of the three monomers, **FQ**, exhibits characteristic peaks at 3340 and 733 cm<sup>-1</sup>, the first one is attributed to N-H stretching of the quinoxaline part and the latter is due to 1,2-disubstituted benzene ring of fluorene moiety [57]. The peaks that appear around 2800–3300 cm<sup>-1</sup> are due to aromatic C-H stretching and the peaks that appear at 1612 and 1452 cm<sup>-1</sup> are due to C=C double bond stretching. Upon substitution of donor units, a new peak appears at 815 cm<sup>-1</sup> indicating the formation of 1,2,4-trisubstituted benzene ring. Furthermore, the new peaks at about 695, 708 and 718 cm<sup>-1</sup> in the FTIR spectrum of **TQT**, **EQE** and **PQP**, respectively, are due to  $\alpha$ -hydrogens of thiophene rings [64]. These peaks disappear and the other peaks still appear as expected in the spectrum of **P(TQT)**, **P(EQE)** and **P(PQP)**. In addition, the new sharp peak appearing at 1042 cm<sup>-1</sup> (for **P(TQT)** and **P(EQE)**) and 835 cm<sup>-1</sup> for **P(PQP)**) indicates the presence of dopant anions ClO<sub>4</sub><sup>-</sup> and PF<sub>6</sub><sup>-</sup>, respectively [72].

#### 3.2.2.5. Spectroelectrochemical behaviour of **P(TQT)**, **P(EQE)** and **P(PQP)**

The electro-optical properties of the polymer films, deposited on ITO electrode via potential cycling, were investigated by monitoring the changes in the electronic absorption spectra under a voltage pulse in a monomer free electrolyte solution. The results are depicted in **Figure 3.20**. The electronic absorption spectra of neutral forms of the films exhibit an absorption band at around 390, 465 and 569 nm for **P(TQT)**, **P(EQE)** and **P(PQP)**, respectively. These bands are due to  $\pi-\pi^*$  transition and they all lose intensity during oxidation which is accompanied by the appearance of new intensifying bands. In the case of **P(TQT)**, as the valance-conduction band at 390 nm diminishes a new band starts to intensify at about 515 nm in the potential range of 0.0–0.45. Upon further oxidation, beyond 0.45 V, a new broad band around 742 nm also starts intensifying. Appearance of these new bands indicates the formation of charge carriers. All spectra recorded during potential cycling between 0.0 V and 1.1 V passes through a clear isosbestic points at 455 nm, indicating that polymer film was being interconverted between its neutral and oxidized states. The changes in the electronic absorption spectra of **P(TQT)** film are also accompanied by a color change, from orange to gray, indicating that **P(TQT)** film exhibits electrochromic behavior. In the case of **P(EQE)**, the new band due to the formation of charge carriers appears at about 576 nm and with an electrochromic response. The spectroelectrochemical changes recorded for **P(PQP)** film, on the other hand, are different than those of **P(TQT)** and **P(EQE)** in terms of the formation of a strong absorption band towards the near-IR region of the spectrum. The two new bands formed at about 864 and 1056 nm indicate the formation of charge carriers, polarons and bipolarons, respectively.

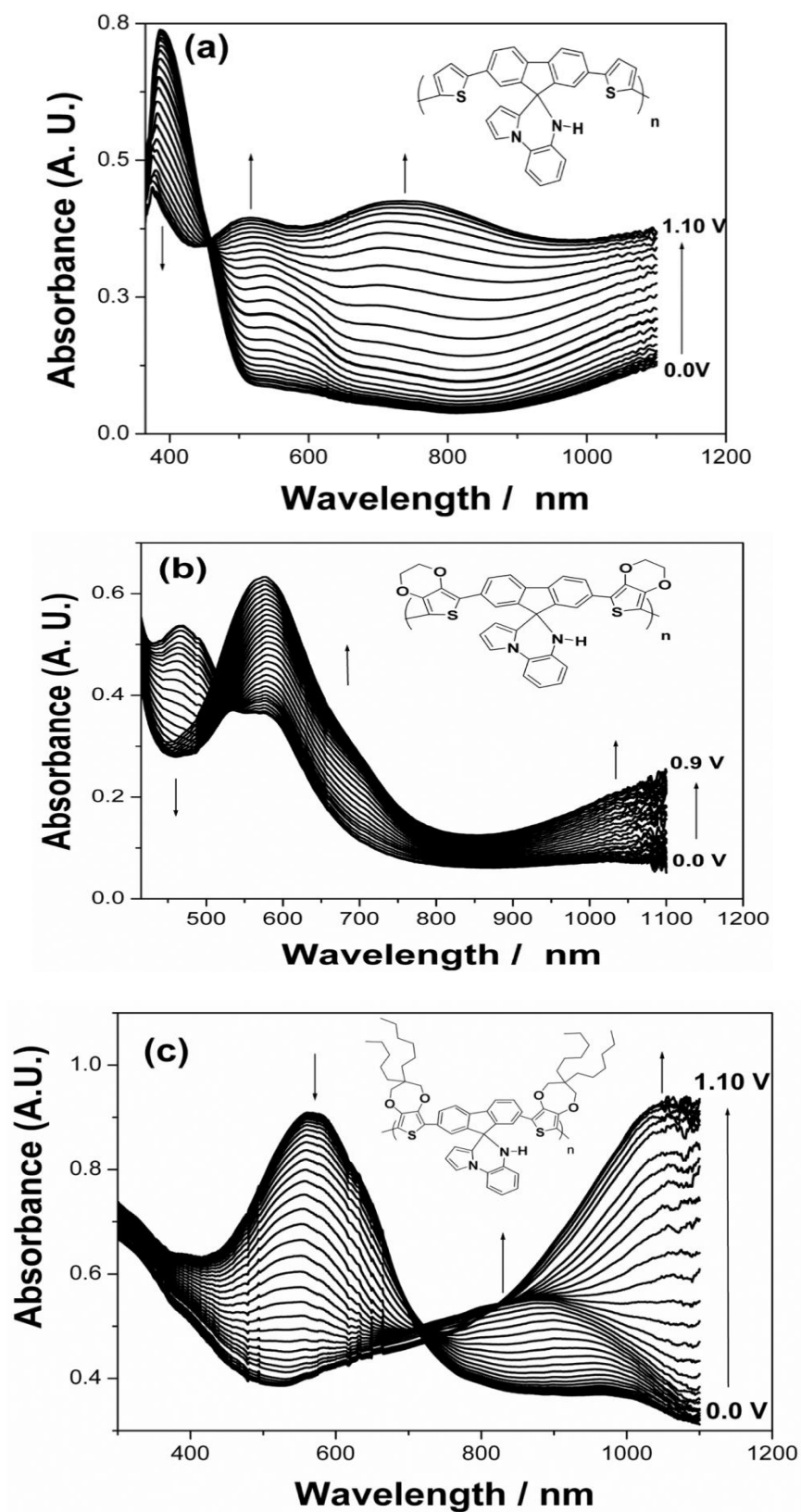


**Figure 3. 20.** Electronic absorption spectra of (a) P(TQT), (b) P(EQE), (c) P(QQP) on ITO (25 cycles) in 0.1 M TBAClO<sub>4</sub>/ACN solution during anodic oxidation of the polymer film.

The band gap ( $E_g$ ) values of polymer films deposited on ITO electrodes via potential cycling were also determined from the commencement of low energy end of  $\pi-\pi^*$  transitions (i.e., 390, 465 and 569 nm for **P(TQT)**, **P(EQE)** and **P(PQP)**, respectively), utilizing spectroelectrochemical data. It was found that  $E_g$  values decreases from 2.47 eV to 1.75 eV and then to 1.66 eV when thiophene side groups are replaced by EDOT and ProDOT side groups. Although, conjugated polymers with Pro-DOT donor groups have higher band gaps than that of PEDOT derivatives, due to lower planarity of the polymer backbone, the higher band gap of **P(EQE)** as compared to **P(PQP)** might be explained as already distorted planarity of **P(EQE)** due to presence of quinoxaline group attached to the 9 position of fluorene moiety. HOMO/LUMO energy levels of the polymers were elucidated utilizing their ionization potentials and electron affinities obtained from experimental data. The onset of oxidation potentials of **P(TQT)** (0.75 V vs. Ag/AgCl), **P(EQE)** (0.65 V vs. Ag/AgCl) and **P(PQP)** (0.44 V vs. Ag/AgCl) were used as  $E_{ox}$  in the equation ( $I_p = (E_{ox} + 4.4)$  eV) [137]. Electron affinities were estimated by subtracting the band gap energy from  $I_p$  and the results are illustrated in **Figure 3.21**. As seen from the figure, HOMO level increases by replacing thiophene with EDOT and then by ProDOT donor groups.

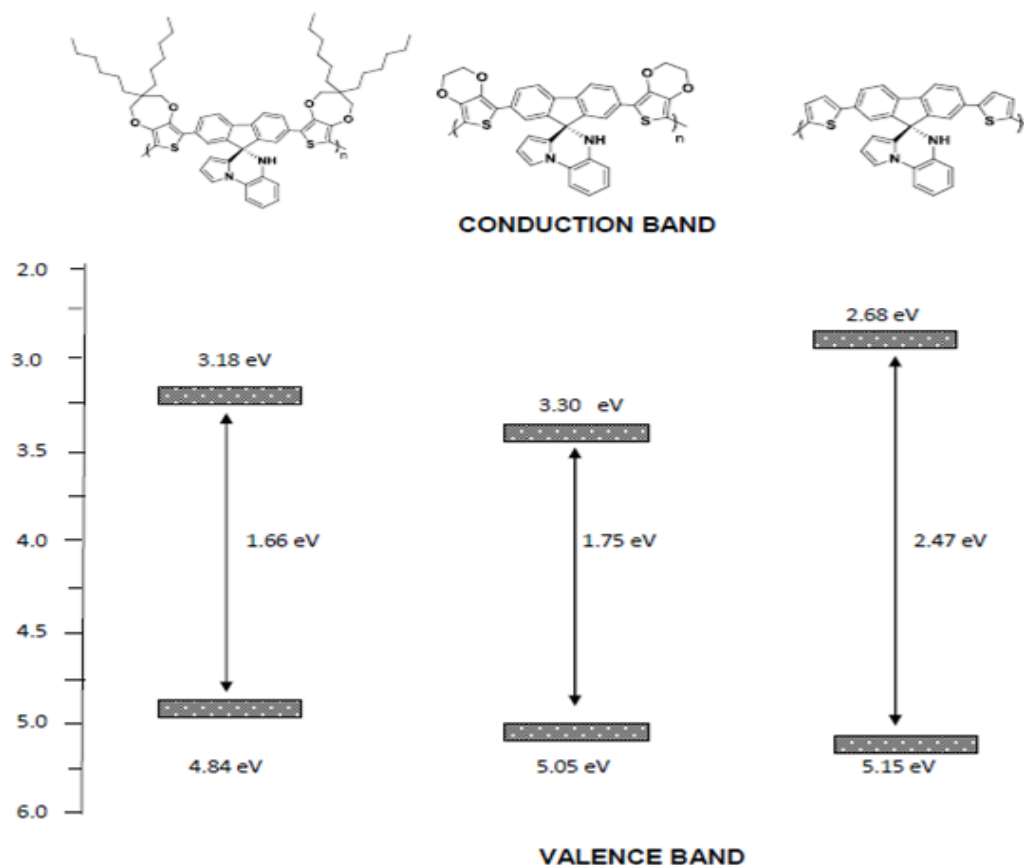
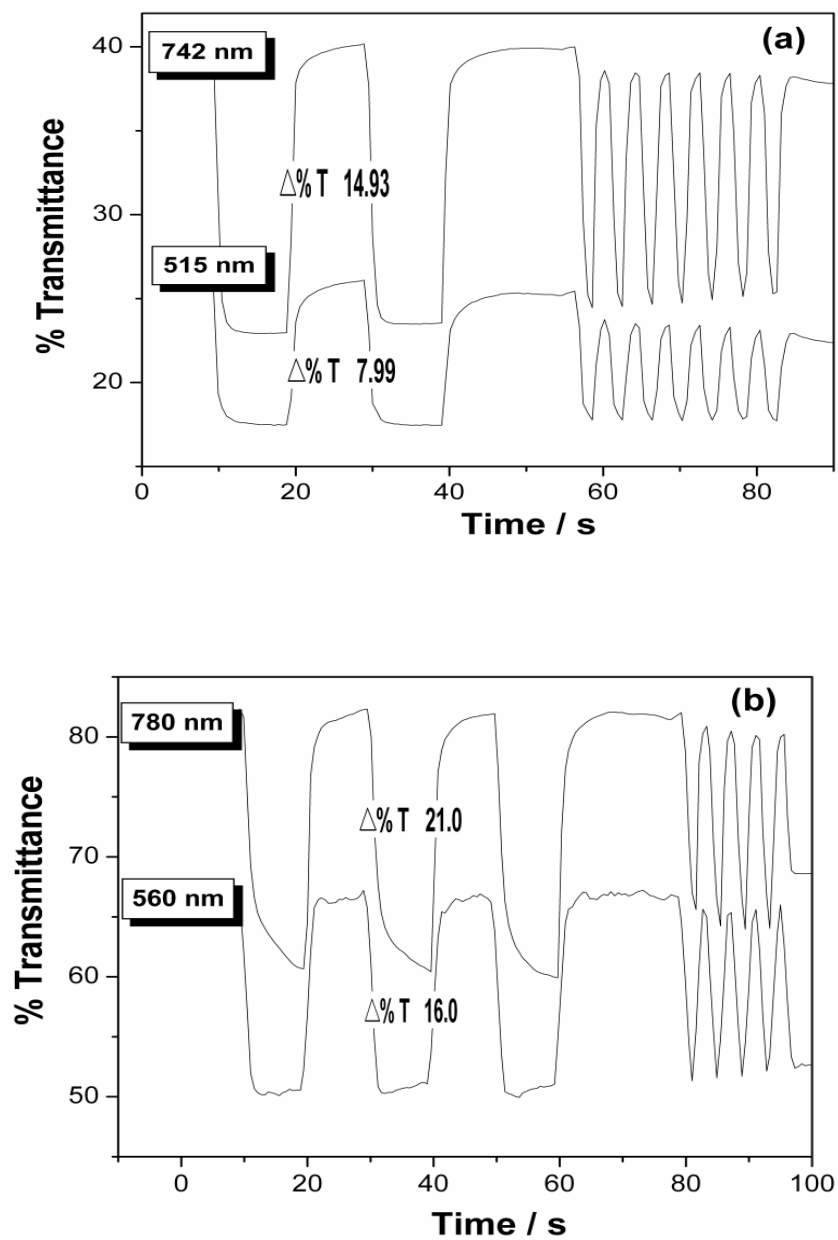


**Figure 3. 21.** Schematic illustration of energy band diagrams for **P(TQT)**, **P(EQE)** and **P(PQP)**.

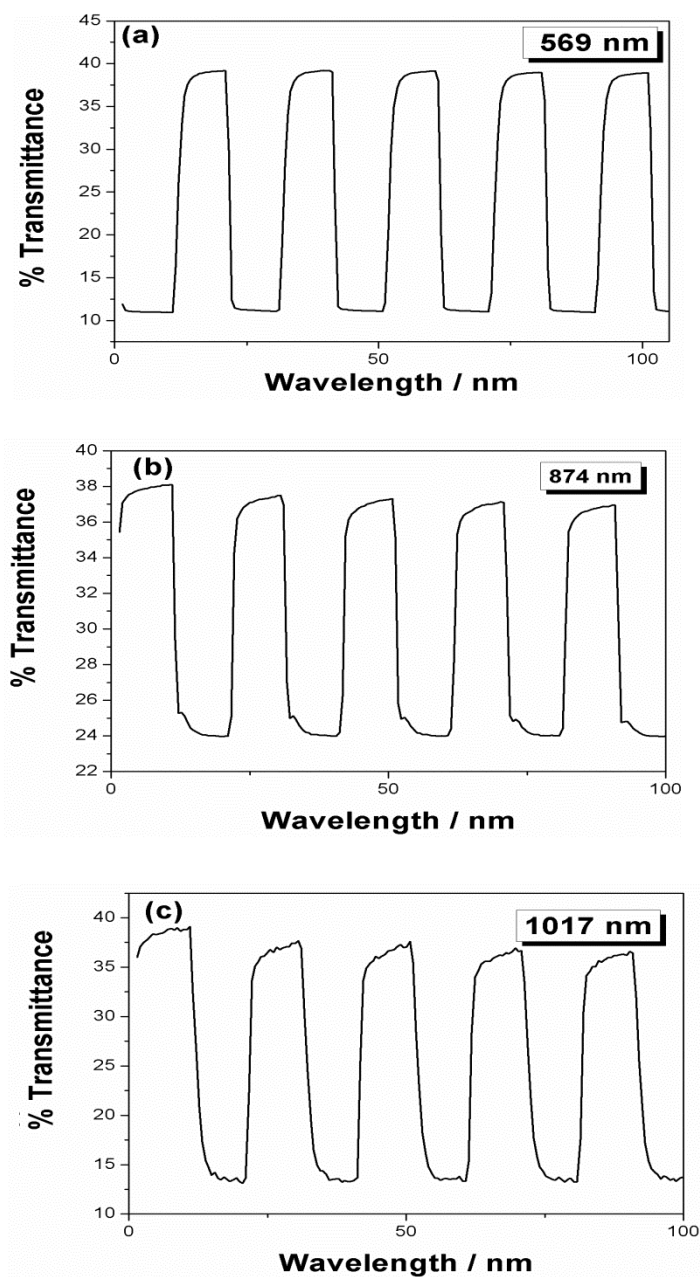
Due to its importance in electrochromic applications, switching times and optical contrast of the polymer films on ITO were also investigated under square wave input of 0.2–1.0 V in 10, and 5 s intervals by monitoring the visible transmittance and the kinetic responses of the film, and the results are shown in **Figure 3.22** and **Figure 3.23**. Inspection of **Figure 3.22** reveals that both **P(TQT)** and **P(EQE)** show a reversible response within the range of applied potential pulses with



a response time of 1.1 s (at 742 nm) and 1.7 s (at 780 nm) at 95% of the maximum transmittance, respectively. The response time of **P(PQP)** was found to be 1.0 s at 1017 nm



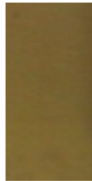
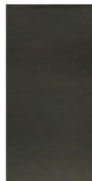
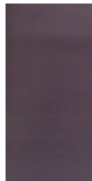



**Figure 3. 22.** Chronoabsorptimetry experiments for (a) **P(TQT)** and (b) **P(EQE)**, with a switching between 0 V and 1.0 V in 10 and 5 s.



**Figure 3. 23.** Optical stability experiments of **P(PQP)** at (a) 569 nm, (b) 874 nm and (c) 1017 nm in a switching between 0 V and 1.0 V in 10 s.

On the basis of this equation, the highest CE values were found as 145.0 cm<sup>2</sup>/C (142 nm), 98.0 cm<sup>2</sup>/C (390 nm) and 253.0 cm<sup>2</sup>/C (1017 nm) for **P(TQT)**, **P(EQE)** and **P(PQP)**, respectively (95 % of full optical switching). CE values for all polymer films are tabulated in **Table 3.3** for comparison reasons. Among the three polymers, **P(PQP)** exhibits the highest value (253 cm<sup>2</sup>/C at 1017 nm) indicating that **P(PQP)** is a promising candidate for electrochromic device applications.

**Table 3. 3.** Optical and switching time data of electrochemically synthesized **P(TQT)**, **P(EQE)**, and **P(PQP)**.

| Polymer       | $\lambda_{\text{max}}$<br>(nm) | Contrast<br>%T | CE<br>(cm <sup>2</sup> / C) | Switching<br>time<br>(s) | Color   |   |
|---------------|--------------------------------|----------------|-----------------------------|--------------------------|---|---|
|               |                                |                |                             |                          | Neutral   | Oxidized  |
| <b>P(TQT)</b> | 390                            | 10.5           | 10.3                        | 0.8                      |    |    |
|               | 515                            | 16.5           | 115.0                       | 1.1                      |   |   |
|               | 742                            | 22.5           | 145.0                       | 1.3                      |   |   |
| <b>P(EQE)</b> | 390                            | 10.0           | 98.0                        | 1.1                      |   |   |
|               | 560                            | 16.0           | 69.6                        | 3.3                      |   |   |
|               | 780                            | 21.0           | 65.0                        | 3.3                      |   |   |
| <b>P(PQP)</b> | 569                            | 11.7           | 235.0                       | 2.7                      |  |  |
|               | 874                            | 23.6           | 90.7                        | 2.0                      |   |   |
|               | 1017                           | 12.4           | 253.0                       | 1.7                      |   |   |

### 3.2.2.6. Fluorescence Study

Among the three polymers prepared electrochemically, only **P(PQP)** was found to be soluble in THF. Therefore, fluorescence property of **P(PQP)** and its monomer, **PQP**, were investigated in this solvent. Although the monomer exhibits an emission at about 520 nm when excited at 327 nm, its polymer emits around 600 nm when excited at 507 nm, corresponding to orange color.

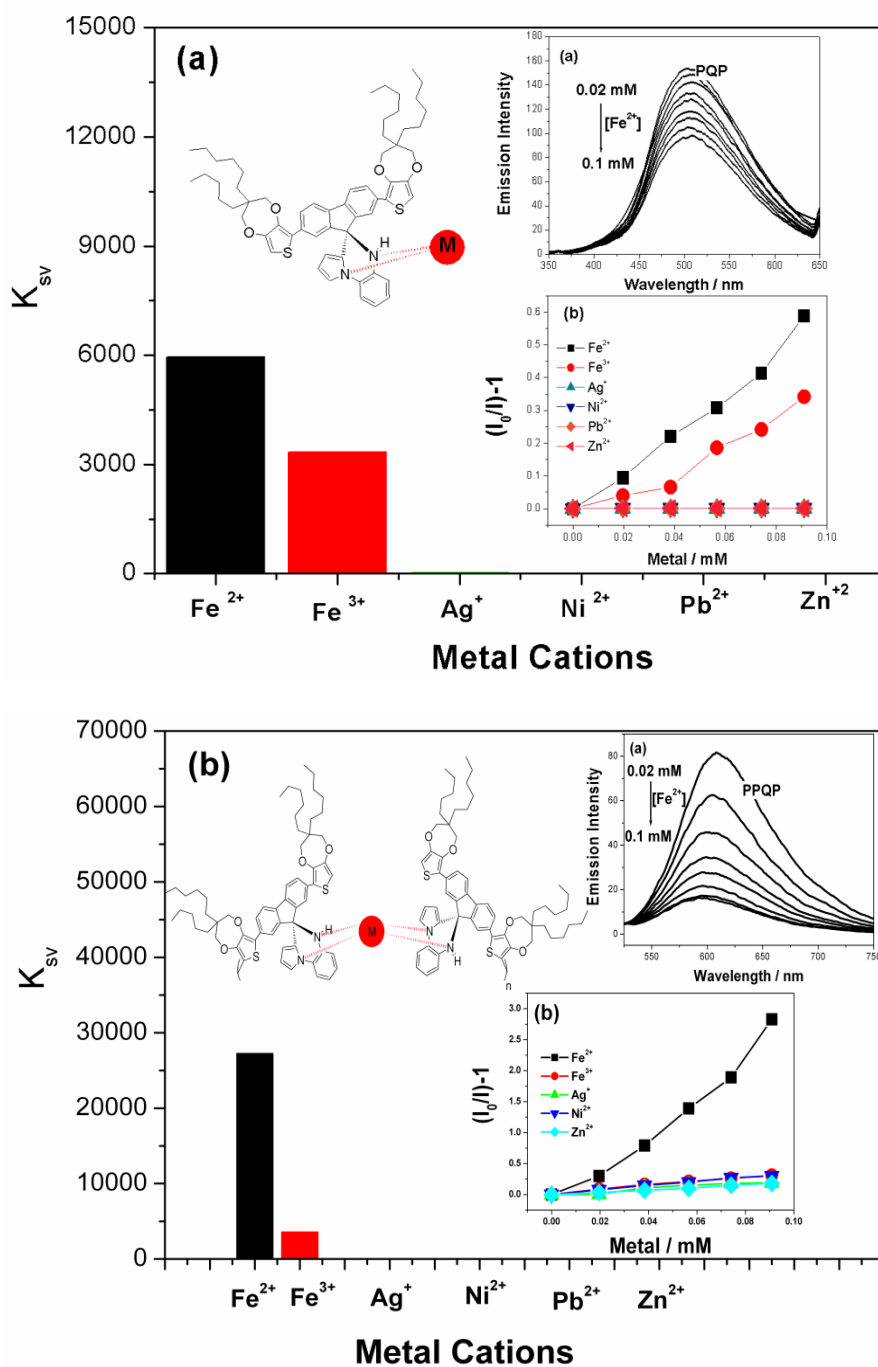


**Figure 3. 24.** The Stern–Volmer plots of (a) P*Q*P, (b) P(P*Q*P), in the presence of various metal ions (each 0.02–0.1 mM). Metal ions prepared from  $Fe(NO_3)_3 \cdot 9H_2O$ ,  $Cu(NO_3)_2 \cdot 3H_2O$ ,  $Ni(NO_3)_2 \cdot 6H_2O$ ,  $Zn(NO_3)_2 \cdot 6H_2O$ ,  $Pb$ ,  $AgNO_3$  in THF. **Inset: (a)** Fluorescence emission spectra of (a) P*Q*P (b) P(P*Q*P) (1 mg in 20 ml THF) with successive addition of 0.02–0.1 mM  $Fe^{2+}$  ion. (b)  $K_{sv}$  values of (a) P*Q*P (b) P(P*Q*P) in the presence of  $Cu^{2+}$ ,  $Ag^+$ ,  $Ni^{2+}$ ,  $Fe^{2+}$ ,  $Zn^{2+}$ ,  $Fe^{3+}$  (each 0.02–0.1 mM).

Binding affinities of **PQP** and **P(PQP)** towards various metal ions were also investigated by monitoring the change in the fluorescence intensity upon addition of metal ions and the results are given in the form of Stern–Volmer plots in **Figure 3.24**. As seen from inset of **Figure 3.24 a** and **b**, fluorescence intensity decreases upon successive addition of  $\text{Fe}^{2+}$  due to energy transfer between  $\text{Fe}^{2+}$  ion and **FQ** fluorophore. Among various common ions, both the monomer and its polymer were found to be selective towards  $\text{Fe}^{2+}$  ions by quenching the fluorescence efficiency. The Stern–Volmer quenching constants ( $K_{sv}$ ) were also determined and are given in **Figure 3.24 a** and **b**. As seen from the figure,  $K_{sv}$  values of monomer and polymer solutions are  $5.9 \times 10^3 \text{ M}^{-1}$  and  $2.7 \times 10^4 \text{ M}^{-1}$ , respectively.

The larger  $K_{sv}$  value in the case of **P(PQP)** can be ascribed to the stronger interaction of metal ion with quinoxaline moiety of two acceptor units along the polymer backbone. Although, fluorescence intensity was found to decrease due to quenching effect of  $\text{Fe}^{2+}$  ions, no significant quenching effect was observed by the addition of  $\text{Pb}^{2+}$ ,  $\text{Ni}^{2+}$ ,  $\text{Zn}^{2+}$ ,  $\text{Fe}^{3+}$ , and  $\text{Ag}^{+}$  ions, indicating that both the monomer and its corresponding polymer can be utilized for fluorometric detection of  $\text{Fe}^{2+}$  at a concentration of around 0.008 mM. The quenching effect of  $\text{Fe}^{2+}$  in the concentration range of 0.002–0.01 mM is provided. This behavior can be clearly seen by naked eye under UV lamp. The emission color of **PQP** in THF, for example, turned from green to colorless after the addition of  $\text{Fe}^{2+}$  ions. Also, the addition of this ion to the polymer solution causes a quenching in the intensity of the reddish orange color emission of the polymer (**Figure 3.25**).



**Figure 3. 25.** Emission colors of (1) **PQP**, (2) **PQP** in the presence of  $\text{Fe}^{2+}$  ion, (3) **P(PQP)** , (4) **P(PQP)** in the presence of  $\text{Fe}^{2+}$  ion in THF under handheld UV lamp.

### 3.2.3. Fluorene-xanthene functionalized D-A-D type Polyfluorene derivatives

A couple of new fluorene derivatives based on spiro-skeleton platform bearing pendant xanthenes unit as acceptor group and thiophene and EDOT as donor groups have been synthesized. It is thought that the acceptor groups endowed with octyl chains will open a door for providing solubility to these newly synthesized polymers, namely **P(TXT)** and **P(EXE)**, bearing electrochromic and fluorescence features. On the other hand, the donor units will provide low oxidation potential eliminating over-oxidation problems during electrochemical polymerization.

#### 3.2.3.1. Electrochemical behavior of **FX**, **TXT** and **EXE**

Electrochemical behavior of fluorene based monomers bearing xanthene moieties; **FX**, **TXT** and **EXE** were investigated by cyclic voltammetry studies in 0.1 M TBAPF<sub>6</sub>/ACN electrolyte solution. It was found that **FX** monomer shows two oxidation peaks at 1.50 V and 1.90 V vs Ag/AgCl. Since the first oxidation potential of fluorene generally appears at about 1.85 V in the same medium with **FX**, the latter might be ascribed to the oxidation of fluorene moiety and the former one to the oxidation of xanthenes moiety. When donor side groups are attached to 2 and 7 positions of fluorene moiety, the oxidation peaks shift to lower potentials as expected, depending

on the donor strength of the side groups. As depicted in **Figure 3.26**, the first oxidation potential of **TXT** and **EXE** appear at 1.06 V and 0.91 V, respectively.

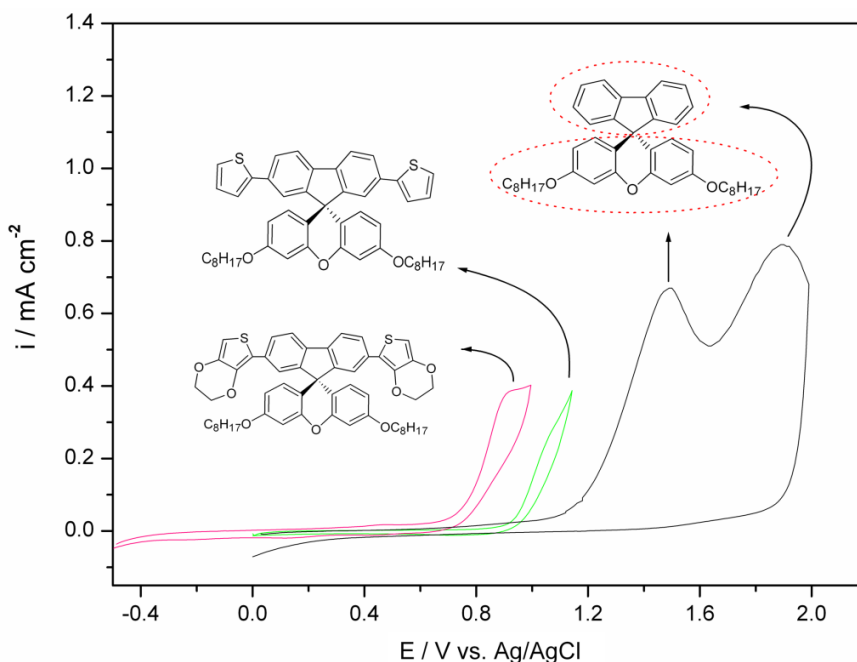


**Figure 3. 26.** First oxidation potential comparison of **FX**, **TXT** and **EXE** in 0.1M TBAPF<sub>6</sub>/ ACN at 100 mV/s onto a Pt disc (area = 0.02 cm<sup>2</sup>).

### 3.2.3.2. Electrochemical polymerization of **TXT** and **EXE**

After the determination of redox behavior of **TXT** and **EXE**, repetitive anodic scans were performed to get their corresponding polymers **P(TXT)** and **P(EXE)**. The electrochemical polymerization of **TXT** was achieved in an electrolyte solution consisting of 0.1 M TBAPF<sub>6</sub> dissolved in DCM: ACN (1:10 by volume) via potential cycling in the range of 0.0–1.20 V. On the other hand, ACN was used as solvent for the polymerization of **EXE** in the potential range of –0.50 V to 0.90 V. As shown in **Figure 3.27**, new redox couples start to intensify during each successive scan indicating the formation of electroactive polymer films on the surface of the working electrode with increasing polymer film thickness.

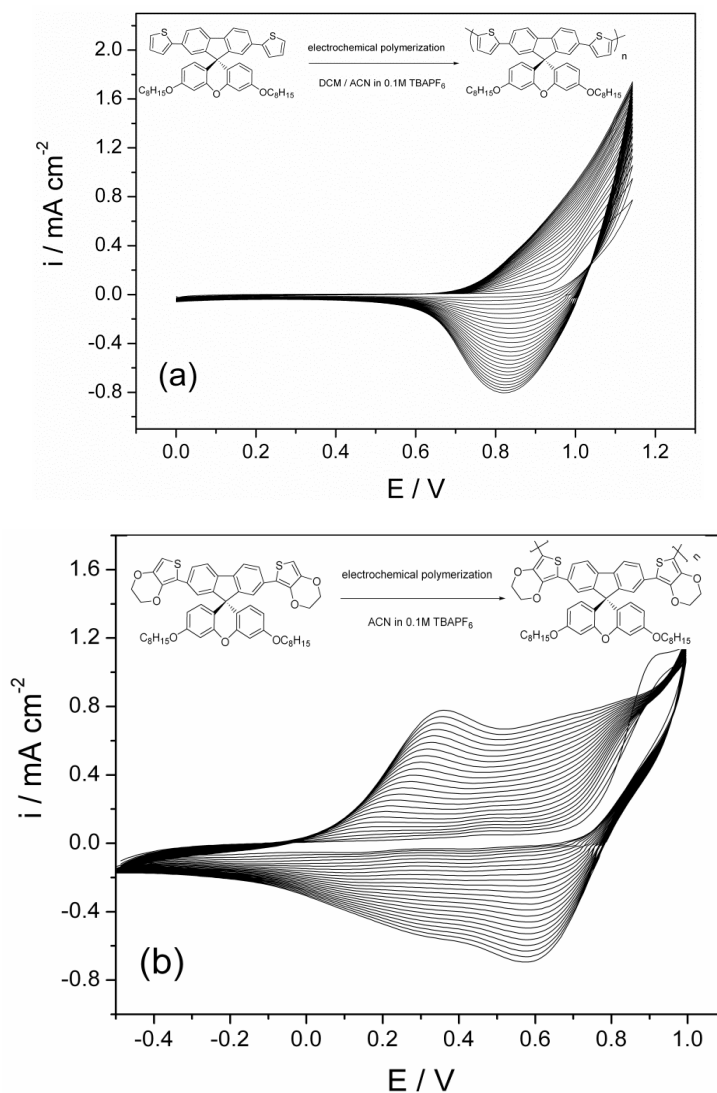


**Figure 3. 27.** (a) Cyclic voltammogram of 10 mM (a) **TXT** 0.1M TBAPF<sub>6</sub> in DCM: ACN = 1:10 and (b) **EXE** 0.1M TBAPF<sub>6</sub> in ACN on a Pt disc electrode at scan rate of 100 mVs<sup>-1</sup> (25 cycle).

### 3.2.3.3. Electrochemical behaviour of P(TXT) and P(EXE)

After electrodeposition step, the polymer film coated electrodes were washed with ACN to remove any unreacted monomer and oligomeric species. For comparison reasons, the electrochemical behavior of the films were investigated in a monomer free electrolyte solution consisting of 0.1 M TBAPF<sub>6</sub> in ACN and the resulting voltammograms are shown in **Figure 3.28**. While **P(TXT)** exhibits one redox couple, **P(EXE)** has two reversible redox couples at 0.45 and 0.80 V, indicating the formation of charge carriers on the main chain backbone.

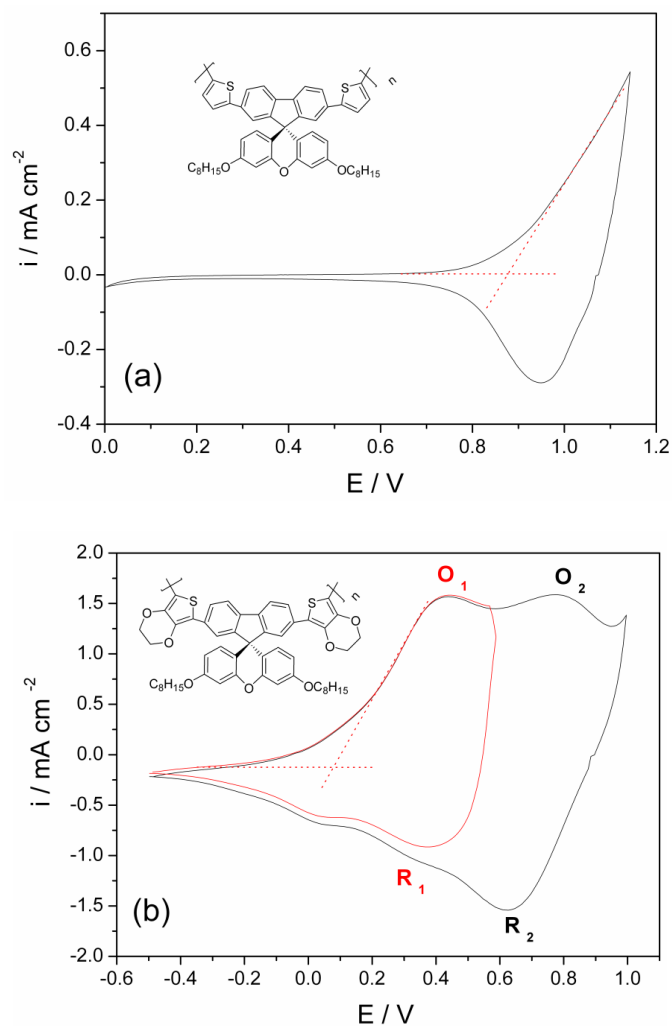


**Figure 3. 28.** Cyclic voltammograms of (a) **P(TXT)** and (b) **P(EXE)** film in TBAPF<sub>6</sub>/ACN at a scan rate of 100 mV/s.

The electrochemical stability of a polymer is also an important parameter for electrochromic devices. Therefore, electrochemical stability of **P(EXE)** film on the electrode was investigated by a square wave potential method. As shown in **Figure 3.29**, **P(EXE)** protects its electroactivity with only 5 % loss after 1000 switches when a potential regime was applied from -0.50 to 0.90 V in 1 s intervals under nitrogen atmosphere.



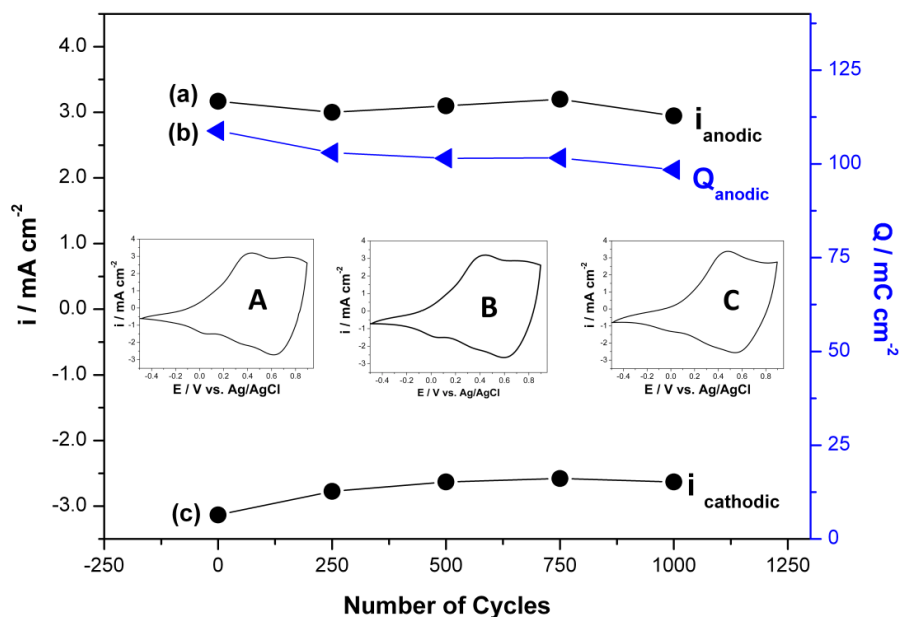


**Figure 3. 29.** Stability test for a **P(EXE)** ( $25 \text{ mC cm}^{-2}$ ) film in  $0.1 \text{ M TBAPF}_6/\text{ACN}$  by a square wave potential method between  $-0.30 \text{ V}$  and  $0.90 \text{ V}$  and cyclic voltammograms of A: 1<sup>st</sup>; B: 500<sup>th</sup>; C: 1,000<sup>th</sup> cycles at a scan rate of  $200 \text{ mVs}^{-1}$ : (a)  $i_{\text{pa}}$  (anodic peak current), (b)  $Q_{\text{a}}$  (Anodic charge stored) (c)  $i_{\text{pc}}$  (cathodic peak current).

#### 3.2.3.4. Spectroelectrochemistry of **P(TXT)** and **P(EXE)**

The band gaps ( $E_{\text{g}}$ ) of the polymer films **P(TXT)** and **P(EXE)** were found to be as  $2.20$  and  $1.74 \text{ eV}$  from the commencement on the low energy end of the absorption bands, respectively. The latter is one of the lower band gap polyfluorenes derivatives [69, 91, 92, 130 and 131]. HOMO/LUMO energy levels of the polymers were elucidated utilizing their ionization potentials and electron affinities obtained from the experimental data. Electron affinities were estimated by subtracting the band gap energy from  $I_{\text{p}}$  and the results were depicted and compared with **PFX** in **Table 3.4**. As shown in the table, HOMO level of **PFX** depends on the donor strength of the units (**Figure 3.30**).

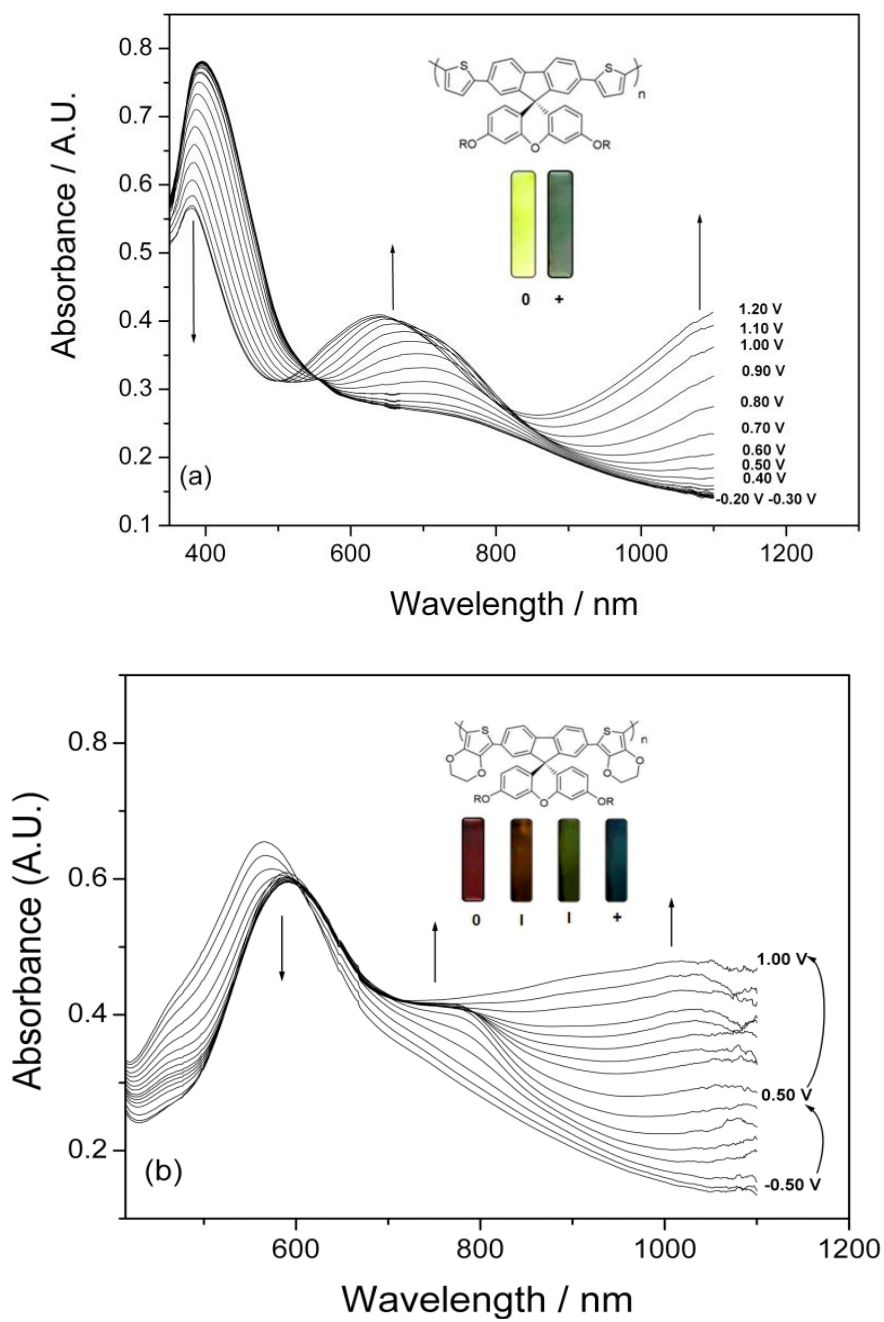


**Figure 3. 30.** Electronic absorption spectra of (a) P(TXT) and (b) P(EXE) on ITO in 0.1 M TBAPF<sub>6</sub>/ACN at various applied potentials. (Inset: The color of oxidized and neutral forms of polymers )

**Table 3. 4.** Voltammetric and spectroelectrochemical data for **PFX**, **P(TXT)**, and **P(EXE)**, in 0.1M TBAPF<sub>6</sub>/ ACN. S (soluble), PS (partially soluble). \*The values were predicted with respect to reference 107 and \*\*  $\Phi f$  of **P(TXT)** (chemically prepared) were found from anthracene as standard in cyclohexane.

| Polymer | $E_{onset}^{ox}$ | HOMO (eV) | LUMO (eV) | $E_g$ (eV) | Solubility | UV-Vis in chloroform solution ( $\lambda_{max}/nm$ ) | PL in chloroform solution ( $\lambda_{max}/nm$ ) | $\Phi f$    |
|---------|------------------|-----------|-----------|------------|------------|--|--|-------------|
|         | 1.10*            | 5.50      | 2.58      | 2.92       | S*<br>PS*  | 280, 390   | 418, 443   | 1*          |
|         | 0.88             | 5.28      | 3.05      | 2.23       | S          | 304, 365   | 418, 398   | 0.59±0.02** |
|         | 0.08             | 4.48      | 2.74      | 1.74       | PS         | 365, 563   | 418, 397   | -           |

Switching times, optical contrast and coloration efficiencies of polymer films were also elucidated. The potential of the WE was stepped between neutral and oxidized states of the polymers with a residence time of 10 s in a monomer free solution, where the polymer coated ITO electrode was used as the WE. During the experiment, the % transmittance at the wavelength of maximum contrast was measured by an UV-vis spectrophotometer. The percentage transmittance change ( $\Delta\%T$ ) in the visible region between the neutral and oxidized states was found to be 10% (at 395 nm) and 14 % (at 655 nm) with a response time of 1.1 s (95 % of full optical switching) for **P(TXT)** (25 mC/cm<sup>2</sup>) and 15% (at 500 nm) and 12 % (at 680 nm) with a response time of 0.8 s for **P(EXE)** (25 mC/cm<sup>2</sup>) (**Figure 3.31**). As **P(TXT)** exhibits  $\eta$  of 187, 136 and 151 cm<sup>2</sup>/C at 395, 655 and 1017 nm, respectively, **P(EXE)** has higher CE values such as 258, 215 and 310 cm<sup>2</sup>/C at 500, 680 and 960 nm, respectively, which indicated that the **P(EXE)** might be a good candidate for electrochromic and optical device applications (**Table 3.5**).

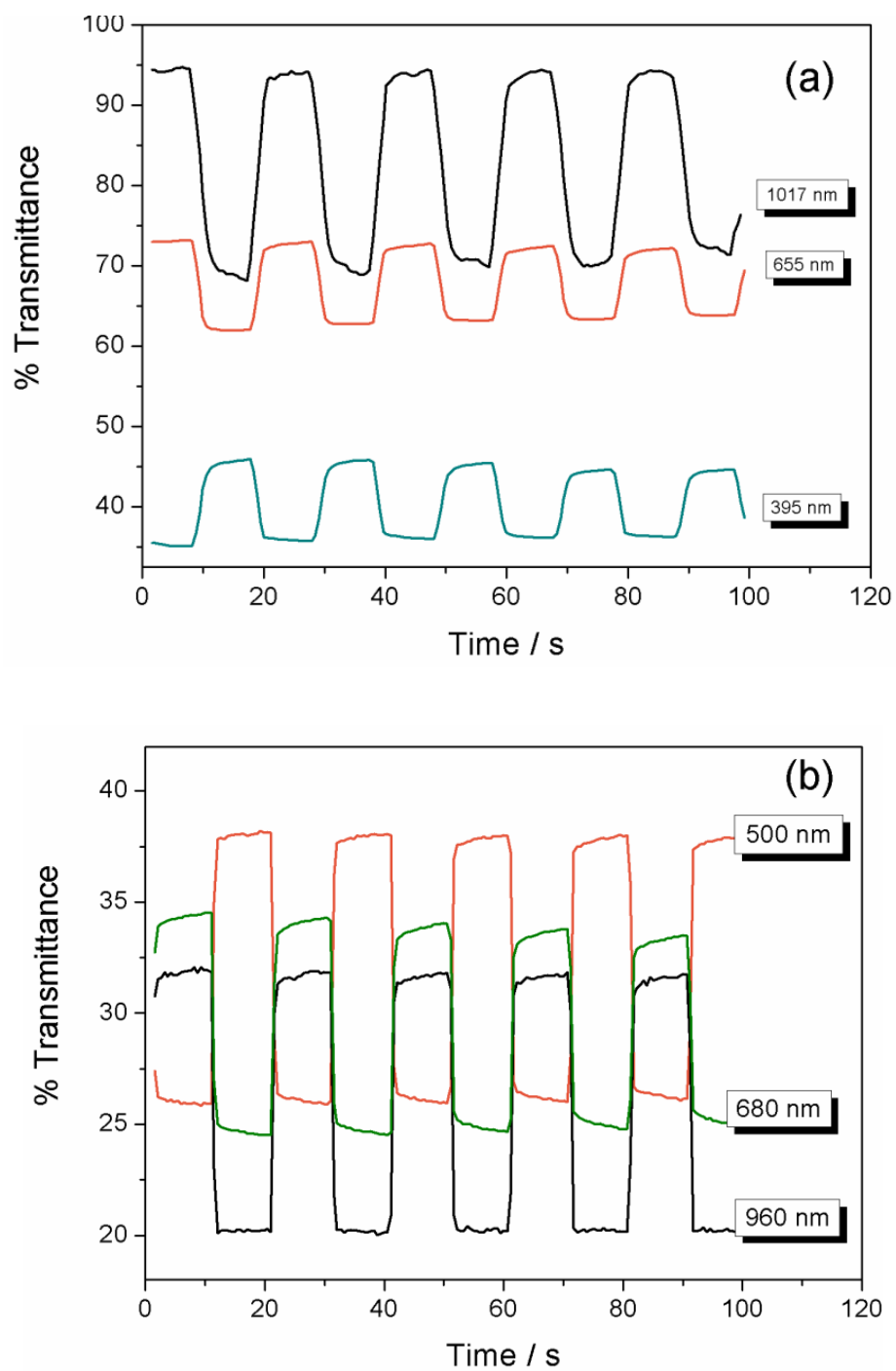


**Figure 3. 31.** Chronoabsorptometry experiments for (a) **P(TXT)** and (b) **P(EXE)** film on ITO in 0.1 M TBAPF<sub>6</sub>/ACN while the polymer was switched with a switching time of 10 s.

**Table 3. 5.** Optical and switching time data of electrochemically synthesized **P(TXT)** and **P(EXE)**.

| Polymer       | $\lambda_{\max}$<br>(nm) | Contrast<br>%T | $\eta$<br>(cm <sup>2</sup> / C) | Switching<br>time<br>(s) |
|---------------|--------------------------|----------------|---------------------------------|--------------------------|
| <b>P(TXT)</b> | 395                      | 10.0           | 187.0                           | 2.4                      |
|               | 655                      | 14.0           | 136.0                           | 1.1                      |
|               | 1017                     | 25.7           | 151.0                           | 1.7                      |
| <b>P(EXE)</b> | 500                      | 15.0           | 258.0                           | 1.1                      |
|               | 680                      | 12.0           | 215.0                           | 0.8                      |
|               | 960                      | 16.0           | 310.0                           | 1.3                      |

### 3.2.3.5. Fluorescence study for **P(TXT)** and **P(EXE)**

It was found that both electrochemically and chemically prepared **P(TXT)** films were soluble in common solvents such as THF, chloroform, DCM, toluene, DMSO, DMF and exhibit fluorescence property **Figure 3.32** presents the UV-vis absorption and fluorescence spectra of **P(TXT)** (chemically prepared) in chloroform. **P(TXT)** exhibits one major band at 365 nm, which is assigned to a  $\pi$ - $\pi^*$  transition derived from the conjugated polymer backbone. The absorption band near 310 nm might be ascribed to  $\pi$ - electron transition that occurs predominately from the spiro pendant units [140]. As it is seen from **Figure 3.32** , excitation at 365 nm resulted in the formation of a weak and relatively intense emission bands at about 405 nm and at 418 nm, which are attributed to blue emission. The fluorescence quantum yield of **P(TXT)** (0.59 $\pm$ 0.02) in cyclohexane was estimated by comparing with the standard of anthracene in cyclohexane. This value is lower than that measured for **PFX** [140] and might be explained by lower fluorescence rates due to the presence of donor side groups.

**Figure 3.32(b)** presents the absorption and emission spectra of a **P(TXT)** film spray-coated from cyclohexane solution onto a quartz plate. The absorption spectrum of the polymer film was slightly broadened but the emission spectrum of the film is red-shifted as compared with that in solution. The presence of intermolecular  $\pi$ - $\pi$  interactions or planarization of the polymer backbones in the thin film might account for the spectral shifts [142-143]. The red shift of fluorescence for **P(TXT)** is as expected due to high extent of  $\pi$ - $\pi$  interaction in the condensed

matter. **P(EXE)** film prepared electrochemically is partially soluble and exhibits fluorescence property in different solvents as it is shown in the inset of the **Figure 3.32 (a)** when excited at 380 nm.

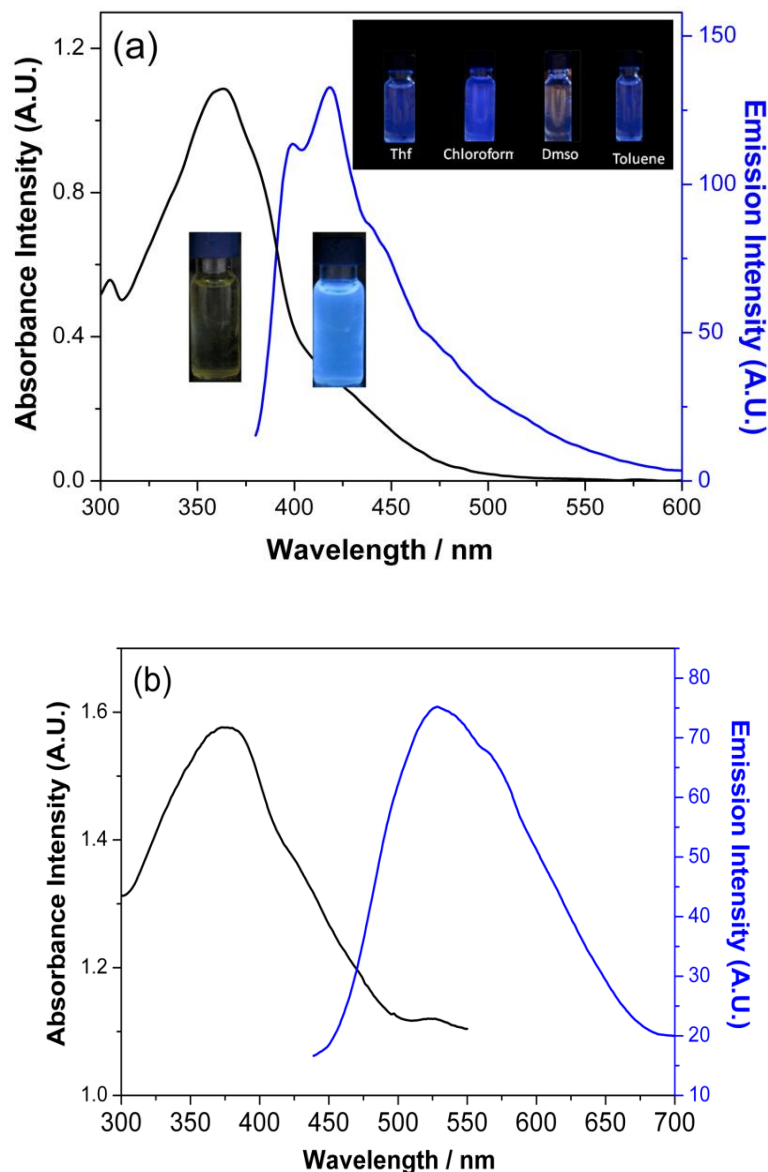


**Figure 3. 32.** Emission and absorbance spectrum of **P(TXT)** (a) in chloroform solution (b) in solid state (inset ; Emission spectrum of **P(EXE)** in different solutions).

### 3.2.3.6. Thermal Characterization of **P(TXT)** and **P(EXE)**

Thermal stability of the material is one of the most important factors in applications for optical devices such as electrochromic devices, PLEDs and solar cells. The thermal stability of the polymers was analyzed by TGA under nitrogen. For comparison sake, the polymers prepared electrochemically were also examined and resulting thermograms are shown in **Figure 3.33**. Both polymers are found to be thermally stable with decomposition temperatures at higher than 300°C.

The complete thermal degradation of polymers occurs in two stages. The initial weight loss (10%) occurs between 200 °C and 320 °C, which might be assigned to the loss of dopant anions in the polymer chain matrix of **P(TXT)**. The last weight loss (30%) between 390 and 580 °C is because of the thermal degradation of the main polymer chain. Similar to **P(TXT)**, **P(EXE)** is also thermally stable; its 25% and 20% weight losses occurred at 320 and 425 °C, respectively.

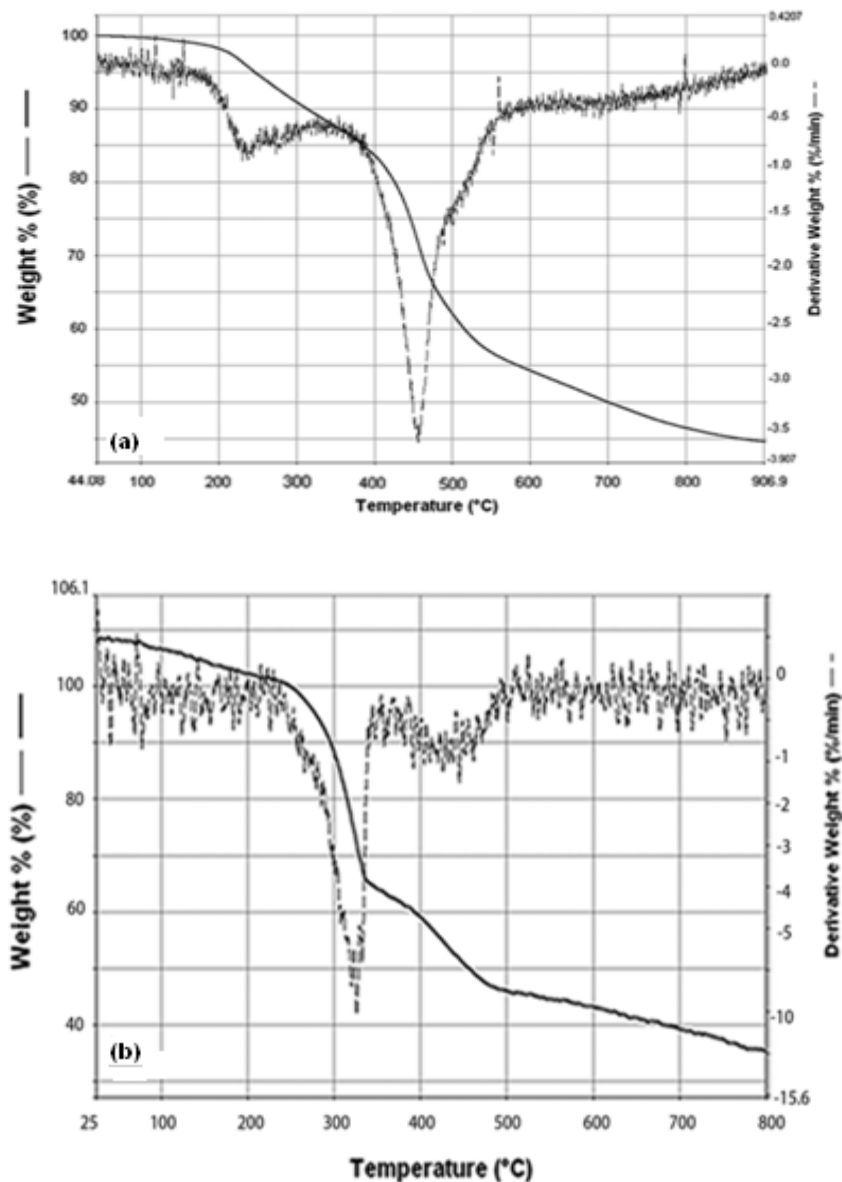


**Figure 3. 33.** Thermogram of (a) **P(TXT)** and (b) **P(EXE)**.

### 3.2.3.7. Characterization of **P(TXT)** and **P(EXE)**

The polymer films formed after 25 consecutive cycles in the potential range of 0.0 to 1.2 V for **P(TXT)** and -0.50 to 0.90 V for **P(EXE)** were washed with ACN and then dried. The FTIR spectra of polymer films, **P(TXT)**, **P(EXE)** and their corresponding monomers together with **FX**,

were recorded. The FTIR spectrum of the acceptor part of the two monomers, **TXT** and **EXE**, exhibits characteristic peaks at 3063–3033  $\text{cm}^{-1}$  (aromatic C–H stretchings), 2900–2950  $\text{cm}^{-1}$  C–H stretchings for octyl chains and 1168, 1260  $\text{cm}^{-1}$  (C–O stretching). Upon substitution of donor units, a new peak appears at 815  $\text{cm}^{-1}$  indicating the formation of 1,2,4-trisubstituted benzene ring. Furthermore, the new peaks at about 695 and 708  $\text{cm}^{-1}$  in the FTIR spectrum of **TXT** and **EXE**, respectively, are due to  $\alpha$ -hydrogens of thiophene rings. These peaks disappear and the other peaks still appear as expected in the spectrum of **P(TXT)** and **P(EXE)**. In addition, the new sharp peak that appears at 1042  $\text{cm}^{-1}$ , is attributed to the  $\text{PF}_6^-$  counter anion.

Since **P(TXT)** was found to be soluble in most of the common organic solvents such as DCM, chloroform, THF and toluene, **TXT** was also polymerized via chemical oxidation to get more amount of polymer for detailed characterization.  $\text{FeCl}_3$  was used as an oxidant for the chemical polymerization. The molecular weight determination of the polymer was carried out by gel permeation chromatography (GPC) by using polystyrene as the standard and THF as the eluent. **P(TXT)** has a weight averaged molecular weight ( $M_w$ ) of  $4.9 \times 10^3$  and a number averaged molecular weight ( $M_n$ ) of  $2.6 \times 10^3$ , with a polydispersity index (PDI) of 1.9, respectively. It refers that the polymer chain of **P(TXT)** consists of approximately 20 repeating units. This value is lower than one of **PFX** ( $M_w = 1.6 \times 10^4$  and  $M_n = 1.1 \times 10^4$ ), which might be because of the synthesis strategy [141].  $^1\text{H}$  NMR spectrum of polymer was also investigated on Bruker-Instrument-NMR Spectrometer (DPX-400) monomers with  $\text{CDCl}_3$  as the solvent and chemical shifts ( $\delta$ ) are given relative to tetramethylsilane as the internal standard.  $^1\text{H}$  NMR (400 MHz,  $\text{CDCl}_3$ ): 0.87–1.80 (broad m, aliphatic octyl units), 3.80–4.00 (broad m, O– $\text{CH}_2$ ), 6.20–6.40 (broad m, xanthene-*H*), 6.60–6.75 (broad m, thienyl-*H*), 6.90–7.10 (broad m, xanthene-*H*), 7.30–7.50 (broad m, fluorene-*H*), 7.60–7.80 (broad m, fluorene-*H*). Broadening of the peaks and the decrease in the intensity of thienyl peaks confirm the polymerization with respect to the monomer spectrum

### 3.3. Fluorene copolymer synthesis

A novel blue emitting and electrochromic conjugated copolymer based on 9,9'-dioctylfluorene (**F8**) and spiro (fluorene-9,9'-xanthene) (**SFX**) has been prepared. Optical, photophysical and electrochemical characterizations are given for the as synthesized polymer; poly [spirofluorene-co-9,9'-dioctylfluorene] **P(F8-SFX)**.

#### 3.3.1. Synthesis and Properties of **P(F8-SFX)**

**P(F8-SFX)** was prepared by Suzuki-Miyaura coupling polymerization of 9,9-dioctylfluorene-2,7 diboronic acid bis(1,3-propanediol) ester and (2,7-dibromospiro[fluorene-9, 9'-2',7'-di-n-octyloxyxanthene]) with tetrakis(palladium catalyst  $\text{Pd}(\text{PPh}_3)_4$  in a toluene/2M potassium carbonate solution. After purification by reprecipitation into methanol, **P(F8-SFX)** was obtained as an ash-colored powder. The chemical structure of the polymer was verified by  $^1\text{H}$  NMR and FT-IR spectra. All aromatic and aliphatic protons of **P(F8-SFX)** resonated in the region of 6.23–7.80 ppm and 0.87–1.94 ppm, respectively. The peak at 3.92 ppm also belongs to the ether protons of octyl chain. FTIR spectrum of the polymer exhibits characteristic peaks at 3063–3033  $\text{cm}^{-1}$  (aromatic C–H stretching), 2850–2930  $\text{cm}^{-1}$  (C–H stretching for octyl chains) and 1184, 1240  $\text{cm}^{-1}$  (C–O stretching of ether linkage). The absorption peaks at 1404, 1450 and 1498  $\text{cm}^{-1}$  can be assigned to the vibration of aromatic ring and one at 1610  $\text{cm}^{-1}$  belongs to asymmetrically substituted benzene. The 810  $\text{cm}^{-1}$  peak in the spectrum of the polymer belongs to the 1,2,4-trisubstituted benzene rings.



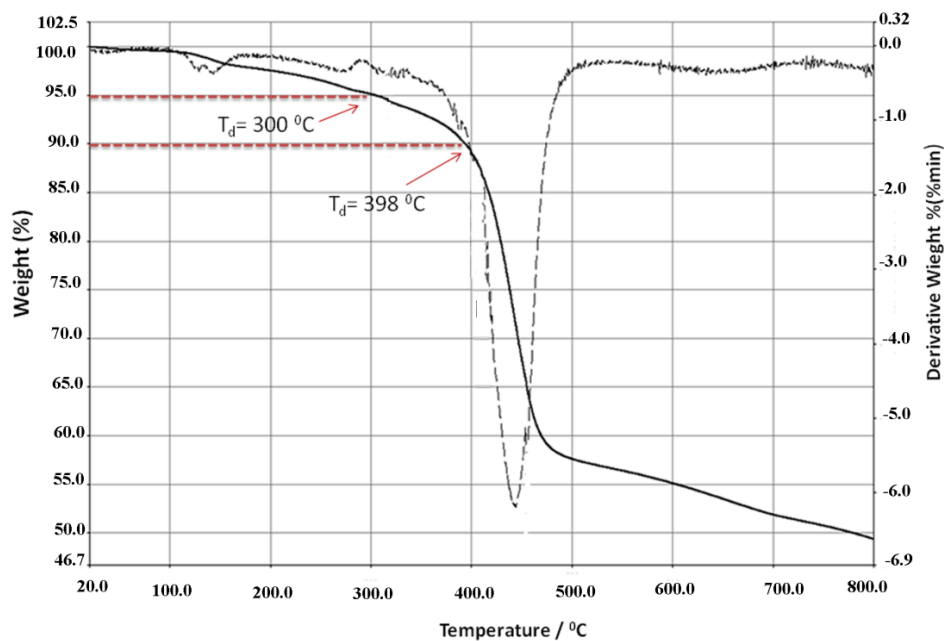


**Figure 3. 34.** Thermal gravimetric analysis of **P(F8-SFX)**

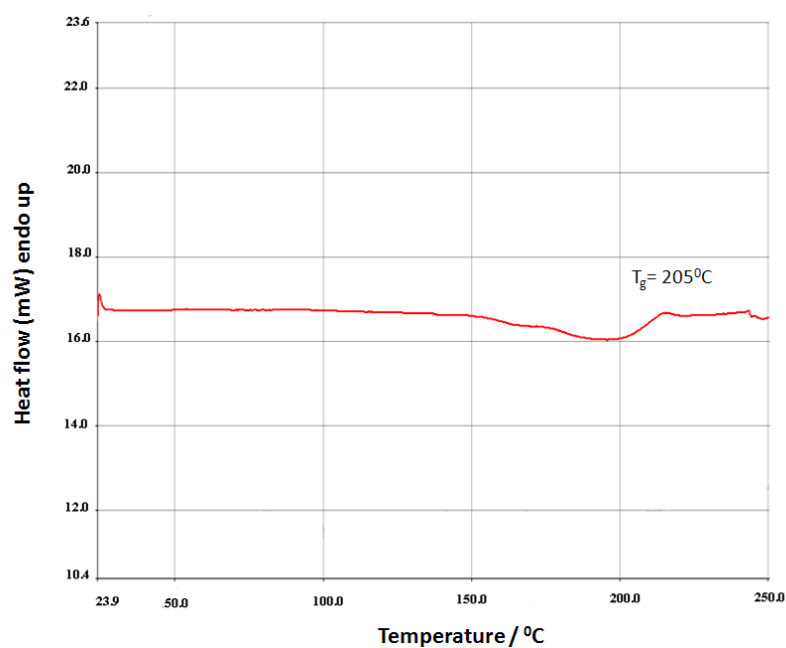


**Figure 3. 35..** DSC analysis of **P(F8-SFX)**

The thermal properties of the synthesized polymers were obtained by means of TGA (**Figure 3.34**) and DSC (**Figure 3.35.**) under nitrogen atmosphere. DSC of **P(F8-SFX)** indicates a glass transition temperature ( $T_g$ ) at around 205 °C for the copolymer. This result shows that the polymer was amorphous like PSFX derivative as depicted in **Table 3.6**. The high  $T_g$  value of **P(F8-SFX)** is most probably arising from reduced segmental mobility due to rigid xanthane units along the

polymer backbone. The copolymer also exhibits good thermal stability, showing only 5% and 10% weight losses at 300 and 398 °C, respectively.

**Table 3. 6.** Comparison of the characteristics properties **P(F8-SFX)** with its analogues.

| Polymer               | $M_n^a$ | $M_w^a$ | DPI  | $T_g(^{\circ}\text{C})^b$ | $T_d(^{\circ}\text{C})^c$ |
|-----------------------|---------|---------|------|---------------------------|---------------------------|
| PF8 <sup>[143]</sup>  | 23200   | 61176   | 2.68 | 67                        | 458*                      |
| PSFX <sup>[107]</sup> | 11000   | 16000   | 1.46 | 149                       | 411, 433**                |
| P(F8-SFX)             | 104480  | 108305  | 1.04 | 205                       | 300, 398**                |

<sup>a</sup> Molecular weights were determined by GPC using polystyrene standards. <sup>b</sup>Glass transition temperature. <sup>c</sup>\*Onset decomposition temperature and \*\* the decomposition temperature at 5% and 10% weight losses measured by TGA under nitrogen .

GPC measurements of **P(F8-SFX)** were conducted to provide the relative molecular weight to the polystyrene standards and polydispersity index. The results of the synthesized copolymer were compared with those of homopolymer poly(9,9-dioctylfluorene) (**POF**) and (poly[2',7'-dioctyloxyspiro(fluorene-9,9'-xanthene)-2,7-diyl] (**PSFX**)) in **Table 3.6** [107, 143]. The synthesized copolymer was highly soluble in most of the organic solvents such as chloroform, THF, 1,2- dichlorobenzene and toluene. The molecular weight of the polymer was determined in THF. **P(F8-SFX)** has a number average molecular weight ( $M_n$ ) of  $1.04 \times 10^5$  g/mol and a weight average molecular weight ( $M_w$ ) of  $1.08 \times 10^5$  g/mol. These values are extremely high than those of **PSFX**, due to solubility problem of **PSFX** in THF [107].

### 3.3.2. Electrochemical characterization of P(F8-SFX)

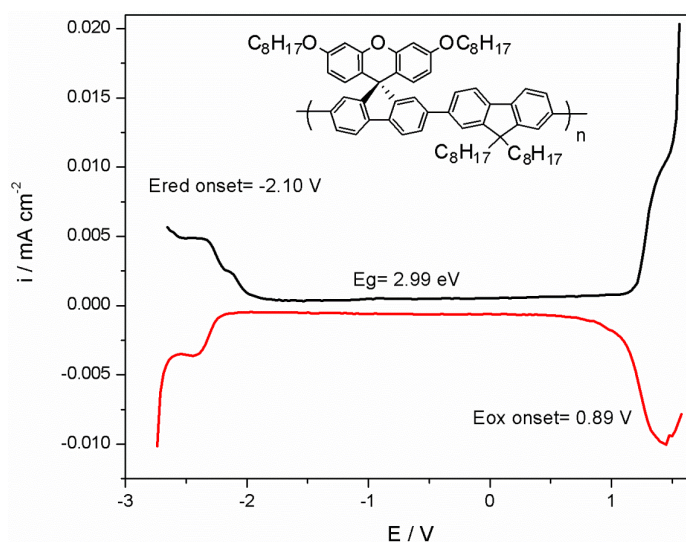


**Figure 3. 36.** DPV of **P(F8-SFX)** measured in the solid state on a glassy carbon disk electrode in the medium of an electrolyte of 0.1 M (TBAPF<sub>6</sub>) in ACN at a scan rate of 100mV s<sup>-1</sup>.

The polymer behavior was carried out in 0.1 M TBAPF<sub>6</sub>/ACN medium after the polymer film was drop-casted onto a glassy carbon electrode. The onset potentials for oxidation and reduction was measured at 0.89 and -2.10 V, respectively. On the basis of this data, the HOMO (5.69 eV) and LUMO (-2.70 eV) with respect to Fc/Fc<sup>+</sup> ferrocenium (4.8 eV) were calculated. The band gap was calculated as 2.99 eV which is in good agreement with optical measurements (**Figure 3.36**).

### 3.3.3. Optical Characterization of P(F8-SFX)

The absorption of **P(F8-SFX)** consists of a strong featureless  $\pi$ - $\pi^*$  transition that peaks around 372 nm (3.3 eV) and a weak  $\pi$ - $\pi^*$  transition at 281 nm coming predominantly from the spiro **SFX** unit. The optical band gap was determined from the absorption onset as 2.99 eV. The optical behavior of the polymer was summarized and compared with other relatives in **Table 2**. As seen in Table 2, while the band gaps of the polymers were too close to each other, HOMO and LUMO levels change depending on the type of the electroanalytical methods used during measurement.

**Table 3. 7.** Summary of optical properties of **P(F8-SFX)**

| Polymer                      | Abs. $\lambda_{\max}$ (nm) |                   | PL <sup>c</sup> $\lambda_{\max}$ (nm) |                        | HOMO <sup>d</sup> (eV) | LUMO <sup>d</sup> (eV) | Band Gap (eV) |
|------------------------------|----------------------------|-------------------|---------------------------------------|------------------------|------------------------|------------------------|---------------|
|                              | Solution <sup>a</sup>      | Film <sup>b</sup> | Solution <sup>a</sup>                 | Film <sup>b</sup>      |                        |                        |               |
| <b>PF8</b> <sup>[143]</sup>  | 389                        | 390               | 418 (443)                             | 424 (448)              | 5.80*                  | 2.85*                  | 2.95          |
| <b>PSFX</b> <sup>[107]</sup> | (280)<br>390               | (281) 393         | 418 (442)                             | 426 (450)              | 5.79*                  | 2.87*                  | 2.96          |
| <b>P(F8-SFX)</b>             | (281)<br>372               | (283) 377         | 415 (437)                             | 422<br>(450, 486, 520) | 5.69**                 | 2.70**                 | 2.99          |

<sup>a</sup>Evaluated in chloroform. <sup>b</sup>Evaluated in the solid state. <sup>c</sup>Excited at 375 nm. <sup>d</sup>Calculated from \*CV and \*\*DPV with regard to the energy level of ferrocene (4.8 eV below vacuum).

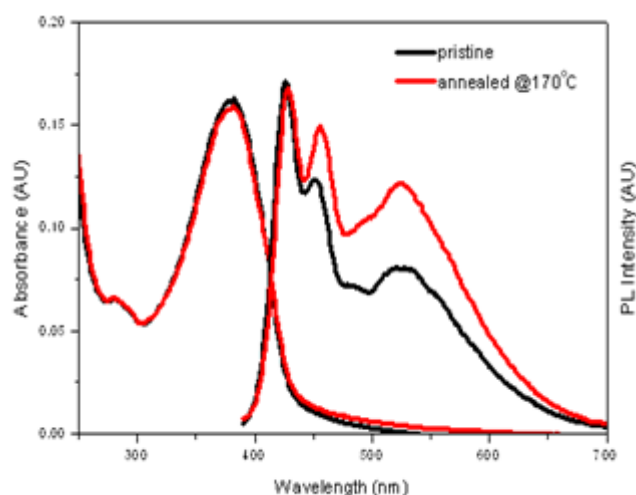


**Figure 3. 37.** PL-spectra of polymer film in 1,2 DCB (15 mg/ml) after annealing (170°C) in ambient atmosphere and normal indoor light.

Preliminary results indicate that after annealing the polymer film at 170 °C in ambient atmosphere and darkness, **P(F8-SFX)** does not show any longer wavelength PL-emission (**Figure 3.37**).

**Figure 3.38** shows a typical absorption and PL spectra in dilute 1,2- dichlorobenzene solution and in the solid state. As expected, the absorption is dominated by the well-known UV band of polyfluorene. The emission of the polymer **P(F8-SFX)** in solution shows a broad emission well resolved structure with peaks at 415, and at 437 nm as a shoulder assigned to the 0-0 and 0-1 intra-chain singlet transitions. In contrast to the emission in solution, the polymer film shows well resolved vibronic structures assigned to 0-0, 0-1, 0-2 transitions at 422, 450 and 486 nm as well as additional transitions at long wavelength region. In comparison with the solution, the absorption spectrum of the thin film slightly broadened and 7 nm red shifted most probably due to stronger interchange interactions in the solid state [144]. The PL spectrum, on the other hand, showed a much more narrow emission with 7 nm red-shift. Additional broad green contribution at 520 nm is assigned to interchain excimers [145,146].

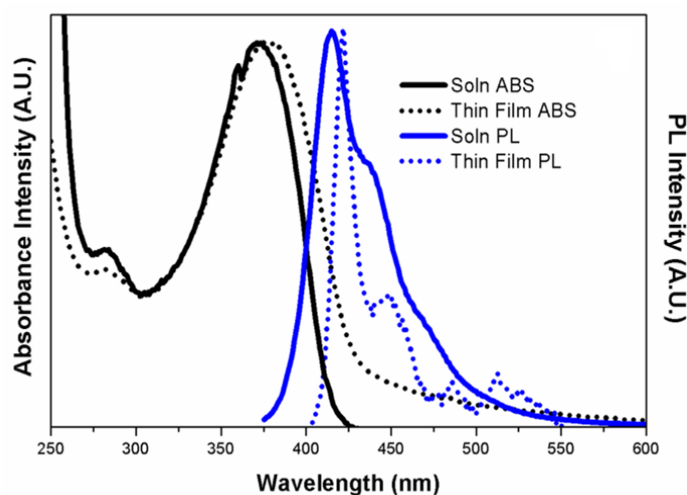


**Figure 3.38.** UV-vis absorption and PL spectra of **P(F8-SFX)** in  $\text{CHCl}_3$ .

### 3.3.4. Electrochromic Properties of **P(F8-SFX)**

#### 3.3.4.1. Electrochromic properties of **P(F8-SFX)** and its switching property

The changes in the electronic absorption spectrum of **P(F8-SFX)** upon changing the applied potentials represent the electro-optical properties of the polymer film. In order to evaluate the electrochromic features and get information about charge carriers, **P(F8-SFX)** film was drop-casted onto ITO (20 mg/mL). Following coating process of the electrode, the SPEL behavior of the polymer film was monitored in monomer-free electrolyte solution, during anodic oxidation. The electronic absorption spectra of neutral forms of the films exhibit absorption bands at around 380 nm, which is due to  $\pi$ - $\pi^*$  transitions for **P(F8-SFX)** (**Figure 3.39**). The electronic band gap defined as the onset energy for the  $\pi$ - $\pi^*$  transition and was found to be 2.80 eV. This value is lower than the values obtained both from electroanalytical measurements and absorption spectrum of polymer solution during UV-vis measurements. It may be due to the red shift effect of ITO electrode to the absorption band during optical measurement. The evolution of the spectra during doping process shows simultaneous increases in the absorbance intensities, corresponding to the formation of the new charge carriers (polarons and bipolarons). In the electronic absorption spectra of **P(F8-SFX)** film, a new increasing absorption band was observed at 527 nm in the potential

range of 0.0–0.40 V and upon further applied potential, another absorption band appears about 1000 nm in the near – IR region with a clear isosbestic points at 440 nm indicating that polymer film was being interconverted between its neutral and oxidized states. As a result of these variations in the absorption spectrum of **P(F8-SFX)**, the color of the polymer changes from yellow in the neutral state to pale purple upon doping.

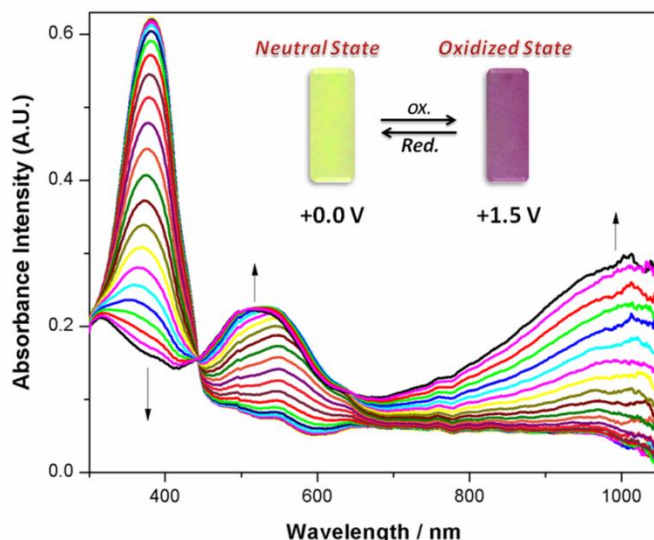


**Figure 3. 39.** Optical characterization of **P(F8-SFX)** by applying different potentials between oxidized and neutral states with an inset of photographs.

Due to its importance in electrochromic applications, switching times and optical contrast of the **P(F8-SFX)** film on ITO were also investigated under square wave input of 0.0 to 1.5 V in 10 s intervals by monitoring the visible transmittance and the kinetic responses of the film at 527 nm. **P(F8-SFX)** film shows a reversible response within the range of applied potential pulses with a response time of 1.62 s for oxidation and 2.2 s for reduction at 95% of the maximum transmittance and the optical contrast (%T) was 14.0 % at 527 nm. On the basis of these equations, **P(F8-SFX)** has  $\eta$  value of 120 cm<sup>2</sup>/ C at 527 nm and 266 cm<sup>2</sup>/ C at 1000 nm which is very close to those fluorene copolymers reported previously [110], indicating that it is a promising candidate for electrochromic device applications.

### 3.3.4.2. Optical Properties of the **P(F8-SFX)/PEDOT** electrochromic device

All-polymer electrochromic device consisting of **P(F8-SFX)** and PEDOT was constructed as shown in the inset (a) of **Figure 3.40** and its spectroelectrochemical properties was investigated by monitoring the optical absorbance spectra at different applied potentials. Electrochromic device showed a reversible response in the potential range of -0.5 V (neutral) and +2.0 V (oxidized). At -0.5 V, the colors of polymer and PEDOT were yellow and transparent, respectively (Inset (b) of **Figure 3.40**). Therefore, the polymer film was yellow colored in its neutral state with a  $\lambda_{\text{max}}$  at 386 nm. As the device was oxidized with the applied potentials, the color of the device became dark purple. A new band at 600 nm because of PEDOT film starts to intensify accompanied with the band of **P(F8-SFX)** at 527 nm.

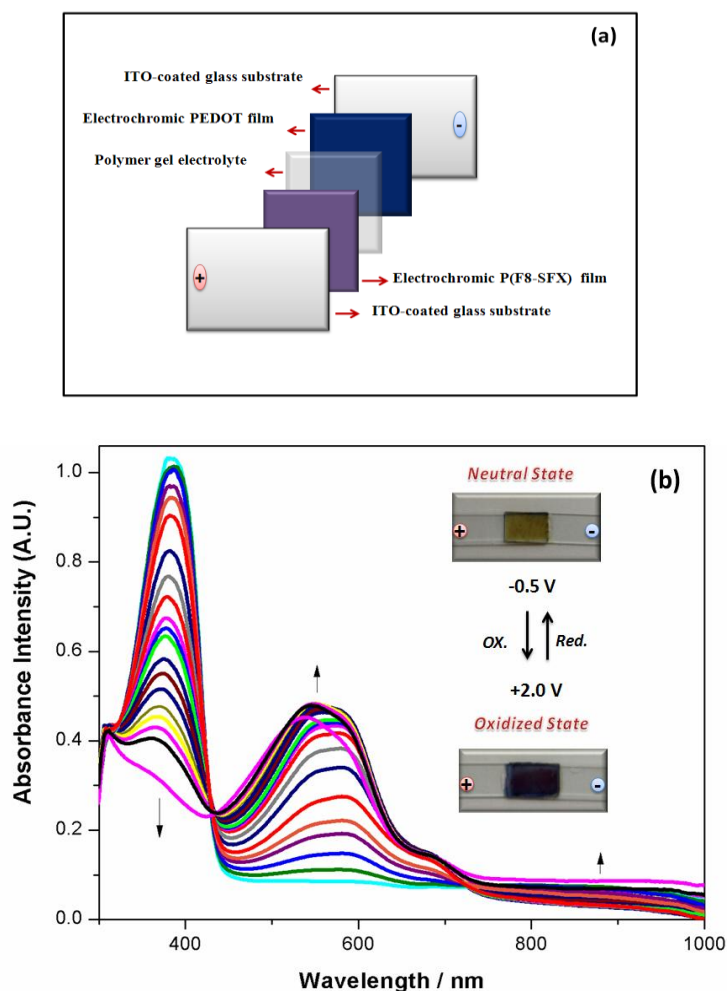


**Figure 3. 40.** Optical characterization of **P(F8-SFX)/PEDOT** electrochromic device by applying different potentials between oxidized and neutral states. **(a)** illustration of electrochromic device construction). **(b)** the colors of oxidized and neutral states and

**Table 3. 8.** Electronic and electrochromic properties of the **P(F8-SFX)** and its electrochromic device (<sup>a</sup>CIE L x x b system: luminance (L), hue (a) and saturation (b). <sup>b</sup>Redox states for PEDOT layer.)

| Polymer / device                | $\lambda_{\max}$<br>(nm) | Redox<br>state        | $L^a$ | $a^a$ | $b^a$ | Color          | CE<br>$\text{cm}^2/\text{C} (\lambda)$  |
|---------------------------------|--------------------------|-----------------------|-------|-------|-------|----------------|---|
| <b>P(F8-SFX)</b> film           | 380                      | Oxidized              | 52.17 | 15.7  | -15.8 | Pale purple    | 120<br>(527 nm)<br><br>266 (1000<br>nm) |
|                                 | 527                      |                       |       |       |       |                |   |
|                                 | 1000                     | Neutral               | 88.92 | -8.62 | 7.44  | Yellow         |   |
| <b>P(F8SFX)/PEDOT</b><br>Device | 386                      | Oxidized <sup>b</sup> | 82.91 | 24.64 | 50.99 | Dark<br>Yellow | -                                       |
|                                 | 561                      | Neutral <sup>b</sup>  | 68.75 | -3.70 | -4.94 | Dark<br>purple |   |
|                                 |                          |                       |       |       |       |                |   |

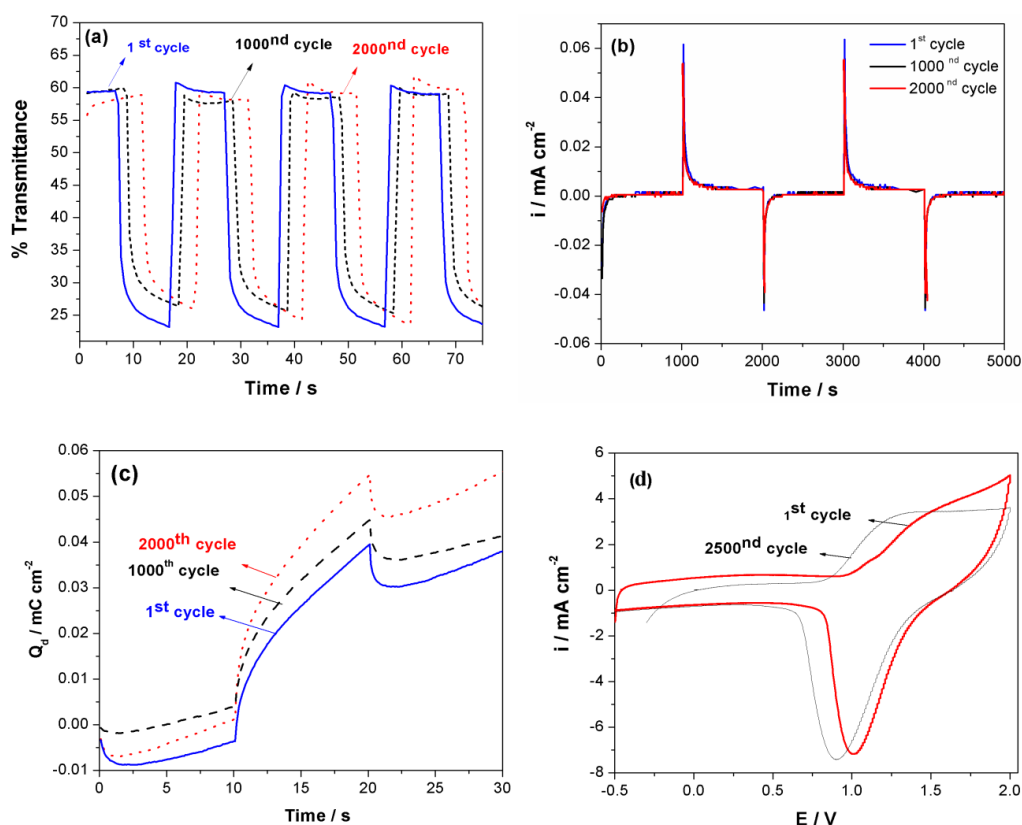


**Figure 3. 41.** (a) Chronoabsorptometry (b) chronocoloumetry and (c) current density experiments for **P(F8-SFX)** electrochromic device at  $\lambda_{\text{max}}$  (562 nm) under an applied square voltage signal between -0.5 V and 2.0 V. (d) Electrochemical stability of **P(F8-SFX)/PEDOT** electrochromic device.

The long cycle life time is also another important parameter in the electrochromic devices. For this purpose, **P(F8-SFX)/PEDOT** device was switched between -0.5 V and +2.0 V by applying potential intervals of 1 s. SPEL and electrochemical behavior of the device were also investigated after switching steps. After 2000 time switching steps, the device still keeps its redox stability, retaining 98.64 % of its optical activity (**Figure 3.41 a, b, c**). The stability of the device was also investigated in the solvent electrolyte solution via cyclic voltammetry method. The results indicate that the polymer film was quite stable and retained 93.0 % of its electroactivity after 2500 cycles (**Figure 3.41**).

### 3.3.5. PLED Characterization

Device from a single layer device of **P(F8-SFX)** gave poor device efficiency. The maximum brightness that could be obtained was  $17 \text{ cd/m}^2$  and the electroluminescence spectrum (**Figure 3.42**) was mostly dominated by long wavelength emissions due to increase in applied voltage which can be attributed to the increase in keto defects and excimer emission [147,148].



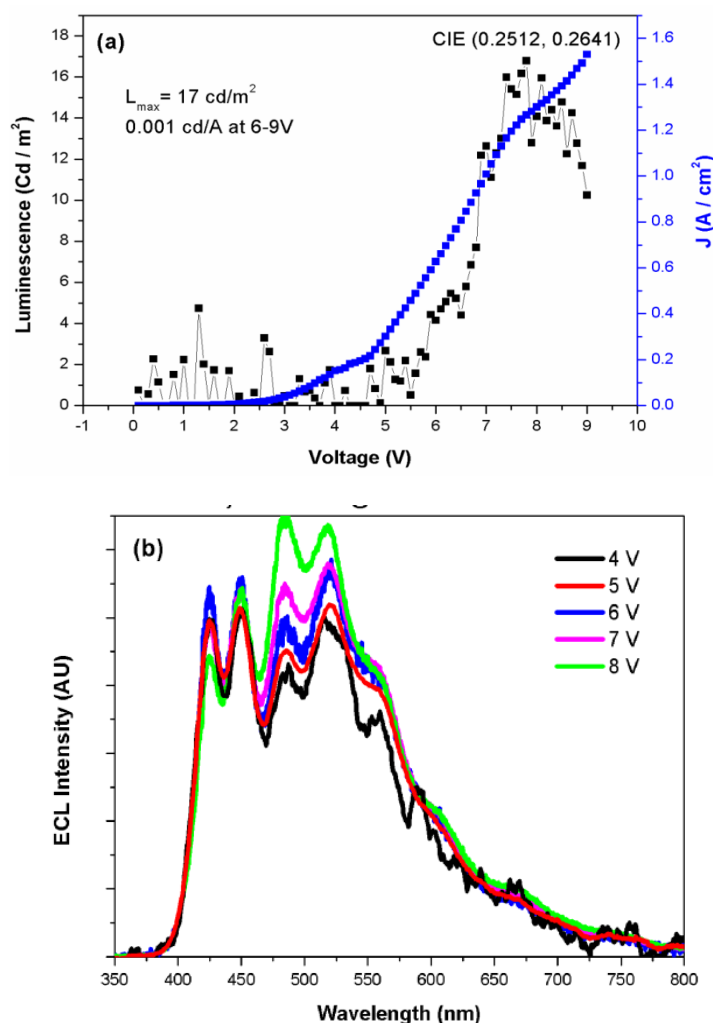


**Figure 3.42.** Behaviour of the single layer device

The contribution from the longer wavelength emission can be overcome either by doping the active material by hole trapping molecules or using hole transporting layers [149-150]. Both of the methods have been tried in this study and it is concluded that inserting a thin layer of F8-TFB could improve both the brightness and the color purity. **Figure 3.43a** illustrates the device fabricated with the structure of ITO/PEDOT/CAV-2/P(F8-SFX)/Ca(20 nm)/Al(100 nm). As the HOMO level of the F8-TFB matches with the PEDOT: PSS (-5.1), it is not expected to see any decrease in total current which shows that F8-TFB does not act as a HTL. The total current did not change when F8-TFB layer is inserted. However, it acts as an electron blocking layer due to its lower LUMO level (-2.2) than P(F8-SFX) (-2.7). Electrons injected from cathode to P(F8-SFX) layer are blocked by F8-TFB; therefore, reaching to PEDOT:PSS and hence ITO. This may result in an increase in the recombination. The device that has a thin layer of F8-TFB between PEDOT:PSS and P(F8-SFX) showed a better luminescence, 73 cd/m<sup>2</sup> at 8.4 V with CIE (0.194, 0.1561) (**Figure 3.43b and c**). Color purity is the main problem for polyfluorene derivatives [153]. Increase in green emission has been attributed to the ketone defects which cause rapid energy transfer from high energy sites to lower energy sites before radiative decay of the excited species [152,153]. For the devices which do not contain F8-TFB, the green emission is very intense. However, when a thin of F8-TFB layer is added between PEDOT: PSS and emitting layer, the green emission is significantly reduced (**Figure 3.43d**).



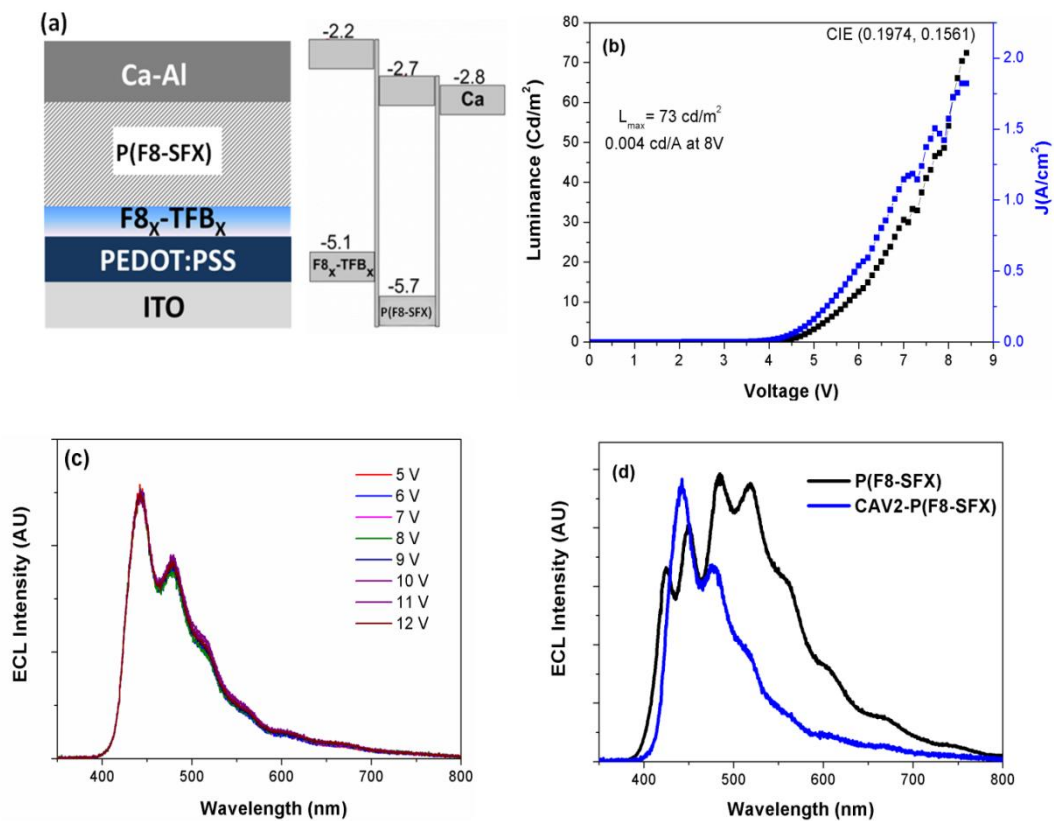


**Figure 3. 43.** (a) Schematic illustration of ITO/PEDOT/F8-TFB/P(F8-SFX)/Ca(20 nm)/Al(100 nm) PLED device and its energy band diagram (b) Device performance and normalized ECL spectrum of the device ITO/PEDOT:PSS/CAV-2/P(F8-SFX)/Ca-Al. (c) Electroluminescence spectrum of single layer device (black) and the device with thin CAV-2 layer. (d) Comparison of ECL spectrum P(F8-SFX) and CAV-2- P(F8-SFX).



## CHAPTER 4

### CONCLUSIONS

In this thesis, the synthesis of new fluorene containing polymers and their applications are described. The investigation carried out in this project allowed for the development of new conjugated fluorene based polymers as electrochromic materials besides their implementation to multiple device configurations. The results presented also bring a new standpoint on the polyfluorene derivatives in terms of multifunctionality and processability. By using a changeable fluorene structure or adjusting the composition of the polyfluorene copolymer, it is possible to obtain varied colored electrochromic and light emitting polymers. Furthermore, polyfluorene and related structures have been used widely in biological and chemical sensing applications because of their facile substitution at fluorene C9 position. As previously mentioned, the research was divided into three parts.

In the first part, a new material **P(FCA)** was synthesized for electrochromic device applications. Electrochemical polymerization, which is one of the fast and reliable synthetic methods, was employed for the generation of polymer on the electrode surface. In electrochemical polymerization, various solvents have been widely applied for different fluorene derivatives to electropolymerize. Furthermore, the polymerization potentials of fluorene derivatives were relatively high and the amount of obtained polymers was little. For that reason, BFEE is generally used to get low-potential electropolymerization of polyfluorene derivatives to obtain better quality films. Fluorene based homopolymer, **P(FCA)** was successfully synthesized via electrochemical polymerization in the medium of nitromethane containing 4% BFEE and 0.1 M TBABF<sub>4</sub> leads to formation of a polymer film on platinum surface. The structural characterization, electrochemistry, electrochromic, and thermal stability were investigated. Indeed, as-formed **P(FCA)** film showed some interesting optoelectronic properties. The thermal analysis results indicated the high thermal stability of **P(FCA)**.

Also, **P(FCA)** can be reversibly switched between its neutral to oxidized state, which is accompanied with a color change from transparent to brownish-orange color as seen in the **Figure 4.1**. An anodically coloring polyfluorene derivative was obtained. Furthermore, the dual type electrochromic device constructed utilizing **P(FCA)** and PEDOT exhibits switching ability with a good optical memory with a color change of transparent to dark blue. These properties make **P(FCA)** a good candidate for display applications. However, its partial solubility in common organic solvents limits its application in organic electronics.

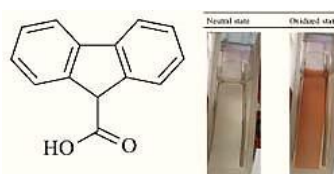
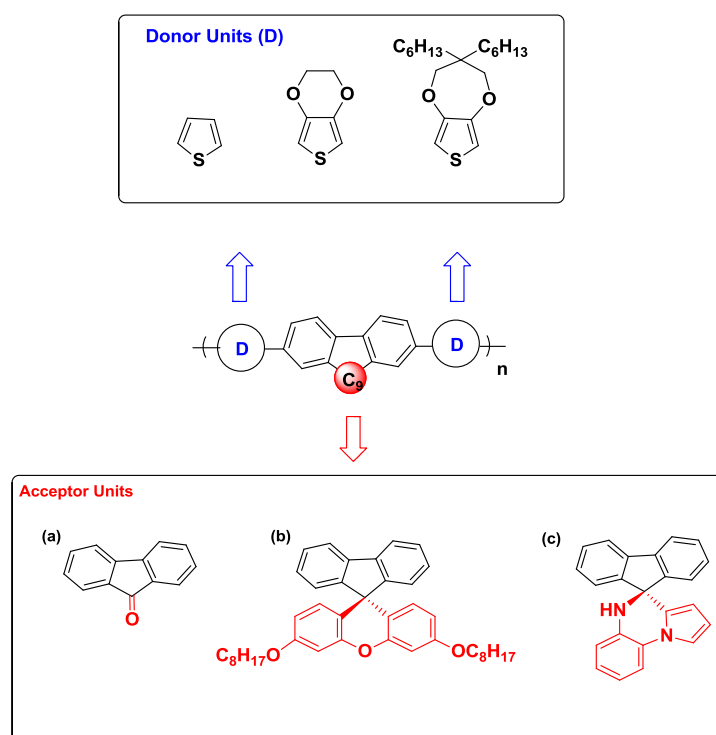


**Figure 4. 1.** The chemical structure of **FCA** and electrochromic performance of its polymer **P(FCA)** in the neutral and oxidized states.

In the next part, a series of new fluorene derivatives bearing different pendant units with different donor units was synthesized as illustrated in **Scheme 4.1**. The fluorene subunits contained ketone functional group, quinoxaline and xanthene pendant groups at the C9 position. The donor-

acceptor-donor segments were derived from this middle functionalized fluorene structures. Three different heterocyclic units along with fluorene moieties were also incorporated especially chosen for their varied electron densities because of the methodology, which is related with the control of the optoelectronic properties of the resulting polymers. Solution processability of electrochromic polymers is a major advantage for the fabrication of large area devices. ProDOT donor group with hexyl units was especially selected for this purpose. Totally, eight thiophene-based D-A-D monomers were also electropolymerized via potential cycling in their proper solvent-electrolyte mixture in this part. It is important that the polymer films obtained have relatively lower band gaps which are also lower than those previously reported PF derivatives. SPEL and electrochemical analyses revealed that polymer films can be reversibly cycled between their neutral and oxidized states with electrochromic response. Beside the electrochromic and fluorescence property of the polymers, processable ones were also used some important applications.



**Scheme 4. 1.** Chemical structures of a series of new fluorene derivatives bearing different pendant units with different donor units.

The fluorescence property of the processable polymers were also investigated. Depending on the functional unit, the color of the polymer was changed as seen in **Figure 4.2**.

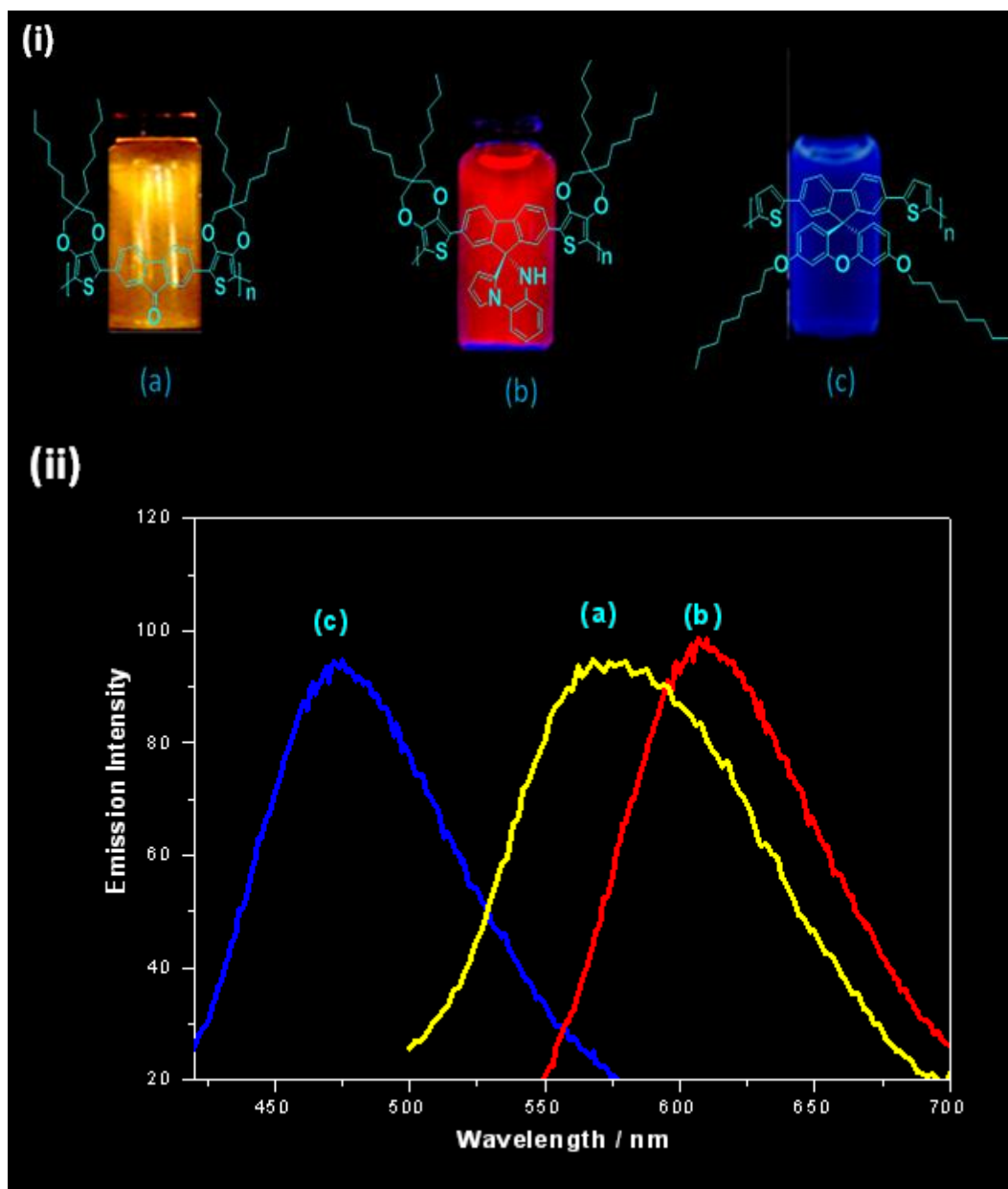


**Figure 4. 2.** Emission (i) colors and (ii) spectrum of (a) **P(PFP)**, (b) **P(PQP)** and (c) **P(TXT)** in the presence of in THF under handheld UV lamp.

The electrochromic colors of all the polymers in reduction (-), neutral (0), oxidation (+) and intermediate (I) states were also summarized in **Figure 4.3**. Same class of polymers (fluorenone, fluoren-quinoxaline and fluoren-xanthene) can be evaluated in terms of colors. While fluorenone derivatives exhibit nearly same colors in the reduced and neutral states and different colors in oxidized states others (spiro-fluoren polymers) shows different colors in neutral and oxidized states. It is also noted that **P(EXE)** shows multichromic property.

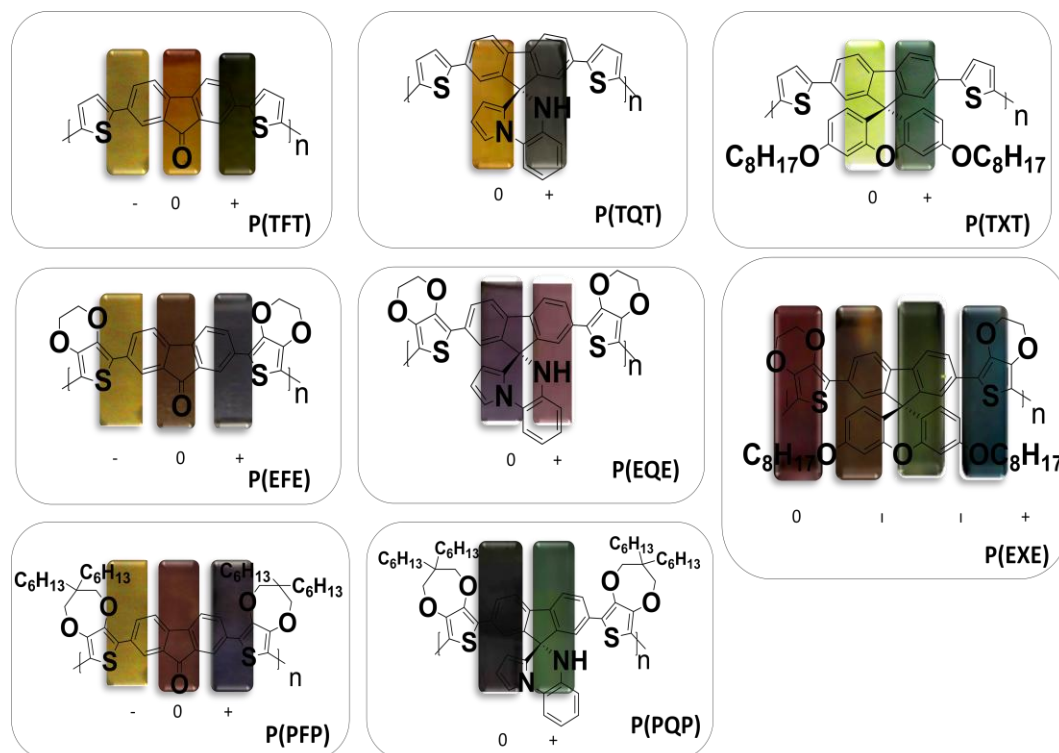


**Figure 4. 3.** Electrochromic colors of the D-A-D type fluorene derivatives.

The electrochemical and optical properties of the fluorene derivatives with different donor groups were summarized in **Table 4.1**. The oxidation potential of the monomers were also compared with each other in the same medium for the same class of fluorene derivatives. The results were showed that the oxidation potential of the monomers changed depending on the donor strength. Electropolymerization of the D-A-D systems provided new low band gap electrochromes. The band gaps of the polymers changes depending on the donor strength in the same class fluorene derivative. Among all the electrochromic polymers for this group, **P(PFP)** had superior properties with high optical stabilities and high coloration efficiency ( $422 \text{ cm}^2/\text{C}$ ).

Each class of the fluorene derivative (fluorenone, fluoren-quinoxaline and fluoren-xanthene) arouses interest because of their usages for some various applications but electrochromism property.

#### • Fluorenone Derivatives

SPEL and electrochemical analysis revealed that the polymer films, **P(TFT)**, **P(EFE)** and **P(PFP)** are both p- and n-dopable and can be successfully cycled and switched between oxidized and neutral states. The results also showed that the polymer film **P(PFP)** showed a higher  $\eta$  value ( $422 \text{ cm}^2/\text{C}$  at 684 nm) than other fluorenone derivatives in **Table 4.1**. The presence of ProDOT donor groups not only lowered the band gap (1.74 eV) of the **P(PFP)** film but also enhanced the solubility. Due to the HOMO level being closer to ITO work function, polymeric films expected to have enhanced hole injection. On the other hand, its LUMO energy ( $-3.4 \text{ eV}$ ) correlates well with the work function of Mg indicating facile electron injection. These properties make these films a promising candidate as an ambipolar charge transport material in LEDs. Furthermore, due to their orange light-emitting fluorescence property **P(EFE)** and **P(PFP)** may find applications in various fields, such as organic lasers and electroluminescent materials.

- **Fluoren-quinoxaline Derivatives**

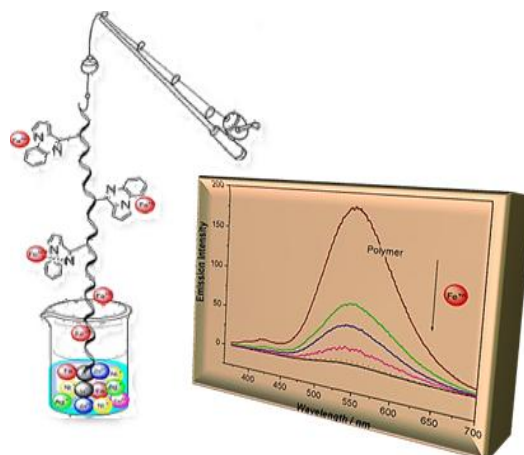


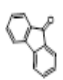
**Figure 4. 4.** An illustration of quinoxaline functionality over the metal cations when it acts a pendant unit over the polymer chain. Fluorescence intensity decreases upon successive addition of  $\text{Fe}^{2+}$  ion due to energy transfer between  $\text{Fe}^{2+}$  ions and fluorene quinoxaline fluorophore.

Among the three fluoren-quinoxaline polymers, **P(PQP)** has the lowest band gap (1.66 eV) and highest  $\eta$  ( $253 \text{ cm}^2/\text{C}$ ) with smallest switching time (1.02 s) as seen in **Table 4.1**. The decrease in the band gap energy indicated not only Pro-DOT side group is a stronger donor group when compared to EDOT and thiophene but also enhances the solubility of polymer film. Fluorescence of **PQP** and its corresponding polymer **P(PQP)**, were found to be highly sensitive towards  $\text{Fe}^{2+}$  ions which make them a promising sensor candidate for  $\text{Fe}^{2+}$  ion detection, besides the use of **P(PQP)** in electronic and optical applications. The ion sensitivity of **PQP** and its polymer **P(PQP)** was also investigated by monitoring the change in the fluorescence intensity. Among various common ions, both **PQP** and **P(PQP)** were found to be selective towards  $\text{Fe}^{2+}$  ions by quenching the fluorescence efficiency with a Stern–Volmer constant ( $K_{\text{sv}}$ ) of ( $5.9 \times 10^3 \text{ M}^{-1}$ ) and ( $2.7 \times 10^4 \text{ M}^{-1}$ ) for monomer and polymer solutions, respectively.

- **Fluoren-xanthene Derivatives**

**P(TXT)** and **P(EXE)** were also achieved via potential cycling in their proper solvent–electrolyte mixture and then characterized with electrochemical and spectroscopic methods. SPEL and electrochemical analyses revealed that the polymer films can be successfully cycled and switched between neutral and oxidized states several times without any appreciable decrease in its electroactivity. As **P(TXT)** transmits yellow and green color in its fully neutral and oxidized forms, **P(EXE)** transmits scarlet red to turquoise with intermediate colors at different applied potentials. Due to its blue light-emitting fluorescence property and thermal as well as attractive optical properties, **P(TXT)** and **P(EXE)** may find potential utility in the field for PLEDs, organic lasers and electrofluorescence or electrochromic devices.

**Table 4. 1.** A summary of electrochemical and optical data for D-A-D type fluorene derivatives

| MONOMER | Chemical Structure  | FLUOREN-ONE DERIVATIVES |               |              |              | FLUOREN-QUINOXALINE DERIVATIVES |              |              |              | FLUOREN-XANTHENE DERIVATIVES |              |             |
|---------|---|-------------------------|---------------|--------------|--------------|---------------------------------|--------------|--------------|--------------|------------------------------|--------------|-------------|
|         |   | FO                      | TFT           | EFE          | PFP          | FQ                              | TQT          | EQE          | PQP          | FX                           | TXT          | EXE         |
|         |  |                         |               |              |              |                                 |              |              |              |                              |              |             |
|         | $E_{ox}^H$ (V)  | 2.40*                   | 1.34          | 1.10         | 1.05         | 1.80 (0.98)                     | 1.35 (0.98)  | 1.00 (0.98)  | 1.10 (0.98)  | 1.50 (1.90)                  | 1.06 (1.90)  | 0.91 (1.90) |
|         | $E_{opt}^{red}$ (eV)  | 2.40                    | 2.27          | 1.68         | 1.79         | -                               | 2.47         | 1.93         | 1.66         | 2.92**                       | 2.23         | 1.74        |
|         | $\eta$ (Å)  |                         | 6.71 (394nm)  | 250 (462nm)  | 144 (441nm)  | -                               | 10.3 (390nm) | 98 (390nm)   | 235 (569nm)  | -                            | 187 (395nm)  | 258 (500nm) |
| POLYMER |   |                         | 46.8 (697nm)  | 242 (697nm)  | 422 (664nm)  |                                 | 115 (515nm)  | 69.6 (560nm) | 90.7 (874nm) |                              | 136 (655nm)  | 215 (680nm) |
|         |   |                         | 9.32 (1050nm) | 218 (1050nm) | 93 (1050nm)  |                                 | 145 (742nm)  | 65 (780nm)   | 253 (1017nm) |                              | 151 (1017nm) | 310 (960nm) |
|         |   |                         | 2.9 (394nm)   | 4.8 (462nm)  | 3.1 (441nm)  |                                 | 0.8 (390nm)  | 1.1 (390nm)  | 2.6 (569nm)  |                              | 2.4 (395nm)  | 2.6 (500nm) |
|         | $t_{switching}$ (s)   |                         | 8.6 (697nm)   | 1.9 (697nm)  | 1.9 (664nm)  |                                 | 1.1 (515nm)  | 3.3 (515nm)  | 2.0 (874nm)  |                              | 1.1 (655nm)  | 0.8 (680nm) |
| POLYMER |   |                         | 1.6 (1050nm)  | 2.3 (1050nm) | 3.1 (1050nm) |                                 | 1.3 (742nm)  | 3.3 (742nm)  | 1.8 (1017nm) |                              | 1.7 (1017nm) | 1.3 (960nm) |



In the third part of the thesis, another class of conjugated copolymer for a dual electrochromic and light emitting display was also synthesized and characterized. The multifunctional polymer, **P(F8-SFX)** exhibits yellow to purple electrochromism upon oxidation with relatively high  $\eta$  ( $120 \text{ cm}^2/\text{C}$  at  $527 \text{ nm}$  and  $266 \text{ cm}^2/\text{C}$  at  $1000 \text{ nm}$ ). The utilization of dual-type complementary colored polymer electrochromic devices using **P(F8-SFX)**/ (PEDOT) in sandwich configuration was also successfully established. The switching ability and spectroelectrochemical properties of the electrochromic device were investigated utilizing UV-vis spectrophotometry and cyclic Voltammetry. The results obtained indicated a high switching ability and redox stability. In the second part of the study, blue emitting (CIE coordinate; (0.19, 0.15)) PLED device using **P(F8-SFX)** was constructed and device performance was optimized utilizing an electron blocking layer. Significant improvement in the color purity and 4 fold increase in the brightness was observed for the devices with the electron blocking layer as compared to the single layer devices.



## REFERENCES

- [1] Staudinger, H. *Nobel Lectures*, Chemistry 1942-1962; Elsevier Publishing Company: Amsterdam, 1964.
- [2] Staudinger H. *Ber. Dtsch. Chem. Ges. B* 1920, 53, 1073.
- [3] Heeger, H. Semiconducting and Metallic Polymers: The Fourth Generation of Polymeric Materials, [http://nobelprize.org/nobel\\_prizes/chemistry/laureates/2000/heegerlecture.pdf](http://nobelprize.org/nobel_prizes/chemistry/laureates/2000/heegerlecture.pdf), 2009.
- [4] Schwendeman, I.; Hickman, R.; Sonmez, G.; Schottland, P.; Zong, K.; Welsh, D.; Reynolds, J. R. *Chem. Mater.* 2002, 14, 3118.
- [5] Meng, H.; Tucker, D.; Chaffins, S.; Chen, Y.; Helgeson, R.; Dunn, B.; Wudl, F. *Adv. Mater.* 2003, 15, 146.
- [6] Bange, K.; Gambke, T. *Adv. Mater.* 1990, 2, 10.
- [7] Pennisi, A.; Simone, F.; Barletta, G.; Di Marco, G.; Lanza, L. *Electrochim. Acta* 1999, 44, 3237.
- [8] Rauh, R. *Electrochim. Acta* 1999, 44, 3165.
- [9] Mortimer, R. G. *Chem. Soc. Rev.* 1997, 26, 147.
- [10] Rosseinsky, D. R.; Mortimer, R. J. *Adv. Mater.* 2001, 13, 783.
- [11] Chandrasekhar, P.; Zay, B. J.; Birur, G. C.; Rawal, S.; Pierson, E. A.; Kauder, L.; Swanson, T. *Adv. Funct. Mater.* 2002, 12, 95.
- [12] Beaupré, S.; Breton, A.-C.; Dumas, J.; Leclerc, M. *Chem. Mater.* 2009, 21, 1504.
- [13] Schmidt-Mende, L.; Fechtenkötter, A.; Mullen, K.; Moons, E.; Friend, R. H.; Mackenzie, J. D. *Science* 2001, 293, 1119.
- [14] Liscio, A.; De Luca, G.; Nolde, F.; Palermo, V.; Müllen, K.; Samori, P. *J. Am. Chem. Soc.* 2008, 130, 780.
- [15] Fréchet, J.M.J.; Thompson, B. C. *Angew. Chem., Int. Ed.* 2008, 47, 58.
- [16] Dance, Z. E. X.; Ahrens, M. J.; Vega, A. M.; Ricks, A. B.; McCamant, D. W.; Ratner, M. A.; Wasielewski, M. R. *J. Am. Chem. Soc.* 2008, 130, 830. 150
- [17] Hagberg, D. P.; Yum, J.-H.; Lee, H.; De Angelis, F.; Marinado, T.; Karlsson, K. M.; Humphry-Baker, R.; Sun, L.; Hagfeldt, A.; Grätzel, M.; Nazeeruddin, Md. K. *J. Am. Chem. Soc.* 2008, 130, 6259.
- [18] Muccini, M. *Nat. Mater.* 2006, 5, 605.
- [19] Gao, P.; Beckmann, D.; Tsao, H. N.; Feng, X.; Enkelmann, V.; Pisula, W.; Müllen, K. *Chem. Commun.* 2008, 1548.
- [20] Usta, H.; Facchetti, A.; Marks, T. J. *J. Am. Chem. Soc.* 2008, 130, 8580.
- [21] Yang, C.; Kim, J. Y.; Cho, S.; Lee, J. K.; Heeger, A. J.; Wudl, F. *J. Am. Chem. Soc.* 2008, 130, 6444.
- [22] Hermans, E.C.M. *Sensors Actuators* 1984, 5, 181.
- [23] Bott, B.; Jones, T.A. *Sensors Actuators* 1986, 9, 19.
- [24] Heiland, G.; Kohl, D. *Sensors Actuators* 1985, 8, 227.
- [25] Nylander, C.; Armgarth, M.; Lundström, I. *Anal Chem Symp Ser* 1983, 17, 203.
- [26] Colla, J.O.; Thoma, P.E. *Nitrogen dioxide sensing element and method of sensing the presence of nitrogen dioxide*. US Pat 4,142,400; 1979.
- [27] Karami, H.; Mousavi, M.F.; Shamsipur, M. *Journal of Power Sources* 2003, 124, 303.
- [28] Nyström, G.; Razaq, A.; Strømme, M.; Nyholm, L.; Mihranyan, A. *Nano Letters* 2009, 10, 3635.
- [29] Gofer, Y.; Sarker, H.; Killian, J. G.; Poehler, T. O.; Searson, P. C. *Appl. Phys. Lett.* 1997, 71, 1582.
- [30] Katz, H.E.; Searson, P.C.; Poehler, T.O. *J. Materials Research* 2010, 25, 1561.
- [31] Zheng, W.; Alici, G.; Clingan, P. R.; Munro, B. J.; Spinks, G. M.; Steele, J.R.; Wallace, G. G. *J. Polym. Sci. Part B: Polym. Phys.* 2013, 51, 57.
- [32] Shoa, T. N.; Shoa, T.; Madden, J. D.W.; Mirfakhrai, T.; Alici, G.; Spinks, G. M.; Wallace, G. G. *Sensor and Actuators A* 2010, 161, 127.
- [33] Skotheim, T.A.; Reynolds, J.R. *Handbook of Conducting Polymers, Theory, Synthesis, Properties and Characterization*, CRC Press/Taylor & Francis 3<sup>rd</sup> ed., 2007.

- [34] Dai, L. *Intelligent Macromolecules for Smart Devices*, Springer, 2004
- [35] Bredas, J.L. ; Street, G.B. *Acc Chem. Res.* 1985, 18, 1309.
- [36] Salaneck, W. R.; Friend, R. H.; Bredas, J. L. *Physics Reports* 1999, 319, 231.
- [37] Wu, J. *Appl. Phys. Lett.* 2002, 80, 3967.
- [38] Nigrey, P. J.; MacDiarmid, A. G.; Heeger A. J. *Chem. Commun.* 1979, 96, 594.
- [39] Mort, N. F.; Davis, E. A. *Electronic Processes in Non-Crystalline Materials*, Clarendon Press, Oxford, 1979.
- [40] Kumar, D.; Sharma, R.C. *Eur. Polym. J.*, 1998, 34,1053.
- [41] Toshima, N.; Hara, S.; *Prog. Polym. Sci.* 1995, 20,155.
- [42] Street, B. G.; Clarke, T. C.; Krounbi, M.; Kanazawa, K.; Lee, V.; Pfluger P.; Scott, J. C.; Weiser, G. *Mol. Cryst. Liq. Cryst.* 1982, 83,1285.
- [43] Salmon, M.; Kanazawa, K. K.; Diaz, F. F.; Krounbi, M. *J. Polym. Sci.* 1982, 20,187.
- [44] Shimidzu, T.; Ohtani, A.; Iyoda, T.; Honda, K. J. *J. Chem. Soc., Chem. Commun.* 1982, 361.
- [45] Wang, J. *Analytical Electrochemistry*, 3<sup>rd</sup> ed., John Wiley & Sons, 2006.
- [46] Chiang, C.K.; Fincher, C.R.; Park, Y.W.; Heeger, A.J.; Shirakawa, H.; Louis, E.J.; Gau, S.C.; MacDiarmid, A.G. *Phys. Rev. Lett.* 1977, 39, 1089.
- [47] Sawyer, D.T.; Roberts Jr., J.L. *Experimental electrochemistry for chemists*, Wiley Interscience, Newyork, 1974.
- [48] Mann, C.K. *Electroan Chem* 1969, 3, 57.
- [49] Baizer, M.M.; Lund, H. *Organic Electrochemistry*, Marcel Dekker, New York, 1983.
- [50] Noel, M ; Vasu, K.I. *Cyclic Voltammetry and the frontiers of Electrochemistry*, Oxford IBH publishing Co. Pvt. LTD, 1990.
- [51] Rieger, P. H. *Electrochemistry*, 2<sup>nd</sup> ed., Chapman & Hall Inc, USA, 1994.
- [52] Hibbert, D.B. *Introduction to Electrochemistry*, Macmillan Press, London, 1993.
- [53] Scholz, F. *Electroanalytical methods*, 2<sup>nd</sup> ed., Springer, 2010.
- [54] Gibson, G.L.; McCormick, T.M.; Seferos, D.S. *J. Am. Chem.Soc.* 2012, 134, 539.
- [55] Pamuk, M.; Tirkeş, S.; Cihaner, A.; Algi, F. *Polymer* 2010, 51, 62.
- [56] Koldemir, U.; Graham, K. R.; Salazar, D. H.; McCarley, T. D.; Reynolds, J. *J. Mater. Chem.* 2011, 21, 6480.
- [57] Bezgin, B.; Cihaner, A.; Önal, A.M. *Thin Solid Films* 2008, 516, 7329.
- [58] Sonmez, G.; Schwendeman, I.; Schottland, P.; Zong, K.; Reynolds, J. R. *Macromolecules* 2003, 36, 639.
- [59] Beaujuge, P. M.; Reynolds, J. R. *Chem.l Rev.* 2010, 110, 268.
- [60] Argun, A. A.; Aubert, P. H.; Thompson, B. C.; Schwendeman, I.; Gaupp, C. L.; Hwang, J.; Pinto, N.J.; Tanner, D. B.; MacDiarmid, A. G.; Reynolds, J. R. *Chem. Mater.* 2004, 16, 4401.
- [61] Sotzing, G. A.; Reddinger, J. L.; Katritzky, A. R.; Soloducho, J.; Musgrave, R.; Reynolds, J. R. *Chem. Mater.* 1997, 9, 1578.
- [62] Amb, C. M.; Dyer, A. L.; Reynolds, J.R. *Chem. Mater.* 2011, 23, 397.
- [63] Dyer, A. L.; Thompson, E. J.; Reynolds, J. R. *Appl. Mater. Interfaces* 2011, 3, 1787.
- [64] Carbas, B. B.; Kivrak, A.; Zora, M.; Önal, A. M. *J. Electroanal.Chem.* 2012, 677–680, 9.
- [65] Lakowicz, J. R. *Principles of Fluorescence Spectroscopy*, Plenum: New York, 1983
- [66] Fery-Forgues, S.; Lavabre, D. *J. Chem. Ed.*,1999, 76, 1260.
- [67] Grimsdale, A. C.; Chan, K. L.; Martin, R. E.; Jokisz, P. G.; Holmes, A. B. *Chem. Rev.* 2009, 109, 897.
- [68] Inaoka, S.; Advincula, R. *Macromolecules* 2002, 35, 2426.
- [69] Tsuie, B.; Reddinger, J. L.; Sotzing, G. A.; Soloducho, J.; Katritzky, A. R.; Reynolds, J. R. *J. Mater. Chem.* 1999, 9, 2189.
- [70] Larmat, F.; Reynolds, J. R.; Reinhardt, B. A.; Brott, L. L.; Clarson, S. I. *J. Polym. Sci., Part A: Polym. Chem.* 1997, 35, 3627.
- [71] Nie, G.; Yang, H.; Chen, J.; Bai, Z. *Organic Electronics: physics, materials, applications* 2012, 13, 2167.
- [72] Çarbaş, B.B.; Kivrak, A.; Önal, A.M. *Electrochim. Acta* 2011, 58, 223.
- [73] Fukuda, M.; Sawada, K.; Yoshino, K. *J. Polym. Sci. A: Polym. Chem.* 1993, 31, 2465.
- [74] Yamamoto, T.; Zhou, Z.H.; Takaki, K.; Shimura, M.; Kizu, K.; Maruyama, T.; Nakamura, Y.; Fukuda, T.; Lee, B.L.; Ooba, N.; Tomaru, S.; Kurihara, T.; Kaino, T.; Kubota, K.; Sasaki, S.J. *J. Am. Chem. Soc.* 1996, 118, 10389.

- [75] Bernius, M.; Inbasekaran, E.; Woo, E.; Wu, W.; Wujkowski, L. *J. Mater. Sci.: Mater. Electron.* 2000, 111.
- [76] Inbasekaran, M.; Wu, W.; Woo, E.P. *US Patent* 5,777,070, 1998.
- [77] Xu, J.K.; Wei, Z.H.; Du, Y.K.; Zhou, W.Q.; Pu S.Z. *Electrochim. Acta* 2006, 51, 4771.
- [78] Fan, C.L.; Xu, J.K.; Chen, W.; Dong, B. *J. Phys. Chem. C* 2008, 112, 12012.
- [79] İmamoğlu, T.; Önal A.M. *Eur. Polym. J.* 2004, 40, 1875.
- [80] Chen, W.; Fan, C.L.; Zeng, L.Q.; Wang, X.C.; Chu, Q.; Xu, J.K. *Acta Polym. Sinica*, 2008, 9, 861.
- [81] Nie, G.M.; Cai, T.; Qu, L.Y.; Xu, J.K.; Wei, Q.; Zhang, S. S. *J. Electroanal. Chem.* 2008, 612, 191.
- [82] Fan, C. L.; Xu, J. K.; Chen, W.; Lu, B. Y.; Miao, H. M.; Liu, C. C.; Liu, G. D. *J. Phys. Chem C* 2009, 113, 9900.
- [83] Nie, G.M.; Guo, Q.F.; Zhang, Y.; Zhang, S. S. *Eur. Polym. J.* 2009, 45, 2600.
- [84] Zhang, S. S.; Nie, G.M.; Han, X.J.; Xu, J.K.; Li, M.S.; Cai T. *Electrochimica Acta* 2006, 51, 5738.
- [85] Cihaner, A.; Tirkes, S.; Onal, A.M. *J. Electroanal. Chem* 2004, 568, 151.
- [86] Lu, B. Y.; Zeng, L. Q.; Xu, J. K.; Le, Z. G.; Rao, H. Y. *Eur. Polym. J.* 2009, 45, 2279.
- [87] Zecchin, S.; Schiavon, G.; Tomat, R.; Zotti, G. *J. Electroanal. Chem.* 1986, 215, 377.
- [88] Uckert, F.; Setayesh, S.; Mullen, K. *Macromolecules* 1999, 32, 4519.
- [89] Eroğlu E. M.S. thesis, Middle East Technical University, 2013.
- [90] Güneş, A.; Cihaner, A.; Önal, A. M., *Electrochim. Acta*, 2013, 89, 339.
- [91] Loganathan, K.; Pickup, P. G. *Electrochim. Acta* 2007, 52, 4685.
- [92] Bezgin, B.; Önal, A.M. *Electrochim. Acta* 2010, 55, 779.
- [93] Çarbaş, B.B.; Kivrak, A.; Önal, A.M. *Electrochim. Acta* 2011, 58, 223.
- [94] List, E. J. W.; Guentner, R.; de Freitas, P. S.; Scherf, U. *Adv. Mater.* 2002, 14, 374.
- [95] Pogantsch, A.; Wenzl, F. P.; List, E. J. W.; Leising, G.; Grimsdale, A. C.; Müllen, K. *Adv. Mater.* 2002, 14, 1061.
- [96] Xiao, S.; Nguyen, M.; Gong, X.; Cao, Y.; Wu, H.; Moses, D.; Heeger, A.J. *Adv. Funct. Mater.* 2003, 13, 25.
- [97] Lee, J.; Cho, H. J.; Jung, B. J.; Cho, S. N.; Shim, H. K. *Macromolecules* 2004, 37, 8523.
- [98] Shu, C. F.; Dodda, R.; Wu, F. I.; Liu, M. S.; Jen, A. K. Y. *Macromolecules* 2003, 36, 6698.
- [99] Klarmer, G.; Davey, M. H.; Chen, W. D.; Scott, J. C.; Miller, R. D. *Adv. Mater.* 1998, 10, 993.
- [100] Klarmer, G.; Lee, J.I.; Lee, V. Y.; Chan, E.; Chen, J.P.; Nelson, A.; Markiewicz, D.; Siemens, R.; Scott, J. C.; Miller, R. D. *Chem. Mater.* 1999, 11, 1800.
- [101] Miteva, T.; Meisel, A.; Knoll, W.; Nothofer, H. G.; Scherf, U.; Müller, D. C.; Meerholz, K.; Yasuda, A.; Neher, D. *Adv. Mater.* 2001, 13, 565.
- [102] Xia, C.; Advincula, R. C. *Macromolecules* 2001, 34, 5854.
- [103] Lee, J.-H.; Hwang, D.H. *Chem. Commun.* 2003, 2836.
- [104] Yu, W. L.; Pei, J.; Huang, W.; Heeger, A. J. *Adv. Mater.* 2000, 12, 828.
- [105] Setayesh, S.; Grimsdale, A. C.; Weil, T.; Enkelmann, V.; Müllen, K.; Meghdadi, F.; List, E. J. W.; Leising, G. *J. Am. Chem. Soc.* 2001, 123, 946.
- [106] Dinakaran, K.; Chiu, M.Y.; Wei, K.H. *Macromolecules* 2005, 38, 745.
- [107] Tseng, Y.H.; Shih, P.I.; Chien, C.H.; Dixit, A.K.; Shu, C.F.; Liu, Y.H.; Lee, G.H. *Macromolecules* 2005, 38, 10055.
- [108] Woo, E. P.; Inbasekaran, M.; Shlang, W. R.; Roof, G. R.; Bernius, M. T.; Wu, W. *US Patent* 6,169,163, 2001.
- [109] Cho, N. S.; Hwang, D. H.; Lee, J. I.; Jung, B. J.; Shim, H. K. *Macromolecules* 2002, 35, 1224.
- [110] Ibrahimova, V.; Kocak, M. E.; Önal, A. M.; Tuncel, D. *Journal of Polymer Science, Part A: Polymer Chemistry* 2013, 51, 815.
- [111] Welsh, D. M.; Kumar, A.; Meijer, E. W.; Reynolds, J. R. *Adv. Mater.* 1999, 11, 1379.
- [112] Bunz, U. H. *Poly(arylene ethynylene)s*, 2005, 1-52.
- [113] Lackowicz, J. R. *Principles of Fluorescence Spectroscopy*, 1983, 262.
- [114] Liu, B.; Yu, W. L.; Pei, J.; Liu, S. Y.; Lai, Y. H.; Huang W. *Macromolecules* 2001, 34, 7932.
- [115] Qin, C.; Wu, X.; Gao, B.; Tong, H.; Wang, L. *Macromolecules* 2009, 42, 5427.
- [116] Li, Z.; Lou, X.; Yu H.; Li, Z.; Qin, J. *Macromolecules* 2008, 41, 7433.

- [117] Zhou, G.; Qian, G.; Ma, L.; Cheng, Y.; Z. Xie, Wang, L.; Jing, X.; Wang, F. *Macromolecules* 2005, 38, 5416.
- [118] Qin, C.; Cheng, Y.; Wang, L.; Jing, X.; Wang, L. *Macromolecules* 2008, 41, 7798.
- [119] Dwivedi, A. T.; Saikia, G.; Iyer, P. K. *J. Mater. Chem.* 2011, 21, 2502.
- [120] Qin, C.; Wu, X.; Tong, H.; Wang, L. *J. Mater. Chem.* 2010, 20, 7957.
- [121] Lerclerc M. *J. Polm. Sci. Part A. Polym. Chem.* 2001, 39, 2687.
- [122] Prieto, I. ; Teetsov, J. ; Fox M.A.; Vanden Bout, D.A.; Bard, A. J. *J. Phys. Chem. A.* 2001, 105, 520.
- [123] Schutz, P.; Carasu, F. *Langmuir* 2001, 17, 7670.
- [124] Rault-Berthelot, J.; Simonet, J. *New J. Chem.* 1986, 10, 169.
- [125] Rault-Berthelot, J.; Angely, L.; Delaunay, J. ; Simonet, J. *New J. Chem.* 1987, 11, 487.
- [126] Le Deit, H.; Rault-Berthelot, J.; Simonet J. *Synth. Met.* 1992, 47, 373.
- [127] Wright M.E.; Cochran, B.B. *Organometallics* 1993, 12, 3873.
- [128] Vak, D.; Jo, J.; Ghim, J. ; Chun, C.; Lim, B.; Heeger, A.J.; Kim, D.Y. *Macromolecules* 2006, 39, 6433.
- [129] McFarlane, L.S.; Piercey, D.G.; McDonald, R.; Veinot, J.G.C. *Macromolecules* 2008, 41, 7780.
- [130] Bischoff, F.; Adkins, H. *J. Am. Chem. Soc.* 1923, 45, 1030.
- [131] Xie, L.H.; Liu, F.; C.Tang, Hou, X.Y.; Hua, Y.R.; Fan, Q.L.; Huang, W. *Org. Lett.* 2006, 8, 2787.
- [132] Atak S. M.S. thesis, Middle East Technical University, 2011.
- [133] Patil, N. T.; Lakshmi, P. G. V. V.; Singh V. *Eur. J. Org. Chem.* 2010, 4719.
- [134] Cihaner, A.; Algi, F. *Adv. Mater.* 2008,18, 3583.
- [135] Beaujuge, P.M.; Pisula, W.; Tsao, H.N.; Ellinger, S.; Müllen, K.; Reynolds, J.R. *J. Am. Chem. Soc.* 2009, 131, 7514.
- [136] Chandrasekhar, P. *Conducting Polymers. Fundamental and Applications*, Kluwer Academic Publisher, Boston, 1999.
- [137] Dierschke, F.; Grimsdale, A.C.; Müllen, K. *Macromol. Chem. Phys.* 2004, 205, 1147.
- [138] Becker, S.; Ego, C.; Grimsdale, A.C.; List, E.J.W.; Marsitzky, D.; Pogantsch, A.; Setayesh, S.; Leising, G.; Müllen, K. *Synth. Met.* 2002, 125, 73.
- [139] Sonmez, G.; Meng, H.; Wudl, F. *Chem. Mater.* 2004; 16; 574.
- [140] Tang, S.; Liu, M.; Gu, C.; Zhao Y., Lu, P.; Lu, D.; Liu, L.L.; Shen, F.; Yang, B.; Ma, Y. *Org.Chem.* 2008, 73, 4212.
- [141] Hassan, J. ; Seignion, M.; Gozzi, C.; Schulz, E.; Lemaire, M. *Chem. Rev.* 2002, 102, 1359.
- [142] Gaupp, C.L. ; Welsh, D.M.; Rauh, R.D.; Reynolds J.R. *Chem. Mater.* 2002, 14, 3964.
- [143] Kulkarni, A. P.; Zhu, Y.; Jenekhe, S. A. *Macromolecules*, 2005, 38, 1553.
- [144] Zhao, Q. Wu, W. *Polymer*, 2009, 50, 998.
- [145] N. C. Greenham, I. D. W. Samuel, G. R. Hayes, R. T. Phillips, Y. A. R. R. Kessener, S. C. Moratti, A. B. Holmes, R. H. Friend, *Chem. Phys. Lett.*, 1995, 241, 89.
- [146] Pei, Q.; B. Yang, Y. *J. Am. Chem. Soc.*, 1996, 118, 7416.
- [147] Chi, C. Y.; Im C.; Enkelmann, V.; Ziegler, A.; Lieser, G.; Wegner, G. *Chem. Eur. J.*, 2005, 11, 6833.
- [148] List, E. J. W.; Guentner, R.; de Freitas, P. S.; Scherf, U. *Adv. Mater.* 2002, 14, 374.
- [149] Tang, C.W.; VanSlyke, S.A. *Appl. Phys. Lett.*, 1987, 51, 913.
- [150] Adachi, C.; Tsutsui, T.; Saito, S. *Appl. Phys. Lett.*, 1990, 57, 531.
- [151] Scherf, U.; Neher, D.; Grimsdale, A.; Müllen, K. *Polyfluorenes*. Leipzig Germany: Springer., 2008, 15.
- [152] Scherf U. ; List, E. J. W. *Adv. Mater.* 2002, 14, 477.
- [153] Lupton, J. M.; Craig, M. R.; Meijer, E. W. *Appl. Phys. Lett.* 2002, 80, 4489.

## APPENDIX A

### FTIR SPECTRA OF MONOMERS AND POLYMER

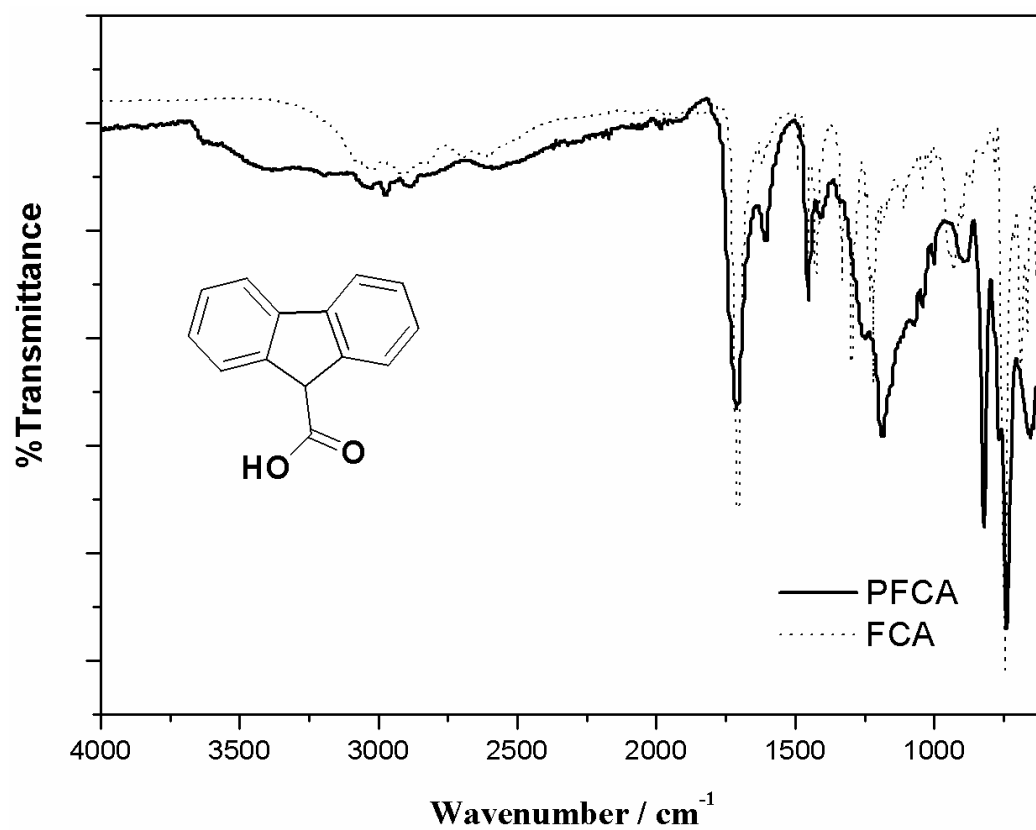
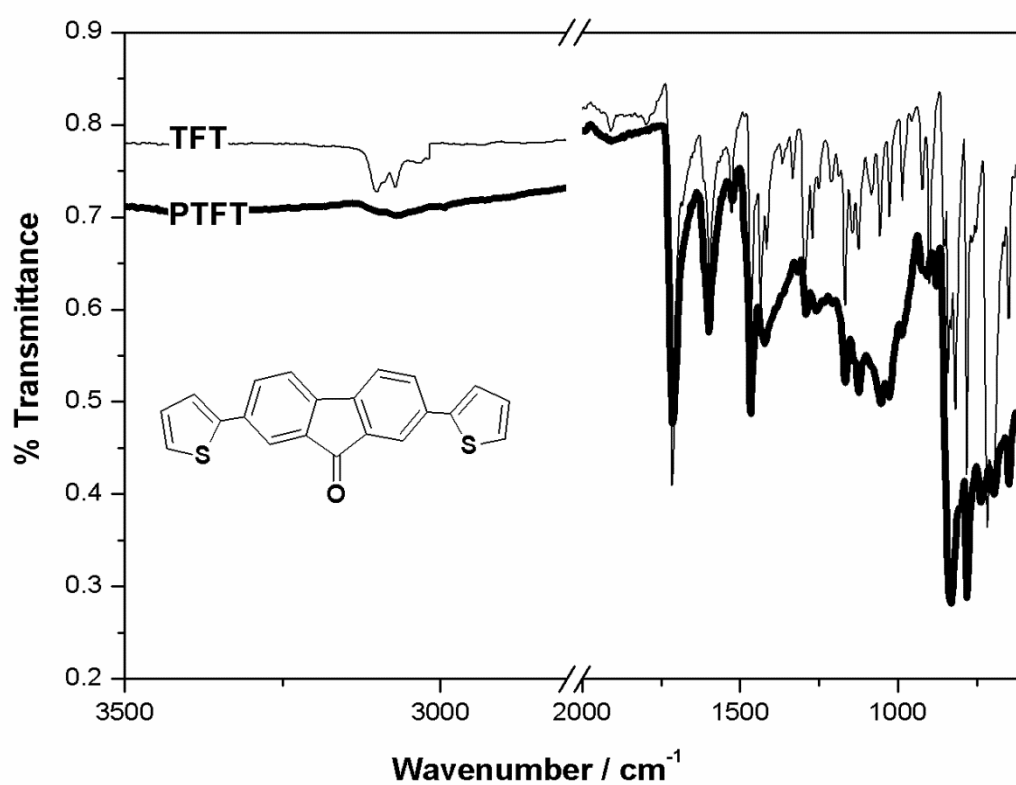
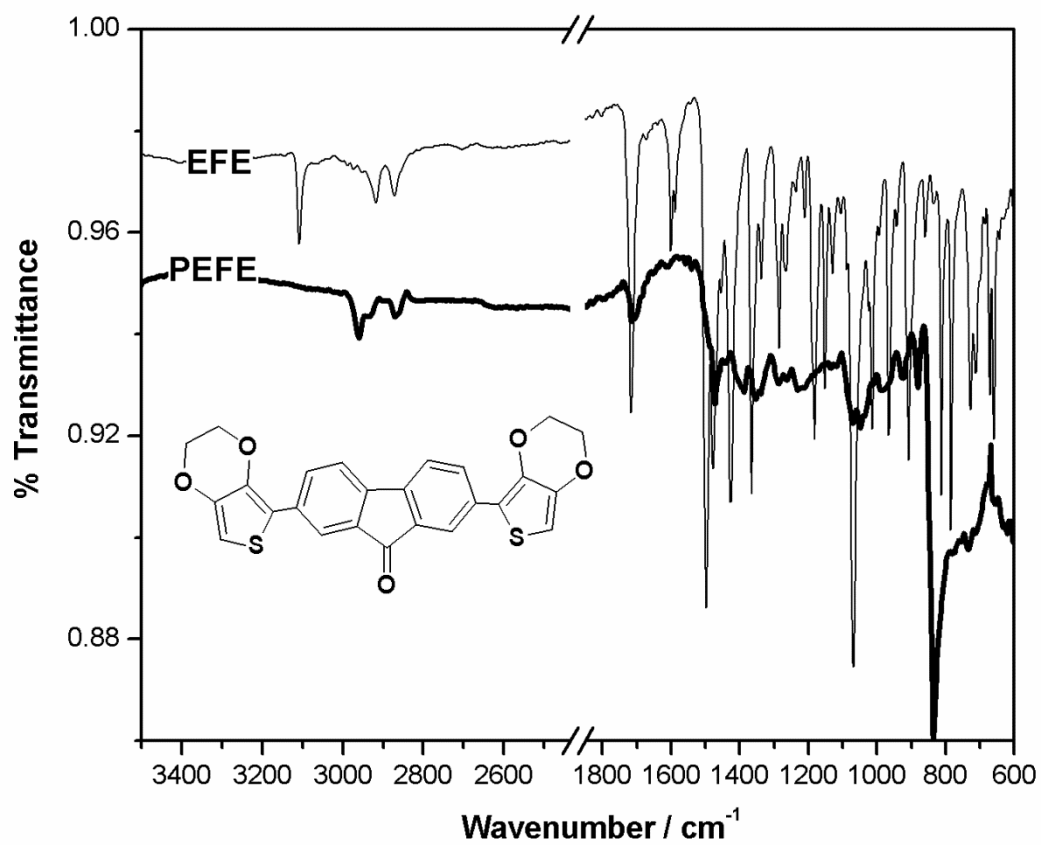


Figure A 1. FTIR spectrum of FCA and P(FCA)



**Figure A 2.** FTIR spectrum of **TFT** and **P(TFT)**.





**Figure A3.** FTIR spectrum of **EFE** and **P(EFE)**.

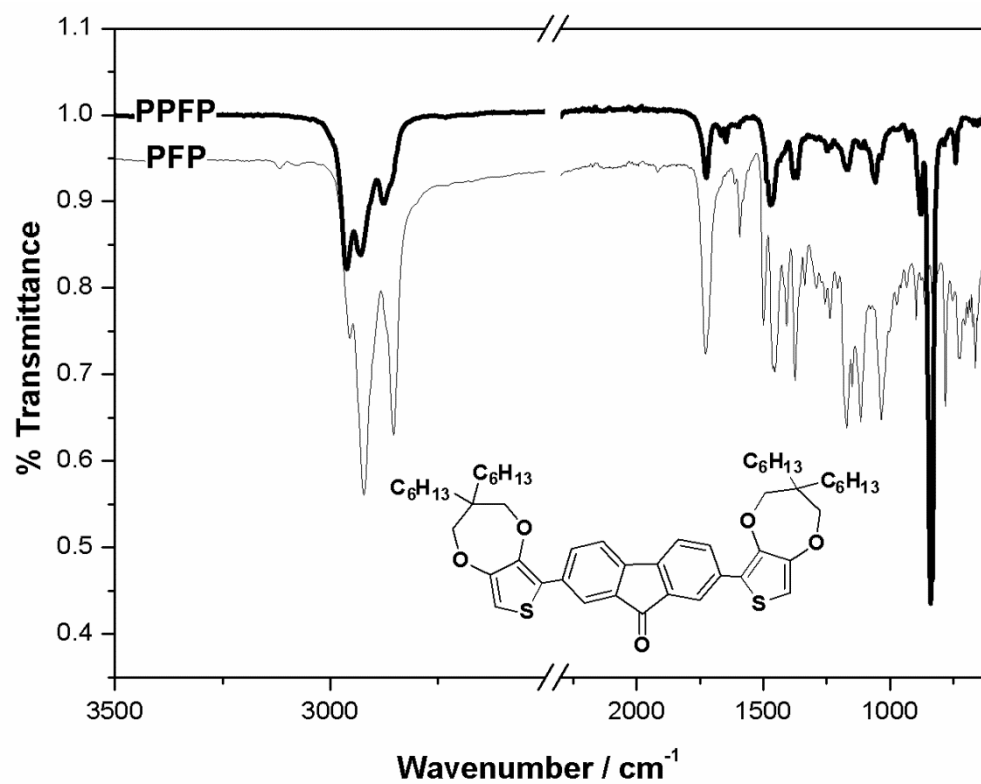


**Figure A4.** FTIR spectrum of **PFP** and **P(PFP)**.

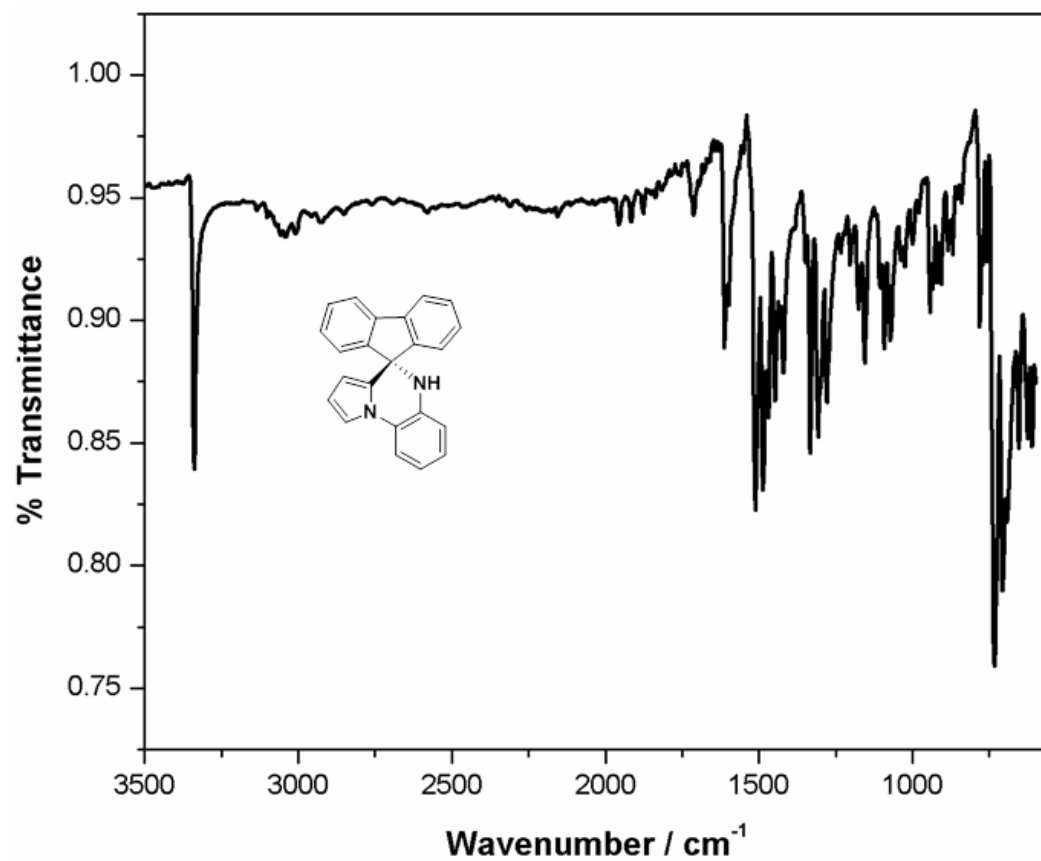


**Figure A5.** FTIR spectrum of FQ

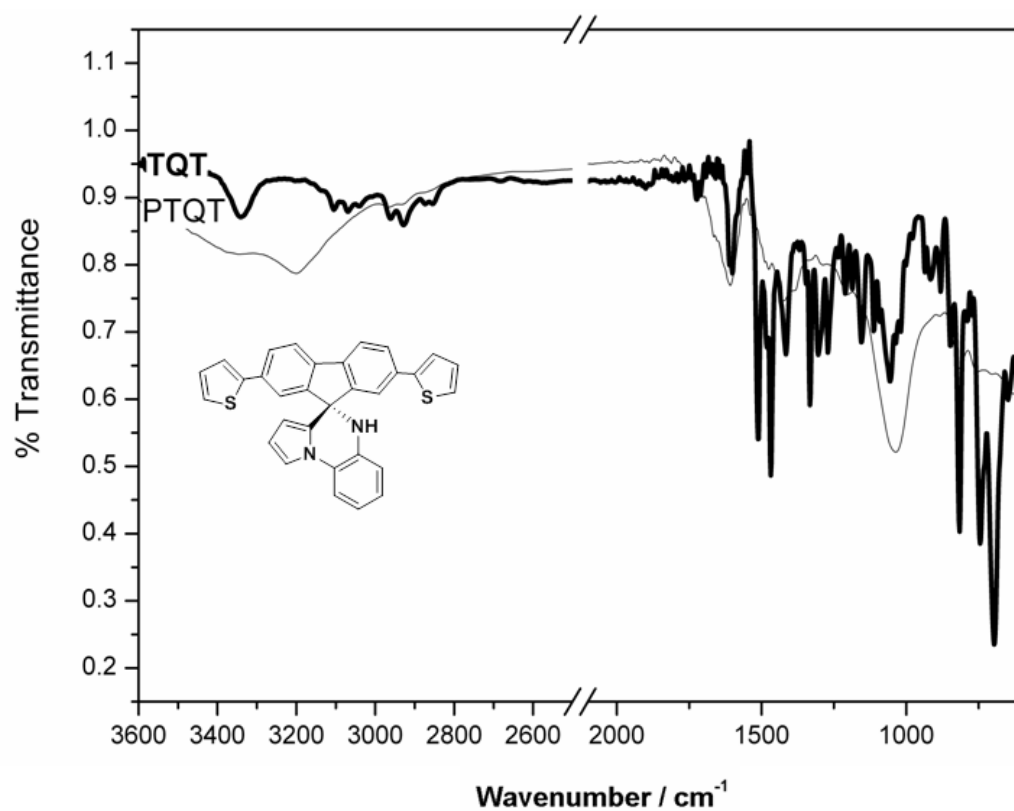


**Figure A6.** FTIR spectrum of TQT and P(TQT)

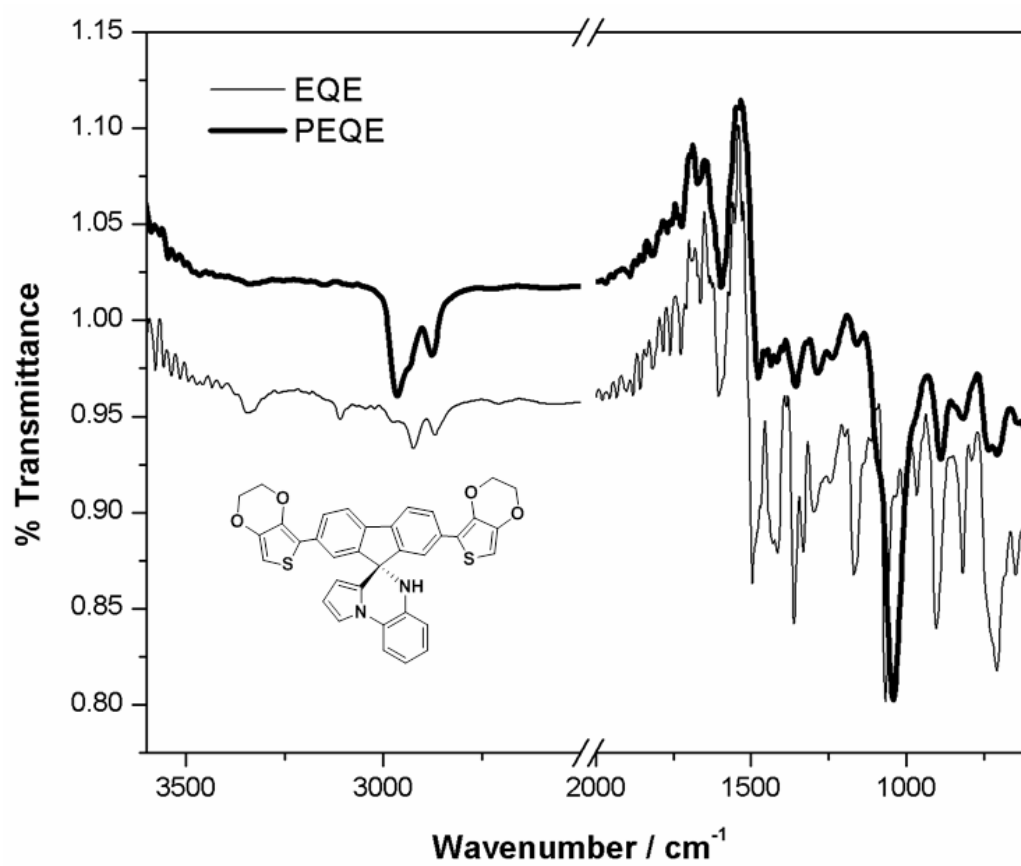


**Figure A7.** FTIR spectrum of EQE and P(EQE).

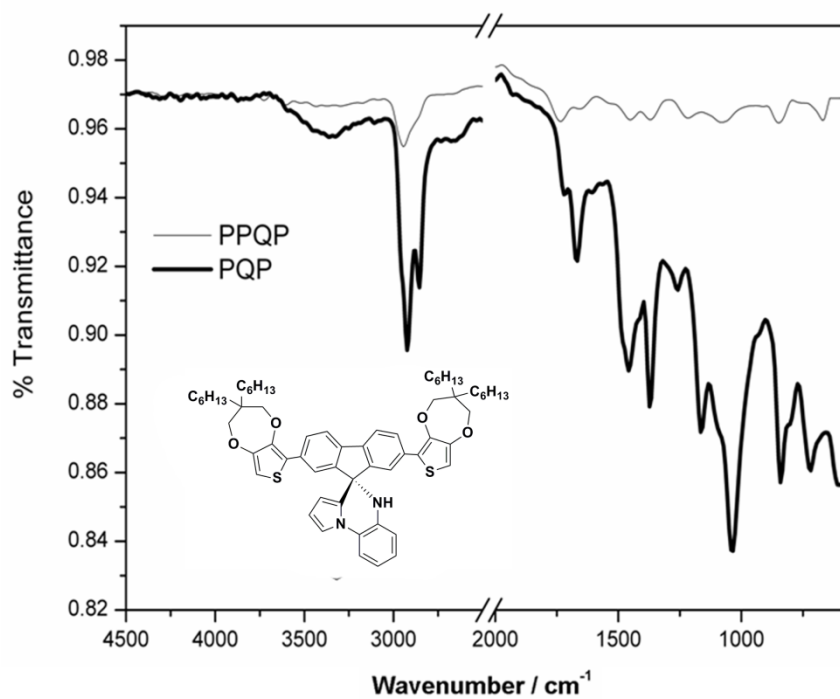


**Figure A8.** FTIR spectrum of **PQP** and **P(PQP)**

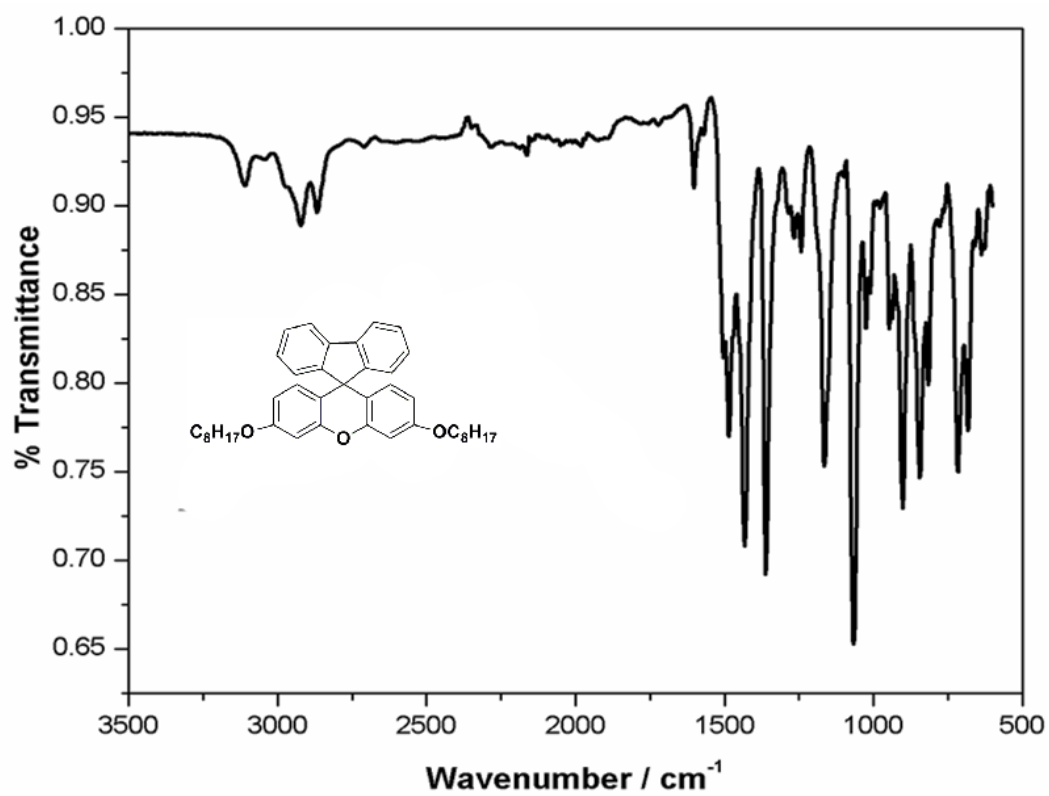


**Figure A9.** FTIR spectrum of **FX**

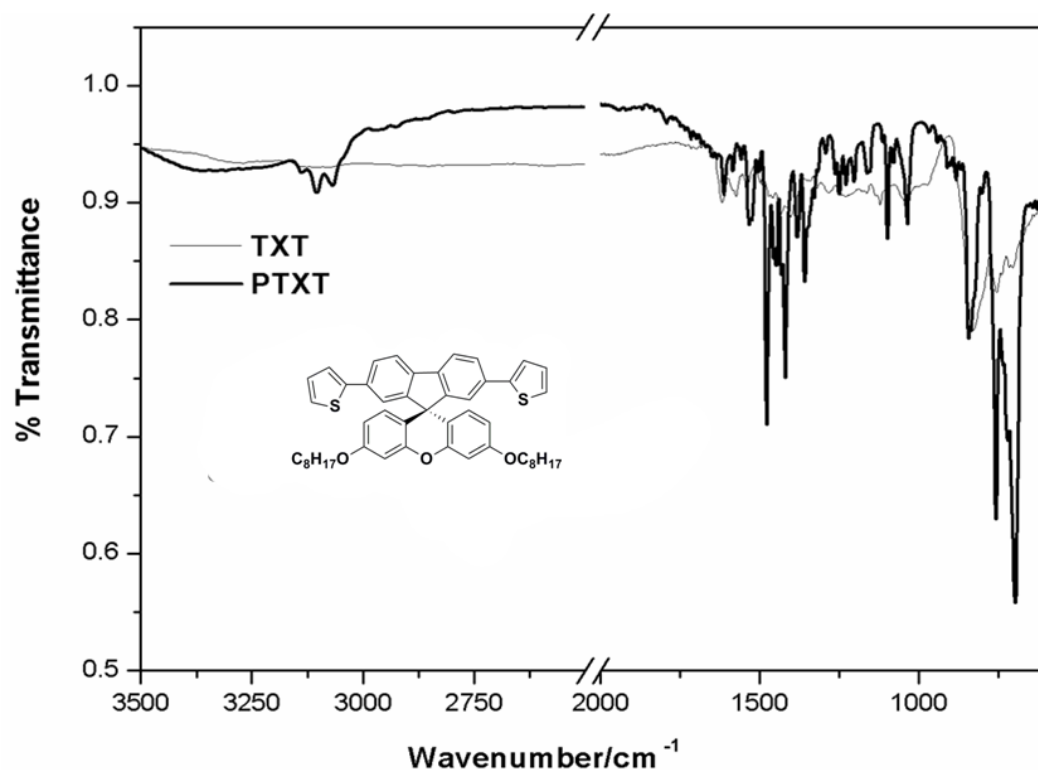


**Figure A10.** FTIR spectrum of **TXT** and **P(TXT)**.





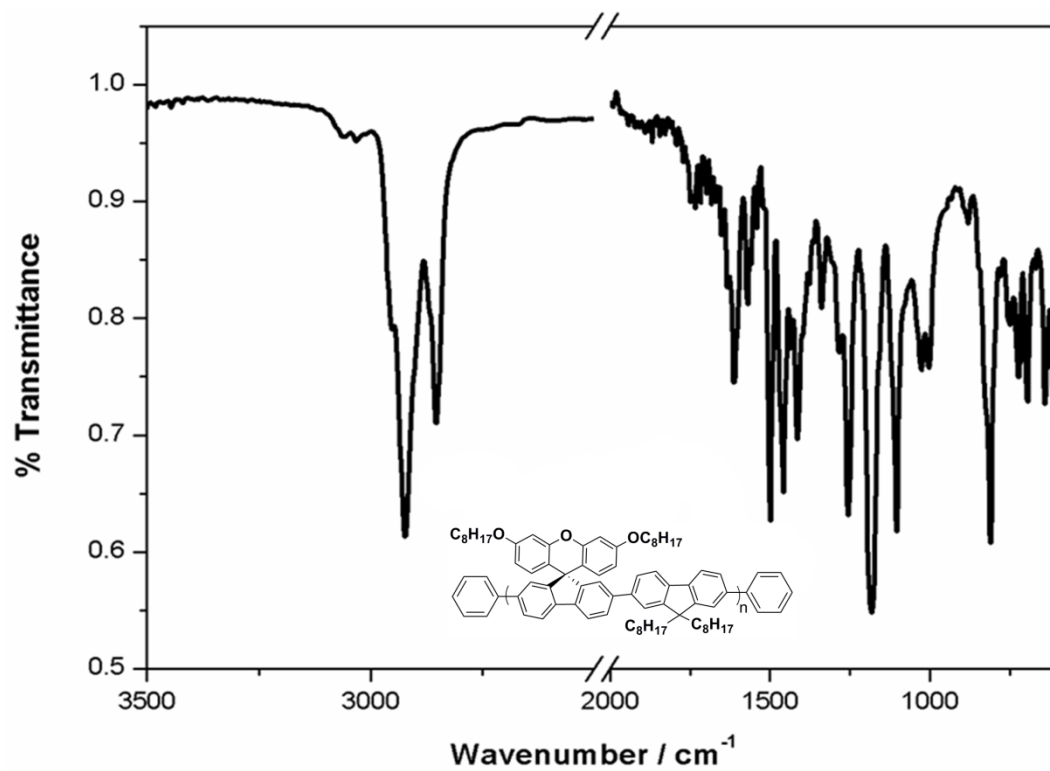


**Figure A12.** FTIR spectrum of P(F8-SFX).

## APPENDIX B

### NMR SPECTRA OF MONOMERS

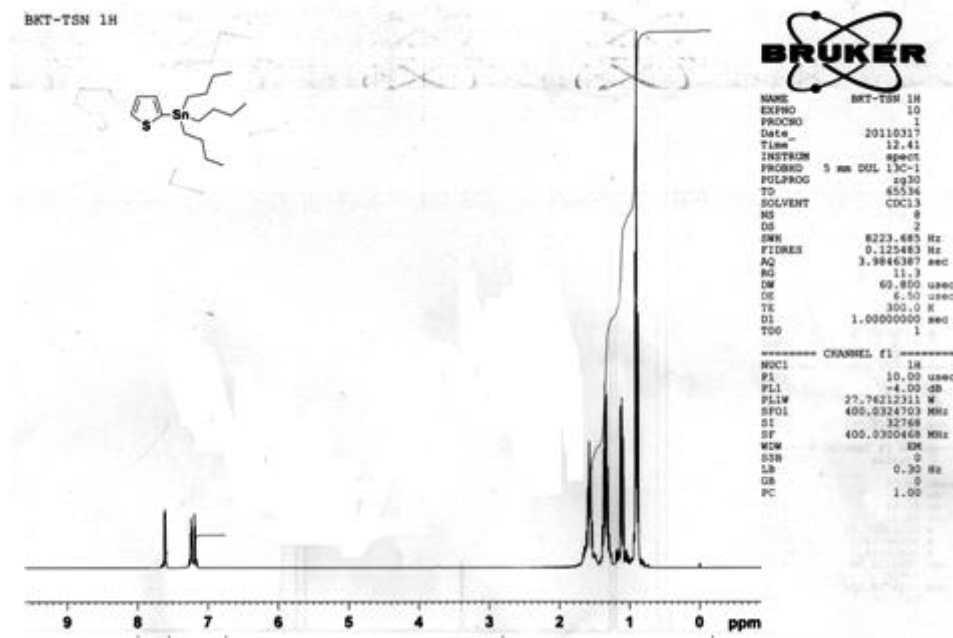


Figure B 1.  $^1\text{H}$  NMR spectrum of **i** in  $\text{CDCl}_3$ .

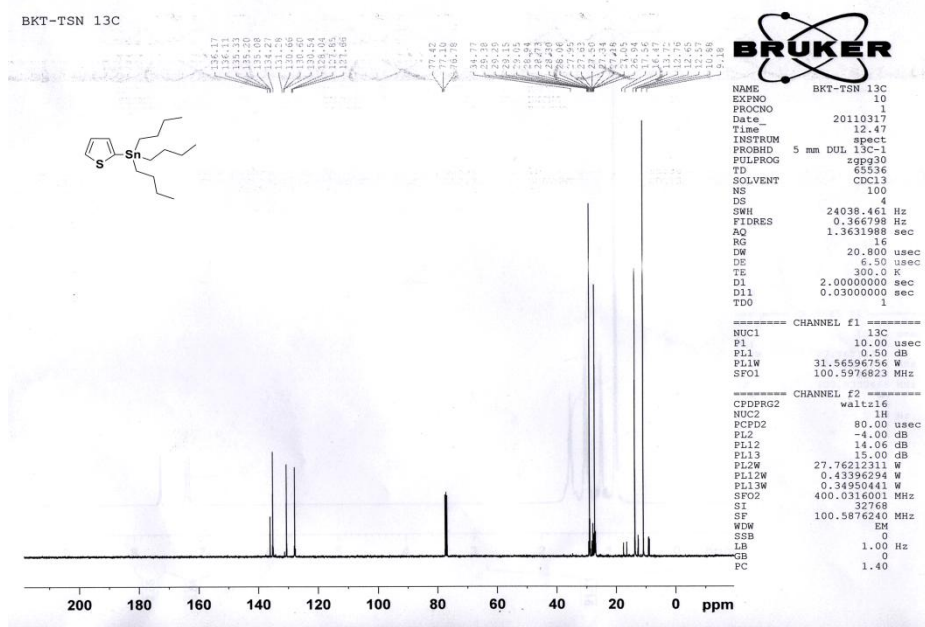


Figure B 2.  $^{13}\text{C}$  NMR spectrum of **i** in  $\text{CDCl}_3$ .

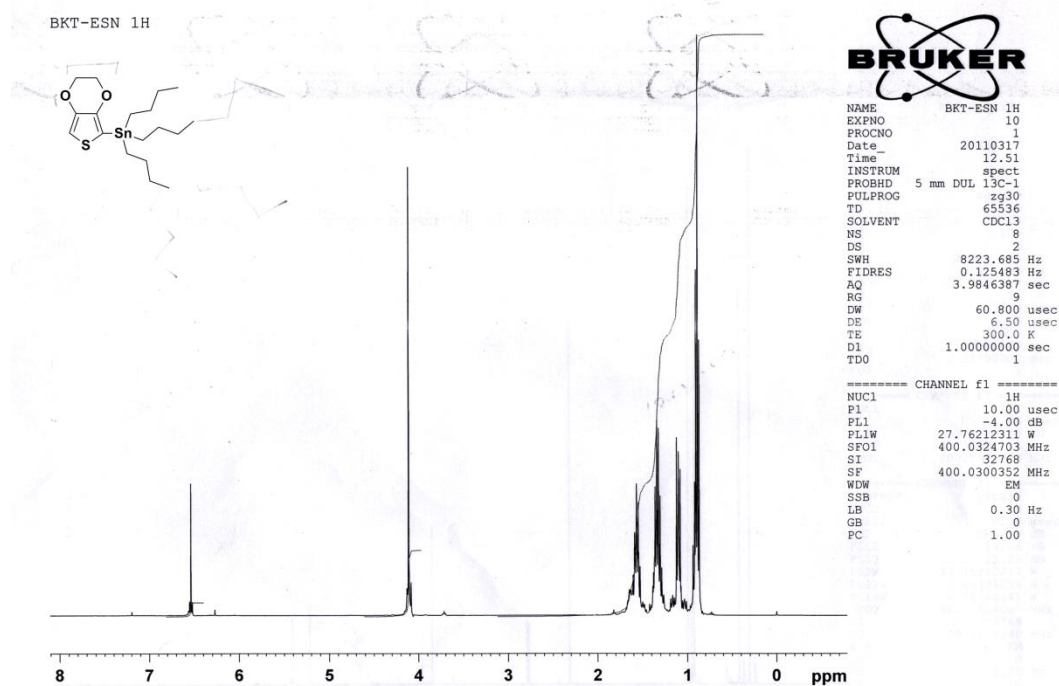


Figure B 3.  $^1\text{H}$  NMR spectrum of **ii** in  $\text{CDCl}_3$ .

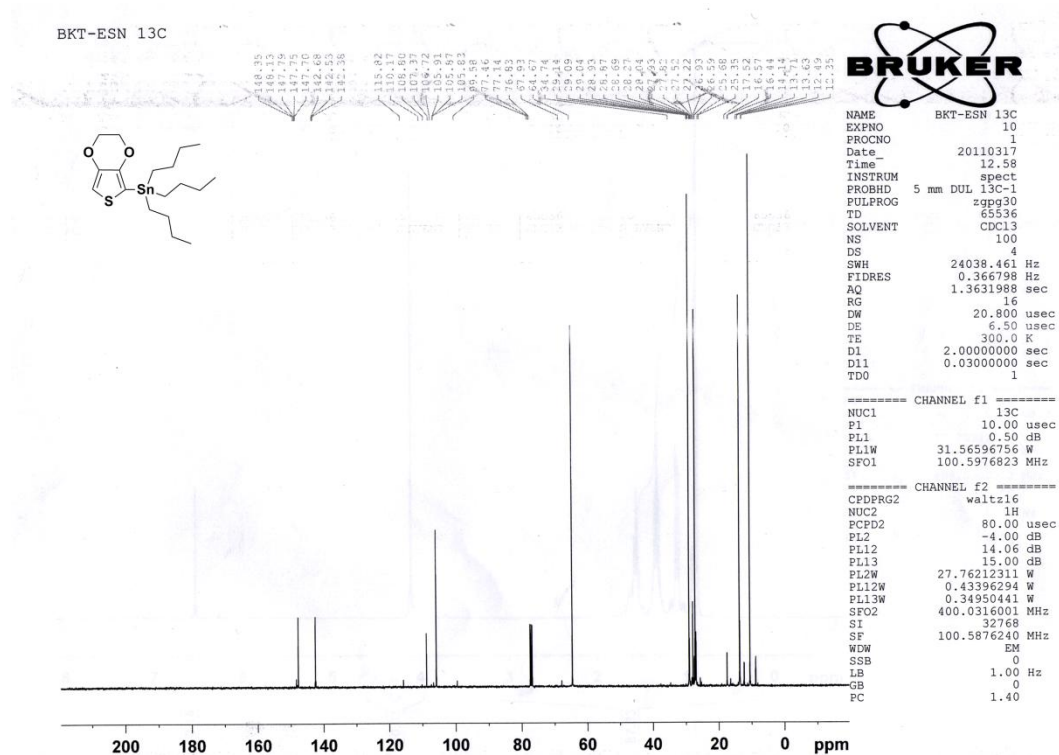


Figure B 4.  $^{13}\text{C}$  NMR spectrum of **ii** in  $\text{CDCl}_3$

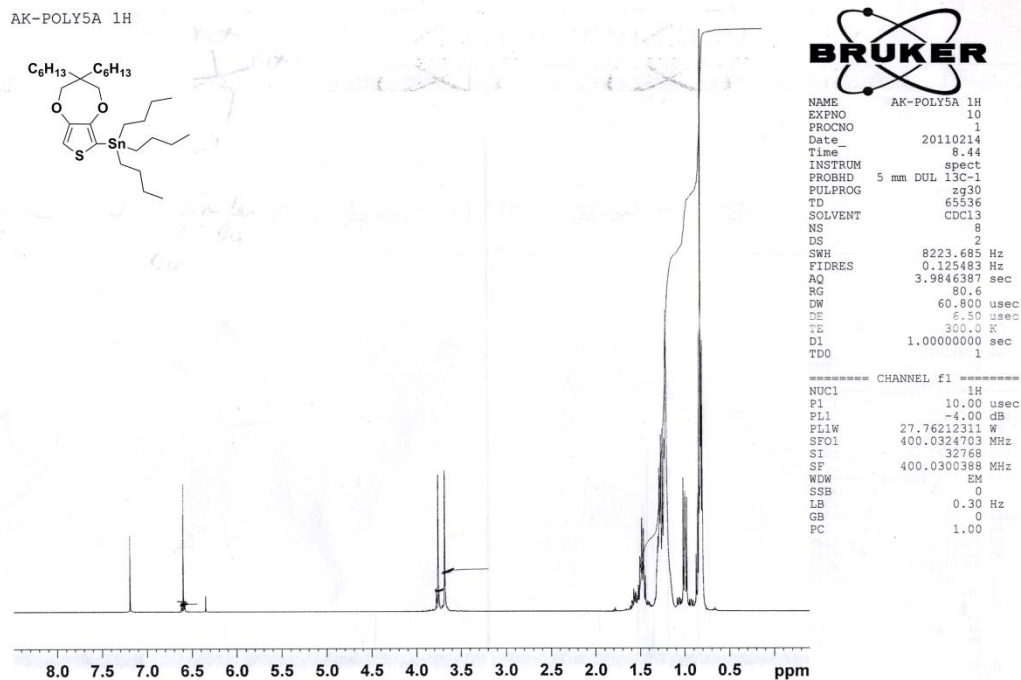


Figure B 5.  $^1\text{H}$  NMR spectrum of iii in  $\text{CDCl}_3$ .

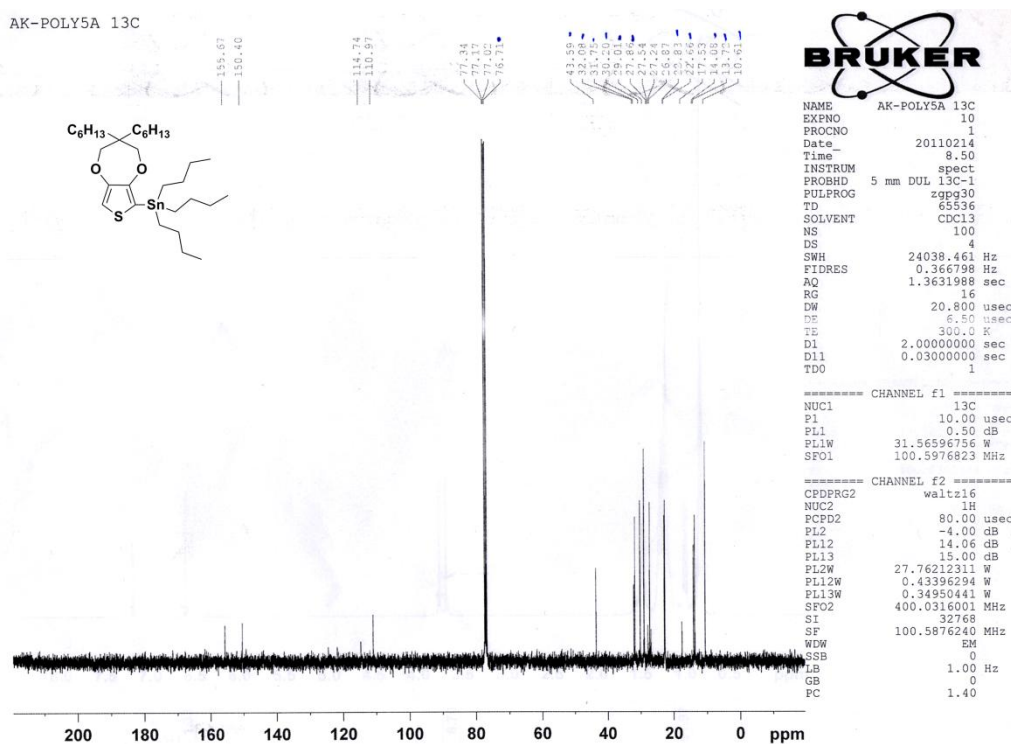
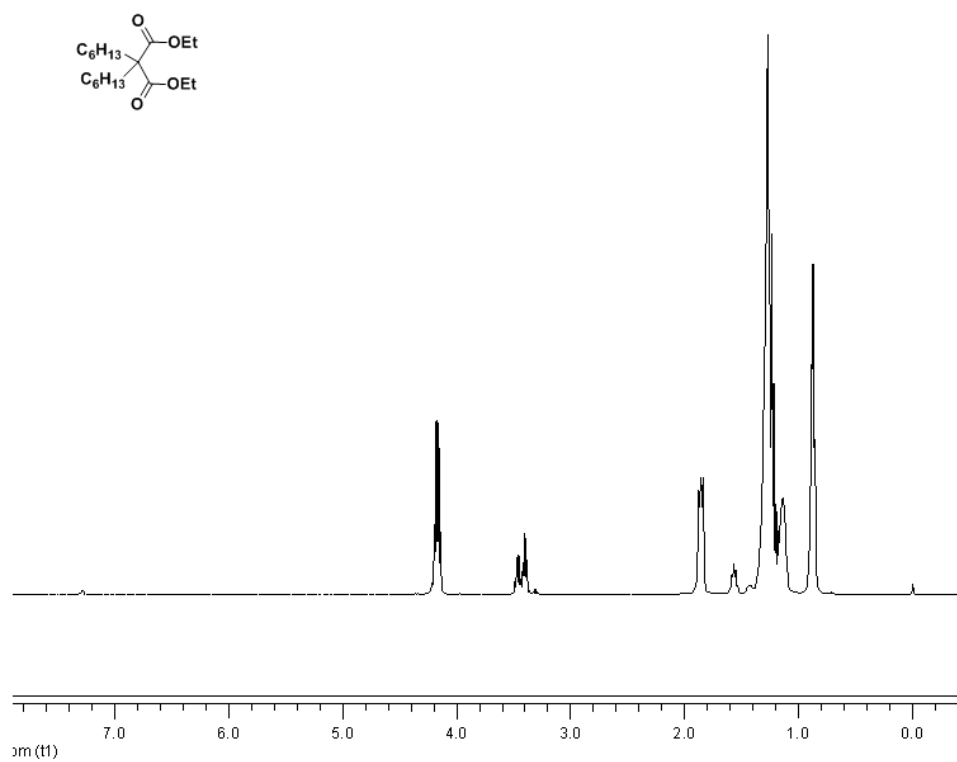
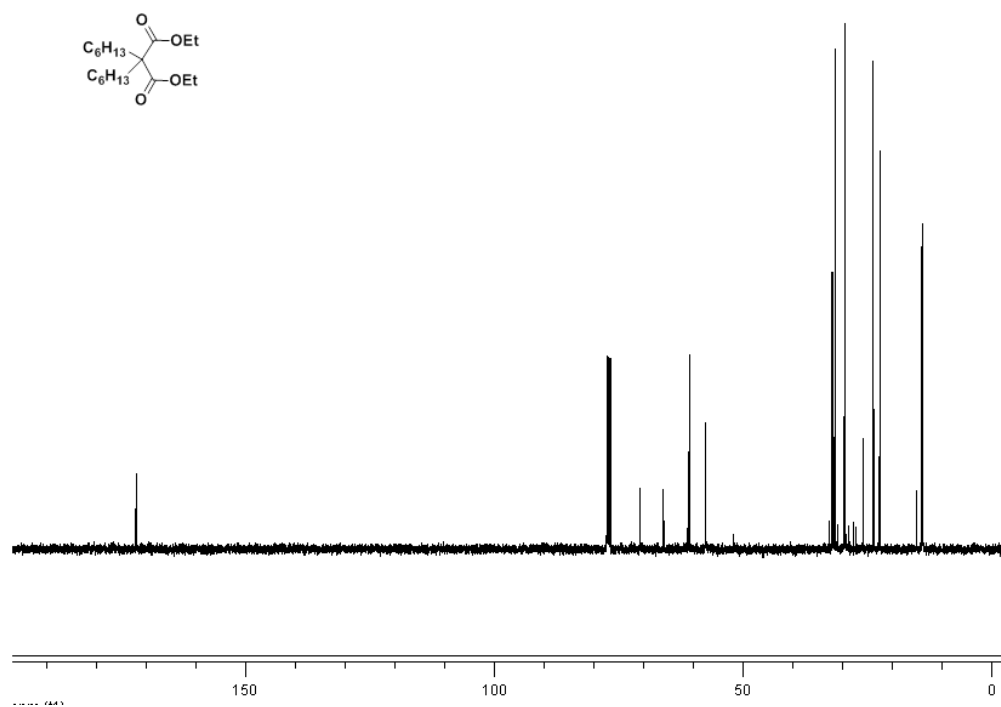


Figure B 6.  $^{13}\text{C}$  NMR spectrum of iii in  $\text{CDCl}_3$



**Figure B 7.** <sup>1</sup>H NMR spectrum of **iii (a)** in CDCl<sub>3</sub>



**Figure B 8.** <sup>13</sup>C NMR spectrum of **iii (a)** in CDCl<sub>3</sub>

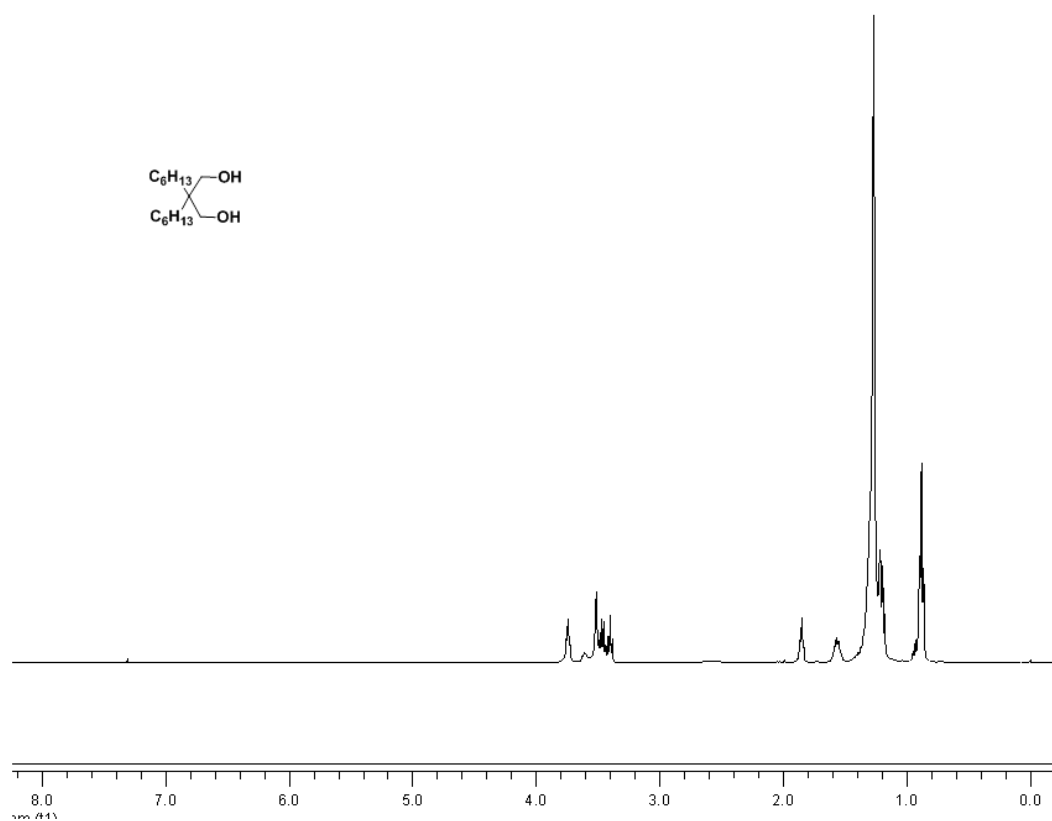


**Figure B 9.** <sup>1</sup>H NMR spectrum of **iii (b)** in CDCl<sub>3</sub>

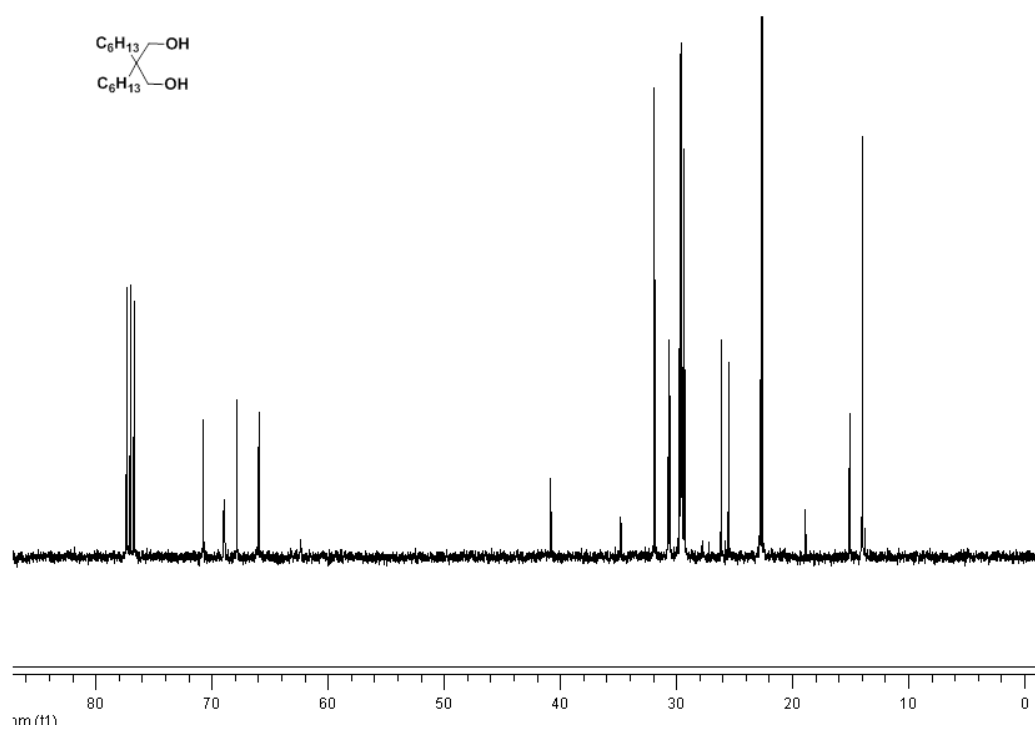


**Figure B 10.** <sup>13</sup>C NMR spectrum of **3b** in CDCl<sub>3</sub>.

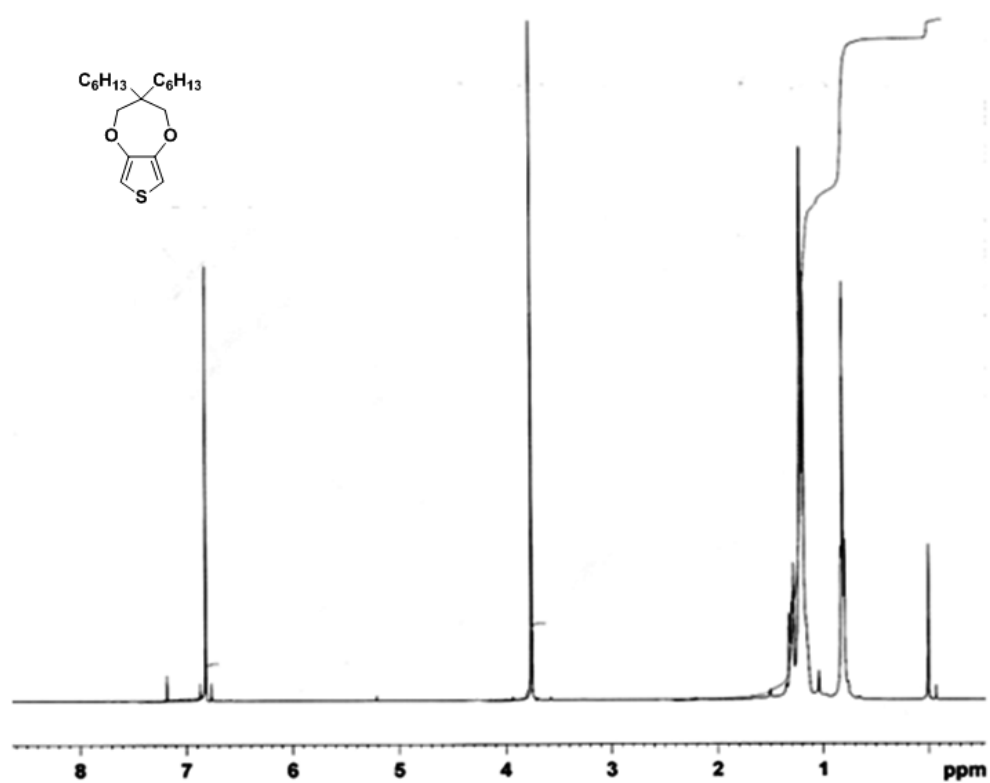


Figure B 11. <sup>1</sup>H NMR spectrum of **3c** in CDCl<sub>3</sub>

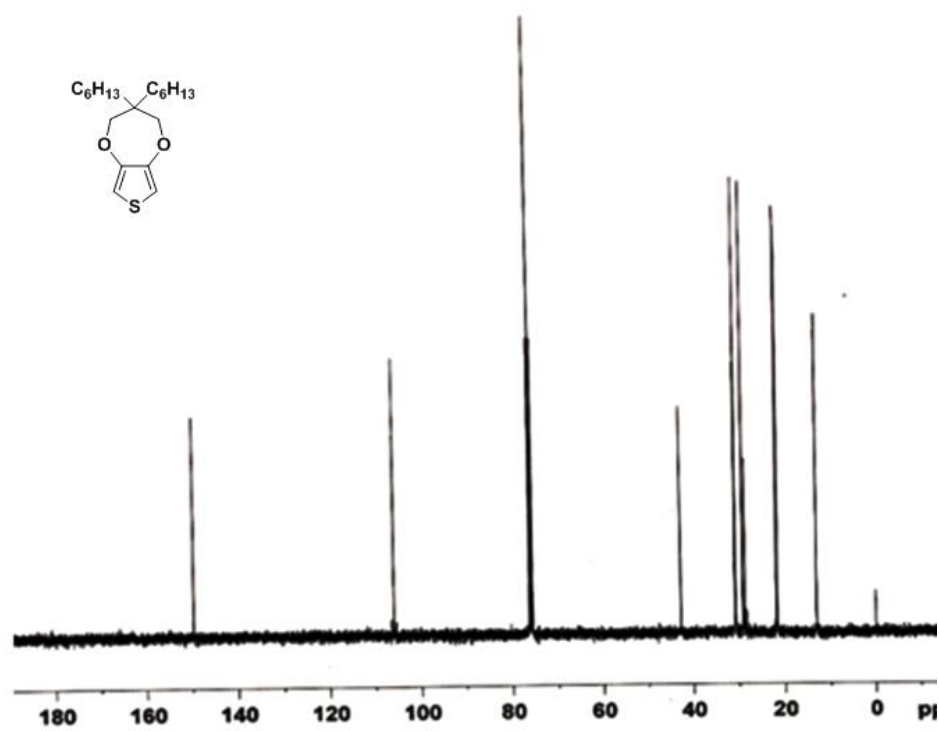
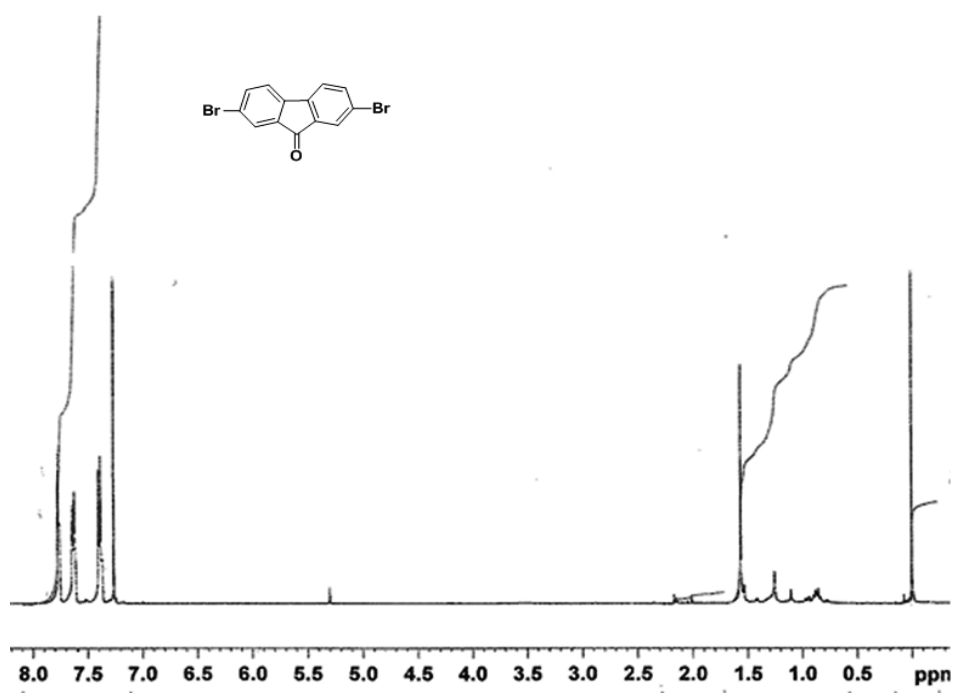
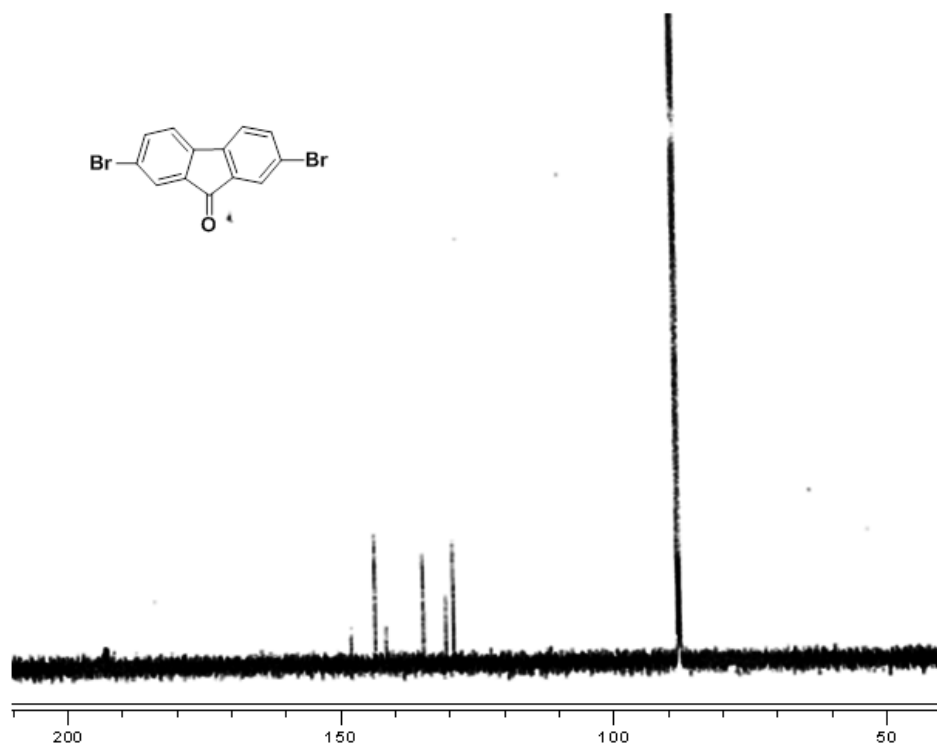


Figure B 12. <sup>13</sup>C NMR spectrum of **3c** in CDCl<sub>3</sub>.





**Figure B 11.** <sup>1</sup>H NMR spectrum of iv in CDCl<sub>3</sub>



**Figure B 12.** <sup>13</sup>C NMR spectrum of iv in CDCl<sub>3</sub>.

ESR-TFT 1H

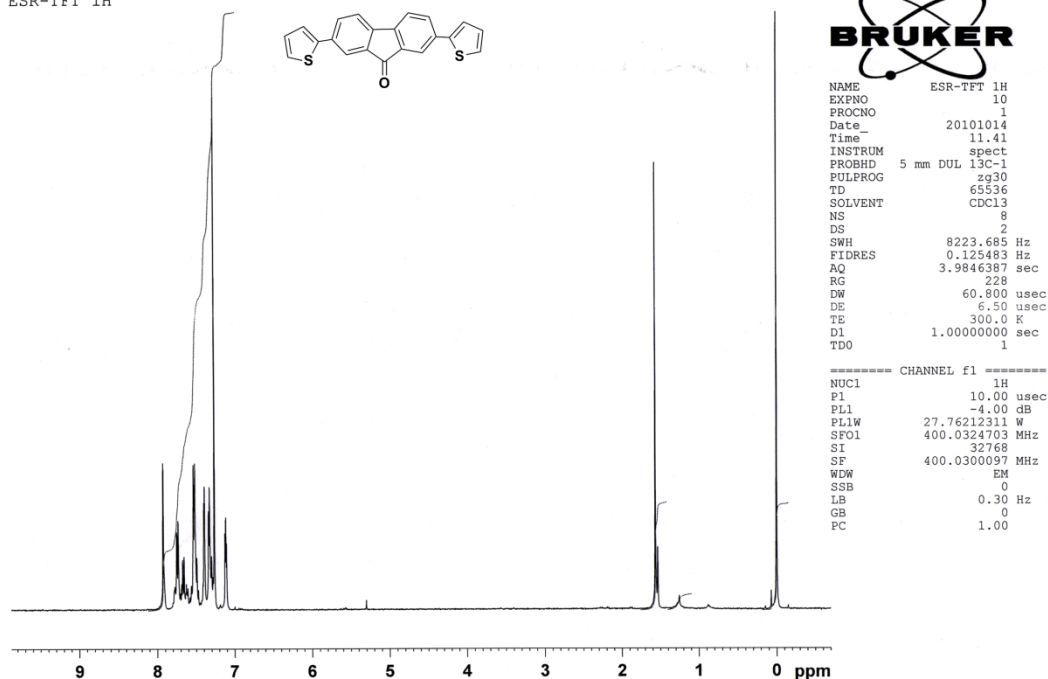


Figure B 13.  $^1\text{H}$  NMR spectrum of TFT in  $\text{CDCl}_3$

BKT-TFT 13C

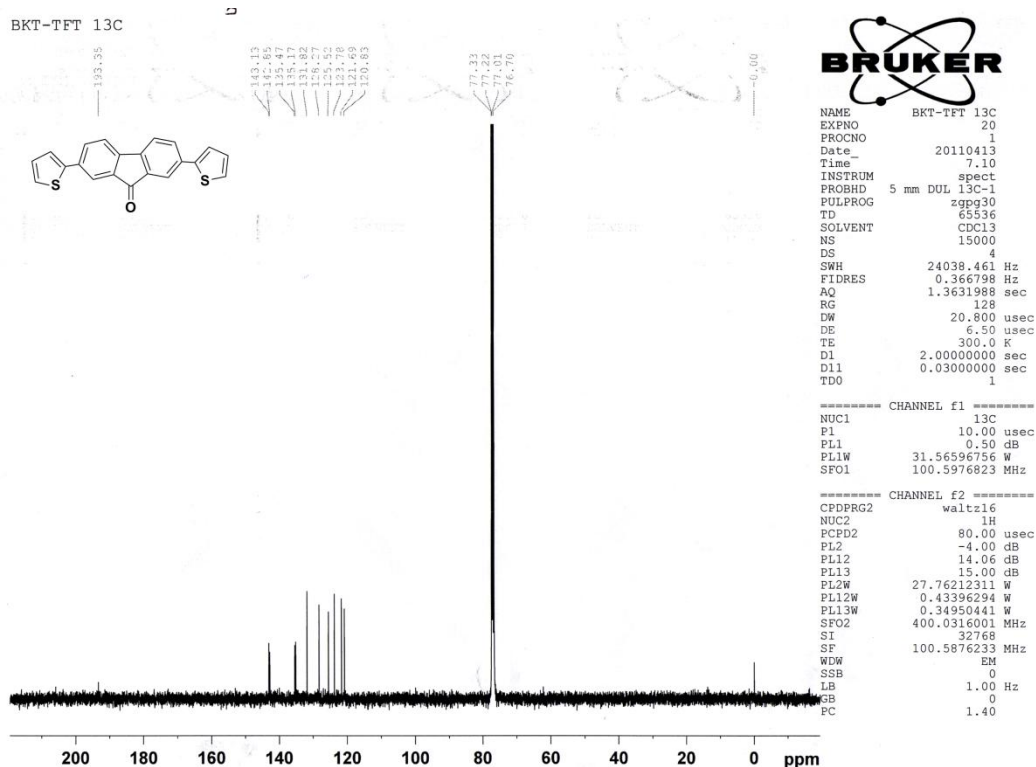


Figure B 14.  $^{13}\text{C}$  NMR spectrum of TFT in  $\text{CDCl}_3$ .

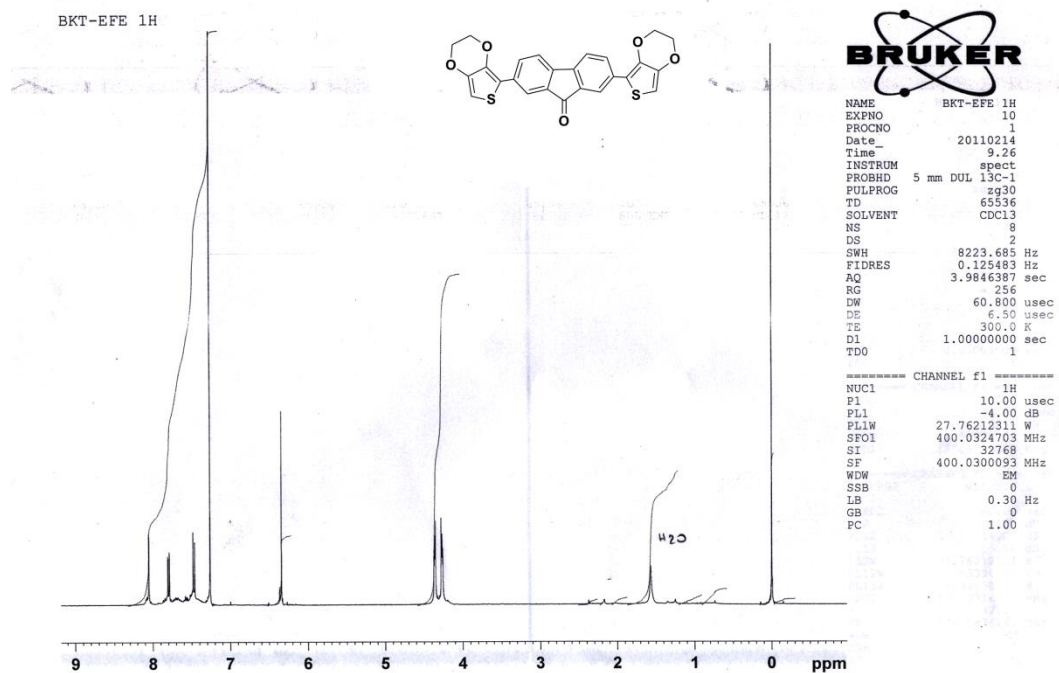


Figure B 13. <sup>1</sup>H NMR spectrum of EFE in CDCl<sub>3</sub>

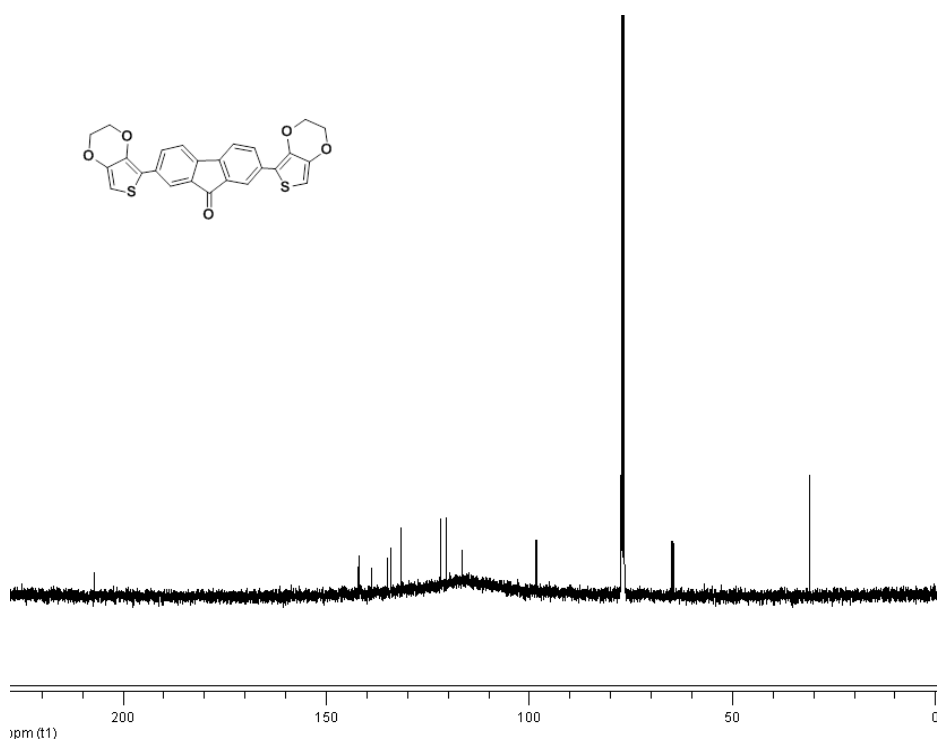


Figure B 16. <sup>13</sup>C NMR spectrum of EFE in CDCl<sub>3</sub>.

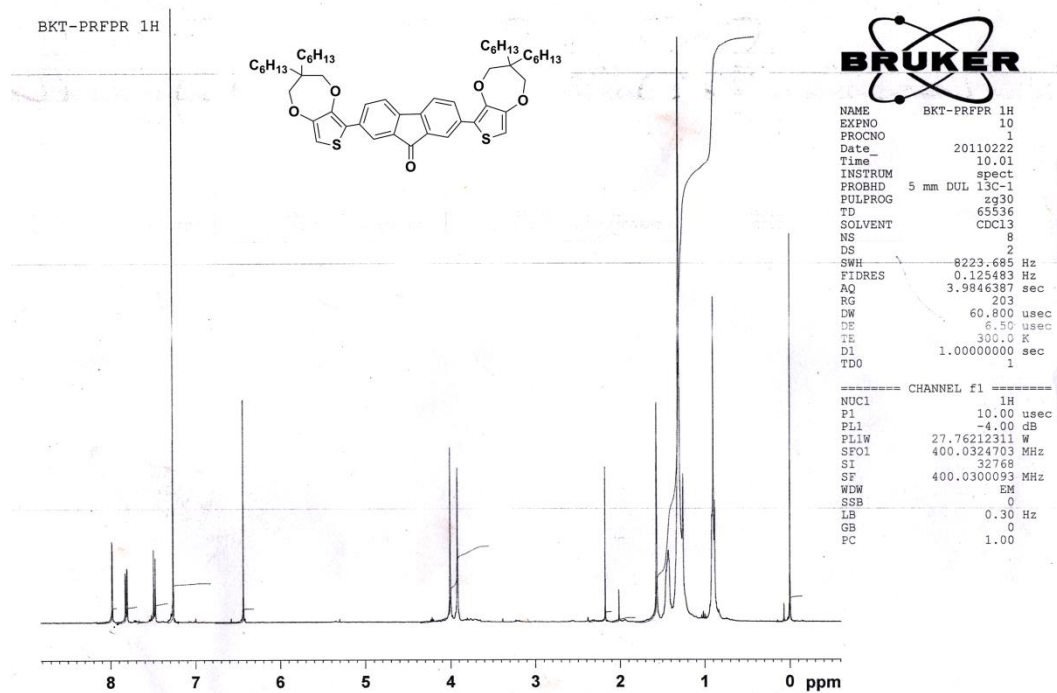


Figure B 17.  $^1\text{H}$  NMR spectrum of PFP in  $\text{CDCl}_3$

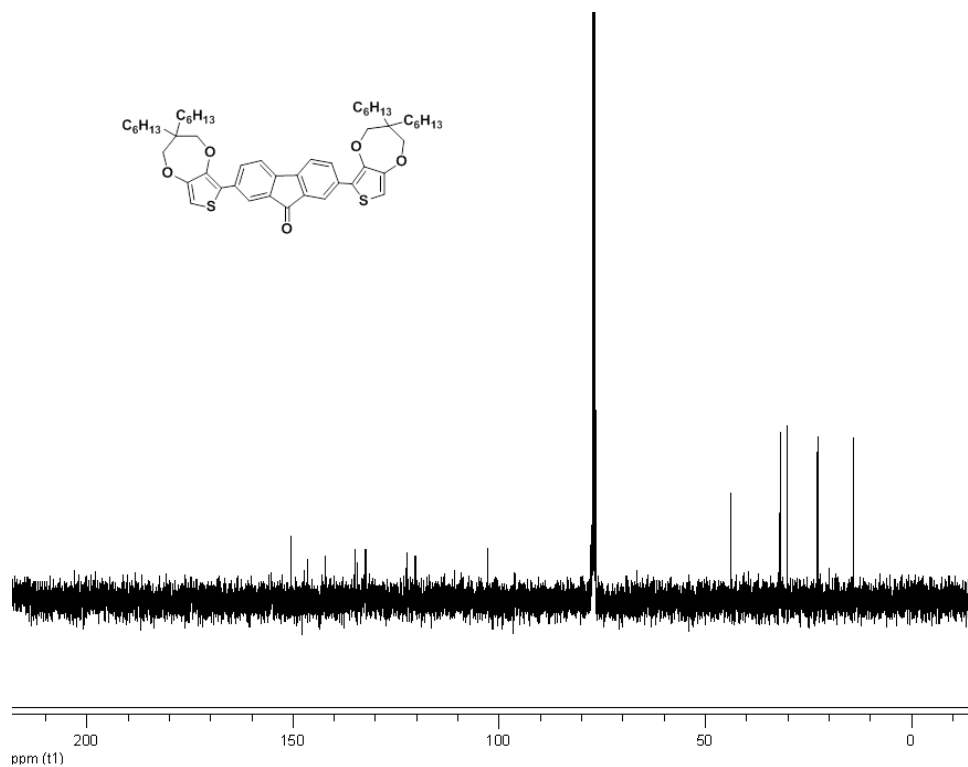
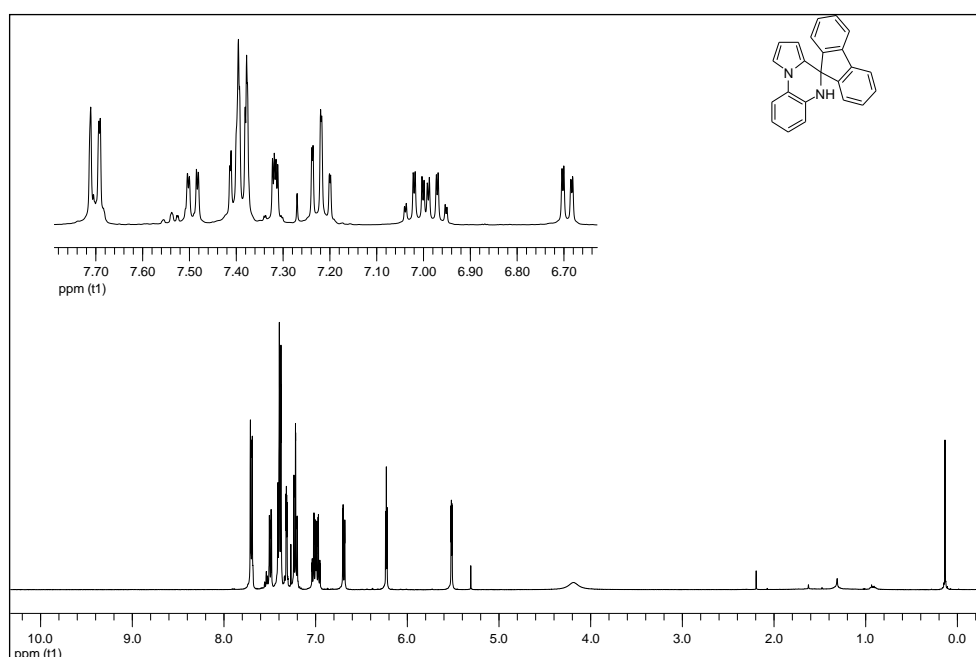
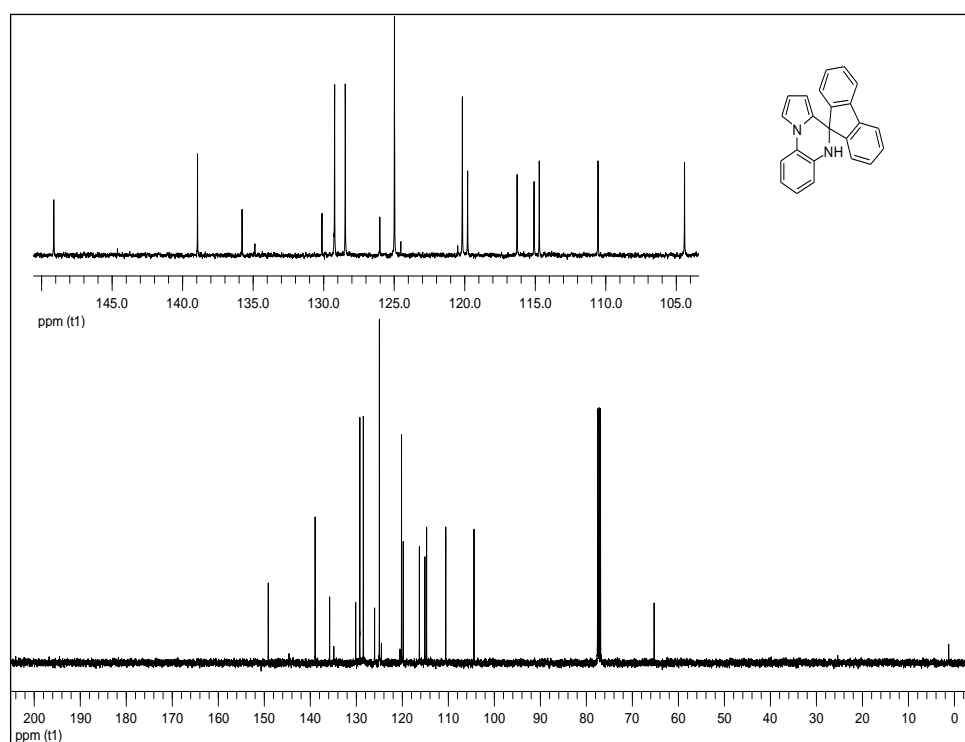


Figure B 18.  $^{13}\text{C}$  NMR spectrum of PFP in  $\text{CDCl}_3$ .



**Figure B 19.**  $^1\text{H}$  NMR spectrum of **FQ** in  $\text{CDCl}_3$



**Figure B 20.**  $^{13}\text{C}$  NMR spectrum of **FQ** in  $\text{CDCl}_3$ .

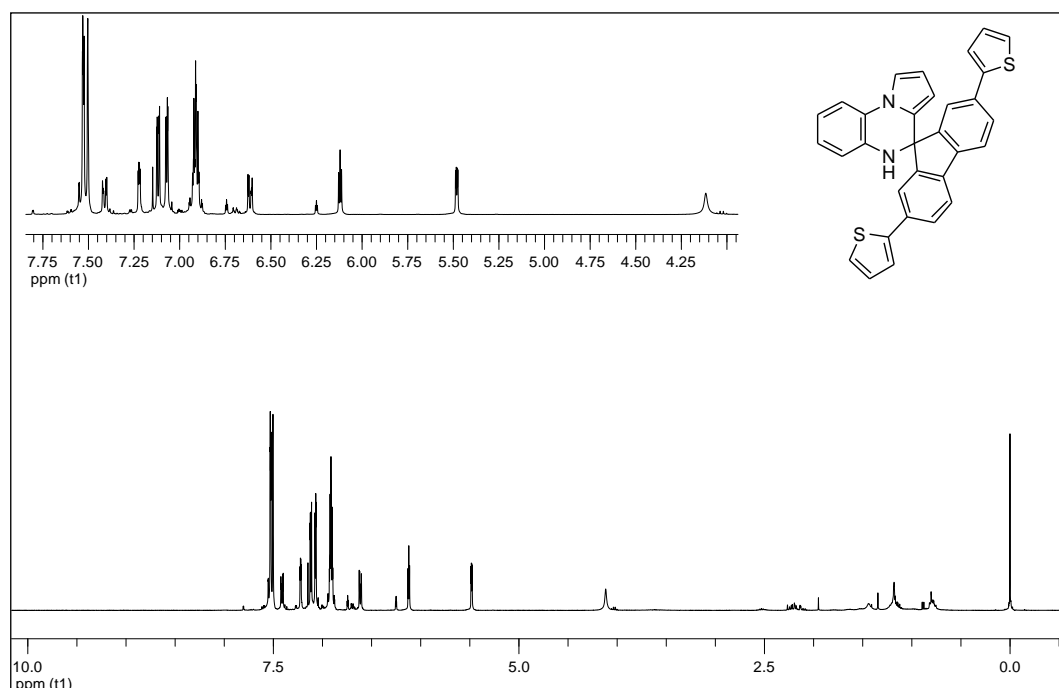


**Figure B 21.**  $^1\text{H}$  NMR spectrum of **TQT** in  $\text{CDCl}_3$

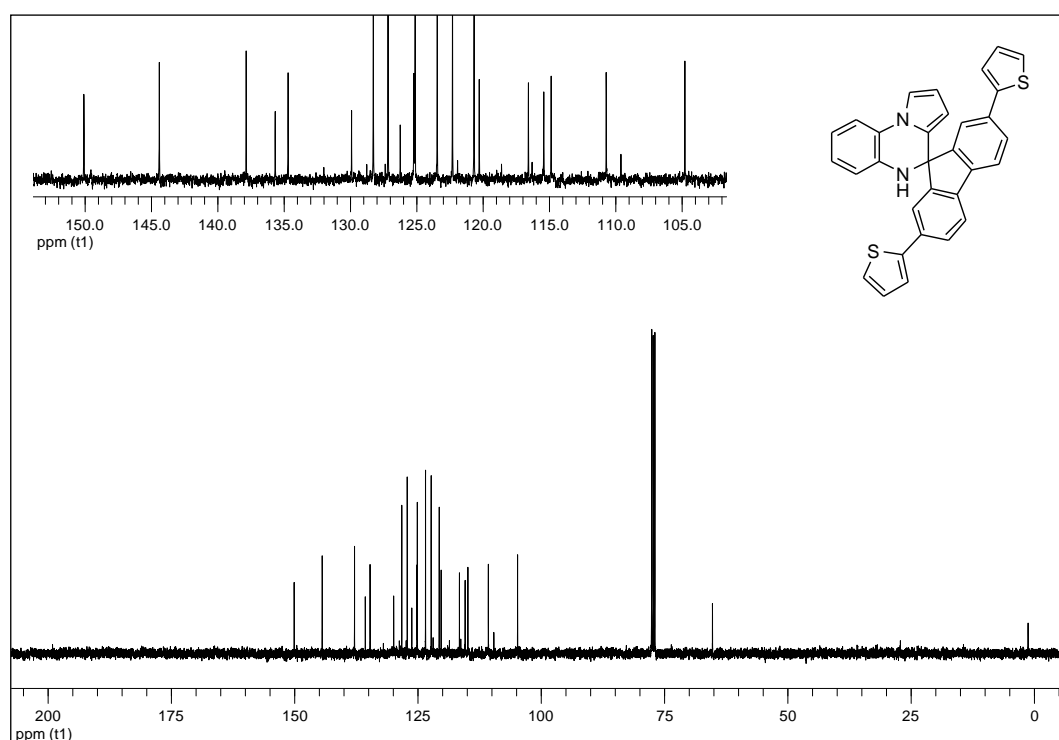


**Figure B 22.**  $^{13}\text{C}$  NMR spectrum of **TQT** in  $\text{CDCl}_3$

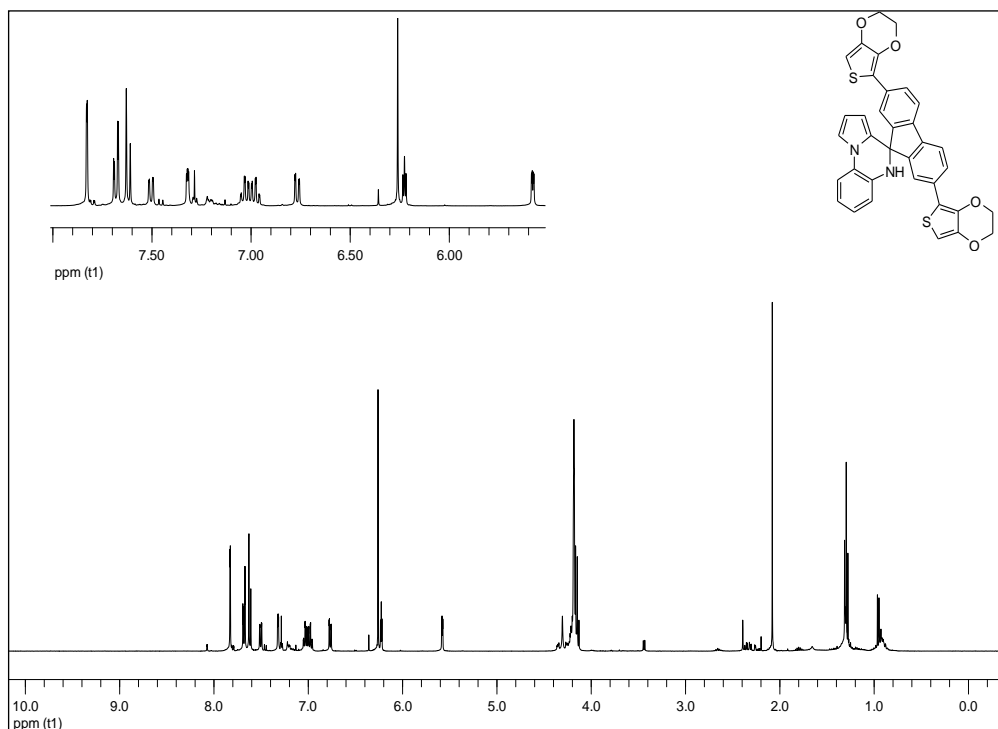


**Figure B 23.**  $^1\text{H}$  NMR spectrum of EQE in  $\text{CDCl}_3$

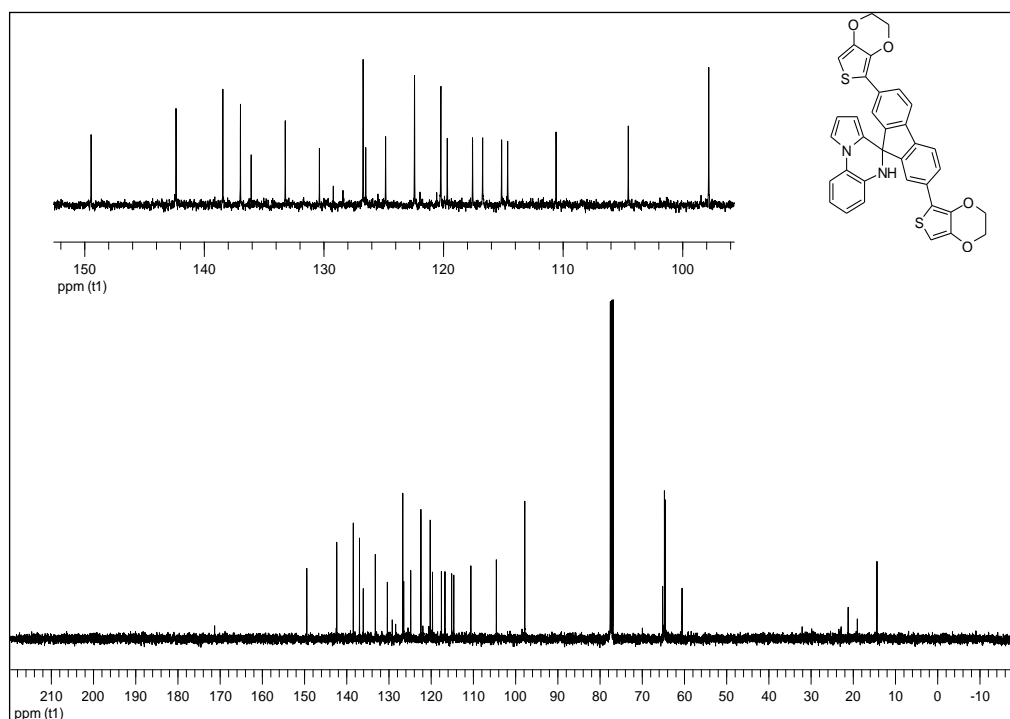


**Figure B 24.**  $^{13}\text{C}$  NMR spectrum of EQE in  $\text{CDCl}_3$

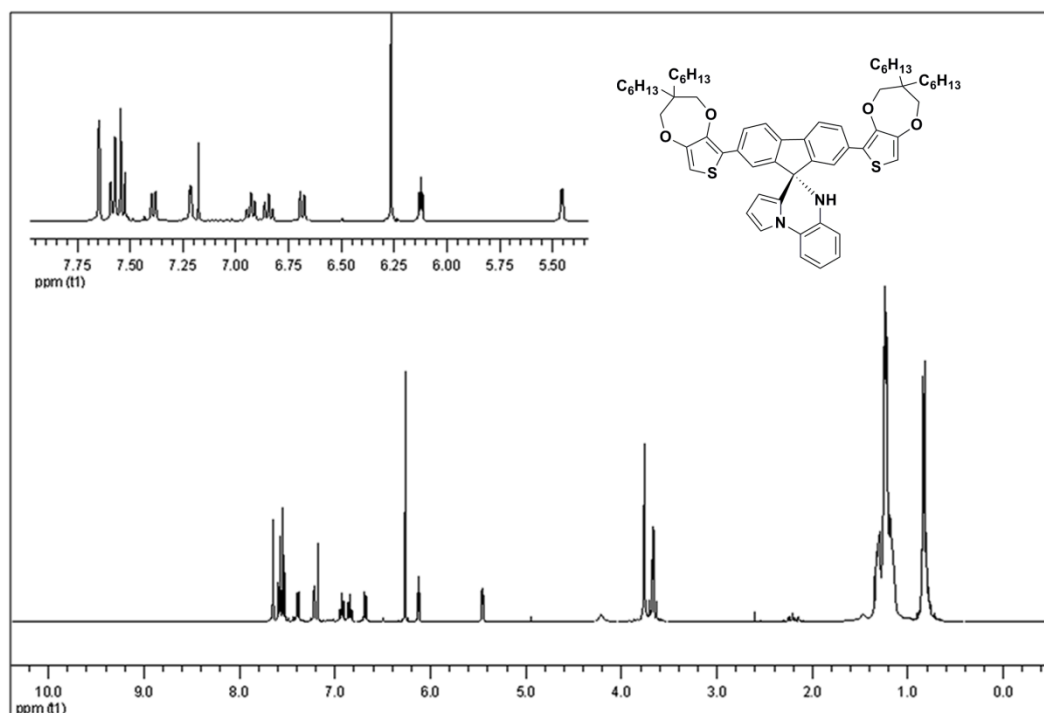


**Figure B 25.** <sup>1</sup>H NMR spectrum of **PQP** in CDCl<sub>3</sub>

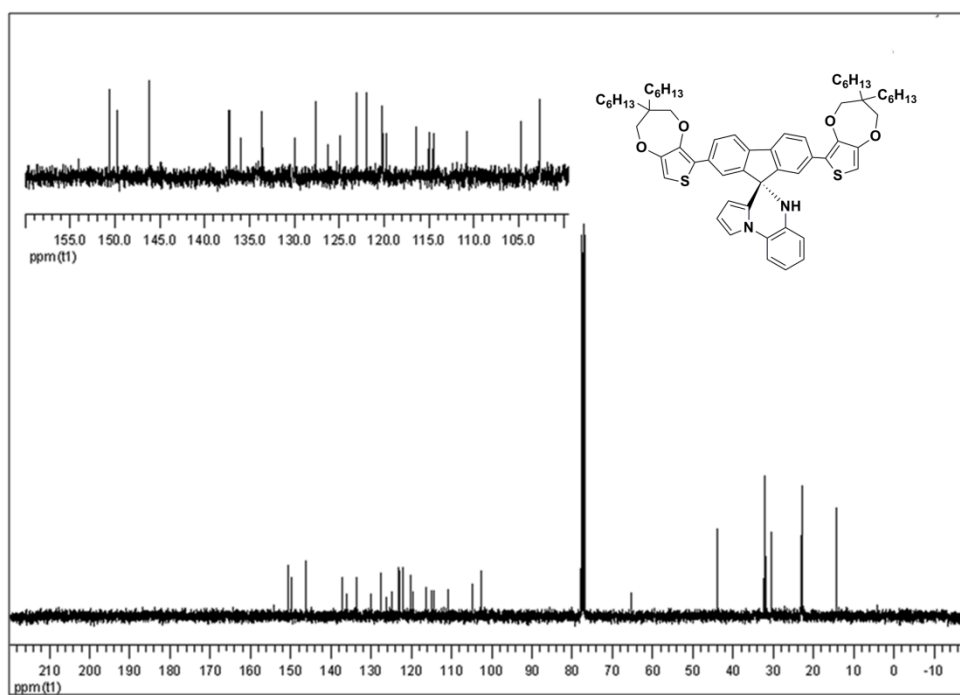


**Figure B 26.** <sup>13</sup>C NMR spectrum of **PQP** in CDCl<sub>3</sub>



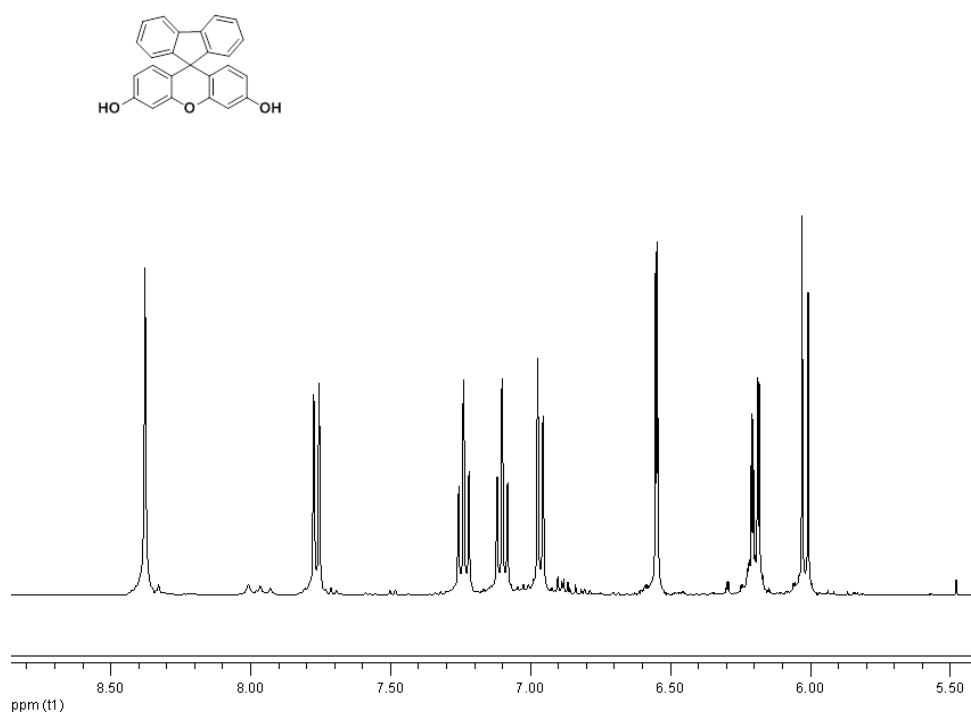


**Figure B 27.** <sup>1</sup>H NMR spectrum of **Spirofluorene** in d-acetone

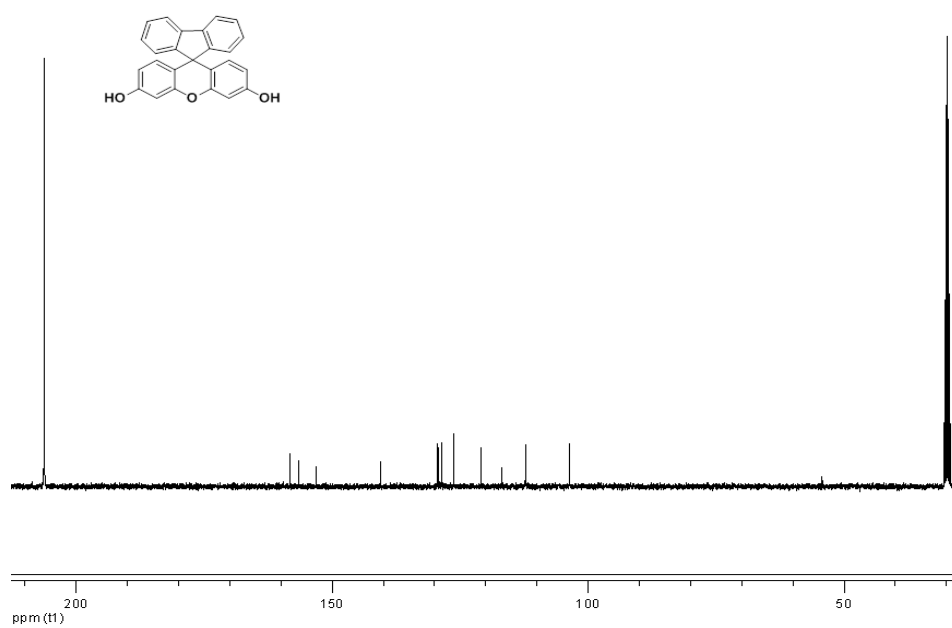


**Figure B 28.** <sup>13</sup>C NMR spectrum of **Spirofluorene** in d-acetone

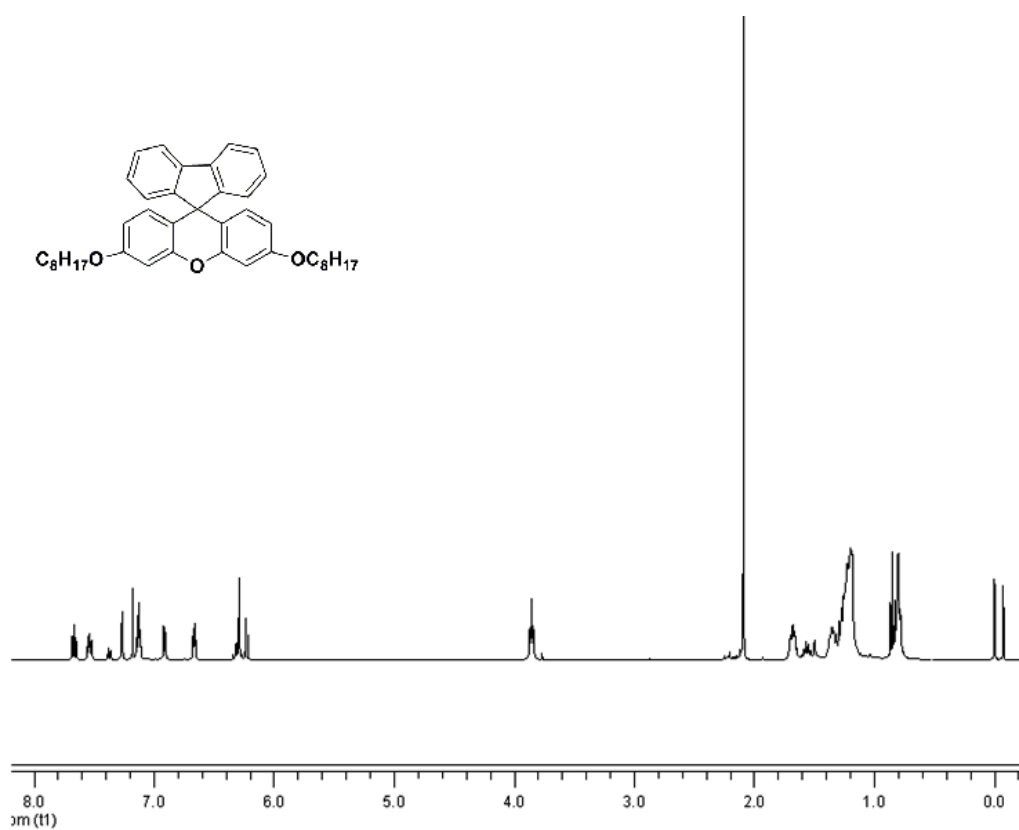


**Figure B 29.** <sup>1</sup>H NMR spectrum of **v** in CDCl<sub>3</sub>

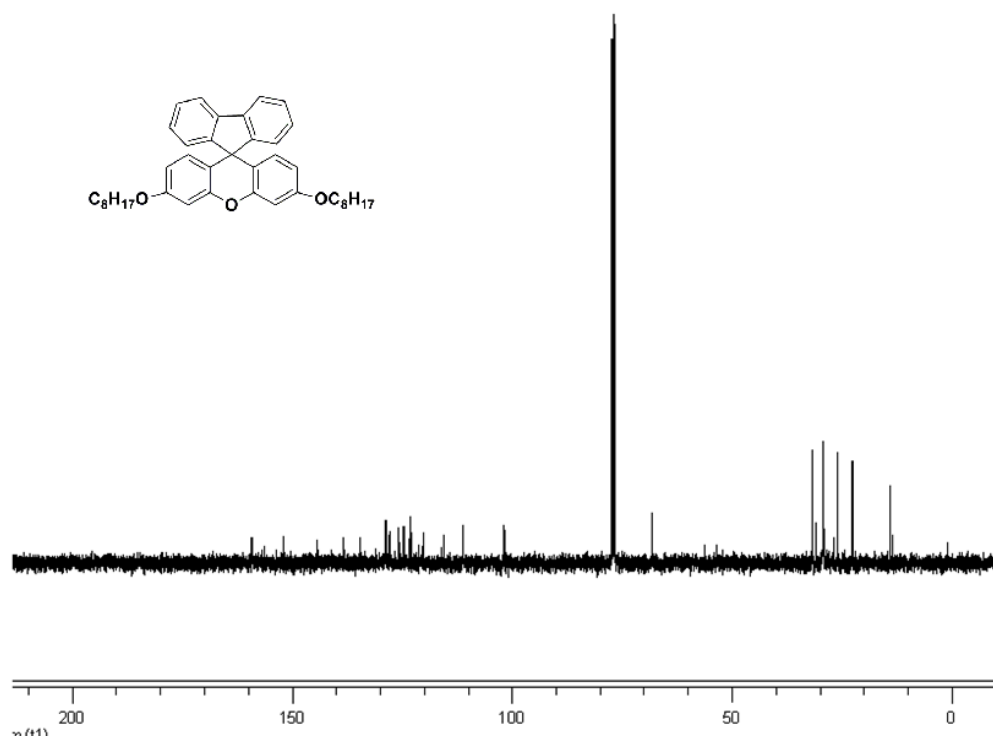


**Figure B 30.** <sup>13</sup>C NMR spectrum of **v** in CDCl<sub>3</sub>.

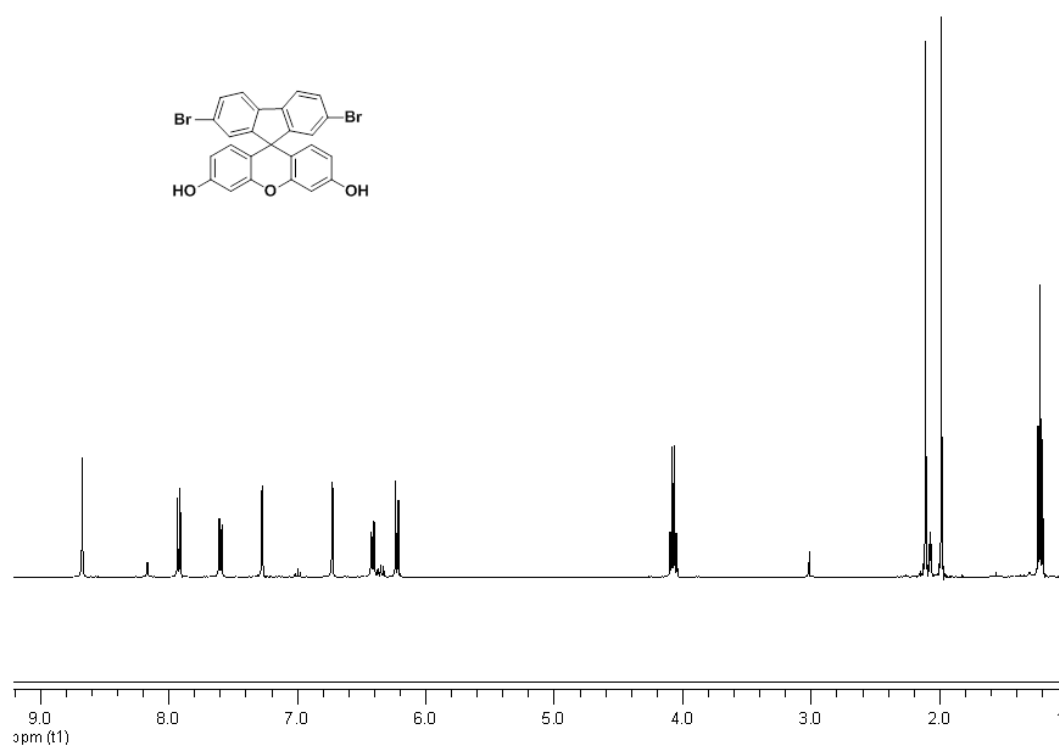


**Figure B 31.** <sup>1</sup>H NMR spectrum of **vi (a)** in CHCl<sub>3</sub>

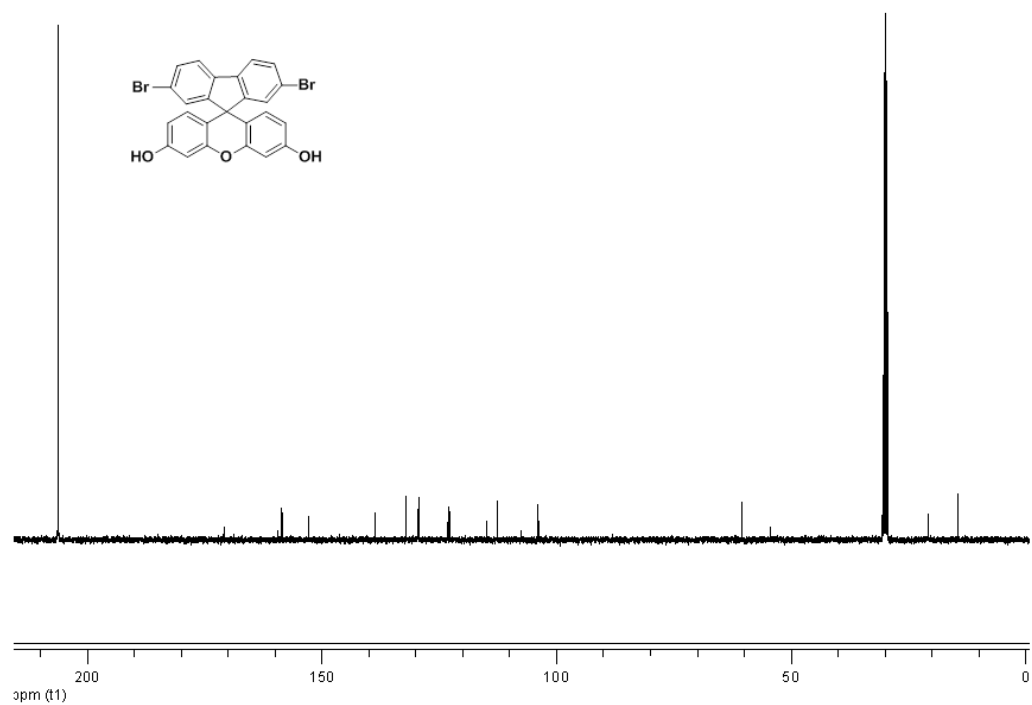


**Figure B 32.** <sup>13</sup>C NMR spectrum of **vi (a)** in CHCl<sub>3</sub>.

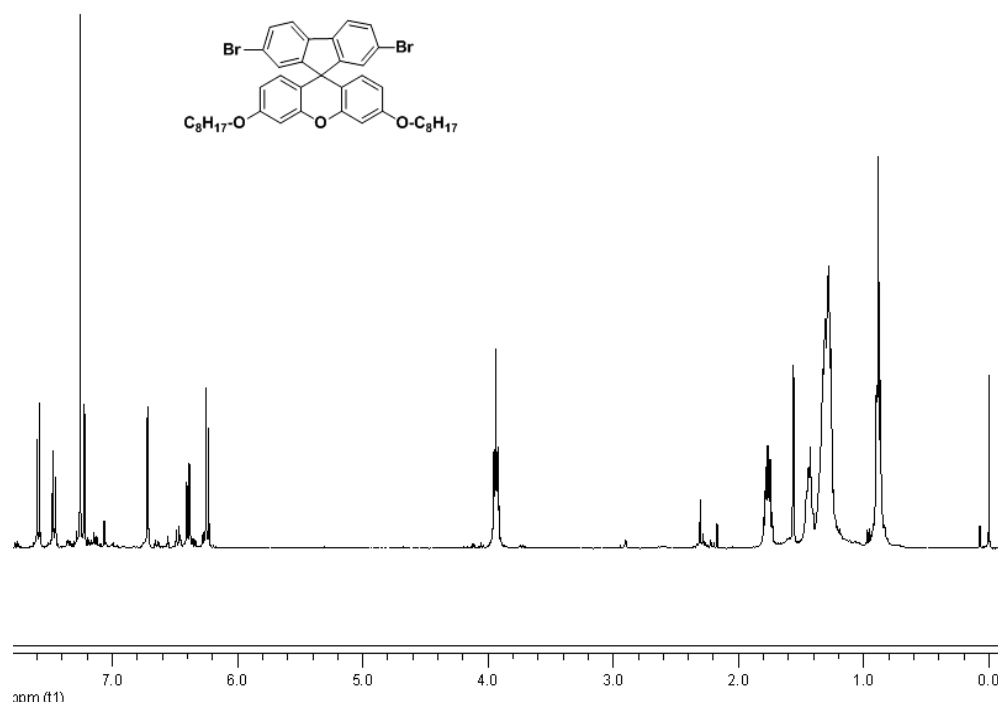


**Figure B 33.** <sup>1</sup>H NMR spectrum of **vi** in CHCl<sub>3</sub>

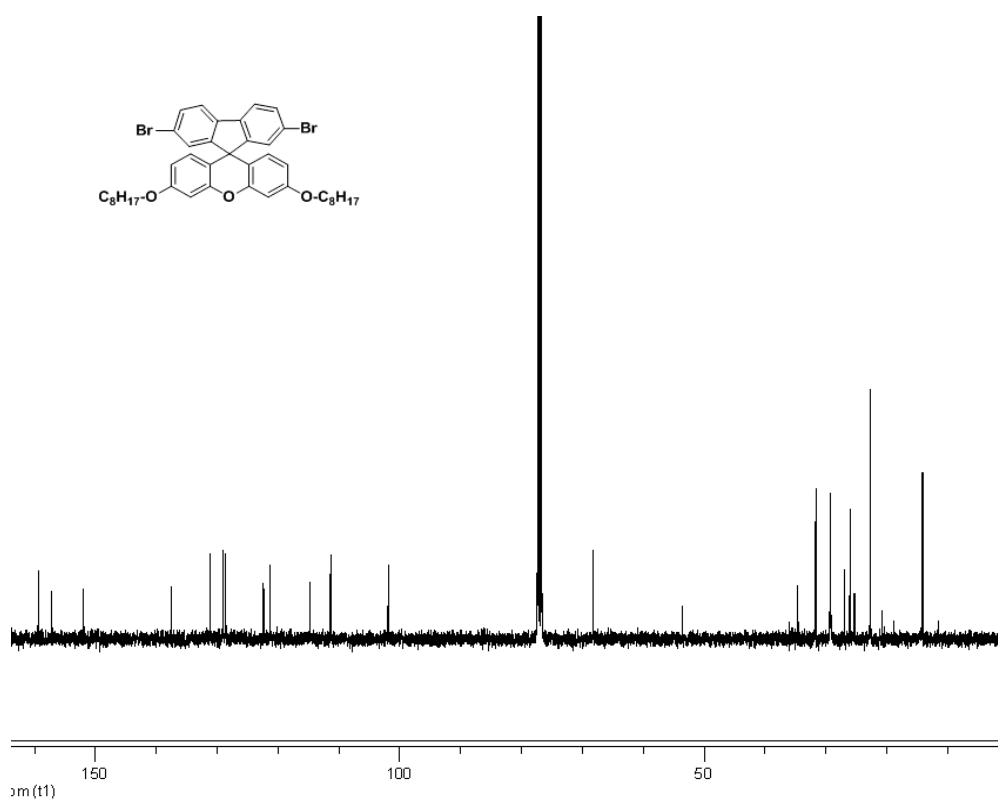


**Figure B 34.** <sup>13</sup>C NMR spectrum of **vi** in CHCl<sub>3</sub>.

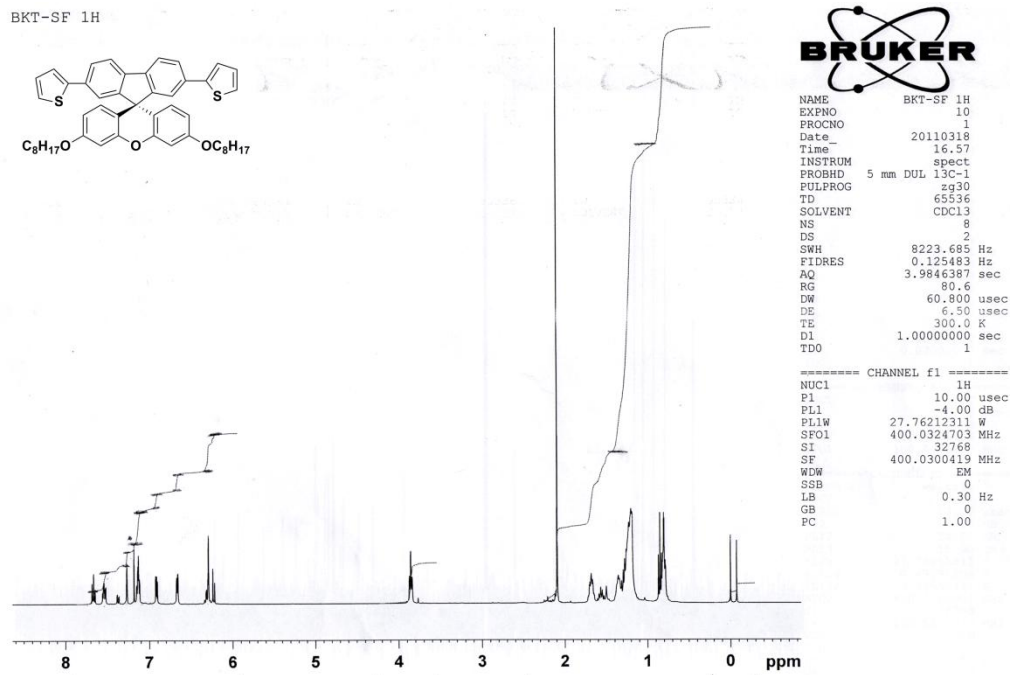


Figure B 35.  $^1\text{H}$  NMR spectrum of TXT in  $\text{CHCl}_3$

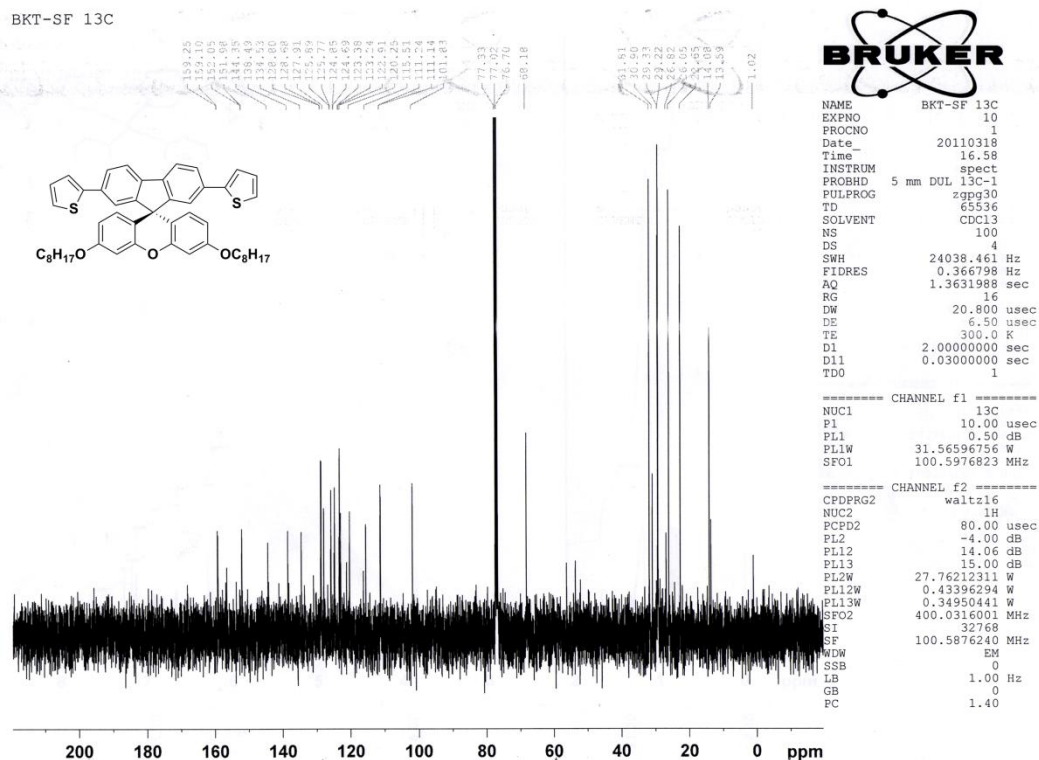


Figure B 36.  $^{13}\text{C}$  NMR spectrum of TXT in  $\text{CHCl}_3$

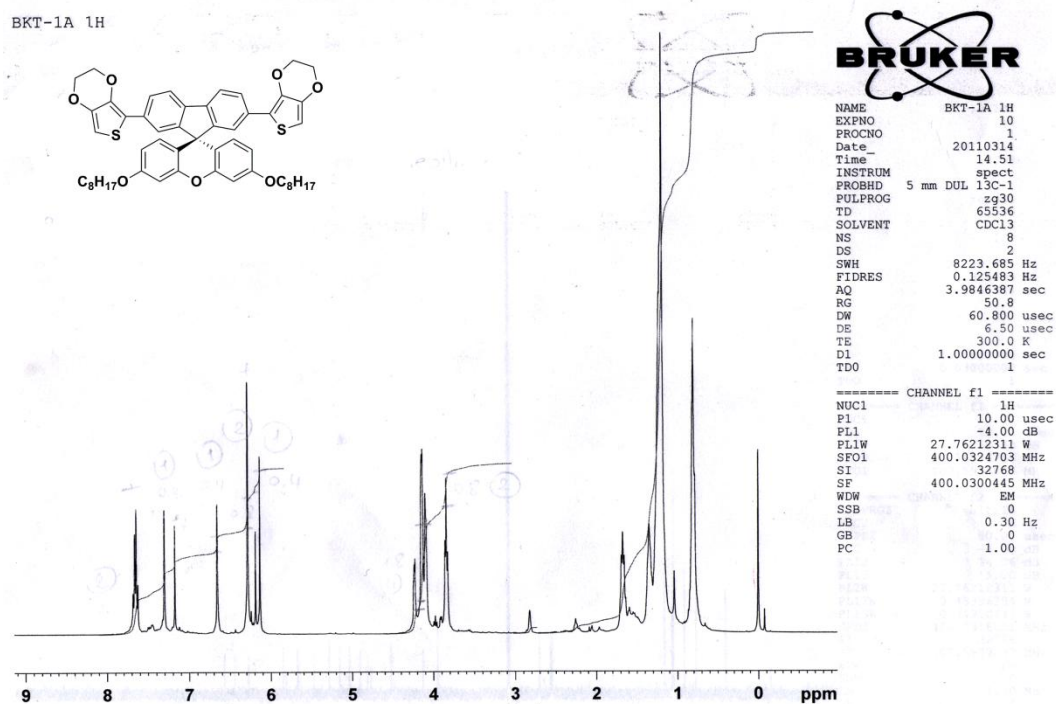


Figure B 37.  $^1\text{H}$  NMR spectrum of EXE in  $\text{CHCl}_3$

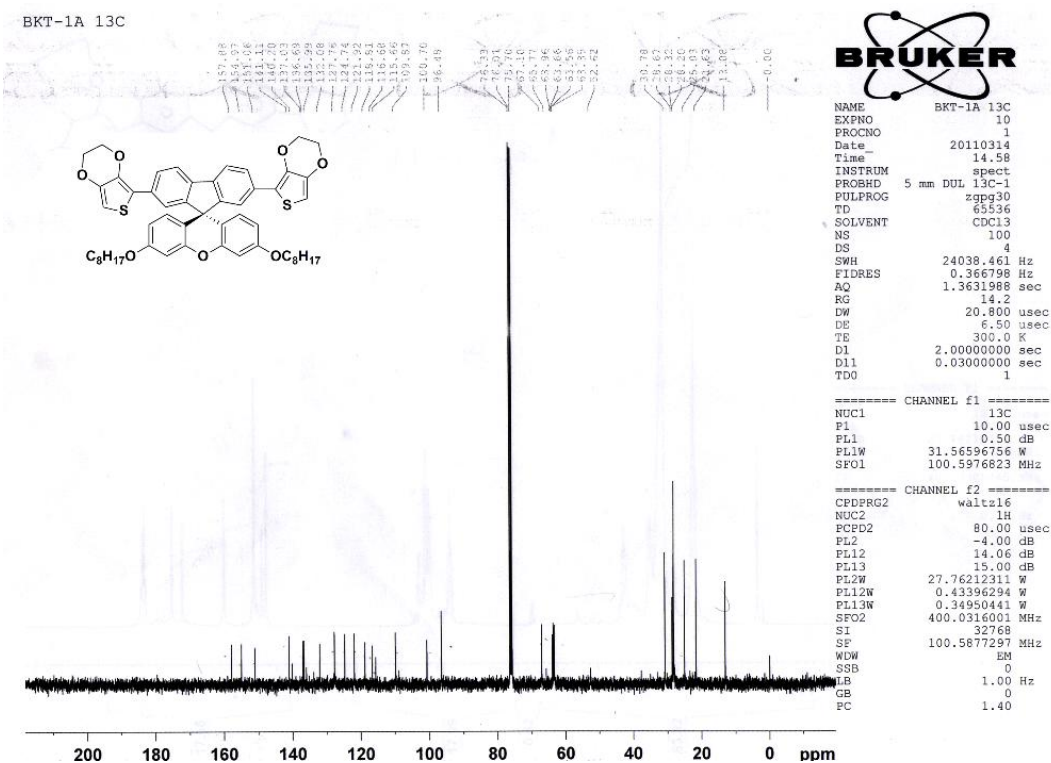


Figure B 38.  $^{13}\text{C}$  NMR spectrum of EXE in  $\text{CHCl}_3$

## APPENDIX C

### NMR SPECTRA OF POLYMERS

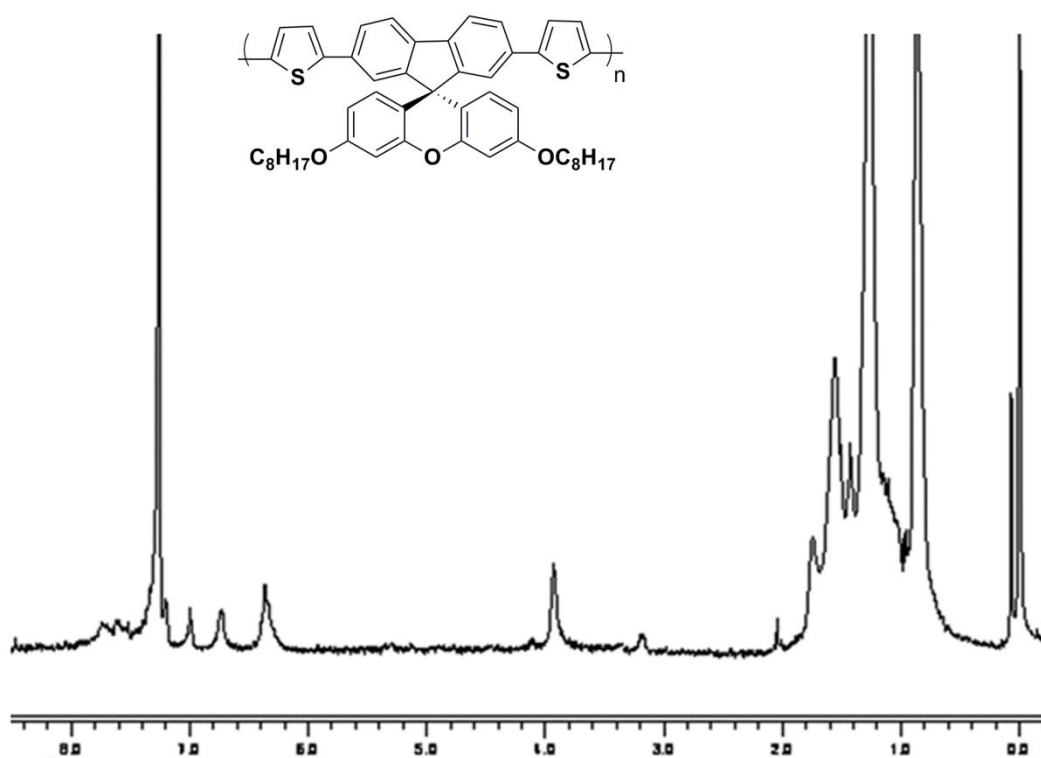
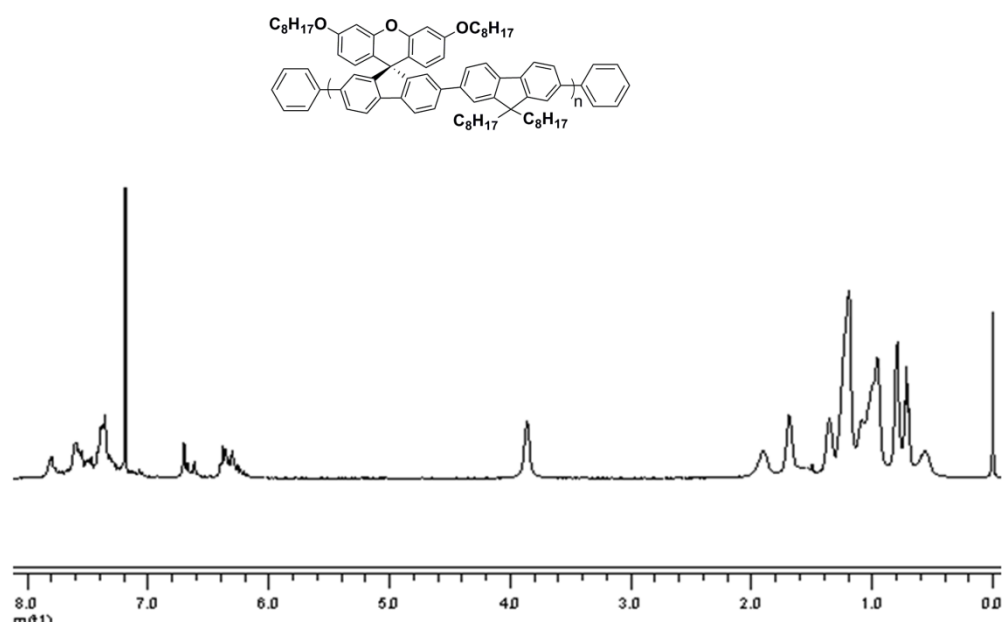


Figure C1.  $^1\text{H}$  NMR spectrum of P(TXT) in  $\text{CHCl}_3$



**Figure C2.**  $^1\text{H}$  NMR spectrum of **P(F8-SFX)** in  $\text{CHCl}_3$



## APPENDIX D

### ELEMENTAL COMPOSITION REPORT OF MONOMERS

#### Single Mass Analysis

Tolerance = 100.0 PPM / DBE: min = -1.5, max = 100.0

Element prediction: Off

Number of isotope peaks used for i-FIT = 3

Monoisotopic Mass, Even Electron Ions

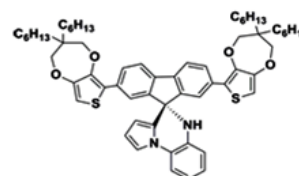
1 formula(e) evaluated with 1 results within limits (all results (up to 1000) for each mass)

Elements Used:

C: 59-62 H: 66-80 N: 2-2 O: 4-4 S: 2-2

Ahmet Onal

20110603\_6318\_BKTPFGP\_01 11 (0.058) Cm (1:283)



1: TOF MS ES+  
1.90e+005

| Minimum: |            |       |       | -1.5 |       |              |                  |  |
|----------|------------|-------|-------|------|-------|--------------|------------------|--|
| Maximum: | 100.0      | 100.0 | 100.0 |      |       |              |                  |  |
| Mass     | Calc. Mass | mDa   | PPM   | DBE  | i-FIT | i-FIT (Norm) | Formula          |  |
| 965.4808 | 965.5325   | -51.7 | -53.5 | 24.5 | 467.4 | 0.0          | C61 H77 N2 O4 S2 |  |

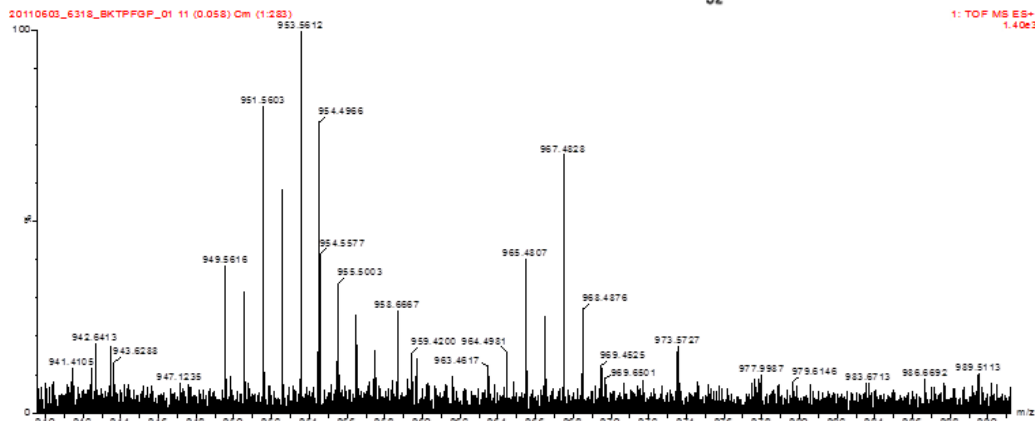


Figure D2. Elemental composition report of PQP.

Number of isotope peaks used for i-FIT = 3

Elements Used:

Minimum:

Maximum:

| Mass     | Calc. Mass | mDa  | PPM  | DBE  | i-FIT    | Formula :    |
|----------|------------|------|------|------|----------|--------------|
| 868.3573 | 868.3467   | 10.6 | 12.2 | 26.0 | 476.00.0 | C53 H56 O7S2 |

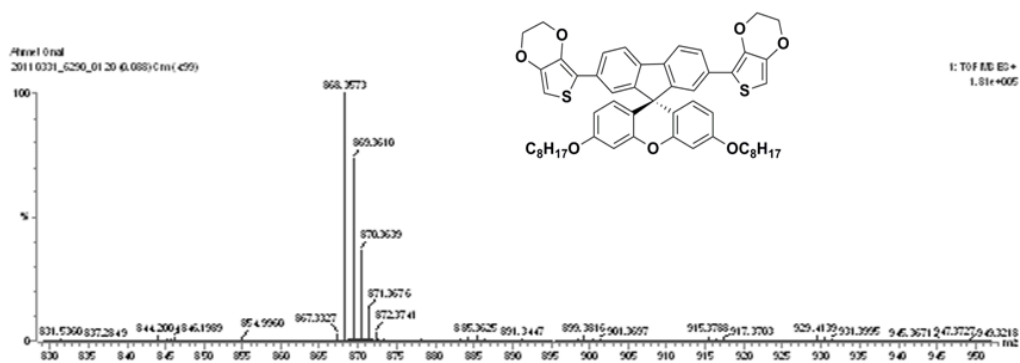


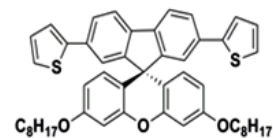
**Figure D3.** Elemental composition report of **EXE**.

### Single Mass Analysis

Tolerance = 10.0 PPM / DBE: min = -1.5, max = 100.0

Element prediction: Off

Number of isotope peaks used for i-FIT = 3



Monoisotopic Mass, Odd and Even Electron Ions

8 formula(e) evaluated with 1 results within limits (all results (up to 1000) for each mass)

Elements Used:

C: 47-49 H: 10-70 O: 3-5 S: 2-2

Ahmet Onal

20110603\_6318\_BKTHSF\_01 80 (0.292) Cm (13:281)

1: TOF MS ES+  
4.44e+005

Minimum: -1.5  
Maximum: 100.0 10.0 100.0

| Mass     | Calc. Mass | mDa  | PPM  | DBE  | i-FIT | i-FIT (Norm) | Formula   |
|----------|------------|------|------|------|-------|--------------|---|
| 752.3292 | 752.3358   | -6.6 | -8.8 | 24.0 | 502.5 | 0.0          | C <sub>49</sub> H <sub>52</sub> O <sub>3</sub> S <sub>2</sub> |

20110603\_6318\_BKTHSF\_01 80 (0.292) Cm (14:284)

1: TOF MS ES+  
3.51e4

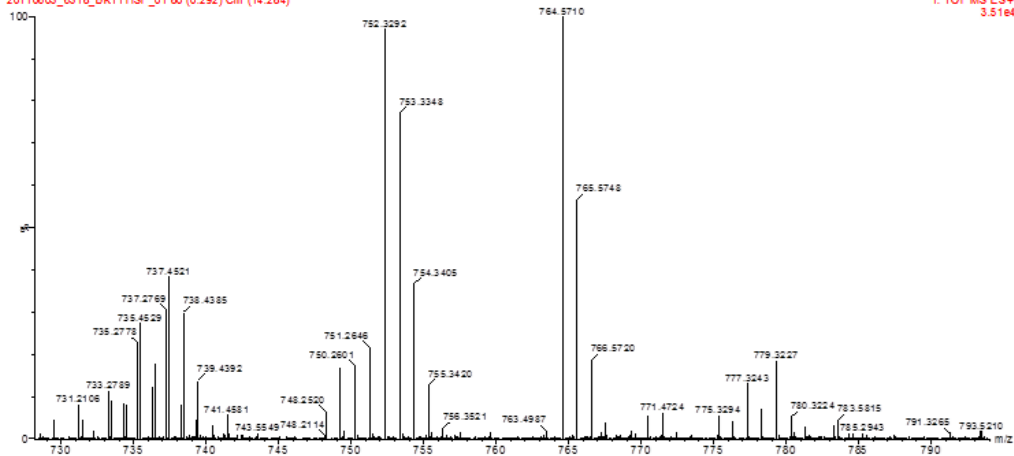


Figure D2. Elemental composition report of TXT.

## APPENDIX E

### MASS ANALYSIS REPORT OF POLYMER

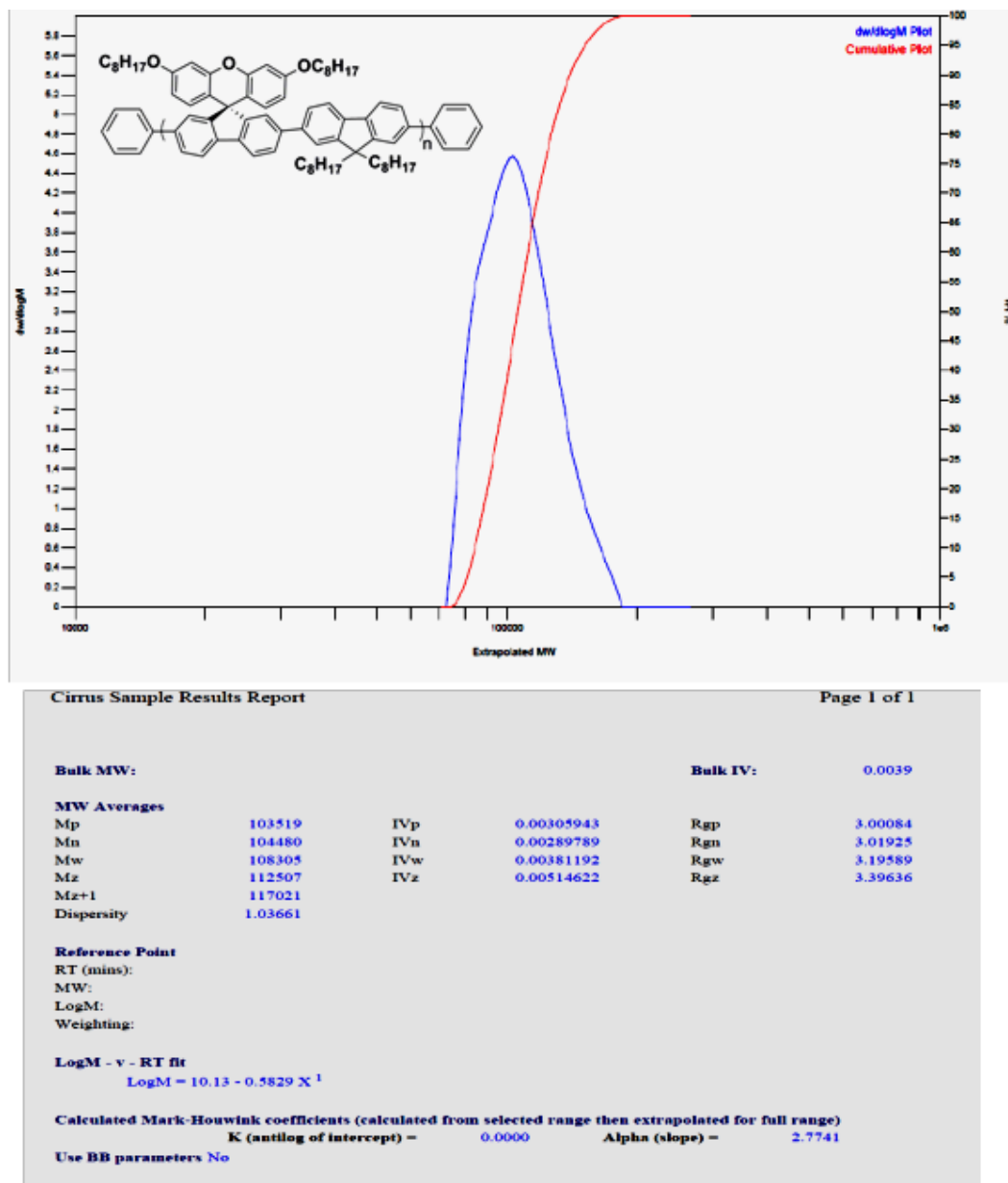


Figure E1. GC mass analysis data for P(F8-SFX)

## CURRICULUM VITAE

### PERSONAL INFORMATION

Surname, Name: Çarbaş Bezgin, Buket  
Nationality: Turkish  
Date and Place of Birth: 29 June 1981, Niksar/Tokat  
Phone: +90 356 527 78 05  
email: [buketbezgin@gmail.com](mailto:buketbezgin@gmail.com)  
bezgin@metu.edu.tr

### EDUCATION

| Degree      | Institution                            | Year of Graduation |
|-------------|--|--------------------|
| Ph.D.       | METU Chemistry Department              | 2013               |
| MS          | Marmara University Chemistry Education | 2004               |
| BS          | Marmara University Chemistry Education | 2004               |
| High School | Danışmend Gazi High School,            | 1999               |

### WORK EXPERIENCE

#### Year Place Enrollment

2004-Present, METU, Department of Chemistry, Research Asistant

2012-2013 Visitor Graduated Researcher in University of California Los Angeles, Depertmant of Material Science and Engineering.

### FOREIGN LANGUAGES

Advanced English.

### PUBLICATIONS

1. Bezgin B., Cihaner A., and Önal A.M., Electrochemical polymerization of 9-fluorene-carboxylic acid and its electrochromic device application , Thin Solid Films, 2008 (516) 7329-7334
2. Yavuz A., Bezgin B., and Önal A.M. Synthesis and Characterization of a New Conducting Polymer Based on 4-(2,5-di-2-thiophen-2-yl-pyrrol-1-yl)-phthalonitrile, Journal of Applied Polymer Science, 114 (2009) 2685.
3. Bezgin B., Yağan A., and Önal A.M, Electrochemical Co-polymerization of a Novel Fluorene Derivative with 3,4-ethylenedioxythiophene, Journal of Electroanalytical Chemistry, 632 (2009) 143-148.
4. Bezgin B., and Önal A. M., Electrochemical Polymerization of an Electron Deficient Fluorene Derivative Bearing Ethylenedioxythiophene Side Groups Electrochimica Acta, , 55 (2010) 779-784.

5. Yavuz A., Bezgin B., Aras L. and Önal A. M, Synthesis and Electropolymerization of the Phthacyanines with 4-(2,5-di-2-thiophen-2-yl-pyrrol-1-yl) Substituents, Journal of Electroanalytical Chemistry, 639 (2010) 116-122.
6. Yavuz A., Çarbaş Bezgin B., Aras L., and Önal A. M Electropolymerization of a new 4-(2,5-di-2-thiophen-2-yl-pyrrol-1-yl) -tetra substituted nickel phthalocyanine derivative, Journal of Applied Polymer Science, 122 (2010) 1293-1299.
7. Çarbaş Bezgin B., Kivrak A., Zora M., and Önal A. M , Synthesis of a novel fluorescent and ion sensitive monomer bearing quinoxaline moieties and its electropolymerization , Reactive and Functional Polymers 71 (2011) 579–587.
8. Çarbaş Bezgin B., Kivrak A., and Önal A. M, A new processable electrochromic polymer based on an electron deficient fluorene derivative with a high coloration efficiency, Electrochimica Acta 58 (2011) 223-230.
9. Çarbaş Bezgin B., Kivrak A., Zora M., and Önal A. M, New fluorene–xanthene-based hybrid electrochromic and fluorescent polymers via donor–acceptor approach, Electrochimica Acta 66 (2012) 38-44.
10. Çarbaş Bezgin B., Kivrak A., Zora M., and Önal A. M, Synthesis and electropolymerization of a new ion sensitive ethylenedioxy-substituted terthiophene monomer bearing a quinoxaline moiety, Journal of Electroanalytical Chemistry, 677 (2012) 9–14.
11. Kivrak A., Çarbaş Bezgin B., Zora M., and Önal A. M, Synthesis and electropolymerization of an ion sensing and fluorescent fluorene derivative bearing a quinoxaline moiety and its analogues with different donor units, Reactive and Functional Polymers 72 (2012) 613-620.